

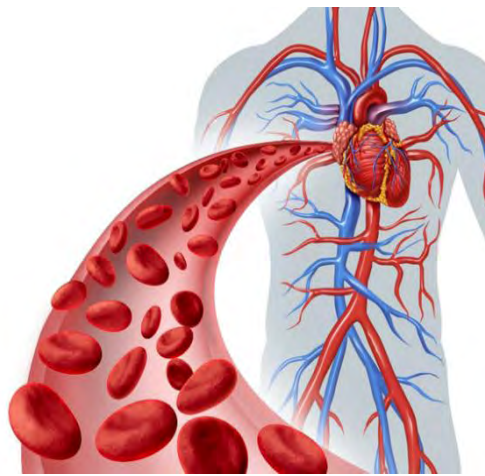
NUMERICAL STUDY OF BLOOD FLOW THROUGH STENOTIC AND ANEURYSMATIC ARTERY OF HUMAN ORGAN

BY

MOHAMMED NASIR UDDIN

Student No. 0412094002P

Registration No. 100709010, Session: April-2012



DOCTOR OF PHILOSOPHY
IN
MATHEMATICS



DEPARTMENT OF MATHEMATICS
BANGLADESH UNIVERSITY OF ENGINEERING AND TECHNOLOGY
DHAKA-1000
FEBRUARY-2018

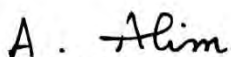
The thesis titled
NUMERICAL STUDY OF BLOOD FLOW THROUGH STENOTIC AND ANEURYSMATIC ARTERY OF HUMAN ORGAN

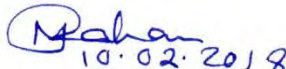
Submitted by

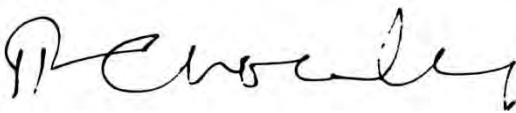
MOHAMMED NASIR UDDIN

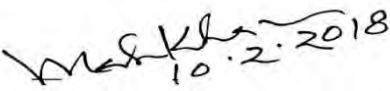
Student No. 0412094002P, Registration No. 100709010, Session: April-2012 has been accepted as satisfactory in partial fulfillment of the requirement for the degree of Doctor of Philosophy (PhD) in Mathematics on 10th February 2018.

BOARD OF DOCTORAL COMMITTEE

1. 
10/02/2018

Dr. Md. Abdul Alim Chairman
Professor (Supervisor)
Department of Mathematics
BUET, Dhaka-1000
2. 
10.02.2018

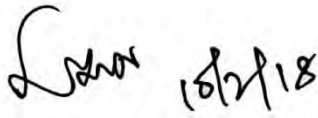


Dr. Md. Mustafizur Rahman Member
Professor and Head (Ex-Officio)
Department of Mathematics
BUET, Dhaka-1000
3. 

Dr. Md. Mustafa Kamal Chowdhury Member
Professor (Rtd), Department of Mathematics
BUET, Dhaka.
Address: 110, Lake Garden, Lake Circus Road,
Kalabagan, Dhaka
4. 
10.2.2018

Dr. Md. Abdul Hakim Khan Member
Professor
Department of Mathematics
BUET, Dhaka-1000

NUMERICAL STUDY OF BLOOD FLOW THROUGH STENOTIC AND ANEURYSMATIC ARTERY OF HUMAN ORGAN

BOARD OF DOCTORAL COMMITTEE (CONTD.)

5.  10/2/18
-
- Dr. Md. Manirul Alam Sarker** Member
Professor
Department of Mathematics
BUET, Dhaka-1000
6.  10.02.18
-
- Dr. Md. Mashud Karim** Member
Professor
Department of NAME,
BUET, Dhaka-1000
7. 
-
- Dr. Mohammad Ali** Member
Professor
Department of ME
BUET, Dhaka-1000
8. 
-
- Dr. Md. Anwar Hossain** Member (External)
Professor (Rtd.), Department of Mathematics
University of Dhaka, Dhaka.
Address: 35/4 Lake Circus (Opposite of Square Hospital)
Kalabagan, Dhanmondi, Dhaka, Bangladesh

Author's Declaration

I am hereby declaring that the work in this dissertation was carried out in accordance with the regulations of Bangladesh University of Engineering and Technology (BUET), Dhaka, Bangladesh. The work is also original except where indicated by and attached with special reference in the context and no part of it has been submitted for any attempt to get other degrees or diplomas.

All views expressed in the dissertation are those of the author and in no way or by no means represent those of Bangladesh University of Engineering and Technology, Dhaka. This dissertation has not been submitted to any other University for examination either in home or abroad.



(MOHAMMED NASIR UDDIN)

Date: 10 February 2018

Certify of Research

This is to endorse that the work presented in this thesis is carried out by the author under the supervision of Dr. Md. Abdul Alim, Professor, Department of Mathematics, Bangladesh University of Engineering & Technology (BUET), Dhaka.

A. Alim
10/02/2018

Dr. Md. Abdul Alim
Professor
Department of Mathematics
BUET, Dhaka

Mik

Md. Nasir Uddin
Student No. 0412094002P
Registration No. 100709010
Session: April-2012

Dedicated to my Parents

Acknowledgements

This PhD thesis would not have been possible without the encouragement, assistance and continuous support of many wellwishers. My deepest gratitude is to all of them.

At first, I would like to acknowledge the noteworthy of Almighty's continual kindness and assist without which no work would have been possible to achieve the aim. I would like to gratefully and sincerely thank my respected supervisor Dr. Md. Abdul Alim, Professor, Department of Mathematics, Bangladesh University of Engineering and Technology, Dhaka for his wonderful guidance, encouragement, patience and cooperation during the preparation of this thesis and throughout the whole period of study in Bangladesh University of Engineering and Technology. It would not have been possible to carry out the outcomes of the research successfully without the continuous inspiration and expert guidance from supervisor.

I would like to take the opportunity to thank the members of the doctoral committee for their inspiring comments, guidance and constructive all criticism during research work. I am pleased to acknowledge with gratefulness to Professor Dr. Md. Mustafa Kamal Chowdhury, Professor Dr. Md Abdul Hakim Khan, Professor Dr. Md. Monirul Alam Sarker and Professor Dr. Md. Mustafizur Rahman, Department of Mathematics, Bangladesh University of Engineering and Technology, for their outstanding recommendation and advice in the course of being successful to reach the objectives of this dissertation.

I would like to thank Professor Dr. Mohammad Ali, Department of Mechanical Engineering, BUET, and Professor Dr. Md. Mashud Karim, Department of Naval Architecture & Marine Engineering, BUET, for their valuable scientific and practical advice, fruitful discussions and useful guidance during my study period.

I am very grateful to my external board member Dr. Md. Anwar Hossain, Professor (Rtd.), Department of Mathematics, University of Dhaka, Dhaka, Bangladesh, for his productive discussions, valuable suggestions and all kind of supports that accelerated my work.

I am very much obliged to Bangladesh University of Professionals to allow and support me for higher study at BUET. I would also like to thank Col Md Shameem Ahsan Jaglul,

Chairman, Department of Information and Communication Technology, BUP, for his all kind of supports and cooperations. I am grateful to all my colleagues for their encouragement and helping mentality in all affairs particularly in my study. Special thank to all staff in my department.

I wish to thank to the staff of the Department of Mathematics, Bangladesh University of Engineering and Technology, for their cooperation during my study period.

Finally, most importantly, I wish to express my deep gratitude towards my family. I am very much thankful to my parent, brothers and sisters, and all relatives for their sacrifices and their love. I express my devoted affection to my wife Mrs. Tahmina Haque, my elder daughter Nusaiba Nuha Nasir and younger daughter Nuzar Nawra Nasir for creating a delightful atmosphere as well as excusing me from family duties in order to complete the courses, research studies and final production of the thesis work.

Abstract

Cardiovascular diseases such as heart attacks, strokes, atherosclerosis, stenosis and aneurysms have been considered as the world's highest cause of death. The frequently affected arteries are the aorta, the coronary, the carotid, and the femoral arteries. It is a vital area of research for the flow behavior of blood, as well as the shear-thinning viscosity of blood. The study of blood flow has attracted the bioengineers, bio-medical researchers and numerical scientists over the past years due to its significant effect on several human cardiovascular diseases. In this thesis entitled "Numerical study of blood flow through stenotic and aneurysmatic artery of human organ", three problems have been studied. The study on various kinds of stenosis and aneurysm enclosures and boundary conditions are summarized below:

Firstly, a computational analysis and simulation of blood flow through symmetric stenosis and asymmetric stenosis with various flow rates have been studied. At inlet, the parabolic velocity profile is used and fixed pressure is used at outlet. No slip conditions are used for velocity and homogeneous Neumann condition for the pressure at blood vessel. The governing mass, momentum and Oldroyd-B equation are expressed in a normalized primitive variables formulation.

Secondly, the blood flow simulation and numerical investigation have been considered through the permeable aneurysmatic artery for Newtonian, Oldroyd-B and their generalized fluids. The velocity profile and constant pressure are used at inlet and outlet respectively. The first aneurysm blood vessel is permeable and no-slip boundary conditions are used for rest of the vessel walls. A set of partial differential equations of conservation of mass, momentum and Oldroyd-B equations are expressed in a normalized primitive variable formulation.

Finally, a comparative study and numerical investigation have been carried out for blood flow through stenotic and aneurysmatic artery with incompressible Newtonian and non-Newtonian fluids including blood clot. The upper surface of blood clot is heated and stenosed vessel wall is cooled down while no slip velocity conditions are applicable for all walls. The parabolic velocity profile is considered at inlet and pressure is remained unchanged at outlet.

The mathematical models are presented by various sets of partial differential equations for different physical problems with the corresponding boundary conditions. The dimensionless governing equations have transformed using appropriate nondimensional scale. The governing equations have solved using a finite element technique based on the Galerkin weighted method.

Results are presented in terms of velocity contour lines, pressure plots, and stream lines with vectors along vessel axis for simulation of blood flow. The graphical study have shown with the effects of the blood velocity, blood pressure along vessel axis, wall shear stress, drag coefficient, stress components, governing parameters namely Reynold numbers Re , Weissenbeg number Wi , Schmidt number Sc , and Pectlet number Pe for all models. Code validation is performed with previously published work and the results are found to be in excellent agreement. Reynold numbers Re , Weissenbeg number Wi , Pectlet number Pe

This results indicate that the blood flow and pressure strongly depends on the parameters such as Reynold numbers Re , Weissenbeg number Wi , Schmidt number Sc , and Pectlet number Pe , the height of stenotic and aneurysmatic artery, permeable aneurysm artery, drag coefficient, and wall shear stress. The following outcomes in the research of numerical study of blood flow through stenotic andaneurysmatic artery of human organ may also be useful in bio-medical engineering.

- (i) It has shown that the effect of blood flow variables related to viscoelasticity is more significant at the throat of stenotic and aneurysmatic artery.
- (ii) The reversal flow have found at behind the stenosis and aneurysm region.
- (iii) The confined area or recirculation zones have originated at constriction of stenosis and middle of two aneurysm.
- (iv) It is found that the hemodynamical factors- blood velocity, pressure, turbulence, stress tensor and wall shear stress, play important roles in the localization of arteriosclerotic lesions affecting mass transfer phenomena at the arterial walls.

- (v) The transport of blood ingredients through permeable walls have played an important role to genesis and progression of arterial diseases.
- (vi) At abrupt contraction region having blood clot, the blood flow characteristics are affected for all modifications.
- (vii) The finding of the blood flow behavior on the wall shear stress is an important factor in the onset of arterial diseases which may be reported in medical science.

Contents

BOARD OF DOCTORAL COMMITTEE	ii
Author's Declaration	iv
Certify of Research	v
Acknowledgements	vii
Abstract.....	ix
Contents	xii
List of Tables	xvii
List of Figures.....	xviii
CHAPTER 1	1
INTRODUCTION AND HISTORICAL REVIEW	1
1.1 Introduction.....	1
1.2 Historical Review	3
1.3.1 Kinematics of fluids	9
1.3.2 Blood circulation and arterial diseases	9
1.3.3 The frame indifference	11
1.3.4 The fluid velocity.....	12
1.3.5 The material derivative	13
1.3.6 The acceleration of fluid.....	13
1.3.7 The deformation gradient tensor	14
1.3.8 The rate of strain and vorticity tensors	14
1.3.9 The forces acting on fluid.....	15
1.3.10 Theorems and lemma	16
1.3.11 Dimensionless parameters.....	18
1.4 Balance Laws.....	20
1.4.1 Conservation of mass.....	20
1.4.2 Conservation of momentum	21
1.5 Formulation and Principles of the Constitutive Relations	23
1.5.1 Newtonian and non-Newtonian fluids.....	23
1.5.2 Generalized Newtonian fluid	24
1.5.3 Viscoelasticity and Development of Viscoelasticity	25
1.5.4 Derivation of Oldroyd model.....	27
1.5.5 Oldroyd-B model for blood flow	28
1.5.6 Navier-Stokes equations	30
1.6 Enthusiasm behind the selection of current work.....	31

1.7	Main objectives of the present study.....	32
1.8	Structure of the Thesis	33
CHAPTER 2		35
COMPUTATIONAL TECHNIQUE		35
2.1	Introduction.....	35
2.2	Elements of Numerical Solution Methods	36
2.2.1	Mathematical model	36
2.2.2	Discretization Process.....	36
2.2.3	Numerical grid	36
2.2.4	Finite approximations	36
2.2.5	Solution technique	37
2.3	Discretization Approaches	37
2.3.1	Finite element analysis	37
2.3.2	Mesh generation	38
2.3.3	Finite Element Formulation and Computational Technique	40
2.3.4	Algorithm.....	40
2.3.5	Solution of system of equations	42
2.4	Chapter Summary	43
CHAPTER 3		44
NUMERICAL STUDY OF BLOOD FLOW THROUGH SYMMETRIC AND ASYMMETRIC STENOSIS UNDER VARIOUS FLOW RATES.....		44
3.1	Physical Configurations	45
3.2	Mathematical Modeling	45
3.2.1	Governing equations.....	45
3.2.2	Shear-thinning viscosity model.....	47
3.2.3	Boundary conditions.....	48
3.2.4	Dimensional analysis	49
3.3	Numerical Analysis.....	49
3.3.1	Finite Element Formulation and Computational Technique	50
3.3.2	Grid Independence Test.....	50
3.4	Code Validation.....	51
3.5	Results and Discussion	51
3.5.1	Symmetric stenosis effects on blood flow field.....	52
3.5.2	Symmetric stenosis effects on pressure distribution	56
3.5.3	Asymmetric stenosis effect.....	58

3.5.4	Effects of dimensionless number	64
3.5.5	Different Flow rates on Blood flow	78
3.5.6	Wall Shear Stress effects	82
3.6	Chapter Summary	84
CHAPTER 4.....		86
BLOOD FLOW STUDY THROUGH ANEURYSMATIC ARTERY WITH PERMEABLE WALLS		86
4.1	Problem Statement	87
4.2	Mathematical Formulation	87
4.2.1	Non-dimensional governing mathematical equations	87
4.2.2	Boundary conditions.....	89
4.3	Computational Analysis	90
4.3.1	Computational procedure	90
4.3.2	Grid independence test.....	90
4.4	Results and Discussion	91
4.4.1	Aneurysm blood vessel effects on blood flow field	92
4.4.2	Aneurysm blood vessel effects on pressure distribution	100
4.4.3	Effects of dimensionless number	104
4.4.4	Stress tensor effects on blood flow	121
4.4.5	Wall shear stress effects on blood flow	125
4.5	Chapter Conclusion.....	128
CHAPTER 5.....		130
NUMERICAL INVESTIGATION OF BLOOD FLOW THROUGH STENOTIC AND ANEURYSMATIC ARTERY HAVING BLOOD CLOT		130
5.1	Problem Formulation	131
5.2	Mathematical Model.....	131
5.2.1	Dimensionless covering equations.....	131
5.2.2	Boundary conditions.....	133
5.3	Numerical Technique	133
5.3.1	Computational procedure	134
5.3.2	Grid sensitivity test	134
5.4	Results and Discussion	135
5.4.1	Stenotic and aneurysmatic effects on blood flow	135
5.4.2	Stenotic and aneurysmatic effects on pressure distribution.....	141

5.4.3	Effects of dimensionless number	144
5.4.4	Wall shear stress effects on blood flow	159
5.4.5	Drag coefficient effects on blood flow	163
5.5	Chapter Ending.....	164
CHAPTER 6	166
6.1	Conclusions.....	166
6.2	Recommendation of Cardiovascular Diseases	168
6.3	Further Research	172
Appendix A	173
Appendix B	178
References	183

Nomenclature

σ	Stress tensor (Pa)	T_b	Arterial blood temperature
σ_v	Viscous stress tensor (Pa)	Pe	Peclet Number
σ_n	Solvent stress tensor (Pa)	Sc	Schmidt Number
L	Height and the enclosure (m)	Pr	Prandtl Number
I	Identity matrix	Q	Heat source
W_i	Weissenberg number	P_f	Perfusion coefficient
p	Pressure (Nm ⁻²)	ρ	Blood density
P	Non-dimensional pressure	C_b	Specific heat capacity of blood
Re	Reynold number	w_b	Blood perfusion rate
q	Flow rate (cm ² /s)	C_p	Tissue specific heat
λ_x	Relaxation time	U_i	Inlet velocity
λ_d	Retardation time	P_o	Outlet pressure
V	Symmetry velocity gradient		

μ_v Polymer viscosity

μ_n Solvent viscosity

V' Anti-symmetry velocity gradient

$\dot{\gamma}$ Rate of deformation tensor

u, v velocity components (ms⁻¹)

U, V Dimensionless velocity components

Subscripts

b blood

s stress

i Inlet state

v Polymer

n Solvent

Greek symbols

μ Viscosity

γ Deformation tensor

ρ density of the fluid (kgm⁻³)

ν kinematic viscosity of the fluid (m²s⁻¹)

τ_s Extra-stress tensor

o Outlet state

x Relaxation

d Retardation

List of Tables

3.1	Models outline	48
3.2	Grid Sensitivity check at $Re = 100$, $Wi = 0.6$ and $q = 0.1 \text{ cm}^3/\text{s}$	51
3.3	Blood velocity is presented along vessel axis for all four cases while $Re = 100$, $Wi = 0.6$ and $q = 0.1 \text{ cm}^3/\text{s}$.	53
3.4	Numerical values of pressure are presented along vessel axis for all four models while $Re = 100$, $Wi = 0.6$ and $q = 0.1 \text{ cm}^3/\text{s}$.	57
3.5	Velocity are obtained along vessel axis for different Reynold numbers, $Re = 100$, 500 and 1000 while $Wi = 0.6$ and $q = 0.1 \text{ cm}^3/\text{s}$.	64
3.6	Numerical value of pressure are obtained along vessel axis for different Effect of various Reynold numbers, $Re = 100$, 500 and 1000 while $Wi = 0.6$ and $q = 0.1 \text{ cm}^3/\text{s}$.	65
3.7	Blood velocity is presented for various Weissenberg numbers, $Wi = 0.0$, 0.5 and 1.0 while $Re = 100$ and $q = 0.2 \text{ cm}^3/\text{s}$.	72
3.8	Numerical pressure is obtained along vessel axis at constriction for different Effects of different Weissenberg numbers while, $Wi = 0.0$, 0.5 and 1.0 while $Re = 100$ and $q = 0.1 \text{ cm}^3/\text{s}$.	72
3.9	Blood velocity is obtained along vessel axis at first and second stenosis for different flow rate, $q = 0.05$, 0.2 and 2.0 cm^3/s at $Re=100$ and $Wi= 0.6$.	79
3.10	Pressure are presented at first and second stenosis along vessel axis for different flow rate, $q = 0.05$, 0.2 and 2.0 cm^3/s at $Re=100$ and $Wi = 0.6$.	79
3.11	Numerical values of wall shear stress are obtained at begining of 1st and 2nd Stenosis of artery for all four models while $Re=100$, $Wi=0.6$ and $q=0.1 \text{ cm}^3/\text{s}$.	82
4.1	Grid Sensitivity Check at $Pe = 100$, $Sc=1$, $Wi = 0.6$ and $q= 0.1 \text{ cm}^3/\text{s}$	91
4.2	Blood velocity is presented for partial permeable aneurysm along vessel axis for all cases while $Pe = 1000$, $Wi = 0.6$ and $q = 0.1 \text{ cm}^3/\text{s}$.	93
4.3	Pressure values of partial permeable aneurysm are inserted along blood vessel axis for all four models while $Pe =1000$, $Wi=0.6$ and $q= 0.1 \text{ cm}^3/\text{s}$.	101
4.4	Velocity deviation are included for various Peclet numbers while $Pe = 1000$, 2000 and 3000.	105
4.5	Pressure variation at inlet and 1 st aneurysm for different Pe with $Wi = 0.6$ and $q = 0.1 \text{ cm}^3/\text{s}$.	106

4.6	Optimal value of velocity are added for various Wi when $Pe= 1000$ and flow rate, $q = 0.1 \text{ cm}^3/\text{s}$.	113
4.7	Minmax pressure are obtained along vessel axis for different Weissenberg numbers while $Wi = 0.0, 0.5$ and 1.0 .	117
4.8	Numerical value of stress components along vessel axis at permeable aneurysm and impermeable aneurysm while $q = 0.1 \text{ cm}^3/\text{s}$, $Pe = 1000$ and $Wi = 0.6$.	122
5.1	Grid Sensitivity Check at $Wi = 0.5$, $Re = 1000$ and $q = 0.1 \text{ cm}^3/\text{s}$	135
5.2	Numerical value of velocity for all four models along blood vessel axis when $Re = 1000$, $Wi = 0.5$ and $q = 0.1 \text{ cm}^3/\text{s}$.	136
5.3	Numerical value of pressure for blood clotted and non-blood clotted models is inserted when $Re = 1000$, $Wi = 0.5$ and $q = 0.1 \text{ cm}^3/\text{s}$.	142
5.4	Velocities are obtained for different Reynold numbers, $Re = 1000, 2000$ and 3000 when $Wi = 0.6$ and $q = 0.1 \text{ cm}^3/\text{s}$.	144
5.5	Pressue value are shown at stenosis and aneurysm with different Re when $Wi = 0.6$ and $q = 0.1 \text{ cm}^3/\text{s}$.	146
5.6	Velocity at the throat of stenosis and aneurysm with various Wi when $Re = 1000$ and $q = 0.1 \text{ cm}^3/\text{s}$.	151
5.7	Pressure at blood lump and swell area of artery along vessel axis for different Weissenberg numbers, $Wi = 0.0, 0.5$ and 1.0 .	156
5.8	The optimal value of wall shear stress along vessel axis for blood clotted and non-blood clotted model while $q = 0.1 \text{ cm}^3/\text{s}$, $Re = 1000$ and $Wi = 0.6$.	160
5.9	The coefficients of drag at stenosed vessel are presented with different dimensionless numbers.	163

List of Figures

1.1	Blood circulatory system	10
1.2	Plaque deposit in stenosed blood vessel (left) and fatty deposit in aneurymatics artery (right)	11
2.1	Finite element discretization of a domain	39
2.2	Current mesh structure for physical systems	39
2.3	Flow chart of the computational procedure	41
3.1	Schematic diagram of the physical system	45

3.2	Viscosity function	47
3.3	Convergence of velocity with grid refinement for $Re = 10^2$ and $Wi = 0.6$ with blood flow rate $0.1 \text{ cm}^3/\text{s}$.	50
3.4	Comparison of velocity contour lines between Prokop and Kozel (2013) and present work	51
3.5	Velocity contour plots on blood flow through symmetric stenosis at $Re=100$ and $Wi = 0.6$	54
3.6	Stream lines of blood flow with vector through symmetric stenosis at $Re=100$ and $Wi = 0.6$	54-55
3.7	Velocity distribution on blood flow with vector arrow through symmetric stenosis at $Re=100$ and $Wi = 0.6$	55
3.8	Velocity profile of blood flow along vessel axis for all models when $Re = 100$, $Wi=0.6$ and $q = 0.1 \text{ cm}^3/\text{s}$.	56
3.9	Pressure distribution on blood flow through Symmetric Stenosis at $Re=100$, $Wi = 0.6$ and $q = 0.1 \text{ cm}^3/\text{s}$.	57-58
3.10	Pressure profile of blood flow along vessel axis for all models when $Re = 100$, $Wi = 0.6$ and $q = 0.1 \text{ cm}^3/\text{s}$.	58
3.11	Velocity distribution on blood flow through non-symmetric Stenosis at $Re=100$ and $Wi = 0.6$ and $q = 0.1 \text{ cm}^3/\text{s}$.	59
3.12	Pressure distribution on blood flow through asymmetric Stenosis at $Re=100$ and $Wi = 0.6$ and $q = 0.1 \text{ cm}^3/\text{s}$.	60
3.13	Comparison of Blood Velocity and Blood Pressure distribution along vessel axis for non-symmetric Stenosis	61
3.14	Comparison of velocity profile for symmetric and asymmetric stenosis effects along vessel axis	62
3.15	Comparison of pressure profile for symmetric (Figure 3.15a) and asymmetric (Figure 3.15b) stenosis effects along vessel axis	63
3.16	Reynold Numbers (Re) effects on Blood flow of Newtonian model at $Wi = 0.6$ and flow rate $0.1 \text{ cm}^3/\text{s}$.	65
3.17	Reynold Numbers (Re) effects on pressure distribution of Blood flow for Newtonian model at $Wi = 0.6$ and flow rate $0.1 \text{ cm}^3/\text{s}$.	66
3.18	Reynold Numbers (Re) effects on Blood flow of generalized Newtonian model at $Wi = 0.6$ and flow rate $0.1 \text{ cm}^3/\text{s}$.	66

3.19	Reynold Numbers (Re) effects on pressure distribution of Blood flow for generalized Newtonian model at $Wi = 0.6$ and flow rate $0.1 \text{ cm}^3/\text{s}$.	67
3.20	Reynold Numbers (Re) effects on Blood flow of Oldroyd-B model at $Wi = 0.6$ and flow rate $0.1 \text{ cm}^3/\text{s}$.	67
3.21	Reynold Numbers (Re) effects on pressure distribution of Blood flow for Oldroyd-B model at $Wi = 0.6$ and flow rate $0.1 \text{ cm}^3/\text{s}$.	68
3.22	Reynold Numbers (Re) effects on Blood flow of generalized Oldroyd-B model at $Wi = 0.6$ and flow rate $0.1 \text{ cm}^3/\text{s}$.	68
3.23	Reynold Numbers (Re) effects on pressure distribution of Blood flow for generalized Oldroyd-B model at $Wi = 0.6$ and flow rate $0.1 \text{ cm}^3/\text{s}$.	69
3.24	Velocity profile of the Effects of Reynold numbers (Re) on Blood flow at $Wi = 0.6$ and flow rate $0.1 \text{ cm}^3/\text{s}$ for all cases	70
3.25	Pressure profile of the Effects of Reynold numbers (Re) on Blood flow at $Wi = 0.6$ and flow rate $0.1 \text{ cm}^3/\text{s}$ for all four cases	71
3.26	Weissenberg Numbers (Wi) effects on blood flow of Newtonian model at $Re = 100$ and flow rate $0.1 \text{ cm}^3/\text{s}$.	73
3.27	Weissenberg Numbers (Wi) effects on pressure distribution of blood flow for Newtonian model at $Re = 100$ and flow rate $0.1 \text{ cm}^3/\text{s}$.	73
3.28	Weissenberg Numbers (Wi) effects on velocity distribution of blood flow for Generalized Newtonian model at $Re = 100$ and flow rate $0.1 \text{ cm}^3/\text{s}$.	74
3.29	Weissenberg Numbers (Wi) effects on pressure distribution of blood flow for Generalized Newtonian model at $Re = 100$ and flow rate $0.1 \text{ cm}^3/\text{s}$.	74
3.30	Weissenberg Numbers (Wi) effects on velocity distribution of blood flow for Oldroyd-B model at $Re = 100$ and flow rate $0.1 \text{ cm}^3/\text{s}$.	75
3.31	Weissenberg Numbers (Wi) effects on pressure distribution of blood flow for Oldroyd-B model at $Re = 100$ and flow rate $0.1 \text{ cm}^3/\text{s}$.	75
3.32	Weissenberg Numbers (Wi) effects on velocity distribution of blood flow for Generalized Oldroyd-B model at $Wi = 0.6$ and flow rate $0.1 \text{ cm}^3/\text{s}$.	76
3.33	Weissenberg Numbers (Wi) effects on pressure distribution of blood flow for generalized Oldroyd-B model at $Wi = 0.6$ and flow rate $0.1 \text{ cm}^3/\text{s}$.	76

3.34	Velocity profile of the Effects of Reynold numbers (Re) on Blood flow at $Wi = 0.6$ and flow rate $0.2 \text{ cm}^3/\text{s}$ for all cases.	77
3.35	Pressure profile of the Effects of Weissenbegr numbers (Re) on Blood flow at $Re = 100$ and flow rate $0.1 \text{ cm}^3/\text{s}$ for all modifications	78
3.36	Velocity profile on Blood flow with various flow rate ($q = 0.05, 0.1, 2 \text{ cm}^3/\text{s}$) at $Wi = 0.6$ and $Re = 100$	80
3.37	Pressure profile on Blood flow with various flow rate ($q = 0.05, 0.1, 2 \text{ cm}^3/\text{s}$) at $Wi = 0.6$ and $Re = 100$	81
3.38	Wall shear stress distribution on blood flow along vessel axis through symmetric stenosis at $Re = 100$ and $Wi = 0.6$ with various flow rate $q = 0.05$ (top) and 2 (bottom) cm^3/s .	83
4.1	Geometry of the physical system	87
4.2	Convergence of velocity with grid refinement for $Pe = 10^3$, $Sc = 1$ and $Wi = 0.6$ with blood flow rate $0.1 \text{ cm}^3/\text{s}$	90
4.3	Velocity contour line on blood flow through aneurysmatic (without permeable) blood vessel at $Pe = 1000$ and $Wi = 0.6$ with $q = 0.1 \text{ cm}^3/\text{s}$.	93
4.4	Velocity contour line on blood flow through partial permeable aneurysmatic blood vessel at $Pe = 1000$ and $Wi = 0.6$ with $q = 0.1 \text{ cm}^3/\text{s}$.	94
4.5	Velocity distribution on blood flow through permeable aneurysmatic blood vessel at $Pe = 1000$ and $Wi = 0.6$ with $q = 0.1 \text{ cm}^3/\text{s}$.	94-95
4.6	Stream lines on blood flow through aneurysmatic (without permeable) blood vessel at $Pe = 1000$ and $Wi = 0.6$ with $q = 0.1 \text{ cm}^3/\text{s}$.	95
4.7	Blood flow with vectors through aneurysmatic (without permeable) blood vessel at $Pe = 1000$ and $Wi = 0.6$ with $q = 0.1 \text{ cm}^3/\text{s}$.	96
4.8	Stream lines on blood flow through permeable aneurysmatic blood vessel at $Pe = 1000$ and $Wi = 0.6$ with $q = 0.1 \text{ cm}^3/\text{s}$.	96-97
4.9	Blood flow patterns with vectors through aneurysmatic (without permeable) blood vessel at $Pe = 1000$ and $Wi = 0.6$ with $q = 0.1 \text{ cm}^3/\text{s}$.	97
4.10	Stream lines on blood flow through partial permeable aneurysmatic blood vessel at $Pe = 1000$ and $Wi = 0.6$ with $q = 0.1 \text{ cm}^3/\text{s}$.	98
4.11	Blood flow patterns with vectors through permeable aneurysmatic blood vessel at $Pe = 1000$ and $Wi = 0.6$ with $q = 0.1 \text{ cm}^3/\text{s}$.	98-99
4.12	Velocity profile with impermeable, partial and both permeable aneurysm along vessel when $Pe = 1000$ and $Wi = 0.6$ with $q = 0.1 \text{ cm}^3/\text{s}$.	99-100

4.13	Pressure distribution on blood flow through aneurysmatic(without permeable) blood vessel at $Pe=1000$ and $Wi = 0.6$ with $q = 0.1 \text{ cm}^3/\text{s}$.	101-102
4.14	Pressure distribution on blood flow through partial permeable aneurysmatic blood vessel at $Pe=1000$ and $Wi = 0.6$ with $q = 0.1 \text{ cm}^3/\text{s}$.	102
4.15	Pressure distribution on blood flow through permeable aneurysmatic blood vessel at $Pe=100$ and $Wi = 0.6$ with $q = 0.1 \text{ cm}^3/\text{s}$.	103
4.16	Pressure profile with no permeable, partial permeable and both permeable aneurysmalong vesselwhen $Pe =1000$ and $Wi =0.6$.	103-104
4.17	Peclet Numbers (Pe) effects on Blood flow of Newtonian Model at $Wi = 0.6$ and flow rate $0.1 \text{ cm}^3/\text{s}$.	107
4.18	Peclet Numbers (Pe) effects on Blood flow of Generalized Newtonian Model at $Wi = 0.6$ and flow rate $0.1 \text{ cm}^3/\text{s}$.	107
4.19	Peclet Numbers (Pe) effects on Blood flow of Oldroyd-B Model at $Wi = 0.6$ and flow rate $0.1 \text{ cm}^3/\text{s}$.	108
4.20	Peclet Numbers (Pe) effects on Blood flow of Generalized Oldroyd-B Model at $Wi = 0.6$ and flow rate $0.1 \text{ cm}^3/\text{s}$.	108
4.21	Velocity profile of different Peclet numbers (Pe) on Blood flow at $Wi = 0.6$ and flow rate $0.1 \text{ cm}^3/\text{s}$.	109
4.22	Peclet Numbers (Pe) effects on pressure distribution of Blood flow for Newtonian Model at $Wi = 0.6$ and flow rate $0.1 \text{ cm}^3/\text{s}$.	110
4.23	Peclet Numbers (Pe) effects on pressure distribution of Blood flow for Generalized Newtonian Model at $Wi = 0.6$ and flow rate $0.1 \text{ cm}^3/\text{s}$.	110
4.24	Peclet Numbers (Pe) effects on pressure distribution of Blood flow for Oldroyd-B Model at $Wi = 0.6$ and flow rate $0.1 \text{ cm}^3/\text{s}$.	111
4.25	Peclet Numbers (Pe) effects on pressure distribution of Blood flow for Generalized Oldroyd-B Model at $Wi = 0.6$ and flow rate $0.1 \text{ cm}^3/\text{s}$.	111
4.26	Pressure profile of different Peclet numbers (Pe) on Blood flow at $Wi = 0.6$ and flow rate $0.1 \text{ cm}^3/\text{s}$	112
4.27	Weissenberg Numbers (Wi) effects on Blood flow of Newtonian Model at $Re = 1000$ and flow rate $0.1 \text{ cm}^3/\text{s}$	114
4.28	Weissenberg Numbers (Wi) effects on velocity distribution of Blood flow for Generalized Newtonian Model at $Re = 1000$ and $q= 0.1 \text{ cm}^3/\text{s}$.	114
4.29	Weissenberg Numbers (Wi) effects on velocity distribution of Blood flow for Oldroyd-B Model at $Re = 1000$ and flow rate $0.1 \text{ cm}^3/\text{s}$.	115

4.30	Weissenberg Numbers (Wi) effects on Velocity distribution of Blood flow for Generalized Oldroyd-B Model at $Pe = 1000$ and $q = 0.1 \text{ cm}^3/\text{s}$.	115
4.31	Velocity profile of the Effects of Weissenbug numbers (Wi) on Blood flow at $Pe = 1000$ and flow rate $0.1 \text{ cm}^3/\text{s}$	116
4.32	Weissenberg Numbers (Wi) effects on pressure distribution of Blood flow for Newtonian Model at $Re = 1000$ and flow rate $0.1 \text{ cm}^3/\text{s}$.	118
4.33	Weissenberg Numbers (Wi) effects on pressure distribution of Blood flow for generalized Newtonian Model at $Re=1000$ and $q = 0.1 \text{ cm}^3/\text{s}$.	118
4.34	Weissenberg Numbers (Wi) effects on pressure distribution of Blood flow for Oldroyd-B Model at $Re = 1000$ and flow rate $0.1 \text{ cm}^3/\text{s}$.	119
4.35	Weissenberg Numbers (Wi) effects on pressure distribution of Blood flow for Generalized Oldroyd-B Model at $Pe = 1000$ and flow rate $0.1 \text{ cm}^3/\text{s}$.	119
4.36	Pressure profile for different Weissenbegr numbers (Wi) on Blood flow at $Pe = 1000$ and flow rate $0.1 \text{ cm}^3/\text{s}$	120
4.37	Stress tensor profile on Blood flow at $Wi = 0.6$, $Pe = 1000$ and flow rate $0.1 \text{ cm}^3/\text{s}$ for all models.	122
4.38	The effects of stress components σ_{11} , σ_{12} and σ_{22} with $Pe = 1000$ and different Wi for all models at permeable aneurysm.	123
4.39	The effects of stress components σ_{11} , σ_{12} and σ_{22} with $Wi = 0.5$ and different Pe for all models at permeable aneurysm.	124
4.40	Wall shear stress effects on bottom wall of impermeable aneurysm for all cases with different Wi at $Pe = 1000$ and $q = 0.1 \text{ cm}^3/\text{s}$.	126
4.41	Wall shear stress effects on bottom wall of partial permeable aneurysm for all cases with different Wi at $Pe = 1000$ and $q = 0.1 \text{ cm}^3/\text{s}$.	127
5.1	Structure of the computational domain	131
5.2	Convergence of velocity with refinement for generalized Newtoninan model.	134
5.3	Velocity contour line on blood flow through stenosed and aneurysmatic vessel with blood clot at $Re = 1000$ and $Wi = 0.6$	137
5.4	Velocity contour line on blood flow through stenosed and aneurysmatic vessel without blood clot at $Re = 1000$ and $Wi = 0.6$	137-138
5.5	Velocity contour line on blood flow through stenosed and aneurysmatic vessel with blood clot at $Re = 1000$ and $Wi = 0.6$	138
5.6	Velocity contour line on blood flow through stenosed and aneurysmatic vessel without blood clot at $Re = 1000$ and $Wi = 0.6$	139

5.7	Velocity contour line on blood flow through stenotic and aneurysmatic vessel with blood clot at $Re=1000$ and $Wi = 0.6$	139-140
5.8	Velocity contour line on blood flow through stenosed and aneurysmatic vessel without blood clot at $Re=1000$ and $Wi = 0.6$	140
5.9	Comparison of Velocity profile with blood clot and without blood clot	141
5.10	Pressure distribution on blood flow through stenosed and aneurysmatic vessel with blood clot at $Re=1000$ and $Wi = 0.6$	142
5.11	Pressure distribution on blood flow through stenosed and aneurysmatic vessel without blood clot at $Re = 1000$ and $Wi = 0.6$	143
5.12	Comparison of pressure profile with blood clot and without blood clot	143
5.13	Reynold Numbers (Re) effects on Blood flow of Newtonian Model at $Wi = 0.6$ and flow rate $0.1 \text{ cm}^3/\text{s}$.	145
5.14	Reynold Numbers (Re) effects on Blood flow of Generalized Newtonian Model at $Wi = 0.6$ and flow rate $0.1 \text{ cm}^3/\text{s}$.	145
5.15	Reynold Numbers (Re) effects on Blood flow of Oldroyd-B Model at $Wi = 0.6$ and flow rate $0.1 \text{ cm}^3/\text{s}$.	146
5.16	Reynold Numbers (Re) effects on Blood flow of Generalized Oldroyd-B Model at $Wi = 0.6$ and flow rate $0.1 \text{ cm}^3/\text{s}$.	146
5.17	Velocity profile of the Effects of Reynold numbers (Re) on Blood flow at $Wi = 0.5$ and flow rate $0.1 \text{ cm}^3/\text{s}$ for all cases	147
5.18	Reynold Numbers (Re) effects on pressure distribution of Blood flow for Newtonian Model at $Wi = 0.6$ and flow rate $0.1 \text{ cm}^3/\text{s}$.	148
5.19	Reynold Numbers (Re) effects on pressure distribution of Blood flow for Generalized Newtonian Model at $Wi = 0.6$ and flow rate $0.1 \text{ cm}^3/\text{s}$.	149
5.20	Reynold Numbers (Re) effects on pressure distribution of Blood flow for Oldroyd-B Model at $Wi = 0.6$ and flow rate $0.1 \text{ cm}^3/\text{s}$.	149
5.21	Reynold Numbers (Re) effects on pressure distribution of Blood flow for Generalized Oldroyd-B Model at $Wi = 0.6$ and flow rate $0.1 \text{ cm}^3/\text{s}$.	150
5.22	Pressure profile of the Effects of Reynold numbers (Re) on Blood flow at $Wi = 0.5$ and flow rate $0.1 \text{ cm}^3/\text{s}$ for all models.	150-151
5.23	Weissenberg Numbers (Wi) effects on Blood flow of Newtonian Model with blood clot at $Re = 1000$ and flow rate $0.1 \text{ cm}^3/\text{s}$.	152
5.24	Weissenberg Numbers (Wi) effects on velocity distribution of Blood flow for Generalized Newtonian Model with blood clot at $Re = 1000$ and flow rate $0.1 \text{ cm}^3/\text{s}$.	153

5.25	Weissenberg Numbers (Wi) effects on velocity distribution of Blood flow for Oldroyd-B Model with blood clot at $Re=1000$ and $q=0.1 \text{ cm}^3/\text{s}$.	153
5.26	Weissenberg Numbers (Wi) effects on Velocity distribution of Blood flow for Generalized Oldroyd-B Model with blood clot at $Re = 1000$ and flow rate $0.1 \text{ cm}^3/\text{s}$.	154
5.27	Velocity profile of the Effects of Weissenbug numbers (Wi) on Blood flow at $Pe = 1000$ and flow rate $0.2 \text{ cm}^3/\text{s}$ for for all models	154-155
5.28	Weissenberg Numbers (Wi) effects on pressure distribution of Blood flow for Newtonian Model with blood clot at $Re = 1000$ and flow rate $0.1 \text{ cm}^3/\text{s}$	156
5.29	Weissenberg Numbers (Wi) effects on pressure distribution of Blood flow for Generalized Newtonian Model with blood clot at $Re = 1000$ and flow rate $0.1 \text{ cm}^3/\text{s}$.	157
5.30	Weissenberg Numbers (Wi) effects on pressure distribution of Blood flow for Oldroyd-B Model with blood clot at $Re = 1000$ and flow rate $0.1 \text{ cm}^3/\text{s}$.	157
5.31	Weissenberg Numbers (Wi) effects on pressure distribution of Blood flow for Generalized Oldroyd-B Model with blood clot at $Re = 1000$ and flow rate $0.1 \text{ cm}^3/\text{s}$.	158
5.32	Pressure profile of the Effects of Weissenbegr numbers (Wi) on Blood flow at $Re =1000$ and flow rate $0.1 \text{ cm}^3/\text{s}$ for for all models.	158-159
5.33	Effects of wall shear stress at upper wall without blood clot at stenotic artery for all cases with different Wi when $Re = 1000$ and $q = 0.1 \text{ cm}^3/\text{s}$.	161
5.34	Effects of wall shear stress on blood flow through stenotic and anuerysmatic artery without blood clot for all cases at $Re=1000$ and $Wi = 0.6$.	162
5.35	Drag effects on blood at bottom stenosed vessel wall with blood clot (left) and without blood clot (right) when $Re = 1000$ and $Wi = 0.6$.	164
5.36	Drag effects of blood at bottom stenosed vessel wall with blood clot with respect to Re (left) and Wi (right) for all models.	164

CHAPTER 1

INTRODUCTION AND HISTORICAL REVIEW

1.1 Introduction

Blood is a complex multi-phase mixture of solid corpuscles that includes red blood cells (RBCs, or erythrocytes), white blood cells (WBCs or leukocytes) and platelets (thrombocytes). These corpuscles are suspended in an aqueous polymeric and ionic solution, the plasma, containing electrolytes, organic molecules and various proteins. Erythrocytes have been shown to exert the most significant influence on the mechanical properties of blood, mainly due to their presence in very high concentration compared to the other formed elements, comprising about 40% to 45% of its volume in healthy individuals (hematocrit). The rheological characteristics of blood are determined by the properties of these components and their interaction with each other as well as with the surrounding structures. Bondar et al. (2011) have studied that the blood rheology is also affected by the external physical conditions such as temperature; however, in living organisms in general, and in large mammals, these conditions are regulated and hence they are subject to minor variations that cannot affect the general properties significantly. Other physical properties, such as mass density, may also play a role in determining the blood overall rheological conduct. Thurston (1972) has studied viscoelasticity properties of human blood flow experimentally. The rheological properties of blood and blood vessels are affected by the body intake of fluids, nutrients and medication although in most cases the effect is not substantial except possibly over short periods of time and normally does not have lasting consequences have described by Breithupt et al. (1997).

Lee et al. (2011) have illustrated that the viscosity of blood is determined by several factors such as the viscosity of plasma, hematocrit level, blood cell distribution, and the mechanical properties of blood cells. The blood viscosity is also affected by the applied deformation forces, extensional as well as shearing, and the ambient physical conditions. While the plasma is essentially a Newtonian fluid, the blood behaves as a non-Newtonian fluid showing all signs of non-Newtonian rheology which includes deformation rate dependency, viscoelasticity, yield stress and thixotropy has presented by Dintenfass (1962). Most non-Newtonian effects originate from the red blood cells due

CHAPTER 1 INTRODUCTION AND HISTORICAL REVIEW

to their high concentration and distinguished mechanical properties such as elasticity and ability to aggregate forming three-dimensional structures at low deformation rates.

There is a strong evidence that hemodynamical factors such as flow separation, flow recirculation, low and oscillatory wall shear stress, as well as changes in the rheological properties of blood and its components, play a major role in the development and progression of atherosclerotic plaques and other arterial lesions have analyzed by Leuprecht and Perktold (2001). Videman (1997) has studied the viscoelastic non-Newtonian fluids mathematically. However, their specific role is not completely understood. The mathematical and numerical study of meaningful constitutive models that can accurately capture the rheological response of blood over a range of physiological flow conditions is recognized as an invaluable tool for the interpretation and analysis of the circulatory system functionality, in both physiological and pathological situations have explained by Charm and Kurland (1965).

While plasma is nearly a Newtonian fluid, whole blood exhibits marked non-Newtonian characteristics, at low shear rates, like shear-thinning viscosity, thixotropy, viscoelasticity, and possibly a yield stress. The non-Newtonian behavior of blood is mainly explained by three phenomena: the tendency of erythrocytes to form three-dimensional microstructures (rouleaux) at low shear rates, their deformability (or breakup) and their tendency to align with the flow field at high shear rates have studied experimentally and theoretically by Chien et al. (1966, 1967, 1978 and 1970). When blood is at rest at low shear rates (below 1 s^{-1}) it seems to have a high apparent viscosity, while at high shear rates there is a reduction in the blood's viscosity. Quemada (1978) has shown there is also experimental evidence that supports the fact that blood exhibits stress relaxation. Moreover, Evans and Hochmuth (1976) have found that the red blood cell membrane, which is a component of blood, has stress relaxation. On the other hand, the experimental results of Thurston (1973) have shown that the relaxation time depends on the shear rate. In view of the experimental work performed so far, a reasonable non-Newtonian fluid model for blood should capture shear-thinning and stress relaxation, with the relaxation time depending on the shear rate. The response of such fluids is still almost unfamiliar and is a subject of dynamic research for future.

The aim of this research is to study the numerical investigation and numerical simulations of blood flow, using finite element methods (FEM), of the non-linear system

CHAPTER 1 INTRODUCTION AND HISTORICAL REVIEW

of partial differential equations (PDE) of a combined elliptic-hyperbolic type, that models the non-Newtonian incompressible viscoelastic Oldroyd-B fluids flows in the steady case. The constitutive equations provide us to characterize the mechanical behavior of fluid which relates the Cauchy stress tensor with the kinematics of different quantities. The constitutive equations for non-Newtonian viscoelastic fluids consist of highly non-linear system of partial differential equations (PDE) of combined elliptic hyperbolic or parabolic-hyperbolic type. The Oldroyd-B fluids model is the constitutive model of rate type which is capable to describe the viscoelastic behavior of blood flows in the polymeric processing. The Oldroyd-B constitutive equations for steady flow are decoupled into two auxiliary problems, namely, the Navier-Stokes like problems for the velocity and pressure (elliptic part of the system) and the steady tensorial transport equation for the extra stress tensor (hyperbolic part of the system). Both the auxiliary problems are studied separately. The iterative Newton-Raphson method is used to obtain the numerical solution of the Navier-Stokes problem which is discretized using P2 - P1 (Hood-Taylor) finite elements. The iterative method based on the application of a fixed-point method is implemented to solve the steady tensorial transport equation which is discretized using the discontinuous Galerkin finite element method.

1.2 Historical Review

At the beginning of the discovery that the fatal cardiovascular disease arteriosclerosis or stenosis and aneurysm affects the flow of blood in the arteries and leads to serious circulatory disorders, this area of biomechanics has been receiving the attention of researchers during the recent decades (2009). At present time medical researchers, bioengineers and numerical scientists join efforts with the purpose of providing numerical simulations of human blood flow system in different conditions. The exchange of knowledge and data information is main purpose of this kind of collaboration that can be used in simulations.

Stenotic Artery:

In our blood circulation system, there are some strong hemodynamical features (such as separation and recirculation of flow, low and oscillatory wall shear stress) that can change in the rheological properties of blood and its components. It plays a major role in the development and progression of atherosclerotic plaques and other arterial lesions. Caro et al. (1978) have investigated the mechanics of the blood circulation. Tu and Deville

CHAPTER 1 INTRODUCTION AND HISTORICAL REVIEW

(1996) also have shown the pulsatile flow of blood fluids through stenotic artery. Flows in stenotic blood vessels have analyzed by Berger and Jou (2000). Atherosclerosis is a common disease of the cardiovascular system, which generates a stenosis of the blood vessels, by partially obstructing them. This reduction in the vessel diameter changes in particular the mechanical behavior of the blood circulation. In any physiological and pathological situations, the numerical study is an important tool for the interpretation and analysis of the circulatory system and can capture the rheological response of blood over a range of physiological flow conditions accurately are shown by Leuprecht and Perktold (2001).

Stenosis is the abnormal and unnatural growth on the arterial wall thickness that develops at various arterial locations of the cardiovascular system under diseased conditions has described by Siddique et al. (2009). Marshall et al. (2004) have analyzed that stenoses developed in the arteries pertaining to brain can cause cerebral strokes and the one developed in the coronary arteries can cause myocardial infarction which leads to heart failure. It has been reported by Verdier (2003) that the fluid dynamical properties of blood flow through nonuniform crosssection of the arteries play a major role in the fundamental understanding and treatment of many cardiovascular diseases.

It has been pointed out by Dwivedi et al. (1982) that the blood vessels bifurcate at frequent intervals, and although the individual segments of arteries may be treated as uniform between bifurcations, the diameter of the artery decreases quite fast at each bifurcation. Hence, Oka and Murata (1969) have examined that the analysis of blood flow through tapered tubes is very important in understanding the behavior of the blood flow as the taper of the tube. Later Oka (1973) has also determined that the pressure development is another important factor in human blood flow.

How and Black (1987) pointed out that the study of blood flow in tapered arteries is also very useful in the design of prosthetic blood vessels as the use of grafts of tapered lumen has the surgical advantage in the blood vessels being wider upstream. The important hydrodynamical factor for tapered tube geometry is the pressure loss which leads to diminished blood flow through the grafts have shown theoretically and experimentally by Yeleswarapu et al. (1998). Hence, the mathematical modeling of blood flow through stenosed tapered or stenosis and aneurysm arteries is very important. Several researchers (Chiu 1998, Chakravarty and Mandal 2000, Chakravarty et al. 2004, Mandal (2005), Mekheimer

CHAPTER 1 INTRODUCTION AND HISTORICAL REVIEW

and Kot 2008) have studied the blood flow characteristics due to the presence of a stenosis in the tapered arteries.

Thurston (1994) was among the earliest to recognize the viscoelastic nature of blood and that the viscoelastic behavior is less prominent with increasing shear rate. Thurston's work (1973) has suggested to be more applicable to venous or low shear unhealthy blood flow than to arterial flows. Other viscoelastic constitutive models for describing blood rheology have been proposed in the recent literature. The empirical three constant generalized Oldroyd-B model studied by Thurston (1972) belongs to this class. It has been obtained by fitting experimental data in one dimensional flows and generalizing such curve fits to three dimensions. This model captures the shear-thinning behavior of blood over a large range of shear rates but it has its limitations, given that the relaxation times do not depend on the shear rate, which does not agree with experimental observations.

Anand et al. (2004) has developed a model that is suitable for blood simulation and it contains Oldroyd-B fluid flow characteristics. Rajagopal and Srinivasa (2000, 2011) have developed a thermodynamic framework requiring the knowledge of how the material stores energy and how it produces entropy, which is particularly well suited for describing the viscoelastic response of bodies with multiple configurations. It is well suited model for blood. Non-Newtonian homogeneous continuum models are very significant in hemodynamics and hemorheology. However, it should be emphasized that blood flow is Newtonian in most parts of the arterial system and attention should be drawn to flow regimes and clinical situations where non-Newtonian effects of blood can probably be observed. These include, for normal blood, regions of stable recirculation like in the venous system and parts of the arterial vasculature where geometry has been altered and RBC aggregates become more stable, like downstream a stenosis, inside a saccular aneurysm or in some cerebral anastomoses. In addition, several pathologies are accompanied by significant changes in the mechanical properties of blood and this results in alterations in blood viscosity and viscoelastic properties, as reported by Truesdell (1991) and in the recent review articles of Robertson et al. (2008).

However, as shown recently Rajagopal and Srinivasa (2000), not all viscoelastic fluids can be described within that earlier framework. In fact, there are (rate type) viscoelastic fluids that cannot have a specific Helmholtz potential associated with them. For certain

CHAPTER 1 INTRODUCTION AND HISTORICAL REVIEW

viscoelastic fluids, one cannot associate a specific Helmholtz potential but only a Gibbs potential. Rate type fluids stemming from a Gibbs potential approach might be useful in describing the response of blood.

Robertson et al. (2009) have explained reliable experimental measurements of velocity, shear stress and interactions between the cellular components of blood and plasma are essential and need further improvement to develop micro structural blood flow models, appropriate in smaller vessels in which the cell and lumen sizes are comparable. For a detailed discussion of the physical properties of blood and corresponding mathematical models see for instance and references therein. To capture the shear-thinning rheological behavior a DA method has developed by Elia et al. (2011) to show the numerical simulation of blood flow in 2D idealized stenosis with wall shear stress effect. G. Telma et al. (2014) discussed the blood flow simulations can be improved by integrating known data in 2D idealized stenosis vessels. Radka and Kozel (2013) have dealt with the numerical simulation of generalized Newtonian and Oldroyd-B fluid flow for four models. Recently, Nasir and Alim (2017) have described a numerical study of blood flow through symmetric and asymmetric stenosis artery under various flow rates. Later, Nasir and Alim (2017) have also studied a numerical investigation of blood flow through stenotic artery.

Aneurysmatic Artery

Up to 75 percent of all patients with a ruptured aneurysm die from the condition before reaching the hospital, which makes screening crucial for people at greatest risk. Ingoldby et al. (1986) have shown these prehospital deaths are counted, the overall mortality rate may exceed 90 percent. Ernst (1993) has studied that the increasing median age of the population contributes to an increasing incidence. An aneurysm is defined as a focal dilatation (balloon) of a blood vessel involving an increase in diameter above 50 percent compared with the expected normal diameter. As an aneurysm increases in size, the risk of rupture increases as reported by Cronenwett et al. (1985). A ruptured aneurysm can lead to bleeding. Aneurysms can occur in any blood vessel, with particularly lethal such that including aneurysms of the circle of Willis in the brain, aortic aneurysms affecting the thoracic aorta, and abdominal aortic aneurysms (AAA). Aneurysms can arise in the heart itself following a heart attack, including both ventricular and atrial septal aneurysms.

CHAPTER 1 INTRODUCTION AND HISTORICAL REVIEW

An aneurysm may occur when the arterial wall loses its structural integrity and gives way to the distending force of the pulsatile intraluminal pressure. A segment of the artery expands to form a balloon-like dilatation: an aneurysm. As the thickness of the wall must play a role in the distension and ultimate rupture of an aneurysm, the stress in the arterial wall has shown to be also inversely proportional to the wall thickness by Johansen (1982). Abdominal aortic aneurysms have usually been characterized as atherosclerotic, although no unified concept of pathogenesis has emerged.

The genesis of blood coagulation is a cascade phenomenon of biochemical events induced by several clotting factors. Transfer of platelets and other clotting factors to the vascular wall is accomplished through diffusive and convective mechanisms. Predilection sites of thrombosis in the human arterial system include geometries which produce nonparallel streamline flow such as bifurcations, branches, curves, stenoses, and aneurysms. Convection of flow aggregates can be locally enhanced or diminished in such geometries that produce localized regions of high and low shear, flow separation, recirculation, and reattachment. The process of thrombosis may be affected by a series of Theological and fluid dynamic parameters.

There are several aneurysm hemodynamics in vitro studies in steady flow have done by Budwig et al. (1993). These studies have shown that the flow field through the aneurysm is characterized by a jet of fluid surrounded by a recirculating vortex and this recirculating vortex effects dramatically the stresses on the aneurysm wall. A typical value of the Reynolds number in a healthy human abdominal aorta is approximately 1800 during peak systole, but this value can dramatically change because of various pathologies.

An insight to the mechanism of thrombus formation in aneurysms was given by Muraki (1983) who performed ultrasonic studies of AAAs and suggested that the mural thrombi in aneurysms is initially formed in the distal area of the expansion and then develops proximally. Muraki also observed that aneurysm rupture typically occurs in the distal area of the aneurysm. Fukushima et al. (1986) have described in vitro studies include numerical studies of pulsatile flow through the aneurysm. Taylor and Yamaguchi (1994) have explored the simulation of blood flow in an abdominal aortic aneurysm steady and unsteady flow cases with three-dimensional.

CHAPTER 1 INTRODUCTION AND HISTORICAL REVIEW

The role of hemodynamics in the growth of aneurysms has been the subject of several studies by Bernsdorf and Wang (2009). Mantha et al. (2009) have studied the stability of pulsatile blood flow at the ostium of cerebral aneurysms. Mukhopadhyay and Layek (2011) have analyzed the systematic analysis of flow features in a tube and modelled as artery, having a local aneurysm in the presence of hematocrit. Kumar and Naidu (1995) discussed the pulsatile suspension flow in a dilated vessel. They discussed the pulsatile suspension flow characteristics by analyzing the flow, pressure and stress fields. The interaction and combination of aneurysm and stenosis further complicate the hemodynamics in diseased arterial vessels. Pincombe et al. (1995) discussed the effects of stenosis and dilatations of the coronary arteries with various combinations on the resistance impedance to flow of by considering blood as Bingham fluid model. Prasad et al. (2014) discussed the steady flow of Jeffrey fluid through a tube with both constriction and dilatations. Numerous theoretical and experimental studies of fluid dynamics through differently geometries of constriction or expansion have been discussed to evaluate the flow pattern are cited in Pincombe and mazumdar (1957). Priyadharshini and Ponalagusamy (2015) analyzed biorheological model on flow of Herschel-Bulkley fluid through a tapered arterial stenosis and dilatation. Fakour et al. (2015) have discussed on the analytical study of micropolar fluid flow and heat transfer in a channel with permeable wall.

Recently, Nadeem and Ijaz (2015) investigated that the influence of metallic nanoparticles reveals that it is important to reduce the significances of the wall shear stress and resistance impedance to flow. More literature is available on nanotechnology that has many advantages in various fields (Rajagopal and Srinivasa 2000, Akbar et al.2014, Zeeshan et al. 2014, Rashidi et al. 2015).

In the present thesis, a numerical investigation of blood flow through stenosis and aneurysm have been studied. The parabolic velocity profile is prescribed at the inlet and constant pressure is used at outlet. On the walls, no-slip conditions are used for velocity and homogeneous Neumann condition for the pressure. The governing mass, momentum and Oldroyd-B equation are expressed in a normalized primitive variables formulation. In this thesis, a finite element method for steady-state incompressible blood flows has been developed. The velocity contour lines and pressure distribution profiles are produced. The results show that the velocity and pressure has changed substantially at the throat of stenosis for the height of stenosis, effect of wall shear stress, symmetric and non-symmetric stenosis effect, different flow rates and dimensionless numbers.

CHAPTER 1 INTRODUCTION AND HISTORICAL REVIEW

1.3 Constitutive Equations

A short overview of the continuum mechanics and basic equations are discussed in this section. We begin with introducing some fundamental concepts of fluid mechanics of continuous medium. Special attention is given to the non-Newtonian viscoelastic fluids of Oldroyd type by researchers (Serrin 1969, Chorin and Marsden 2000, Quarteroni. and Formaggia 2002, Shaughnessy et al. 2005).

1.3.1 Kinematics of fluids

We need to introduce some basic concepts of kinematics and quantities, to originate the partial differential equations of fluid motions. We assume that a fluid may be treated as a continuous medium or continuum, rather than as a group of discrete molecules. In continuum hypothesis, the underlying molecular structure of a fluid is conveniently ignored and replaced by a limited set of fluid properties, defined at each point in the fluid at every instant. Mathematically, this hypothesis allows the use of differential calculus in the modelling and solution of fluid mechanics properties. Here each fluid particle is a continuous function of position and time.

1.3.2 Blood circulation and arterial diseases

The blood circulatory system that permits blood to circulate and transport nutrients oxygen, carbon dioxide, hormones etc to all cell in the body. It consists of cardiovascular and lymphatic system. It helps us in fighting against diseases and keep human body in stable. The blood circulates by pumping of heart and spread throughout the body by the blood vessels. The blood vessels are formed of aorta and capillaries network have referred in Menche (2012) and Pschyrembel (2014). The arteries bear blood away from the heart and the veins carry it back to the heart. The blood circulation in human body are shown by Menche (2012) in Figure 1.1,

CHAPTER 1 INTRODUCTION AND HISTORICAL REVIEW

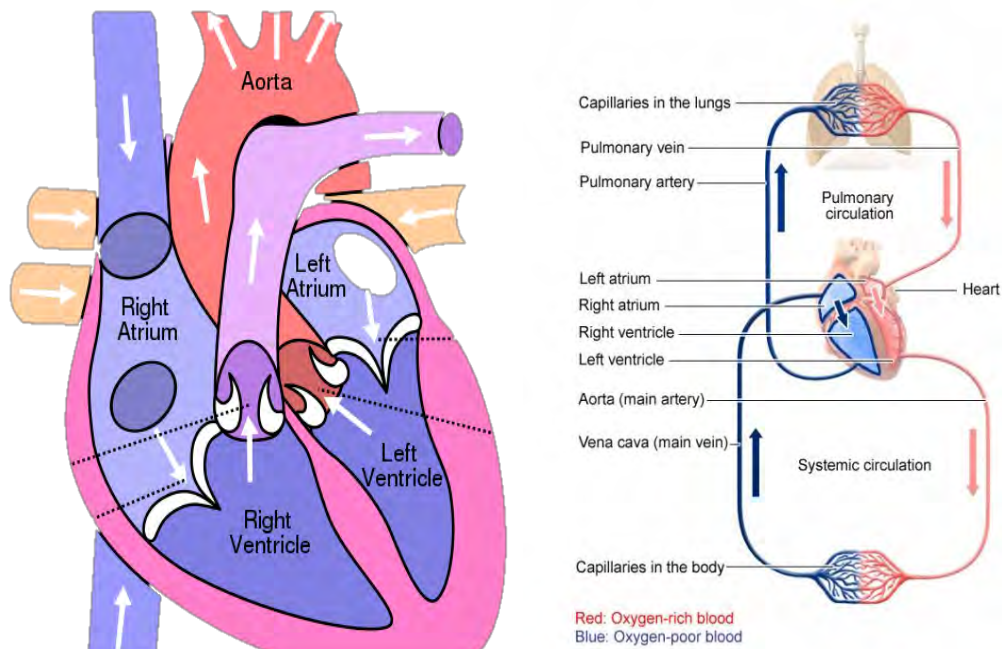


Figure 1.1: Blood circulatory system

The essential components of the human cardiovascular system are the heart, blood and blood vessels. The heart pumps oxygenated blood to the body and deoxygenated blood to the lungs. The right atrium receives deoxygenated (poor in oxygen) blood from upper and lower parts of our body. The blood is passed into the right ventricle to be pumped through the pulmonary artery to the lungs for re-oxygenation and removal of carbon dioxide. The left atrium receives newly oxygenated blood from the lungs as well as the pulmonary vein. It is passed into the strong left ventricle to be pumped through the aorta to the different organs of the body. The blood circulation may be poor in human body for accumulate (build up) of blood clot, external force, external pressure, injury of blood artery, overgrowth of bone, abnormal growths (Tumor), long-term elevated blood pressure (hypertension), Weaken of blood artery, medical surgery, inactive cells, genetic conditions, any kind of trauma are main reasons. The development of stenosis (abnormal narrowing) and aneurysm (dilation) in artery are the main cause of cardiovascular disease arteriosclerosis which leads to serious circulatory disorders. The stenotic and aneurysmatic artery are shown in Figure 1.2.

CHAPTER 1 INTRODUCTION AND HISTORICAL REVIEW

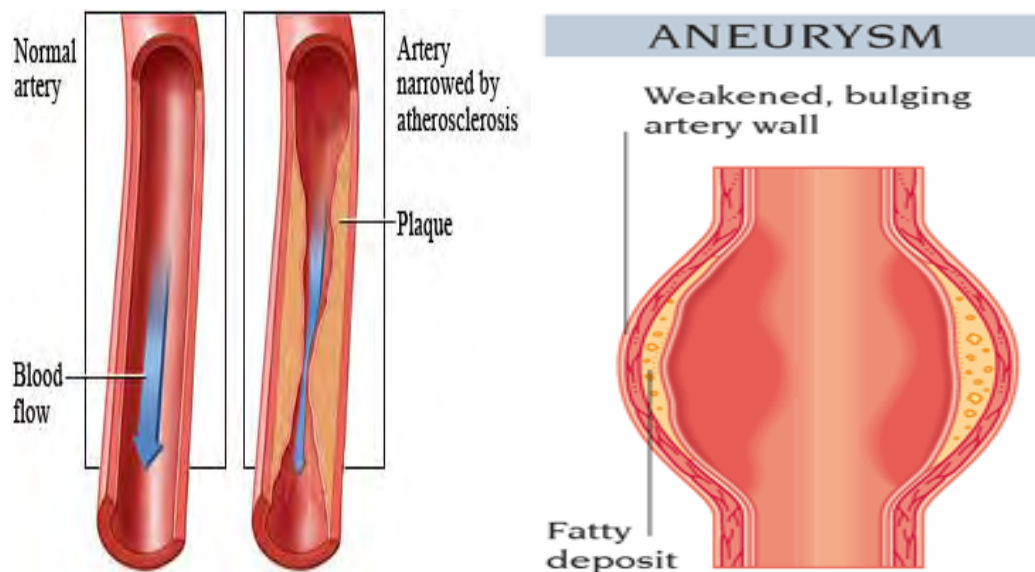


Figure 1.2: Plaque deposit in stenosed blood vessel (left) and fatty deposit in aneurysm artery (right)

1.3.3 The frame indifference

In fluid mechanics, the material response independent of the observer is the main axioms. The principle of frame indifference or material objectivity is demonstrated by Coleman et al. (1966). It states that if a given process is compatible with a constitutive equation, then all processes obtained from the given process by changes of frame must also be compatible with the same constitutive equation. To study the kinematics of fluids, the motion of the continuous medium, two reference frames can be used. These are Lagrangian and Eulerian descriptions and refer to individual time-rate of change and local time-rate of change respectively.

Consider the Euclidean coordinate system R^i ($i = 2, 3$). We assume that the motion will take place during a time interval $I = [t_0; t_1] \subset R^+$. Suppose at the reference initial time $t_0 \geq 0$, the domain occupied by the fluid is Ω_0 called initial or reference configuration and at time $t \in I$ the portion of space occupied by the same fluid (Ω_t) is called current or spatial configuration. The motion of each fluid particle which is on position, $e \in \Omega_0$ at initial time t_0 and on position $x \in \Omega_t$ at time $t \in I$ is described by the family of mappings L_m . Precisely, $L_m : \Omega_0 \rightarrow \Omega_t$ and $e \rightarrow x = x(t, e) = L_m(e)$. Where, L_m is called Lagrangian mapping at time t .

We suppose that L_m is continuous and invertible on \mathcal{D}_0 , with continuous inverse. The position $x \in \Omega_t$ of a material particle is a function of time and the position, $e \in \Omega_0$ of the

CHAPTER 1 INTRODUCTION AND HISTROCAL REVIEW

same material particle. We can relate the pairs (t, e) and (t, x) which are respectively called the material or Lagrangian variables and spatial or Eulerian variables. We focus on a set of specific locations in the flow field for Eulerian variables as independent variables. When we use Lagrangian variables as independent variables we focus on the position e of a specific fluid particle at the initial time t_0 . In fact, we are tracking the trajectory σ_e describes by the particle during the time interval $[t_0, t]$ which was on position „ e “ at instant t_0 . The trajectory is given by

$$\sigma_e = \{(t, x(t, e)) : t \in I\}$$

Though it is more convenient to work with the Eulerian variables, the basic principles of mechanics are more easily formulated with reference to the moving particles, i.e, in the Lagrangian frame. We will mark with the hat symbol „ $\hat{\cdot}$ “ a quantity expressed as a function of Lagrangian variables, that is, if $f : I \times \mathbb{R}$ we have the quantity

$$\hat{F}(t, e) = f(t, x), \text{ with } x \in L_m^{-1}(e)$$

To indicate the gradient with respect to the Eulerian variable x we use the symbol ∇ . Gradient with respect to Lagrangian variable „ e “ is indicated by the symbol ∇_e , defined by

$$\nabla_e \hat{F} = \sum_{i=1}^3 \frac{\partial \hat{F}}{\partial e_i} n_i$$

For the other differential operators such as divergence, Laplacian, etc., we use same convention.

1.3.4 The fluid velocity

The fluid velocity is the fundamental variable in fluid dynamics. It is the major kinematic quantity. In the Lagrangian frame it is expressed by means of a vector field

$$\bar{u} = \frac{\partial x}{\partial t} \text{ i.e. } \bar{u}(t, e) = \frac{\partial x}{\partial t}(t, e)$$

\bar{u} is called the Lagrangian velocity field and it denotes the time derivative along the trajectory σ_e of the fluid particle which was located at position „ e “ at the reference time.

For $(t, x) \in I \times \Omega_t$, the velocity in the Eulerian frame is defined as

$$u = \bar{u} \circ L_m^{-1} \text{ i.e. } u(t, x) = \bar{u}(t, L_m^{-1}(x))$$

In general, the velocity field is a three-dimensional or two-dimensional time dependent vector field.

CHAPTER 1 INTRODUCTION AND HISTROCAL REVIEW

1.3.5 The material derivative

The derivative of a vector field with respect to a fixed position in space is called a Eulerian derivative. On the other hand, the derivative of a vector field following a moving particle of fluid along its path is called substantial, material, co-moving or Lagrangian derivative. This derivative relates the time derivatives computed with respect to the Lagrangian and Eulerian frames. The material or Lagrangian time derivative of a function f , which is denoted by $\frac{Df}{Dt}$, is defined as the time derivative in the Lagrangian frame. It is expressed as a function in the Eulerian variables.

If f be a mapping such that

$$f: I \times \Omega_t \rightarrow R \text{ and } \hat{F} = f \circ L_m \text{ then}$$

$$\frac{Df}{Dt}: I \times \Omega_t \rightarrow R, \quad \frac{Df}{Dt}(t, x) = \frac{d\hat{F}}{dt}(t, e), \quad e = L_m^{-1}(x)$$

So, for any fixed $e \in \Omega_0$ we can write

$$\frac{Df}{Dt}(t, x) = \frac{d}{dt} f(t, x(t, e))$$

We can observe that the material derivative represents the rate of variation of f along the trajectory T_e . Applying the chain-rule of derivation of composed functions we can write

$$\begin{aligned} \frac{Df}{Dt}(t, x) &= \frac{df}{dt}(t, x(t, e)) = \left[\frac{\partial}{\partial t} (f \circ L_m) \right] \circ L_m^{-1} \\ &= \frac{df}{dt}(t, x) + \sum_{i=1}^d \frac{df}{dx_i}(t, x) \frac{dx_i}{dt} = \frac{df}{dt}(t, x) + \sum_{i=1}^d u_i(t, x) \frac{df}{dx_i}(t, x) \end{aligned}$$

So, material derivative operator is defined by

$$\frac{D}{Dt} = \frac{\partial}{\partial t} + \mathbf{u} \cdot \nabla$$

The term $\frac{\partial}{\partial t}$ is a partial time derivative, and the term $\mathbf{u} \cdot \nabla$, called the convective derivative, involves partial space derivatives.

1.3.6 The acceleration of fluid

The fluid acceleration is a kinematic quantity. In the Lagrangian frame the acceleration

$\hat{a}(t, e)$ is a vector field $\hat{a}: I \rightarrow R$ defined by

$$\hat{a}(t, e) = \frac{\partial \hat{u}}{\partial t}(t, e) = \frac{\partial^2 \mathbf{x}}{\partial t^2}(t, e)$$

If we use the definition of material derivative, we can write the acceleration in Eulerian frame as

CHAPTER 1 INTRODUCTION AND HISTROCAL REVIEW

$$\mathbf{a} = \frac{D\mathbf{u}}{Dt} = \frac{\partial\mathbf{u}}{\partial t} + (\mathbf{u} \cdot \nabla)\mathbf{u}$$

We observe that the total acceleration at a point in a fluid can be written as the sum of two different types of acceleration called the local and convective accelerations. The components of the acceleration in Cartesian coordinates can be written as

$$a_i = \frac{\partial u_i}{\partial t} + \sum_{j=1}^d u_j \frac{\partial u_i}{\partial x_j}, \quad i=1,2,\dots,d$$

1.3.7 The deformation gradient tensor

The deformation gradient tensor is the kinematic quantity necessary for the derivation of the mathematical model in fluid dynamics. The deformation gradient tensor g_t , which is defined, at each $t \in I$, as

$$g_t : \Omega_0 \rightarrow R^{d \times d}, \quad g_t(\mathbf{e}) = \nabla_{\mathbf{e}} L_m(\mathbf{e}) = \frac{\partial \mathbf{x}}{\partial \mathbf{e}}(t, \mathbf{e})$$

Where $\nabla_{\mathbf{e}} L_m$ is the derivative of L_m with respect to Lagrangian variable „ \mathbf{e} “

We can write component wise

$$[g_t]_{ij} = \frac{\partial x_i}{\partial e_j}, \quad i, j = 1, 2, \dots, d$$

The Jacobian of the mapping L_m is the determinant, $J_t = \det g_t > 0$. In the Eulerian frame its counterpart is indicated by J_t . Using the determinant of deformation gradient tensor, we can transform integrals from the current to the reference configuration by Chorin and Marsden (2000).

1.3.8 The rate of strain and vorticity tensors

We define the rate of deformation tensor or strain rate tensor by Landau and Lifshitz (1997)

$$\mathbf{V} = \frac{1}{2}(\nabla\mathbf{u} + \nabla\mathbf{u}^T)$$

and the rate of vorticity tensor by

$$\mathbf{V}' = \frac{1}{2}(\nabla\mathbf{u} - \nabla\mathbf{u}^T)$$

Here, $\mathbf{V}(\mathbf{u})$ is the symmetric part of the velocity gradient and $\mathbf{V}'(\mathbf{u})$ is the antisymmetric part. The rate of deformation gives us information about the rate of change of volume element along the time without rotation effects.

Component wise,

CHAPTER 1 INTRODUCTION AND HISTORICAL REVIEW

$$[V(u)]_{ij} = \frac{1}{2} \left(\frac{\partial u_i}{\partial x_j} + \frac{\partial u_j}{\partial x_i} \right), \quad i, j = 1, \dots, d \quad (d = 2, 3)$$

and

$$[V'(u)]_{ij} = \frac{1}{2} \left(\frac{\partial u_i}{\partial x_j} - \frac{\partial u_j}{\partial x_i} \right), \quad i, j = 1, \dots, d \quad (d = 2, 3)$$

1.3.9 The forces acting on fluid

For any continuum, forces acting on a piece of material inside Ω_t are three types.

External or Body forces:

Body forces are long-range forces whose magnitudes are proportional to the mass. They are external forces act on a fluid, but are not applied by a fluid. Body forces are represented by a vector field $\mathbf{f} : I \times \Omega_t \rightarrow R^d$ called specific body force. Its dimension unit is $N/kg = m/s^2$ as like an acceleration. The body force acting on fluid of volume V_t is given by

$$\int_{V_t} \rho \mathbf{f}$$

Gravity force and electromagnetic forces are the familiar examples of body forces.

Surface forces or Forces of Stress:

Surface forces are short-range forces that act on a fluid element through physical contact between the element and its surroundings. Surface forces represent that part of forces which are imposed on the media through its surface. The magnitude of a surface force is proportional to the contact area between the fluid and its surroundings. Surface forces act on a fluid, and also are applied by a fluid to its surroundings. We suppose that the surface force can be represented through a vector $\mathbf{t}^e : I \times \Gamma_t \rightarrow R^d$, called applied stresses, defined on a measurable subset of the domain boundary $\Gamma_t \subset \partial\Omega_t$. The resultant force acting through the surface is given by

$$\int_{\Gamma_t} \mathbf{t}^e$$

Internal continuity forces:

The forces that the continuum media particles exert on each other are the internal continuity forces. They are responsible for maintaining material continuity during the movement. We recall Principle of Cauchy, to model the internal continuity force from Chorin and Marsden (2000).

CHAPTER 1 INTRODUCTION AND HISTROCAL REVIEW

1.3.10 Theorems and lemma

Theorem 1.1.1

Suppose $V_t \subset \Omega_t$ be a subdomain of Ω_t and let us consider the function $\hat{F} : I \times V_t \rightarrow \mathcal{R}$.

Then, f is integrable on V_t if and only if $(f \circ L_m) J_t$ is integrable on $V_0 = L_m^{-1}(V_t)$, and

$$\int_{V_t} f(t, \mathbf{x}) dx = \int_{V_0} \hat{F}(t, \mathbf{e}) J_t de, \text{ Where } \hat{F}(t, \mathbf{e}) = f(t, L_m(\mathbf{e})).$$

Beriefly,

$$\int_{V_t} f = \int_{V_0} \hat{F} J_t$$

The next lemma tells us that the time derivative of the Jacobian is linked to the divergence of the velocity field. This relation is called Euler expansion formula. Its proof can be found in Chorin and Marsden (2000).

Lemma 1.1.1 : Euler expansion formula

Let J_t denote the Jacobian in the Eulerian frame. Then

$$\frac{\partial}{\partial t} J_t(\mathbf{x}) = \frac{\partial}{\partial t} J_t(t, \mathbf{x}) = J_t(\mathbf{x}) \nabla \cdot \mathbf{u}(t, \mathbf{x}) = J(t, \mathbf{x}) \nabla \cdot \mathbf{u}(t, L_t(\mathbf{e})) \quad (1.1)$$

Theorem 1.1.2: Reynolds Transport Theorem

Suppose $V_0 \subset \Omega_0$ and $V_t \subset \Omega_t$ be its image under the mapping L_t . let us consider the function $f : I \times \Omega_t \rightarrow \mathcal{R}$ be continuously differentiable with respect to both variables. Then,

$$\frac{d}{dt} \int_{V_t} f = \int_{V_t} \left[\frac{Df}{Dt} + f \nabla \cdot \mathbf{u} \right] = \int_{V_t} \left[\frac{\partial f}{\partial t} + \nabla \cdot (f \mathbf{u}) \right] \quad (1.2)$$

The proof of this theorem can be found in Chorin and Marsden (2000).

Theorem 1.1.3: Divergence Theorem

Let Ω is open bounden domain in R^d , ($d=2,3$) with a piecewise smooth boundary $\partial\Omega$. If \mathbf{u} is continuously differentiable vector field on a neighborhood of Ω , then

$$\int_{\Omega} (\nabla \cdot \mathbf{u}) d\Omega = \int_{\partial\Omega} (\mathbf{u} \cdot \mathbf{n}) ds \quad (1.3)$$

Where $\mathbf{n} = (n_1, n_2, \dots, n_d)$ is the unit outward normal vector field to the boundary $\partial\Omega$.

In index notation, we can write

$$\int_{\Omega} \frac{\partial u_i}{\partial x_i} = \int_{\partial\Omega} u_i n_i, \quad i = 1, 2, \dots, d \quad (1.4)$$

Applying the divergence theorem, we can rewrite (1.2) as

$$\frac{d}{dt} \int_{V_t} f = \int_{V_t} \frac{\partial f}{\partial t} + \int_{\partial V_t} f \mathbf{u} \cdot \mathbf{n}$$

CHAPTER 1 INTRODUCTION AND HISTROCAL REVIEW

Theorem 1.1.4: The Cauchy Theorem

There exists a vector field, $\mathbf{t}: I \times \Omega_t \times S_t \rightarrow R$, called the Cauchy stress with $S_t = \{n \in R^d: \|n\| = 1\}$ ($d = 2, 3$) such that its integral on the surface of any material domain $V_t \subset \Omega_t$, given by

$$\int_{\partial V_t} \mathbf{t}(\mathbf{t}, \mathbf{x}, \mathbf{n}) ds$$

is equivalent to the resultant of the material continuity forces acting on V_t . Here \mathbf{n} is the outward normal of ∂V_t and ds is the area element. This principle states that the only dependence of the internal forces on the geometry of ∂V_t is through \mathbf{n} . We also have

$$\mathbf{t} = \mathbf{t}^\ell \text{ on } \partial V_t \cap \Gamma_t.$$

Now, we can write the law of conservation of linear momentum. The momentum of the mass at time t of the volume V_t known as linear momentum is defined by

$$\int_{V_t} \rho \mathbf{u}$$

For any $t \in I$ and $V_t \subset \Omega_t$ completely contained in Ω_t ,

$$\frac{d}{dt} \int_{V_t} \rho(t, \mathbf{x}) \mathbf{u}(t, \mathbf{x}) dx = \int_{V_t} \rho(t, \mathbf{x}) \mathbf{f}(t, \mathbf{x}) + \int_{\partial V_t} \mathbf{t}(t, \mathbf{x}, \mathbf{n}) ds \quad (1.5)$$

The equation (1.5) tells us the property that the variation of the linear momentum of V_t is balanced by the resultant of the internal and the body forces. With the following Cauchy Stress Tensor theorem, we can relate the internal continuity forces to a tensor field assuming some regularity of the Cauchy stresses. The proof can be found in Serrin (1969).

Theorem 1.1.5: The Cauchy Stress Tensor Theorem

Suppose that for all $t \in I$, the body forces \mathbf{f} , the density ρ and the fluid acceleration $\frac{D\mathbf{u}}{Dt}$ are all bounded functions on Ω_t , and let the Cauchy stress vector field \mathbf{t} is continuously differentiable with respect to the variable \mathbf{x} for each $\mathbf{n} \in S_t$, where S_t is the set $\{n \in R^d: \|n\| = 1\}$ ($d = 2, 3$) and continuous with respect to \mathbf{n} . Then, there exists a continuously differentiable symmetric tensor field, called Cauchy stress tensor

$$\boldsymbol{\sigma}: I \times \overline{\Omega_t} \rightarrow R^{d \times d} \text{ such that } \mathbf{t}(t, \mathbf{x}, \mathbf{n}) = \boldsymbol{\sigma}(t, \mathbf{x}) \cdot \mathbf{n}, \quad \forall t \in I, \mathbf{x} \in \Omega_t, \forall \mathbf{n} \in S_t.$$

With the hypothesis of the Cauchy stress tensor theorem, we have

$$\boldsymbol{\sigma}(t, \mathbf{x}) \cdot \mathbf{n} = \mathbf{t} = \mathbf{t}^\ell \text{ on } \partial \Omega_t \cap \Gamma_t \quad (1.6)$$

and the resultant of the internal forces on V_t is expressed by $\boldsymbol{\sigma} \cdot \mathbf{n}$. So, we can write

CHAPTER 1 INTRODUCTION AND HISTORICAL REVIEW

$$\int \frac{\sigma \cdot n}{\partial v_i} = \int \frac{t^e}{\partial v_i} \quad (1.7)$$

The stress tensor σ represents the forces which the material develops in response to being deformed.

1.3.11 Dimensionless parameters

The dimensionless parameters can be thought of as measures of the relative importance of certain aspects of the flow. Some dimensionless parameters related to our study are discussed below:

Reynold number, Re

The Reynolds number (Re) is an important dimensionless quantity in fluid mechanics used to help predict flow patterns in different fluid flow situations. It has wide applications, ranging from liquid flow in a pipe to the passage of air over an aircraft wing. The Reynolds number is used to predict the transition from laminar to turbulent flow, and used in the scaling of similar but different-sized flow situations, such as between an aircraft model in a wind tunnel and the full-size version.

The Reynolds number is the ratio of inertial forces to viscous forces within a fluid which is subjected to relative internal movement due to different fluid velocities

$$Re = \frac{\text{Inertial forces}}{\text{Viscous forces}} = \frac{\rho u L}{\mu} = \frac{u L}{\nu}$$

Where, ρ is the density of the fluid, u is the velocity of the fluid with respect to the object, L is a characteristic linear dimension, μ is the dynamic viscosity of the fluid, ν is the kinematic viscosity of the fluid. Reynold number (Re) plays important role to separation of lamina and turbulent flow regimes. At low Reynolds numbers ($Re < 2000$), viscous forces are dominant and is called laminar flow regimes. On the other hand, inertial forces are dominated at high Reynolds numbers ($Re > 4000$) which is turbulent flow regimes. At transition regimes, the value of Reynold numbers is between 2000 to 4000. The transition Reynolds number is called critical Reynolds number.

Weissenberg Number, Wi

A non-Newtonian Fluid is one for which stress is not linearly related to strain-rate. All non-Newtonian fluids are elasticoviscous, that is they combine elastic and viscous properties. The Weissenberg number (Wi) is a dimensionless number used in the study of viscoelastic flows. It is named after Karl Weissenberg. The dimensionless number

CHAPTER 1 INTRODUCTION AND HISTORICAL REVIEW

compares the viscous forces to the elastic forces. Weissenberg numbers have proved invaluable for rheologists in quantifying viscoelastic effects. It can be variously defined, but it is usually given by the relation of stress relaxation time of the fluid and a specific process time. For instance, in simple steady shear, the Weissenberg number, often abbreviated as Wi or We , is defined as the shear rate $\dot{\gamma}$ times the relaxation time, λ . Using the Maxwell Model and the Oldroyd Model, the elastic forces can be written as the first Normal force.

$$Wi = \frac{\text{Elastic Forces}}{\text{Viscous Forces}} = \dot{\gamma} \lambda = \frac{\lambda U}{L}$$

Where, λ is the relaxation time, U is the velocity of the fluid with respect to the object, L is a characteristic linear dimension. Three ranges of Weissenberg numbers are identified as that; if $Wi < 1$ then the fluid is viscous, if $Wi \approx 1$, the fluid is viscoelasticity, if $Wi > 1$, the fluid is elastic. If the value of Wi is above a critical value, usually in the order of one, the elastic properties of the blood have to be taken into account. The most appropriate choice of relaxation time of the RBCs 0.06s and the characteristic time of the flow is equal to the period time of the physiological flow pulse. Generally, viscoelastic computations in complex flows at high Weissenberg numbers have proven to be a tremendous challenge, in particular for systems where singularities are present. A zero Weissenberg number corresponds to no elastic response while an infinite Weissenberg number corresponds to a purely elastic response over a given scale.

Peclet Number, Pe

The Peclet number (Pe) is a vital dimensionless quantity in the study for transport phenomena in a continuum and it's named by Jean Claude Eugene Peclet. It is used in engineering, bio-medical, and biomechanics etc. to predict the transition from laminar to turbulent flow. The Peclet number is the ratio of the rate of advection to diffusion of a physical quantity by the flow of the same quantity driven by an appropriate gradient. So, the Peclet number is defined as

$$Pe = \frac{\text{Advection transport rate}}{\text{Diffusive transport rate}}$$

In the case of mass transfer, the Peclet number is the product of the Reynolds number (Re) and the Schmidt number (Sc). It is defined as

CHAPTER 1 INTRODUCTION AND HISTROCAL REVIEW

$$Pe = \frac{Lu}{D} = ReSc$$

In the case of heat transfer, the thermal Peclet number is equivalent to the product of the Reynolds number (Re) and the Prandtl number (Pr) which can be written as

$$Pe = \frac{Lu}{\alpha} = RePr$$

where L is the characteristic length, u the local flow velocity, D the mass diffusion coefficient, and α the thermal diffusivity. Peclet number (Pe) plays an important role to separatethe laminar and turbulent flow region at the relation $Pe = Re Sc$ when $Sc = 1$. In that case Peclet number and Reynold number play same character to illustrate the blood flow.

1.4 Balance Laws

Balance laws or conservation laws state the physical principles governing the fluid motion in a continuum medium. According to the conservation laws, a particular measurable property of an isolated physical system does not change as the system evolves. Lavoisier states that “in nature nothing is created, nothing is lost, everything is transformed”. The mathematical formulations of these conservation laws are given below.

1.4.1 Conservation of mass

Conservation of mass is a fundamental principle of classical mechanics governing thebehavior of a continuum medium. It states that in a fixed region, the total time rateof change of mass is identically zero, i.e, mass is neither created nor destroyed duringthe motion. Physically, this interprets that the rate of change of the density of a fluidin motion is equal to the sum of the fluid convected into and out of the fixed region. Suppose V_t indicates a material volume at time t , i.e. V_t is the image under theLagrangian mapping of $V_0 \in \Omega_0$, i.e. $V_t = L_m(V_0)$: If m_0 is the mass of material in V_0 and m_t is the mass of that material in V_t , then according to the conservation of mass we can say $m_0 = m_t$: Mathematically,

$$m_0 = m(V_0) = m(L_m(V_0)) = m(V_t) = m_t$$

For each time t , we suppose that the uid has well-defined mass density ρ (mass per unit volume of material $[\rho] = kg/m^3$) which is strictly positive, measurable function $\rho: I \times \Omega_t \rightarrow \mathbb{R}$ such that on each $V_t \subset \Omega_t$

$$m(V_t) = \int_{V_t} \rho$$

CHAPTER 1 INTRODUCTION AND HISTROCAL REVIEW

If V_t is a fixed region in Ω_t , then with the mathematical statement of conservation of mass we can write

$$0 = \frac{d}{dt} m(V_t) = \frac{d}{dt} \int_{V_t} \rho$$

Applying the Reynold Transport theorem, we obtain the integral form of the law of conservation of mass

$$\begin{aligned} \int_{V_t} \left(\frac{D\rho}{Dt} + \rho \nabla \cdot \mathbf{u} \right) &= 0 \\ \Rightarrow \int_{V_t} \left(\frac{d\rho}{dt} + \rho (\nabla \cdot \mathbf{u}) \right) &= 0 \end{aligned} \quad (1.8)$$

We suppose that the terms under the integral are continuous. Since the volume V_t is arbitrary, So the equation is equivalent to the differential equation of this law, called continuity equation (expressing conservation of mass)

$$\int_{V_t} \left(\frac{d\rho}{dt} + \rho (\nabla \cdot \mathbf{u}) \right) = 0 \quad (1.9)$$

If the density is constant or its material derivative $\frac{D\rho}{Dt} = 0$, then the equation of continuity is simplified to

$$\nabla \cdot \mathbf{u} = 0 \quad (1.10)$$

The above relation in the case of incompressible fluid is in fact a kinematic constraint.

Using Euler expansion formula, we can write the above equation as

$$\frac{\partial}{\partial t} \mathbf{J}_t = 0$$

This is an incompressibility constraint. A flow satisfying the incompressibility constraint is called incompressible flow. By the continuity equation we get the following implication:

Constant density fluid \Rightarrow incompressible flow

but the converse is not always true. Mathematically, we mean that the velocity field of an incompressible flow is divergence free.

1.4.2 Conservation of momentum

The second principal physical law that fluid obeys is the conservation of momentum.

This quantity is defined as the product of mass and velocity

$$\int_{V_t} \rho \mathbf{u} \, dx$$

CHAPTER 1 INTRODUCTION AND HISTROCAL REVIEW

Where $\rho = \rho(x,t)$ and $\mathbf{u} = \mathbf{u}(x,t)$. According to the second Newton's law, the rate of change of the momentum of the fluid contained in the volume $v(t)$ is equal to all forces acting on this fluid. There are three types of forces acting on the fluid, body forces, surface forces and internal forces. The body force like gravity acts on a fluid particle and is proportional to its mass. It can be expressed as $\int_{v_t} \rho \mathbf{g} dx$ where $\mathbf{g} = \mathbf{g}(x,t)$ denotes the density of gravity force. The surface forces are the one acting on the boundaries $\partial V(t)$ of the fluid volume $V(t)$, and is usually described by the stress tensor $\boldsymbol{\sigma}$. The stress consists of pressure and friction forces, which are coming from the interactions between fluid layers sliding one relative to the other. Taking all together, conservation of momentum reads as

$$\frac{d}{dt} \int_{v_t} \rho \mathbf{u} = \int_{v_t} \rho \mathbf{f} + \int_{\partial v_t} \boldsymbol{\sigma} \cdot \mathbf{n} \quad (1.11)$$

Applying theorem 1.1.1 to the left-hand side and theorem 1.1.2 to the second term on the right-hand side transforms the above equation to

$$\frac{d}{dt} \int_{v_t} \rho \mathbf{u} = \int_{v_t} \left[\frac{D}{Dt} (\rho \mathbf{u}) + \rho \mathbf{u} \nabla \cdot \mathbf{u} \right] = \int_{v_t} \rho \frac{D}{Dt} (\mathbf{u})$$

So the relation (1.11) can be written as

$$\int_{v_t} \rho \frac{D\mathbf{u}}{Dt} = \int_{v_t} \rho \mathbf{f} + \int_{\partial v_t} \boldsymbol{\sigma} \cdot \mathbf{n} \quad (1.12)$$

Applying the divergence theorem and assuming that $\nabla \cdot \boldsymbol{\sigma}$ is integrable, the above relation (1.12) becomes

$$\int_{v_t} \rho \frac{D\mathbf{u}}{Dt} dx = \int_{v_t} \rho \mathbf{f} + \int_{v_t} \nabla \cdot \boldsymbol{\sigma} \quad (1.13)$$

$$\text{Which implies } \int_{v_t} \left(\rho \frac{D\mathbf{u}}{Dt} - \nabla \cdot \boldsymbol{\sigma} - \rho \mathbf{f} \right) = 0 \quad (1.14)$$

Since the volume V_t is arbitrary, with the hypothesis that the terms under the integrals are continuous in space, we derive the differential form of principle of linear momentum

$$\rho \frac{D\mathbf{u}}{Dt} - \nabla \cdot \boldsymbol{\sigma} = \rho \mathbf{f} \text{ in } \Omega_t \quad (1.15)$$

Writing the fluid acceleration $\frac{D\mathbf{u}}{Dt} = \frac{\partial \mathbf{u}}{\partial t} + (\mathbf{u} \cdot \nabla) \mathbf{u}$, the relation (1.15) finally can be written as

$$\rho \frac{\partial \mathbf{u}}{\partial t} + \rho (\mathbf{u} \cdot \nabla) \mathbf{u} - \nabla \cdot \boldsymbol{\sigma} = \rho \mathbf{f} \quad (1.16)$$

CHAPTER 1 INTRODUCTION AND HISTROCAL REVIEW

Component wise,

$$\rho \frac{\partial \mathbf{u}_i}{\partial t} + \rho \sum_{j=1}^d \mathbf{u}_j \frac{\partial \mathbf{u}_i}{\partial \mathbf{x}_j} - \sum_{j=1}^d \mathbf{u}_j \frac{\partial T_{ij}}{\partial \mathbf{x}_j} = \rho \mathbf{f}_i \quad \text{where, } i = 1, 2, \dots, d.$$

The non linear term $(\mathbf{u} \cdot \nabla)\mathbf{u}$ is called the convective term.

1.5 Formulation and Principles of the Constitutive Relations

All materials mostly satisfy the fundamental conservation principles stated above. The mathematical specification of 'material response' laws is said to be the set of constitutive relations. This law relates the Cauchy stress tensor with the kinematics of different quantities, in particular, the velocity field. Constitutive relations provide us to characterize the mechanical behavior of fluid. In this work, we are concerned with non-Newtonian fluids type, with the flows of incompressible viscoelastic Oldroyd-B fluids. We first give the general form of constitutive equations and then we give the overview of differential constitutive equations for viscoelastic fluids of Oldroyd-B having properties of elastic solids and viscous fluids characterized by aviscous behavior when subject to slow request and elastic behavior subjected to fastrequest. We take into account several principles and assumptions to formulate a constitutive equation.

Principle of determinism: We can determine the stress only by history and present state of material.

Principle of material objectivity: The structure of constitutive equation is independent of the motion of an observer. We assume that the stress at a material point is determined by the deformationgradient at this point, i.e., we assume the material is simple fluid.

Under the above principles, for simple, isotropic, incompressible fluid, the Cauchystress tensor $\boldsymbol{\sigma}$ can be expressed as

$$\boldsymbol{\sigma} = -p\mathbf{I} + \boldsymbol{\tau}_s$$

Where, p is the hydrostatic pressure, $\boldsymbol{\tau}_s$ is the extra stress tensor and \mathbf{I} is the identitymatrix or Kronecker tensor.

1.5.1 Newtonian and non-Newtonian fluids

If for a fluid, the dissipative effects of frictional forces can be described by a linearrelation between the extra stress tensor and rate of strain tensor, i.e,

$$\boldsymbol{\tau}_s = 2\mu\mathbf{V}(\mathbf{u}) \quad (1.17)$$

then this fluid is called Newtonian fluid. In (1.17), μ is the dynamic viscosity coefficient expressing the fluid's resistance which it offers to shear strain during the displacement.

CHAPTER 1 INTRODUCTION AND HISTORICAL REVIEW

On the other hand, the fluids for which the relation between the Cauchy stress tensor and the strain rate tensor is non-linear (doesn't obey the Stokes law) are called non-Newtonian fluids. The fluids with complex microstructures such as polymeric liquids, foams, inks, magma or biological fluids are some examples of non-Newtonian fluids. They are characterized by the fact that they exhibit at least one behavior such as shear-thinning or shear-thickening, stress-relaxation, non-linear creep, normal stress differences or yielding. Some properties of non-Newtonian fluids:

- (i) The non-Newtonian fluid has the ability to thinning and thickening by the action of shear or tangential stress forces, i.e. it has the ability to become more or less viscous as the shear rate increases. In a Newtonian fluid, the viscosity remains constant in time.
- (ii) The non-Newtonian fluids deform by the presence of constant tensions, with strain rate is not constant in time. But the Newtonian fluid does not deform under the presence of constant tensions.
- (iii) In contrast to Newtonian fluids, some non-Newtonian fluids do not relax stress immediately.
- (iv) In some non-Newtonian fluids, the normal tensions vary in simple flows (flows with one-dimensional velocity and velocity gradients), generally normal tension increases with shear rate.
- (v) In the presence of threshold tensions (stress of transfer), some non-Newtonian fluids do not flow immediately, they resist until a certain value of tension.

1.5.2 Generalized Newtonian fluid

Sometimes, it is possible to model the fluid by replacing Newton's law by another explicit, nonlinear law. In this case, it is said that the considered fluid is of generalized Newtonian type. An example is given by the viscoplastic law

$$\sigma^E = 2\mu(|V|) V \quad (1.18)$$

Where, the general viscosity is a nonlinear (power) function of the second invariant $|V| = \sqrt{V:V}$. Power law models (1.18) have been found to be successful in describing the behavior of rubber solutions, adhesives, biological fluids, colloids, suspensions and a variety of polymeric liquids.

CHAPTER 1 INTRODUCTION AND HISTORICAL REVIEW

1.5.3 Viscoelasticity and Development of Viscoelasticity

Continuum mechanics provides the physical laws that materials obey and imposes requirements for the constitutive laws. There isn't a distinction in a continuum mechanical sense between solids and fluids though instinctively the difference is obvious: fluids flow whereas solids do not. Alternatively, one can say that a solid is elastic that is if a force is applied upon it the solid deforms, with the work stored as elastic energy. A fluid is viscous and transforms its work into heat. When the force is removed the solid returns to its original state (if it is a purely elastic material) but the fluid „forgets“ its original configuration. Viscoelastic materials lie somewhere between the purely elastic and Newtonian flow characteristics. Some of the applied work done is stored as elastic energy with the rest transformed into heat. At a characteristic time λ say, the material forgets its initial form after unloading some of its elastic energy into kinetic energy. For purely elastic materials $\lambda = \infty$, i.e. the material doesn't forget its original state and for purely viscous materials $\lambda = 0$. For materials which show both viscous and elastic properties, λ lies within these ranges and is termed a “viscoelastic” material.

It should be said that just knowing the characteristic time isn't generally that useful unless it is compared against the timescale of the flow (if the history of deformation is important). Having a characteristic time of a ratio between characteristic velocity and length scales respectively introduces a dimensionless number called the „Weissenberg number“ Wi . This way of characterizing materials by the time it remembers its deformation history motivates calculating the total stress in a system over all past deformations, thus taking into account the memory of the fluid when calculating stress. We can formulate this by defining the total stress $\boldsymbol{\sigma}(t)$ at a time t to be

$$\boldsymbol{\sigma}(t) = -p\mathbf{I} + \mathbf{F}_{t'=-\infty}^{t'=\infty}(\mathbf{C}(t'))$$

where p is the pressure, $\boldsymbol{\sigma}(t)$ is decomposed into an isotropic part and the extra-stress tensor with \mathbf{C} a suitable strain tensor. The functional \mathbf{F} weights the past deformations less than the most recent ones. As an initial attempt this is too general an approach to model many viscoelastic fluids, a better way to do it is to represent the functional \mathbf{F} as an integral with a weighting function in it, the weighting function chosen to calibrate with real data (such as the measured viscosity).

CHAPTER 1 INTRODUCTION AND HISTORICAL REVIEW

As mentioned later in this introduction, the continuum approach to modelling viscoelastic fluids is limited and one is better served looking at the microstructure of fluids and building up constitutive models this way. The Oldroyd-B fluid is derived this way later from the properties of polymer molecules in such a fluid type. The development and application of viscoelastic theory has arisen from the wide development of polymeric materials in industry. These materials display characteristics that cannot be adequately explained by the classical theories of elasticity or viscosity.

Such studies lead to the need for a more general theory encompassing both fields. One way to characterize such materials is to measure their response to a uniform stress. A standard elastic material when subject to such a stress, will respond instantaneously with a constant rate of deformation. However, materials exist for which such a stress will induce an instant deformation that is not constant, i.e. some flow process will subsequently happen. This flow process may not be linear and may change with magnitude or form as time evolves. Materials which exhibit this are said to show creep characteristics and cannot be fully described by either elasticity or viscosity theory.

Further complications arise when the materials show memory properties. Application of a stress can produce an instantaneous deformation that in turn responds in a time-dependent manner to the first applied stress. An elastic material does not show this property: responses are governed at a particular time only by the total stress levels at that given moment. This property of „memory“ is of fundamental importance to viscoelastic fluids. It should be noted, that memory in viscoelastic theory is time-dependent, contrasting with other theories such as plasticity theory given by Lubliner (1900).

Viscoelastic fluids retain many of the properties associated with Newtonian Fluids; namely that stresses depend upon the current motion of the fluid, along with the property that stresses are dependent upon the history of its motion. Viscoelastic properties are usually measured as responses to an instantaneously applied/removed constant or dynamic stress or strain. The fluid can therefore be thought of as having both a viscous and an elastic element. The Oldroyd-B model includes both Newtonian and Maxwell models, allowing it to model, for example, the case where an elastic fluid obeying the Maxwell relation is mixed with a fluid governed by a Newtonian Law. Various fluid models exhibit viscoelastic behavior.

CHAPTER 1 INTRODUCTION AND HISTROCAL REVIEW

1.5.4 Derivation of Oldroyd model

The constitutive equation in differential form or integral form is suitable to use in a numerical simulation. Oldroyd observed that the convected time derivative

$\frac{D\pi}{Dt} = \frac{\partial\pi}{\partial t} + (\mathbf{u} \cdot \nabla)\pi$ of a tensor π is not the objective. The objective form of the time

derivative of a tensor can be expressed as

$$\begin{aligned} \frac{D_a\pi}{Dt} &= \frac{d\pi}{dt} + \pi V'(\mathbf{u}) + (\pi V'(\mathbf{u}))^t - a[\pi(\pi\mathbf{u}) + (\pi V(\mathbf{u}))^t] \\ \Rightarrow \frac{D_a\pi}{Dt} &= \frac{\partial\pi}{\partial t} + (\mathbf{u} \cdot \nabla)\pi + \pi V'(\mathbf{u}) - V'(\mathbf{u})\pi - a[\pi V(\mathbf{u}) + V(\mathbf{u})\pi] \end{aligned} \quad (1.19)$$

Where $-1 \leq a \leq 1$ is a parameter.

The case with $a = -1$, $a = 1$ and $a = 0$ are respectively called lower, upper and co-rotational convected time derivative. Oldroyd suggested a general form of constitutive Equation by Hron (1997) as

$$\lambda_x \frac{D_a \boldsymbol{\tau}_s}{Dt} + \boldsymbol{\tau}_s + \gamma(\boldsymbol{\tau}_s, \nabla \mathbf{u}) = 2\mu \left[\lambda_d \frac{D_a V(\mathbf{u})}{Dt} + V(\mathbf{u}) \right], \quad 0 \leq \lambda_d \leq \lambda_x \quad (1.20)$$

where the tensor $\boldsymbol{\tau}_s$ is the extra stress, μ is the dynamic viscosity coefficient of fluid which is assumed to be constant and positive, $\lambda_x \geq 0$ and $\lambda_d \geq 0$ are the constants depend on the continuous medium, respectively, called the relaxation and retardation time of fluid. λ_x characterizes the time it takes the fluid to decrease the tension after have been applied a constant deformation and λ_d characterizes the time it takes the fluid to decrease their state of deformation after having an applied tension. $\gamma(\boldsymbol{\tau}_s, \nabla \mathbf{u})$ is a tensor defined by the traces of $\boldsymbol{\tau}_s$ and /or $V(\mathbf{u})$. There are several types of general model. Here we write some models with $\gamma(\boldsymbol{\tau}_s, \nabla \mathbf{u}) = 0$.

- (i) Maxwell type fluid models ($\lambda_d = 0$)
- (ii) Jeffreys type fluid models ($\lambda_d \neq 0$)
- (iii) Oldroyd-A fluid ($\lambda_x > \lambda_d > 0$ and $a = -1$)
- (iv) Oldroyd-B fluid ($\lambda_x > \lambda_d > 0$ and $a = 1$)

We can generalize these models. For example, the extra-stress $\boldsymbol{\tau}_s$ can be written as a sum of partial stresses $\boldsymbol{\tau}_s = \sum \boldsymbol{\tau}_s^i$. For each partial stress $\boldsymbol{\tau}_s^i$ there is a constitutive equation with different relaxation time λ_x^i .

CHAPTER 1 INTRODUCTION AND HISTROCAL REVIEW

1.5.5 Oldroyd-B model for blood flow

The Cauchy stress tensor is given by

$$\boldsymbol{\sigma} = -p\mathbf{I} + \boldsymbol{\tau}_s$$

In viscoelastic fluids, the stresses depend not only on the current motion of the fluid, but on the history of the motion. We can say that λ_x and λ_d are the measures of the time for which the fluid remembers the flow history. Decomposing the extra-stress tensor $\boldsymbol{\tau}_s$ into the sum of its Newtonian part $\boldsymbol{\sigma}_n$ and its viscoelastic part $\boldsymbol{\sigma}_v$, we can write

$$\boldsymbol{\tau}_s = \boldsymbol{\sigma}_n + \boldsymbol{\sigma}_v$$

Where $\boldsymbol{\sigma}_n = 2\mu \frac{\lambda_d}{\lambda_x} \mathbf{V}(\mathbf{u})$, with $\mu_n = \mu \frac{\lambda_d}{\lambda_x}$ the coefficient of Newtonian viscosity

Therefore, the Cauchy stress tensor can be written as

$$\boldsymbol{\sigma} = -p\mathbf{I} + \boldsymbol{\sigma}_n + \boldsymbol{\sigma}_v = -p\mathbf{I} + 2\mu \frac{\lambda_d}{\lambda_x} \mathbf{V}(\mathbf{u}) + \boldsymbol{\sigma}_v \quad (1.21)$$

From (1.20), for Oldroyd-B fluid, i.e., for $\gamma(\boldsymbol{\tau}_s, \nabla \mathbf{u}) = 0$, $\lambda_x > 0$ and $\lambda_d > 0$ and $a = 1$, the general form of the constitutive equation can be written as

$$\begin{aligned} \lambda_x \frac{D_a \boldsymbol{\tau}_s}{Dt} + \boldsymbol{\tau}_s &= 2\mu \left[\lambda_d \frac{D_a \mathbf{V}(\mathbf{u})}{Dt} + \mathbf{V}(\mathbf{u}) \right] \\ \Rightarrow \lambda_x \frac{D_a (\boldsymbol{\sigma}_v + \boldsymbol{\sigma}_n)}{Dt} + \boldsymbol{\sigma}_v + \boldsymbol{\sigma}_n &= 2\mu \left[\lambda_d \frac{D_a \mathbf{V}(\mathbf{u})}{Dt} + \mathbf{V}(\mathbf{u}) \right] \\ \Rightarrow \lambda_x \frac{D_a \boldsymbol{\sigma}_v}{Dt} + \lambda_x 2\mu \frac{\lambda_d}{\lambda_x} \frac{D_a \mathbf{V}(\mathbf{u})}{Dt} + \boldsymbol{\sigma}_v + 2\mu \frac{\lambda_d}{\lambda_x} \mathbf{V}(\mathbf{u}) &= 2\mu \left[\lambda_d \frac{D_a \mathbf{V}(\mathbf{u})}{Dt} + \mathbf{V}(\mathbf{u}) \right] \\ \Rightarrow \lambda_x \frac{D_a \boldsymbol{\sigma}_v}{Dt} + \boldsymbol{\sigma}_v &= 2\mu \mu \left(-\frac{\lambda_d}{\lambda_x} \right) \mathbf{V}(\mathbf{u}) \\ \Rightarrow \lambda_x \frac{D_a \boldsymbol{\sigma}_v}{Dt} + \boldsymbol{\sigma}_v &= 2(\mu - \mu_n) \mathbf{V}(\mathbf{u}) \\ \Rightarrow \lambda_x \frac{D_a \boldsymbol{\sigma}_v}{Dt} + \boldsymbol{\sigma}_v &= 2\mu_v \mathbf{V}(\mathbf{u}) \end{aligned}$$

Where $\mu_v = \mu - \mu_n$ is the coefficient of elastic viscosity and $\mu = \mu_v + \mu_n$.

So, we have

$$\lambda_x \frac{D_a \boldsymbol{\sigma}_v}{Dt} + \boldsymbol{\sigma}_v = 2\mu_v \mathbf{V}(\mathbf{u}) \quad (1.22)$$

Finally, we can write by (1.19)

$$\lambda_x \left[\frac{\partial \boldsymbol{\sigma}_v}{\partial t} + (\mathbf{u} \cdot \nabla) \boldsymbol{\sigma}_v \right] + \boldsymbol{\sigma}_v = 2\mu_v \mathbf{V}(\mathbf{u}) - \lambda_x \left[\boldsymbol{\sigma}_v \mathbf{V}'(\mathbf{u}) - \mathbf{V}'(\mathbf{u}) \boldsymbol{\sigma}_v - \boldsymbol{\sigma}_v \mathbf{V}(\mathbf{u}) - \mathbf{V}(\mathbf{u}) \boldsymbol{\sigma}_v \right] \quad (1.23)$$

Taking into account (2.21), the conservation law of momentum (1.16) can be written as follows

CHAPTER 1 INTRODUCTION AND HISTROCAL REVIEW

$$\begin{aligned}
 \rho \frac{\partial \mathbf{u}}{\partial t} + \rho(\mathbf{u} \cdot \nabla) \mathbf{u} &= \nabla \cdot \boldsymbol{\sigma} + \rho \mathbf{f} \\
 &= \nabla \cdot [-p\mathbf{I} + 2\mu_n V(\mathbf{u}) + \boldsymbol{\sigma}_v] + \rho \mathbf{f} \\
 &= \nabla \cdot (-p\mathbf{I}) + \nabla \cdot [2\mu_n [\nabla \mathbf{u} + (\nabla \mathbf{u})^t]] + \nabla \cdot \boldsymbol{\sigma}_v + \rho \mathbf{f} \\
 &= -\nabla p \cdot \mathbf{I} - \nabla p \cdot \mathbf{I} + \mu_n \nabla \cdot (2V(\mathbf{u})) + \nabla \cdot \boldsymbol{\sigma}_v + \rho \mathbf{f} \\
 &= -\nabla p + 2\mu_n \nabla \cdot V(\mathbf{u}) + \nabla \cdot \boldsymbol{\sigma}_v + \rho \mathbf{f}
 \end{aligned} \tag{1.24}$$

If $\nabla \cdot \mathbf{u} = 0$, then we have $2 \nabla \cdot V(\mathbf{u}) = \Delta \mathbf{u}$.

So, we can also write the conservation of momentum as

$$\rho \frac{\partial \mathbf{u}}{\partial t} + \rho(\mathbf{u} \cdot \nabla) \mathbf{u} = -\nabla p + 2\mu_n \Delta \mathbf{u} + \nabla \cdot \boldsymbol{\sigma}_v + \rho \mathbf{f}$$

For the simplicity, we write $\boldsymbol{\sigma}$ instead of $\boldsymbol{\sigma}_v$. We have the system of non-linear equations formed by the law of conservation of mass (1.10), the momentum equations (1.16) and the Oldroyd-B constitutive equation (1.23) as

$$\nabla \cdot \mathbf{u} = 0, \text{ in } \Omega$$

$$\rho \frac{\partial \mathbf{u}}{\partial t} + \rho(\mathbf{u} \cdot \nabla) \mathbf{u} = -\nabla p + \mu_n \Delta \mathbf{u} + \nabla \cdot \boldsymbol{\sigma} + \rho \mathbf{f}, \text{ in } \Omega$$

$$\lambda_x \left[\frac{\partial \boldsymbol{\sigma}}{\partial t} + (\mathbf{u} \cdot \nabla) \boldsymbol{\sigma} \right] + \boldsymbol{\sigma} = 2\mu_v V(\mathbf{u}) - \lambda_x [\boldsymbol{\sigma} V'(\mathbf{u}) - V'(\mathbf{u}) \boldsymbol{\sigma} - \boldsymbol{\sigma} V(\mathbf{u}) - V(\mathbf{u}) \boldsymbol{\sigma}], \text{ in } \Omega \tag{1.25}$$

Assuming,

$$M(\boldsymbol{\sigma}, \nabla \mathbf{u}) = 2\mu_v V(\mathbf{u}) - \lambda_x [\boldsymbol{\sigma} V'(\mathbf{u}) - V'(\mathbf{u}) \boldsymbol{\sigma} - \boldsymbol{\sigma} V(\mathbf{u}) - V(\mathbf{u}) \boldsymbol{\sigma}]$$

$$M(\boldsymbol{\sigma}, \nabla \mathbf{u}) = 2\mu_v V(\mathbf{u}) + \lambda_x [(\nabla \mathbf{u}) \boldsymbol{\sigma} - \boldsymbol{\sigma} (\nabla \mathbf{u})^t]$$

The oldroyd-B constitutive equations (2.28) can be written as

$$\nabla \cdot \mathbf{u} = 0, \text{ in } \Omega$$

$$\rho \frac{\partial \mathbf{u}}{\partial t} + \rho(\mathbf{u} \cdot \nabla) \mathbf{u} = -\nabla p + 2\mu_n \Delta \mathbf{u} + \nabla \cdot \boldsymbol{\sigma} + \rho \mathbf{f}, \text{ in } \Omega$$

$$\lambda_x \left[\frac{\partial \boldsymbol{\sigma}}{\partial t} + (\mathbf{u} \cdot \nabla) \boldsymbol{\sigma} \right] + \boldsymbol{\sigma} = M(\boldsymbol{\sigma}, \nabla \mathbf{u}), \text{ in } \Omega \tag{1.26}$$

The above set of equations describes the behavior of an incompressible viscoelastic fluid of Oldroyd-B type, in a certain open subset of R^d ($d = 2; 3$) where the fluid is homogeneous. We observe that the conservation of momentum leads the symmetry properties of the tensor $\boldsymbol{\sigma}$ i.e. $\boldsymbol{\sigma}^t = \boldsymbol{\sigma}$.

The first two equations form a parabolic system for (\mathbf{u}, p) which is in the form of Navier-stokes equation. The last equation has a hyperbolic characteristic which is in the form of transport equation.

CHAPTER 1 INTRODUCTION AND HISTORICAL REVIEW

If the flow state (velocity, pressure, density, etc.) of a flow does not change with time, then it is called a steady or stationary flow. Therefore, in case of steady flow, \mathbf{u} is independent of time and then $\frac{\partial \mathbf{u}}{\partial t} = 0$. So, the Oldroyd-B constitutive equations in case of steady flow is a non-linear system of partial differential equations (PDE) of a combined elliptic-hyperbolic type

$$\begin{aligned} \nabla \cdot \mathbf{u} &= 0, \text{ in } \Omega \\ \rho \frac{\partial \mathbf{u}}{\partial t} + \rho(\mathbf{u} \cdot \nabla) \mathbf{u} &= -\nabla p + 2\mu_n \Delta \mathbf{u} + \nabla \cdot \boldsymbol{\sigma}_v + \rho \mathbf{f}, \text{ in } \Omega \\ \lambda_x \left[\frac{\partial \boldsymbol{\sigma}}{\partial t} + (\mathbf{u} \cdot \nabla) \boldsymbol{\sigma} \right] + \boldsymbol{\sigma} &= M(\boldsymbol{\sigma}, \nabla \mathbf{u}), \text{ in } \Omega \end{aligned} \quad (1.27)$$

1.5.6 Navier-Stokes equations

The limit case $\lambda_x = 0$ leads us from equation (1.22)

$$\boldsymbol{\sigma}_v = 2\mu_v \mathbf{V}(\mathbf{u})$$

The Cauchy stress tensor is given by

$$\begin{aligned} \boldsymbol{\sigma} &= -pI + \boldsymbol{\sigma}_n + \boldsymbol{\sigma}_v \\ &= -pI + 2\mu_n \mathbf{V}(\mathbf{u}) + 2\mu_v \mathbf{V}(\mathbf{u}) \\ &= -pI + 2(\mu_n + \mu_v) \mathbf{V}(\mathbf{u}) \\ &= -pI + 2\mu \mathbf{V}(\mathbf{u}) \\ &= -pI + \mu [\nabla \mathbf{u} + (\nabla \mathbf{u})^t] \end{aligned} \quad (1.28)$$

The Cauchy stress tensor can be written as a linear function of strain rate tensor or the velocity derivative. The fluids for which the above property holds are called the incompressible Newtonian fluids. The Newtonian fluids are a subclass of Stokesian fluids, which are isotropic (with the properties independent of direction) viscous fluids where the stress tensor $\boldsymbol{\sigma}$ is the sum of the tension caused by the hydrostatic pressure in the fluid, the tension that causes deformation fluid and the tension due to volumetric expansion. Newtonian fluids are modeled by Navier-Stokes equations

$$\begin{aligned} \nabla \cdot \mathbf{u} &= 0 \\ \rho \frac{\partial \mathbf{u}}{\partial t} + \rho(\mathbf{u} \cdot \nabla) \mathbf{u} &= \nabla \cdot \boldsymbol{\sigma} + \rho \mathbf{f} \\ \text{Where, } \boldsymbol{\sigma} &= -pI + \mu [\nabla \mathbf{u} + (\nabla \mathbf{u})^t] \end{aligned}$$

$$\nabla \cdot \mathbf{u} = 0$$

CHAPTER 1 INTRODUCTION AND HISTORICAL REVIEW

$$\rho \frac{\partial \mathbf{u}}{\partial t} + \rho(\mathbf{u} \cdot \nabla) \mathbf{u} + \nabla p = \nabla \cdot \boldsymbol{\mu}[\nabla \mathbf{u} + (\nabla \mathbf{u})^t] + \rho \mathbf{f}$$

$$\nabla \cdot \mathbf{u} = 0$$

$$\rho \frac{\partial \mathbf{u}}{\partial t} + \rho(\mathbf{u} \cdot \nabla) \mathbf{u} - \mu \Delta \mathbf{u} + \nabla p = \rho \mathbf{f} \quad (1.29)$$

The above system defines the Navier-Stokes equations for incompressible fluids. For steady flow, the Navier-Stokes equations (2:32) can be written as

$$\nabla \cdot \mathbf{u} = 0$$

$$\rho \frac{\partial \mathbf{u}}{\partial t} + \rho(\mathbf{u} \cdot \nabla) \mathbf{u} + \nabla p - \mu \Delta \mathbf{u} = \rho \mathbf{f} \quad (1.30)$$

Considering ρ as a constant, we define the kinematic viscosity by $\nu = \mu/\rho$ [m^2/s] and the scaled pressure $p = p/\rho$ (m^2/s^2) still denoted by p and we obtain from (1.30)

$$\nabla \cdot \mathbf{u} = 0$$

$$(\mathbf{u} \cdot \nabla) \mathbf{u} + \nabla p - \nu \Delta \mathbf{u} = \mathbf{f}$$

1.6 Enthusiasm behind the selection of current work

According to the World Health Organization (WHO), cardiovascular diseases such as heart attacks, strokes, atherosclerosis, stenosis and aneurysms have been accepted the world's highest cause of death, claiming approximately 17.5 million lives per year is reported in Fuat et al. (2011). The most commonly affected arteries are the abdominal aorta, the carotid, the coronary and the femoral arteries. In such cases, it is important the study of non-Newtonian blood flow behavior, including the shear-thinning viscosity, thixotropy, viscoelasticity, or the yield stress. The Bioengineers, numerical scientists and medical researchers have been receiving the additional attention during the recent decades to exchange the knowledge and data information that can be used to simulation of blood flow.

In the present thesis, a computational analysis and simulation of blood flow through stenosis and aneurysm in aorta have been studied. At inlet, the parabolic velocity profile is used and fixed pressure is used at outlet. No slip conditions are used for velocity and homogeneous Neumann condition for the pressure at blood vessel. The governing mass, momentum, Oldroyd-B and bioheat equations are expressed in a normalized primitive variables formulation. In this thesis, a finite element method for steady-state incompressible blood flows has been developed. The velocity contour lines and pressure distribution profiles are produced. Numerical investigation and simulation are essential

CHAPTER 1 INTRODUCTION AND HISTORICAL REVIEW

to observe the variation in blood flow and pressure distribution due to the above physical changes with boundary conditions, which forms the basis of the motivation behind the present study.

1.7 Main objectives of the present study

The present study has focused on the development of a mathematical model, numerical investigation and simulation regarding the effects of stenosis and aneurysm blood vessel on blood flow in cardiovascular system for Newtonian model, Generalized Newtonian model, Oldroyd-B model and Generalized Oldroyd-B.

This thesis aims to contribute:

- ◆ To solve the governing equations using finite element method with various boundary conditions
- ◆ To study the blood flow through symmetric and non-symmetric stenotic artery, aneurysmatic artery, and stenotic and aneurysmatic artery numerically.
- ◆ To develop a mathematical model regarding the effect of wavy symmetry and non-symmetry stenosis, permeable aneurysmatic artery, and stenotic and aneurysmatic artery on blood flow for all four models.
- ◆ To study the flow characteristics of blood flow through stenotic and aneurysmatic arteries with different flow rates.
- ◆ To visualize the blood flow patterns and pressure distribution of blood flow inside the stenotic and aneurysmatic artery.
- ◆ To investigate the stress characteristics and drag coefficient of the blood flow at the throat of stenosed vessel.
- ◆ To investigate the effects of Weissenberg number (Wi), Peclet number (Re) and Reynold Number (Re) on the blood flow.
- ◆ To show the comparison of symmetric and asymmetric stenosis effect, blood clot and without blood clot model effect on blood flow.
- ◆ To carry out the validation of the present finite element model by investigating the effect of blood flow through stenotic and aneurysmatic artery.
- ◆ To examine the effects of wall shear stress on blood flow with various flow rates and different boundary conditions.

CHAPTER 1 INTRODUCTION AND HISTORICAL REVIEW

1.8 Structure of the Thesis

This dissertation contains six chapters and the thesis is organized as follows.

Chapter 1 has introduced blood rheology and discussed the derivations of the Navier-Stokes equations and Oldroyd-B fluid as well as literature review. The literature review consists of the past studies on blood flow stenosis or aneurysm in arteries or cavities. The different aspects of the previous studies have been mentioned categorically. This is followed by the post-mortem of a recent historical event for the illustration of blood flow and various effects in stenosis or aneurysm. The balance laws have been stated, which are the equations that we wish to investigate for blood flow analysis and numerical study. The aim and specific objectives have been mentioned at the end of this chapter. Our study of equations has commenced with a preliminary analysis from this chapter.

Chapter 2, the computational technique and discretized approaches of the problem has been discussed for viscous incompressible flow. Throughout the thesis, incompressible fluid is considered. Numerical process and finite element method is a vital part in this thesis. This chapter describes discretization and numerical methods to solve the system of partial differential equations supplemented by the constitutive equations, given in the forthcoming Chapters 3, 4 & 5.

Chapter 3 describes a detailed parametric study on Numerical investigation and simulation of blood flow in two-dimensional laminar steady-state through symmetry and non-symmetry wavy Stenosis under various flow rates. Firstly, we describe the governing equations with boundary conditions. The differential constitutive equations have expressed in dimensionless form and written as a continuity equation, the momentum equations and Oldroyd-B equation which are fully coupled. Next, the numerical procedure used to solve the governing equations and iteration technique is used also. Further, the finite element discretization has been used in the blood flow simulation. The effects of the major parameters such as Reynold numbers and Weissenberg number, symmetric and non-symmetric stenosis, wall shear stress and various flow rate of blood flow have been presented for better understanding of the velocity and pressure distribution of blood for mention four models. The results of velocity and pressure distribution of blood flow with different flow rates have been studied.

CHAPTER 1 INTRODUCTION AND HISTORICAL REVIEW

Chapter 4 considers the permeable aneurysm blood flow problem for parameters values $0 < Pe \leq 3000$ and $0 \leq Wi \leq 1$. The present problem has been solved numerically using finite element method. First, Simulation of Newtonian, Oldroyd-B, generalized Newtonian and Oldroyd-B fluids are discussed. In this problem, we have studied that the influence of permeable aneurysm on blood flow and the effects of dimensionless numbers, wall shear stress and stress tensor for all cases. The mathematical models are expressed in terms of continuity equation, momentum and Oldroyd-B equations and a finite element model has been developed. The transport of blood elements through the porous walls play a significant role on blood flow and recirculation zones have migrated to vessel wall for all fluid models. Blood turbulence has reduced at porous permeable artery and elliptical recirculation bubbles are found between the enlargement arteries. The effects of all blood parameters on blood flow are shown graphically for all modifications.

In Chapter 5, the blood flow analysis through stenotic and aneurysmatic artery with blood clot is discussed. The bioheat equation has been inserted for the presence of blood clot at stenosis region. The constitutive equations can be written as mass of conservation, momentum, viscoelastic and bioheat equations, and derive a set of dimensionless form using dimensionless scales. The finite element method and iterative technique is used to solve the non-linear mathematical equations. The finite element discretization has been used to blood flow simulation. It is very important objectives to find out the correlation of blood shear thinning and blood variables, and studies the effects of dimensionless numbers, stenotic and aneurysmatic artery, wall shear stress and drag coefficient on blood flow for all cases. We observe that, the blood flow variables have a rigorous transformed at the throat of stenosis for nonblood clot model. The blood flow patterns have a significant changed at $Re = 3000$ for generalized Oldroyd-B model and immaterial various among models for Wi . At the end of this chapter, we have presented the graphical discussion of blood flow behaviors for Newtonian, generalized Newtonian, Oldroyd-B, and generalized Oldroyd-B models.

Finally, an overview of the results in this thesis is presented, as well as possible extensions through concluding remarks.

CHAPTER 2

COMPUTATIONAL TECHNIQUE

2.1 Introduction

Computational fluid dynamics (CFD) has been rapidly gaining popularity over the past several years for technological as well as scientific interests. For many problems of industrial interest, experimental techniques are extremely expensive or even impossible due to the complex nature of the flow configuration. Analytical methods are often useful in studying the basic physics involved in a certain flow problem, however, in many interesting problems; these methods have limited direct applicability. The dramatic increase in computational power over the past several years has led to a heightened interest in numerical simulations as a cost-effective method of providing additional flow information, not readily available from experiments, for industrial applications, as well as a complementary tool in the investigation of the fundamental physics of turbulent flows, where analytical solutions have so far been unattainable. It is not expected (or advocated), however, that numerical simulations replace theory or experiment, but that they be used in conjunction with these other methods to provide a more complete understanding of the physical problem at hand.

Mathematical model of physical phenomena may be ordinary or partial differential equations, which have been the subject of analytical and numerical investigations. The partial differential equations of fluid mechanics and heat transfer are solvable for only a limited number of flows. To obtain an approximate solution numerically, we have to use a discretization method, which approximated the differential equations by a system of algebraic equations, which can then be solved on a computer. The approximations are applied to small domains in space and / or time so the numerical solution provides results at discrete locations in space and time. Much as the accuracy of experimental data depends on the quality of the tools used, the accuracy of numerical solutions depend on the quality of discretizations used. Computational fluid dynamics (CFD) computation involves the formation of a set numbers that constitutes a practical approximation of a real life system. The outcome of computation process improves the understanding of the performance of a system. Thereby, engineers need CFD codes that can make physically realistic results with good quality accuracy in simulations with finite grids. Contained within the broad field of computational fluid dynamics are activities that cover the range

CHAPTER 2 COMPUTATIONAL TECHNIQUE

from the automation of well established engineering design methods to the use of detailed solutions of the Navier-Stokes equations as substitutes for experimental research into the nature of complex flows. CFD have been used for solving wide range of fluid dynamics problem. It is more frequently used in fields of engineering where the geometry is complicated or some important feature that cannot be dealt with standard methods. More details are available in Ferziger & Perić (1997) and Patankar (1980).

2.2 Elements of Numerical Solution Methods

Several components of numerical solution methods are available in Reddy and Gartling (2001) here only the main steps will be demonstrated in the following.

2.2.1 Mathematical model

The starting point of any numerical method is the mathematical model, i.e. the set of partial differential equations and boundary conditions. A solution method is usually designed for a particular set of equations. Trying to produce a general-purpose solution method, i.e. one which is applicable to all flows, is impractical, is not impossible and as with most general-purpose tools, they are usually not optimum for any one application.

2.2.2 Discretization Process

After selecting the mathematical model, one has to choose a suitable discretization method, i.e. a method of approximating the differential equations by a system of algebraic equations for the variable at some set of discrete locations in space and time.

2.2.3 Numerical grid

The numerical grid defines the discrete locations at which the variables are to be calculated, which is essentially a discrete representation of the geometric domain on which the problem is to be solved. It divided the solution domain into a finite number of sub-domains (elements, control volumes etc). Some of the options available are structural (regular) grid, block structured grid, unstructured grids etc.

2.2.4 Finite approximations

Following the choice of grid type, one has to select the approximations to be used in the discretization process. In a finite difference method, approximations for the derivatives at the grid points have to be selected. In a finite volume method, one has to select the methods of approximating surface and volume integrals. In a finite element method, one has to choose the functions and weighting functions.

CHAPTER 2 COMPUTATIONAL TECHNIQUE

2.2.5 Solution technique

Discretization yields a large system of non-linear algebraic equations. The method of solution depends on the problem. For unsteady flows, methods based on those used for initial value problems for ordinary differential equation (marching in time) is used. At each time step an elliptic problem has to be solved. Pseudo-time marching or an equivalent iteration scheme usually solves steady flow problems. Since the equations are non-linear, an iteration scheme is used to solve them. These methods use successive linearization of the equations and the resulting linear systems are almost always solved by iterative techniques. The choice of solver depends on the grid type and the number of nodes involved in each algebraic equation.

2.3 Discretization Approaches

The first step to numerically solve a mathematical model of physical phenomena is its numerical discretization. This means that each component of the differential equations is transformed into a “numerical analogue” which can be represented in the computer and then processed by a computer program, built on some algorithm. Many different methodologies were devised for this purpose in the past and the development still continues. In order to short them, we can at first divide the spatial discretisation schemes into the following three main categories: finite difference (FD), finite volume (FV) finite element (FE) methods, Boundary element (BE) method and Boundary volume (BV) method.

In the present numerical computation, Galerkin finite element method (FEM) is used. Detailed discussion of this method is available in Chung (2002) and Dechaumphai (1995, 1999).

2.3.1 Finite element analysis

The finite element method (FEM) is a powerful computational method for solving problems, which are described with partial differential equations. The fundamental idea of the finite element method is to outlook a given domain as an assemblage of simple geometric shapes, called finite elements, for which it is possible to systematically generate the approximation functions needed in the solution of partial differential equations by the weighted residual method. The computational domains with irregular geometries by a collection of finite elements makes the method a valuable practical tool for the solution of boundary value problems arising in various fields of engineering. The approximation functions, which satisfy the governing equations and boundary

CHAPTER 2 COMPUTATIONAL TECHNIQUE

conditions, are often constructed using ideas from interpolation theory. Approximating functions in finite elements are determined in terms of nodal values of a physical field, which is required. A continuous physical problem is transformed into a discretized finite element problem with unknown nodal values. For a linear problem, a system of linear algebraic equations should be solved. Values inside finite elements can be recovered using nodal values.

The finite element method is one of the numerical methods that have received popularity due to its capability for solving complex structural problem. The method has been extended to solve problems in several other fields such as in the field of heat transfer, computational fluid dynamics, electromagnetic, biomechanics etc. In spite of the great success of the method in these fields, its application to fluid mechanics, particularly to convective viscous flows, is still under intensive research.

The major steps involved in finite element analysis of a typical problem are:

1. Discretization of the domain into a set of finite elements (mesh generation).
2. Weighted-integral or weak formulation of the differential equation to be analyzed.
3. Development of the finite element model of the problem using its weighted-integral or weak form.
4. Assembly of finite elements to obtain the global system of algebraic equations.
5. Imposition of boundary conditions.
6. Solution of equations.
7. Post-computation of solution and quantities of interest.

2.3.2 Mesh generation

The area of numerical grid generation is relatively young in practice, although its roots in mathematics are old. The arrangement of discrete points throughout the flow field is simply called a grid. The determination of a proper grid for the flow through a given geometric shape is important. The way that such a grid is determined is called grid generation. The grid generation is a significant consideration in CFD. Finite element method can be applied to unstructured grids. This is because the governing equations in this method are written in integral form and numerical integration can be carried out directly on the unstructured grid domain in which no coordinate transformation is required. A two-dimensional domain may be triangulated as shown in Figure 2.1. In

CHAPTER 2 COMPUTATIONAL TECHNIQUE

finite element method, the mesh generation is the technique to subdivide a domain into a set of sub-domains, called finite elements. Figure 2.1 shows a domain, Ω is subdivided into a set of sub-domains, Ω^e with boundary Γ^e .

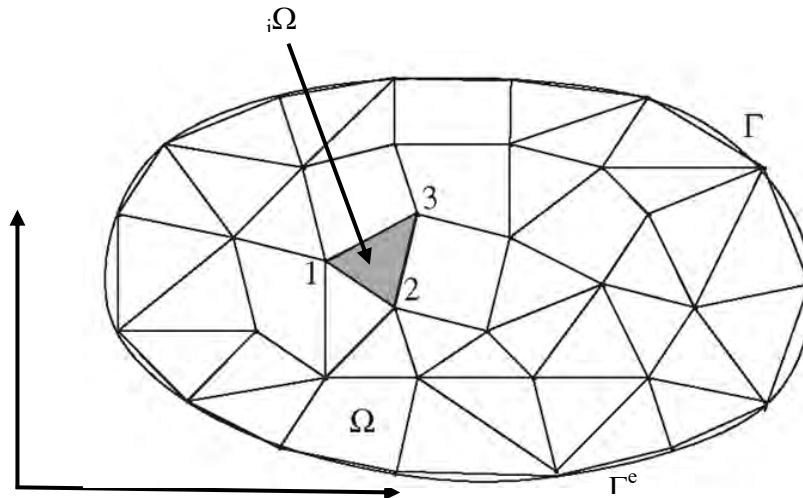


Figure 2.1: A typical FE discretization of a domain, Reddy & Gartling [69].

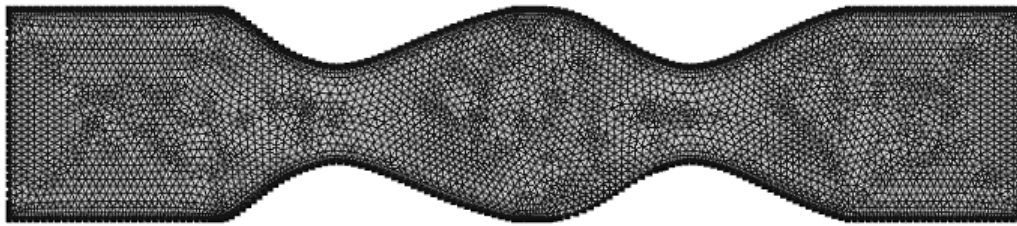


Figure 2.2a: Mesh structure of elements for stenotic artery.

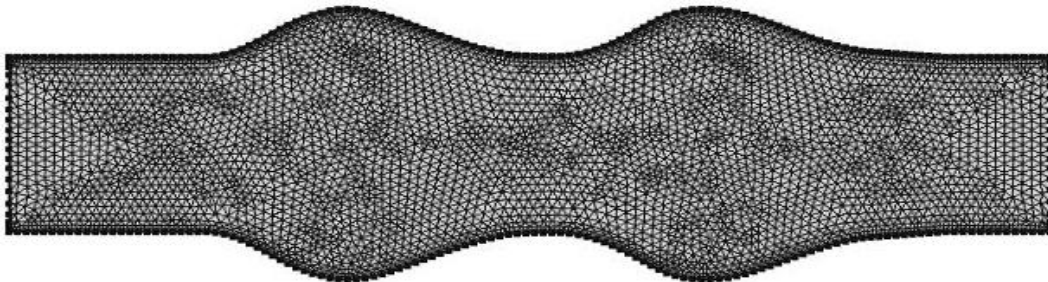


Figure 2.2b: Mesh structure of elements for aneurysmatic artery.



Figure 2.2c: Current mesh structure of elements for stenotic and aneurysmatic artery.

Figure 2.2: Current mesh structure for physical systems

CHAPTER 2 COMPUTATIONAL TECHNIQUE

2.3.3 Finite Element Formulation and Computational Technique

Viscous incompressible blood flows have been the subject of our investigation. The problem is relatively complex due to the coupling between the viscoelasticity equation and the Navier-Stokes equations, which govern the fluid motion. These equations comprise a set of coupled nonlinear partial differential equations, which is difficult to solve especially with complicated geometries and boundary conditions. The finite element formulation and computational procedure for Navier-Stokes equations along with Oldroyd-B equations will be discussed in Chapter 3.

2.3.4 Algorithm

The algorithm was originally put forward by the iterative Newton-Raphson algorithm; the discrete forms of the continuity, momentum and viscoelasticity equations are solved to find out the value of the velocity, pressure and the extra stress tensor. It is essential to guess the initial values of the variables. Then the numerical solutions of the variables are obtained while the convergent criterion is fulfilled. The simple algorithm is shown by the flow chart below.

CHAPTER 2 COMPUTATIONAL TECHNIQUE

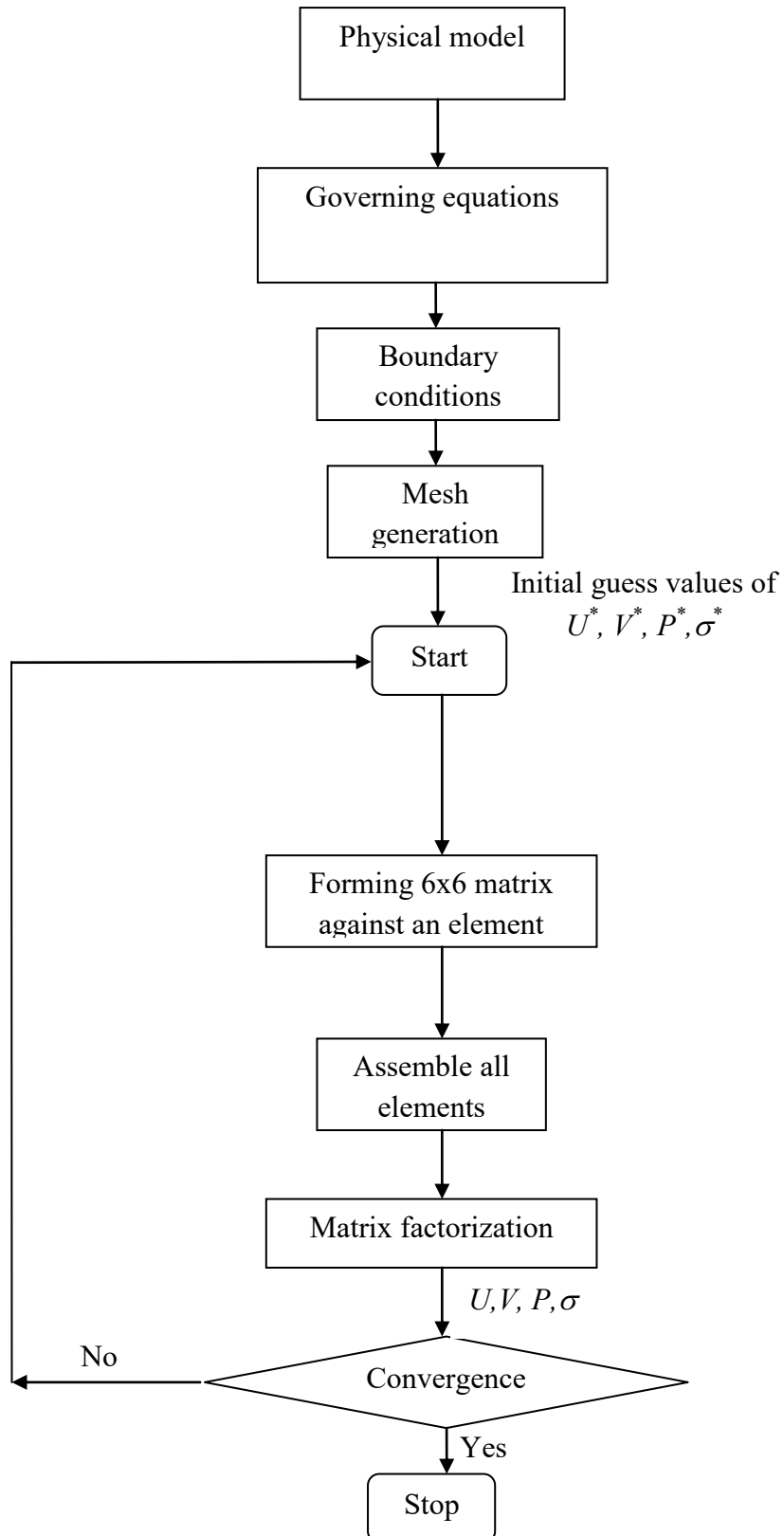


Figure 2.3: Flow chart of the computational procedure

CHAPTER 2 COMPUTATIONAL TECHNIQUE

2.3.5 Solution of system of equations

A system of linear algebraic equations has been solved by the UMFPACK with COMSOL MULTIPHYSICS (2013) package interface and in own MATLAB programming (2010). UMFPACK is a set of routines for solving asymmetric sparse linear systems $Ax = b$, using the Asymmetric Multi-Frontal method and direct sparse LU factorization. Five primary UMFPACK routines are required to factorize A or $Ax = b$:

1. Pre-orders the columns of A to reduce fill-in and performs a symbolic analysis.
2. Numerically scales and then factorizes a sparse matrix.
3. Solves a sparse linear system using the numeric factorization.
4. Frees the Symbolic object.
5. Frees the Numeric object.

Additional routines are:

1. Passing a different column ordering
2. Changing default parameters
3. Manipulating sparse matrices
4. Getting LU factors
5. Solving the LU factors
6. Computing determinant

UMFPACK factorizes PAQ , $PRAQ$, or $PR^{-1}AQ$ into the product LU , where L and U are lower and upper triangular, respectively, P and Q are permutation matrices, and R is a diagonal matrix of row scaling factors (or $R = I$ if row-scaling is not used). Both P and Q are chosen to reduce fill-in (new non-zeros in L and U that are not present in A). The permutation P has the dual role of reducing fill-in and maintaining numerical accuracy (via relaxed partial pivoting and row interchanges). The sparse matrix A can be square or rectangular, singular or non-singular, and real or complex (or any combination). Only square matrices A can be used to solve $Ax = b$ or related systems. Rectangular matrices can only be factorized. UMFPACK first finds a column pre-ordering that reduces fill-in, without regard to numerical values. It scales and analyzes the matrix, and then automatically selects one of three strategies for pre-ordering the rows and columns: asymmetric, 2-by-2 and symmetric. These strategies are described below.

CHAPTER 2 COMPUTATIONAL TECHNIQUE

One notable attribute of the UMFPACK is that whenever a matrix is factored, the factorization is stored as a part of the original matrix so that further operations on the matrix can reuse this factorization. Whenever a factorization or decomposition is calculated, it is preserved as a list (element) in the factor slot of the original object. In this way a sequence of operations, such as determining the condition number of a matrix and then solving a linear system based on the matrix, do not require multiple factorizations of the intermediate results.

Conceptually, the simplest representation of a sparse matrix is as a triplet of an integer vector \mathbf{i} giving the row numbers, an integer vector \mathbf{j} giving the column numbers, and a numeric vector \mathbf{x} giving the non-zero values in the matrix. The triplet representation is row-oriented if elements in the same row were adjacent and column-oriented if elements in the same column were adjacent. The compressed sparse row (csr) or compressed sparse column (csc) representation is similar to row-oriented triplet or column-oriented triplet respectively. These compressed representations remove the redundant row or column in indices and provide faster access to a given location in the matrix.

2.4 Chapter Summary

This chapter has presented an introduction to computational method with advantages of numerical investigation. Because numerical method has played a central role in this thesis. Various components of numerical method have been also explained. Finally, the major steps involved in finite element analysis of a typical problem have been discussed.

CHAPTER 3

NUMERICAL STUDY OF BLOOD FLOW THROUGH SYMMETRIC AND ASYMMETRIC STENOSIS UNDER VARIOUS FLOW RATES

Stenotic artery affects the human blood flow and leads to severe disorders in our circulatory system as a result cardiovascular diseases arise in human body. Now a days, medical researcher, bioengineers and scientists have been receiving the attention during the recent decades. The main purpose of this efforts is to provide numerical simulations of blood flow system, exchange of knowledge and data information in different conditions. The details are available in Caro et al. (1978), Tu and Deville (1996), Shaughnessy et al. (2005), and Robertson et al. (2008). Stenosis is an abnormal reduction of blood vessel that develops various arterial locations of the cardiovascular system under diseased conditions has described by Siddique et al. (2009). Development of stenosis in brain arteries can reason of cerebaral strokes and myocardial infraction which leads to heart inactive. Verdier (2003) has studied that the hemodynamical properties of blood flow through non uniform cross section of arteries play an important role to identify arthrosclerorsis diseases. To have a clear understanding of blood flow behavior through the obstacles a number of studies were carried out in the past by many researchers Chien et al. (1968), Lowe (1990), Chakravarty and Mandal (2000), Baskurt and Meiselman (2003), Mandal (2005).

The chapter describes the numereical study of blood flow through symmetric and asymmetric stenotic artery under various flow rates. The governing equations along with appropriate boundary conditions are transformed into a dimensionless equation then solved numerically with finite element technique. Numerical investigation and simulation are essential to observe the variation in blood flow and pressure distribution due to the physical changes with boundary conditions. Mathematical tests are performed on an idealized symmetric stenosis and a realistic stenosed carotid bifurcation reconstructed from medical images. Model sensitivity tests are achieved with respect to the characteristic flow rate to evaluate its impact on the observed non-Newtonian effects. Different effects on blood flow of stenosis for these models are presented numerically.

The remainder of this chapter is as follows. The physical schematic diagram descriptions of the present work are shown in section 3.1. In section 3.2, the dimensionless governing

equations with boundary conditions using dimensionless parameters is considered. After that a computational method is derived in the section 3.3. Later results are presented in section 3.5 with code validation. Finally, section 3.6 gives a summary of this chapter.

3.1 Physical Configurations

The physical model considered here is shown in Figure 3.1, along with the important geometric parameters. The stenosed vessel is assumed to be two-dimensional with diameter $D=2R= 6.2$ which reduces smoothly to one half in the stenosed region. The parabolic velocity profile (U_i) and extra stress tensor (σ_v) are prescribed at the inlet with Reynolds number, $Re = 100$ and Weissenberg number, $Wi = 0.6$. At outlet, pressure is fixed to a constant. On the walls no-slip conditions are used for velocity and homogeneous Neumann condition for the pressure. For Oldroyd-B model and generalized Oldroyd-B model, the homogeneous Neumann conditions are considered at the walls and outlet. The stenosis cross-sectional area ratio is 2:1 and thus a significant local acceleration of the flow is expected.

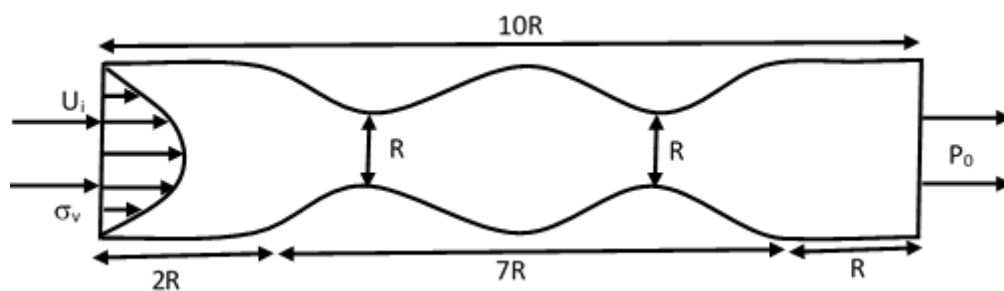


Figure 3.1: Schematic diagram of the physical system

3.2 Mathematical Modeling

The several steps of the mathematical formulation for the above physical configurations are shown as follows

3.2.1 Governing equations

Mathematical model is based on incompressible Navier-Stokes equations which are generalized to take into account viscoelasticity and shear-thinning properties of blood flow. The model used to capture viscoelastic properties of the blood flow is the generalized Oldroyd-B model. The numerical method used for solution of the governing system of equations is based on the Finite Element discretization. The governing system of equations is based on Navier Stokes equations using Johnson-Segalman model for stress tensor. The governing equations can be written as:

Continuity Equation

$$\nabla \cdot \mathbf{u} = 0 \quad (3.1)$$

Momentum Equations

$$\rho \frac{\partial \mathbf{u}}{\partial t} + \rho(\mathbf{u} \cdot \nabla) \mathbf{u} = -\nabla p + \mu_n \Delta \mathbf{u} + \nabla \cdot \boldsymbol{\sigma} + \rho \mathbf{f} \quad (3.2)$$

Oldroyd-B constitutive equation:

$$\boldsymbol{\sigma} + \lambda_x \left[\frac{\partial \boldsymbol{\sigma}}{\partial t} + (\mathbf{u} \cdot \nabla) \boldsymbol{\sigma} \right] = 2\mu_v \mathbf{V}(\mathbf{u}) + \lambda_x [\boldsymbol{\sigma} \mathbf{V}' - \mathbf{V}' \boldsymbol{\sigma} - \boldsymbol{\sigma} \mathbf{V} - \mathbf{V} \boldsymbol{\sigma}] \quad (3.3)$$

Here \mathbf{u} is the velocity vector, $\mathbf{u} = (u_1, u_2, u_3)^T$, ρ is the constant density, $\boldsymbol{\sigma}$ is the extra stress tensor, μ is dynamic viscosity, λ_x and λ_d denote the relaxation and retardation time respectively, and the symmetric part of the velocity gradient, $\mathbf{V} = \frac{1}{2}(\nabla \mathbf{u} + \nabla \mathbf{u}^T)$ i.e.

$\boldsymbol{\sigma} = 2\mu \mathbf{V}$. The total viscosity composed of Newtonian viscosity (solvent, μ_n) and viscoelasticity (polymer, μ_v) components, $\mu = \mu_n + \mu_v$. Decomposing the extra-stress tensor $\boldsymbol{\sigma}$ into the sum of its Newtonian part $\boldsymbol{\sigma}_n$ and its viscoelastic part $\boldsymbol{\sigma}_v$, we can write $\boldsymbol{\sigma} = \boldsymbol{\sigma}_n + \boldsymbol{\sigma}_v$.

Where, $\boldsymbol{\sigma}_n = 2\mu_n \mathbf{V}$, $\boldsymbol{\sigma}_v + \lambda_x \frac{\partial \boldsymbol{\sigma}_v}{\partial t} = 2\mu_v \mathbf{V}$, $\mu = \mu_n + \mu_v$ and $\frac{\lambda_d}{\lambda_x} = \frac{\mu_n}{\mu_n + \mu_v}$

The upper convective $\frac{\delta}{\delta t}$ can be express for the general quantity N

$$\frac{\delta N}{\delta t} = \frac{\partial N}{\partial t} + (\mathbf{u} \cdot \nabla) N - (\mathbf{V}' N - N \mathbf{V}') - (\mathbf{V} N + N \mathbf{V}) \quad (3.4)$$

Where, Velocity gradient for symmetric part

$$\mathbf{V} = \frac{1}{2}(\nabla \mathbf{u} + \nabla \mathbf{u}^T) = \frac{1}{2} \begin{pmatrix} 2u_x & u_y + v_x \\ u_y + v_x & 2v_y \end{pmatrix} \quad (3.5)$$

and Velocity gradient for anti-symmetric part

$$\mathbf{V}' = \frac{1}{2}(\nabla \mathbf{u} - \nabla \mathbf{u}^T) = \frac{1}{2} \begin{pmatrix} 0 & u_y - v_x \\ v_x - u_y & 0 \end{pmatrix} \quad (3.6)$$

The Oldroyd-B constitutive equation for viscoelastic part is

$$\frac{\partial \boldsymbol{\sigma}_v}{\partial t} + (\mathbf{u} \cdot \nabla) \boldsymbol{\sigma}_v = \frac{2\mu_v}{\lambda_x} \mathbf{V} - \frac{1}{\lambda_x} \boldsymbol{\sigma}_v + (\mathbf{V}' \boldsymbol{\sigma}_v - \boldsymbol{\sigma}_v \mathbf{V}') + (\mathbf{V} \boldsymbol{\sigma}_v + \boldsymbol{\sigma}_v \mathbf{V}) \quad (3.7)$$

3.2.2 Shear-thinning viscosity model

In the case of blood flow the shear-thinning behaviors, the shear rate dependent viscosity function $\mu(\dot{\gamma})$ instead of the constant viscosity coefficient μ_n .

The shear rate is defined by $\dot{\gamma} = 2\sqrt{V : V} = 2|V|$. The non-dimensional form of this function is

$$F(\dot{\gamma}) = \frac{\mu(\dot{\gamma}) - \mu_\infty}{(\mu_0 - \mu_\infty)}$$

Here μ_0 and μ_∞ are the asymptotic viscosity values at zero and infinity shear rates. The appropriate transition between these values is carried out by the shear rate dependent function $F(\dot{\gamma})$ which satisfies the limit conditions

$$\lim_{\dot{\gamma} \rightarrow 0^+} F(\dot{\gamma}) = 1 \text{ and } \lim_{\dot{\gamma} \rightarrow \infty} F(\dot{\gamma}) = 0$$

There are many possible choices for such a function $F(\dot{\gamma})$. It is very important to select the blood viscosity for accuracy in blood flow simulations. For 2D stenosis case, one of the most frequently used shear-thinning models for blood is the generalized Cross model given by

$$\mu(\dot{\gamma}) = \mu_\infty + \frac{\mu_0 - \mu_\infty}{(1 + (\lambda \dot{\gamma})^b)^a} \tag{3.8}$$

with the parameters $a, b, \lambda > 0$ and $\gamma = \sqrt{(2 \text{ tr} V^2)}$.

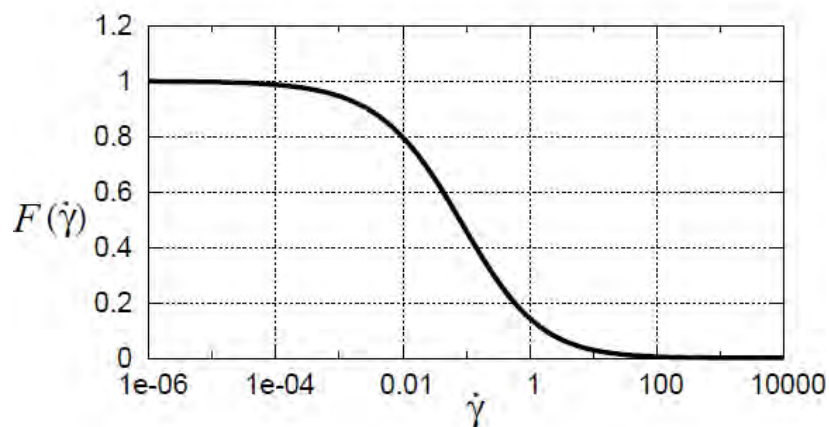


Figure 3.2: Viscosity function

To account for the viscoelasticity of blood we consider the equations for the conservation mass equation (3.1), conservation momentum equation (3.2) and Oldroyd-B equation (3.3). For the combination of shear-thinning and viscoelasticity we have four models and all the following models are tested for different flow rates ($q = 0.05, 0.1, 2 \text{ cm}^3/\text{s}$), that correspond to the common blood flow rates in human body.

Table 3.1: Models outline

Name of Model	Shear-thinning (μ_n)	Viscoelasticity (σ_v)
Newtonian	$\mu_n = \mu_\infty = \text{constant}$	$\sigma_v = 0$
Generalized Newtonian	$\mu_n = \mu(\dot{\gamma})$	$\sigma_v = 0$
Oldroyd-B	$\mu_n = \mu_\infty = \text{constant}$	σ_v
Generalized Oldroyd-B	$\mu_n = \mu(\dot{\gamma})$	σ_v

3.2.3 Boundary conditions

The flow is modeled in a bounded computational domain where a boundary is divided into three mutually disjoint parts: a solid wall, an outlet and an inlet.

(i) At inlet:

a. Dirichlet boundary conditions for velocity vector are used on the boundary $\partial\Omega$

$u = g$ on $\partial\Omega$ with compatibility condition $\int_{\partial\Omega} g \cdot \mathbf{n} = 0$, where \mathbf{n} is the unit outward normal vector to Ω at the boundary $\partial\Omega$. For homogenous case, $g=0$.

b. For a pressure and the stress tensor Neumann boundary condition is used on the boundary $\partial\Omega$. This boundary condition can be defined by

$$\boldsymbol{\sigma} \cdot \mathbf{n} = (-p\mathbf{I} + \nu \nabla \cdot \mathbf{u}). \mathbf{n} = \mathbf{h}$$

c. The developed parabolic velocity profile and the corresponding extra stresses components

$$\mathbf{u} = 1.5 U_i (1 - y^2), \mathbf{v} = 0$$

$$\sigma_{11} = 2\mu_v Wi \left(\frac{\partial \mathbf{u}}{\partial y}\right)^2, \sigma_{12} = \mu_v \frac{\partial \mathbf{u}}{\partial y}, \sigma_{22} = 0$$

Where, y is along the inlet boundary, and U_i is the average fluid velocity at the inlet.

(ii) At outlet:

a. At outflow boundary pressure value is constant and for the velocity vector and the stress tensor Neumann boundary condition is used.

b. Due to pressure force (P_o) the stress is acting at the boundary, $\boldsymbol{\sigma} \cdot \mathbf{n} = -P_o \mathbf{n}$

(iii) At boundary wall:

a. On the walls no slip conditions are used for the velocity together with the condition for the normal component of the extra stress:

$$\mathbf{u} = 0, (\boldsymbol{\sigma} \cdot \mathbf{n}) \cdot \mathbf{n} = 0$$

Where \mathbf{n} is the boundary unit normal vector.

b. Homogenous Neumann boundary conditions are used for the pressure.

3.2.4 Dimensional analysis

The fundamental laws used to solve for the variables velocity, pressure and shear stress, provided the viscosity function, and flow parameters. With respect to boundary conditions the problems are the conservation of mass (continuity equations), conservation of momentums (momentum equations), and Oldroyd-B (viscoelasticity equations), which constitute a set of coupled, nonlinear, and partial differential equations. To obtain a system of dimensionless variables, we use some scaling properties of the system to introduce Reynolds number (Re) and Weissenberg number (Wi) that measures the effect of viscosity and elasticity on blood flow for steady state.

Using non-dimensional variables defined in the nomenclature, the non-dimensional governing equations 3.1, 3.2 and 3.7 are obtained for 2D stenosis vessel in domain Ω as follows:

Continuity Equation

$$\nabla \cdot \mathbf{U} = 0 \quad (3.9)$$

Momentum Equations

$$Re[(\mathbf{U} \cdot \nabla) \mathbf{U}] = -\nabla P + (1 - \lambda) \Delta \mathbf{U} + \nabla \cdot \boldsymbol{\sigma} + \mathbf{f} \quad (3.10)$$

$$Re[(\mathbf{V} \cdot \nabla) \mathbf{V}] = -\nabla P + (1 - \lambda) \Delta \mathbf{V} + \nabla \cdot \boldsymbol{\sigma} + \mathbf{f} \quad (3.11)$$

Oldroyd-B constitutive equation:

$$Wi[(\mathbf{U} \cdot \nabla) \boldsymbol{\sigma}] + \boldsymbol{\sigma} = 2\mu_v V(\mathbf{U}) + Wi_i[(\nabla \mathbf{U}) \boldsymbol{\sigma} + \boldsymbol{\sigma}(\nabla \mathbf{U})^t] \quad (3.12)$$

Equations (3.9)-(3.12) were non-dimensional using the following dimensionless scales:

$$x = LX, \quad t = Lt^*/U, \quad u = UU_o, \quad \mathbf{v} = VU_o, \quad p = \mu UP/L, \quad T = U\mu T^*/L, \\ f = f^* \mu U/L^2, \quad \nabla = \nabla^*/L, \quad Wi = \lambda_x U/L, \quad Re = \rho UL/\mu$$

Reynolds number (Re) and Weissenberg number (Wi) are dimensionless numbers. Small values of Wi mean that the fluid is little elastic and small values of Re means that the fluid is very viscous.

3.3 Numerical Analysis

The differential constitutive equations are solved by numerical methods, in particular the commercial high-level finite element package COMSOL Multiphysics (2013) and MATLAB Programming (2010). The Galerkin weighted residual finite element techniques discussed below.

3.3.1 Finite Element Formulation and Computational Technique

The numerical procedure used to solve the governing equations for the present work is based on the Galerkin weighted residual method of finite-element formulation. The finite element technique is explained in appendix A, which includes a detail analysis.

3.3.2 Grid Independence Test

Preliminary results are obtained to inspect the field variables grid independency solutions. Test for the accuracy of grid fineness has been carried out to find out the optimum grid number.

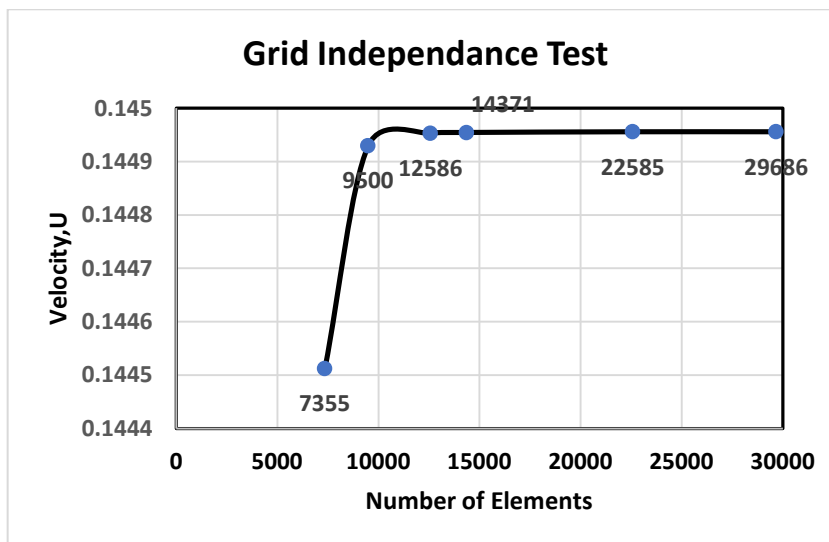


Figure 3.3: Convergence of velocity with grid refinement for $Re = 10^2$ and $Wi = 0.6$ with blood flow rate $0.1 \text{ cm}^3/\text{s}$.

To obtain grid independent solution, a grid refinement study is performed for a stenosis cavity with $Re = 10^2$ and $Wi = 0.6$ with blood flow rate $0.2 \text{ cm}^3/\text{s}$. Figure 3.3 shows the convergence of velocity (U) along the vessel axis with grid refinement. It is observed that grid independence is achieved with 22585 elements where there is an insignificant change in velocity with further increase of mesh elements. Six different non-uniform grids with the following number of nodes and elements were considered for the grid refinement tests: 28442 nodes, 7355 elements; 50346 nodes, 9500 elements; 64240 nodes, 12586 elements; 69887 nodes, 14371 elements; 92573 nodes, 22585 elements, 98388 nodes, 29686 elements. From these values, 92573 nodes, 22585 elements can be chosen throughout the simulation to optimize the relation between the accuracy required and the computing time.

Table 3.2: Grid Sensitivity Check at $Re = 100$, $Wi = 0.6$ and $q = 0.2 \text{ cm}^3/\text{s}$

Nodes	28442	50346	64240	69887	92573	98388
(elements)	(7355)	(9500)	(12586)	(14371)	(22585)	(29686)
U	0.14451252	0.14492982	0.14495304	0.14495446	0.14495578	0.14495579
Time (s)	255.6	283.43	301.51	332.25	551.61	1007.65

3.4 Code Validation

For code validation, the blood flow simulation with above mentioned parameters for Newtonian model have solved, and the results have compared with those reported in Prokop and Kozel (2013), obtained with an extended computational domain. A comparison between the simulations of velocity field is presented in Figure 3.4. The results from the present experiment are almost same as Prokop and Kozel (2013).

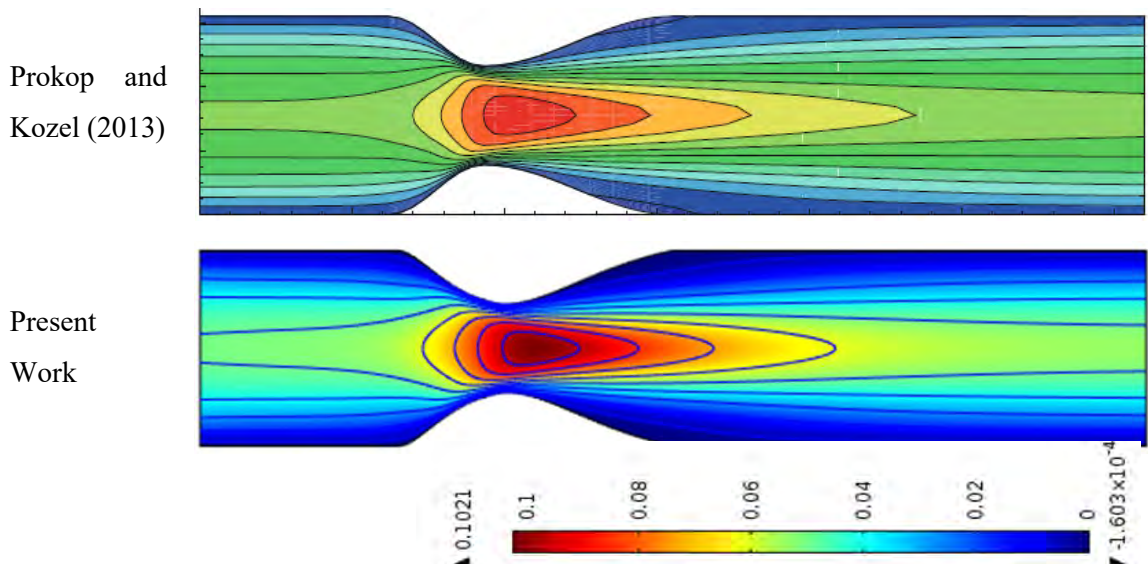


Figure 3.4: Comparison of velocity contour lines between Prokop and Kozel (2013) and present work

3.5 Results and Discussion

The objective of the present mathematical model is to understand and bring out the effects of symmetric stenosis, non-symmetric stenosis, wall shear stenosis, dimensionless numbers and various flow rates on blood flow for the Newtonian (N), generalized Newtonian (GN), Oldroyd-B (OD) and generalized Oldroyd-B (GD) models. We have used the models mentioned in Section 3.2.2 to investigate the influence of the shear-thinning and viscoelastic effects on the behavior of blood in different flow situations.

CHAPTER 3 NUMERICAL STUDY OF BLOOD FLOW... ..

The solution of the Naiver-Stoke equations is obtained under the same conditions as the solutions of the non-Newtonian equations. To show the non-Newtonian effects are used the comparison of flow field. We assume that the only change of blood viscosity μ_n and extra stress σ_v for developed all four models. Numerical simulations and investigation have performed and compared for all four models. The following parameters are repoted in Prokop and Kozel (2013) and have been used for blood flow simulations in aorta

$$\begin{array}{llll} \mu_0 = 0.16 \text{ Pa.s} & \mu_n = 0.0036 \text{ Pa.s} & a = 1.23 & b=0.64 \\ \lambda = 8.2\text{s} & \rho = 1050 \text{ kg.m-3} & L_w = 0.003\text{m} & L = 0.03\text{m} \end{array}$$

The effect of stenosis is examined for all four different models with various flow rates. A comparison between velocity and pressure distribution for above mentioned models with $Wi = 0.6$ and $Re = 100$ is presented in terms of contour lines and stream lines with vectors in Figures 3.5-3.7. The velocity and pressure profiles have a significant changed on blood flow at throat of stenosis. The wall shear stress is another parameter to identify the artery diseases and its effect has shown in Figure 3.38. For the effect of dimensionless numbers have shown in Figures 3.16 -3.35 at Reynold number, Re (100, 500 and 1000) and Weissenberg number, Wi (0.0, 0.5, 1.0). The parabolic profile has developed at constriction zone in artery and the pattern of blood flow for velocity and pressure distributions in terms of contour lines are shown in Figures 3.16 -3.35. The velocity and pressure distribution of blood flow which have changed with the change of flow rate are presented graphically in Figures 3.24-3.25 and 3.34-3.35 for considerable models.

3.5.1 Symmetric stenosis effects on blood flow field

The axial velocity contours and stream lines with vectors of the four models Newtonian, Generalized Newtonian, Oldroyd-B, Generalized Oldroyd-B are presented in Figures 3.5-3.7 with the flow rate $q = 0.1 \text{ cm}^3/\text{s}$. Just behind the stenosis the reversal flow regions and flow separation are found with respect to the centerline. It is interesting to note that there are some permanent recirculation zones or confined zones formed at the throat of stenosis for four models. These confined zones are indicative of regions where the blood flow is almost identical over a significant portion of each model. The confined zone becomes little shorter for generalized Newtonian and Oldroyd-B model. It is easy to comprehend, in the Newtonian case the characteristic blood viscosity is μ_n and thus a shear-thinning viscosity of the form equation (3.8), leads to the increase in the local viscosity in the low-shear regions. Different results are found to choices of the other

characteristic viscosity for the Newtonian model. The axial velocity profiles are shown in Figure 3.8 for all four models at dimensionless number $Wi = 0.6$ and $Re = 100$. From Figure 3.8, the minimum value of velocity is found in 1st constriction regions. It is clearly visible that the main effect of the blood shear-thinning behavior is noticeable in the recirculation zone, where the resistance to flow (local viscosity) increases substantially. The effects of viscoelasticity are about one order of magnitude lower in this case. For pulsatile flow or other flow rates or geometries, the viscoelastic effects may become more vital. In Table 3.3, blood velocity obtained along blood vessel axis for all four models while $Re = 100$, $Wi = 0.6$ and $q = 0.1 \text{ cm}^3/\text{s}$ is presented.

Table 3.3: Blood velocity is presented along vessel axis for all four cases while $Re = 100$, $Wi = 0.6$ and $q = 0.1 \text{ cm}^3/\text{s}$.

Along vessel axis	Velocity (U)			
	Newtonian Model	Generalized Newtonian Model	Oldroyd-B Model	Generalized Oldroyd-B Model
0	0.072441613	0.07179703	0.073790151	0.074216232
1	0.073659585	0.073220394	0.074457772	0.074775967
2	0.078958292	0.078622927	0.079394602	0.079839732
3	0.122305168	0.123011724	0.122420933	0.126968168
4	0.136198205	0.135461351	0.1362318	0.137490551
5	0.119060907	0.114177162	0.119078516	0.11014374
6	0.114595236	0.110281144	0.114600092	0.107498954
7	0.144967463	0.144195034	0.144971072	0.147781529
8	0.128953238	0.124620332	0.128956833	0.12208713
9	0.112582709	0.105268318	0.112584813	0.099287073
10	0.100114693	0.089927309	0.100113836	0.082873143

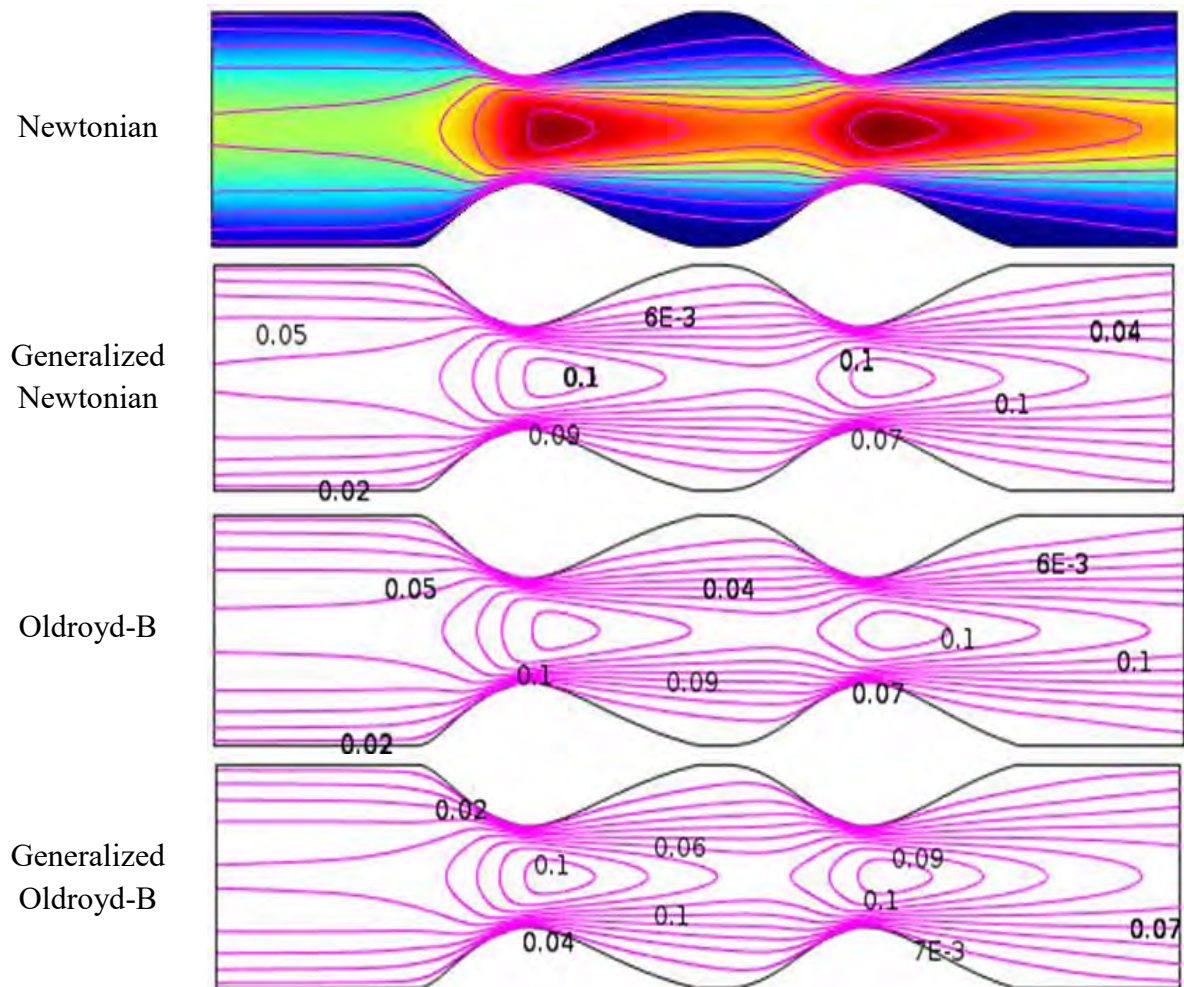
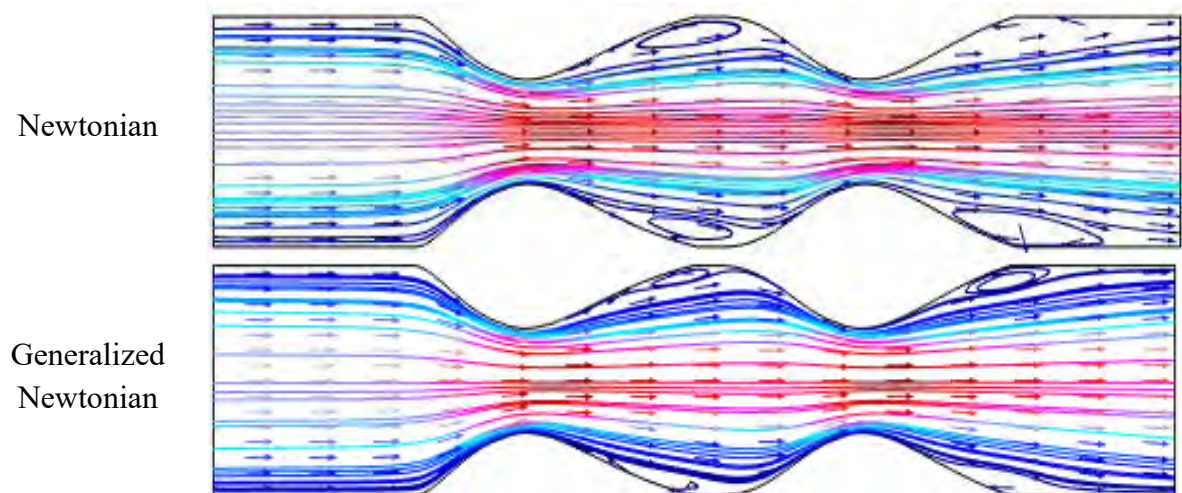


Figure 3.5: Velocity contour plots on blood flow through symmetric stenosis at $Re=100$ and $Wi = 0.6$



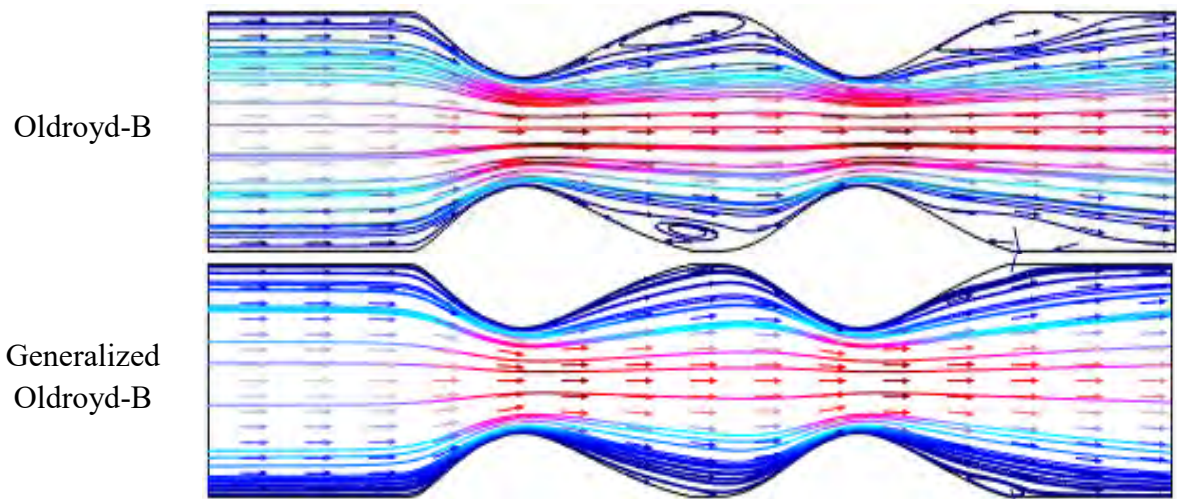


Figure 3.6: Stream lines of blood flow with vector through symmetric stenosis at $Re=100$ and $Wi = 0.6$

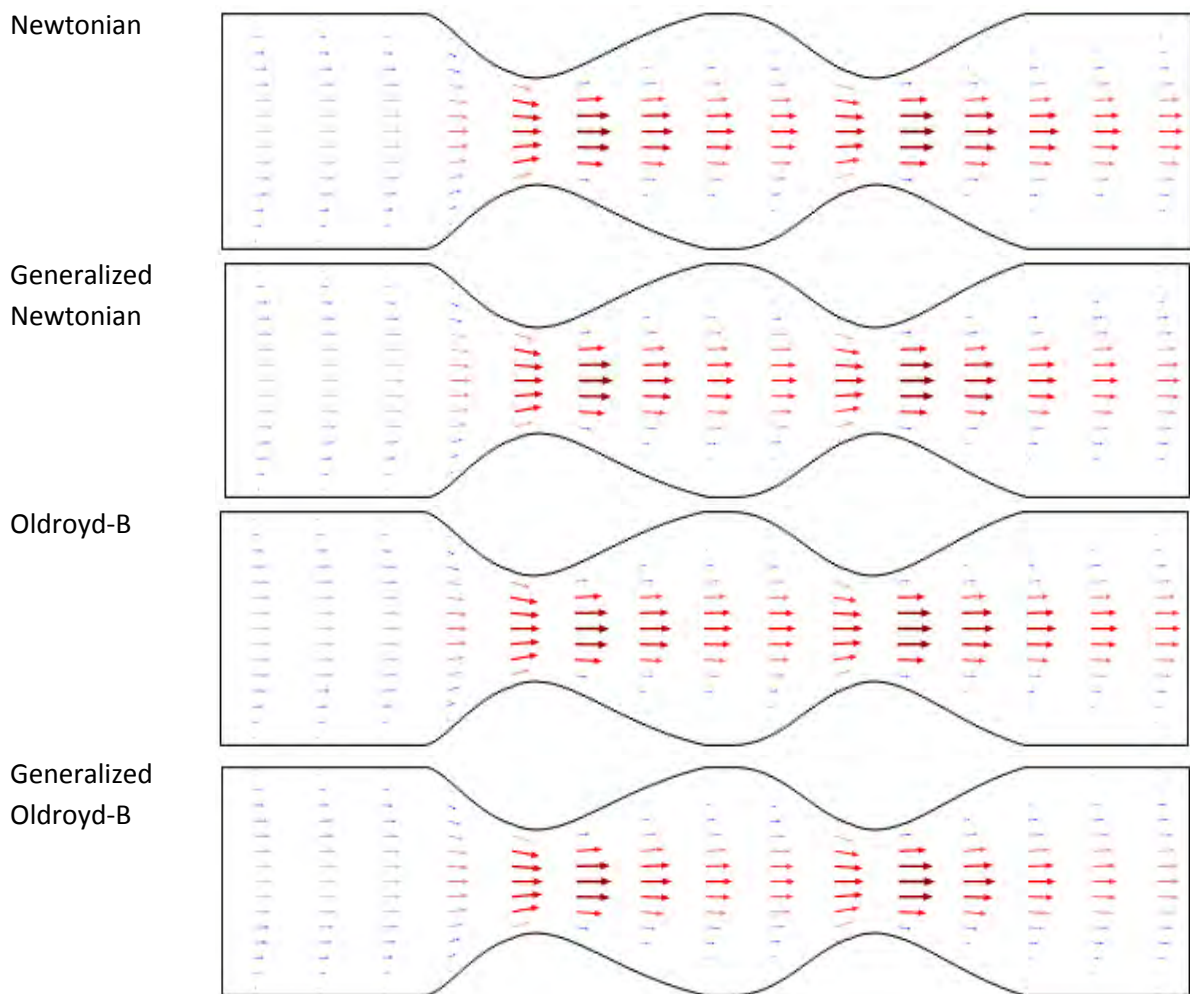


Figure 3.7: Velocity distribution on blood flow with vector arrow through symmetric stenosis at $Re=100$ and $Wi = 0.6$

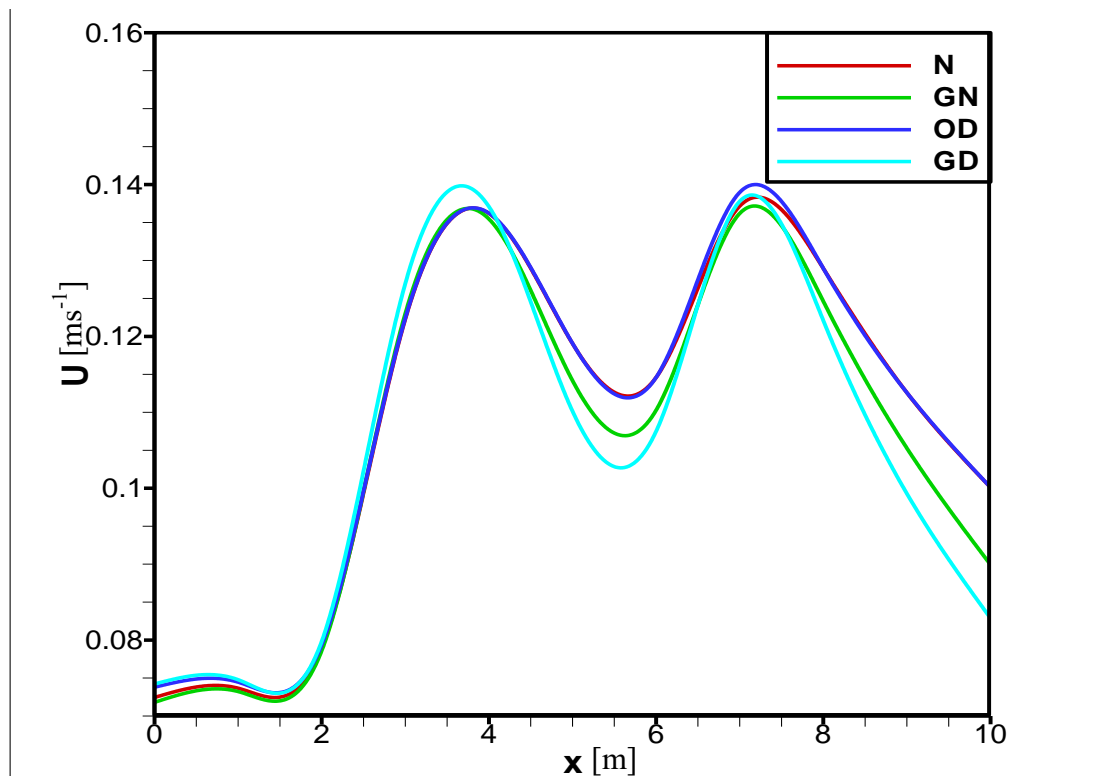


Figure 3.8: Velocity profile of blood flow along vessel axis for all models when $Re = 100$, $Wi=0.6$ and $q = 0.1\text{cm}^3/\text{s}$.

3.5.2 Symmetric stenosis effects on pressure distribution

In blood flow experiments blood pressure can easily be measured, in particular the pressure drops (i.e. the inlet-outlet pressure difference) needed to achieve a prescribed flow rate. In Figure 3.9, the axial pressure contours are presented for all the four models Newtonian, Generalized Newtonian, Oldroyd-B, Generalized Oldroyd-B with the flow rate $q = 0.2\text{ cm}^3/\text{s}$. These figures clearly show similarities among the four models at the inflow and outflow (far from the stenosis) of the artery with a developed pressure profile. While the difference in axial pressure profiles are pronounced at the around of stenosis, with some departures from the parabolic profile at second stenosis, due to great shear acting on the fluid in these regions. The pressure contour obtained relatively steep at far from the constriction regions but very intensive pressure gradient at stenosis.

Pressure is more dominated at stenosis regions because of the shear-thinning behavior of blood viscosity. It implies that, the flow is quicker than the non-Newtonian ones and its patterns remain in a disturbed state compare to others. In shear-thinning viscosity function (3.8) leads to the growth of the local viscosity in the low-shear regions at all cases. The axial pressure profiles are shown in Figure 3.10 for all four models at dimensionless number $Wi = 0.6$ and $Re=100$. Form Figure 3.10, the lowest value of

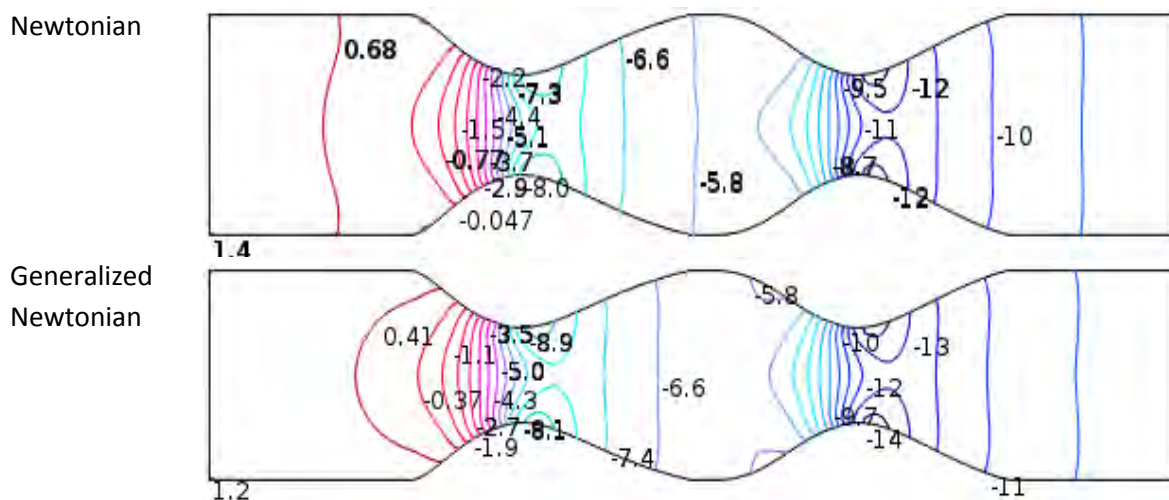
CHAPTER 3 NUMERICAL STUDY OF BLOOD FLOW... ..

pressure is found in second stenosis region. The main effect of the blood shear-thinning behavior is visible in the throat of stenosis, where the local viscosity increases greatly.

In Figure 3.10 the more negative values are found in the second stenosis region for generalized Newtonian and Oldroyd-B model which leads to non-Newtonian fluid is slower than Newtonian fluid. In Table 3.4, the numerical value of pressure obtained along blood vessel axis for all four models while $Re = 100$, $Wi = 0.6$ and $q = 0.2$ is presented.

Table 3.4: Numerical values of pressure are presented along vessel axis for all four models while $Re = 100$, $Wi = 0.6$ and $q = 0.1 \text{ cm}^3/\text{s}$.

Along vessel axis	Pressure (P)			
	Newtonian Model	Generalized Newtonian Model	Oldroyd-B Model	Generalized Oldroyd-B Model
0	0.995079141	0.998610322	0.998448191	0.997242004
1	0.735498997	0.641601056	0.754884445	0.61650652
2	0.122876754	-0.055150764	0.154373106	-0.145772918
3	-4.690719793	-5.066619856	-4.648226035	-5.706156529
4	-7.049941317	-7.565015747	-7.003165415	-8.66326103
5	-5.890207742	-6.315599669	-5.843389238	-7.313790517
6	-6.413371938	-7.092404681	-6.36541262	-8.401036198
7	-11.51431898	-12.66428871	-11.46724914	-15.03906105
8	-10.32620926	-11.38024981	-10.27869818	-13.68324387
9	-9.502362283	-10.50455761	-9.454816021	-12.79217817
10	-9.041404005	-10.13914344	-8.994475968	-12.51618949



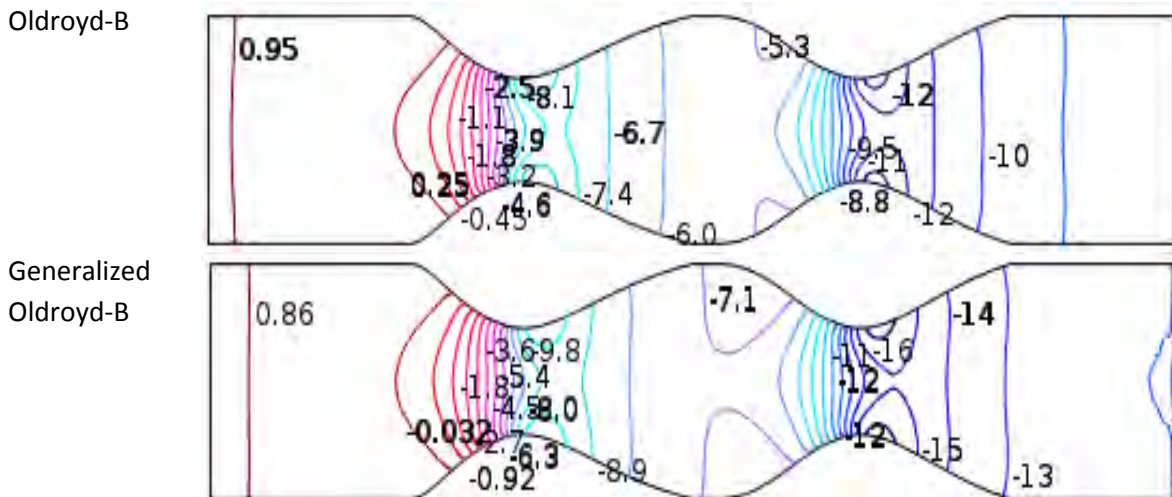


Figure 3.9: Pressure distribution on blood flow through Symmetric Stenosis at $Re=100$, $Wi = 0.6$ and $q = 0.1 \text{ cm}^3/\text{s}$.

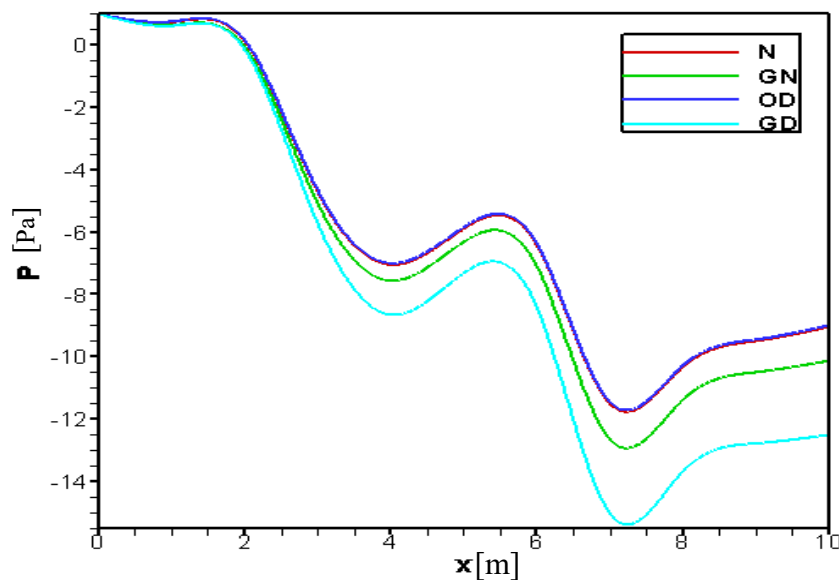


Figure 3.10: Pressure profile of blood flow along vessel axis for all models when $Re = 100$, $Wi = 0.6$ and $q = 0.1 \text{ cm}^3/\text{s}$.

3.5.3 Asymmetric stenosis effect

It is another remarkable effect on blood flow if the height of stenosis is different for velocity pressure distribution of the four dissimilar models as presented in Figures 3.11-3.12 with the flow rate $q = 0.1 \text{ cm}^3/\text{s}$. The different confine or recirculation zones are found in the stenotic height for various models. We observed that the vacuum space found which have created back flow of blood at close to the vessel wall after constriction zone for Newtonian and Oldroyd-B model. The parabolic profile has little deformed for non-symmetric stenosis. The comparable study of velocity and pressure for symmetric and asymmetric models has shown in Figures 3.13-3.15. From Figure 3.13a, the

CHAPTER 3 NUMERICAL STUDY OF BLOOD FLOW... ..

maximum velocity is found in second stenosis but lower velocity at non-symmetric stenosis.

On the other hand, the pressure distribution is presented for our considerable model with flow rate in Figure 3.12. There are some clearly dissimilarities among the four models at the first stenosis and second stenosis of the artery with developed parabolic pressure profile. Due to great shear acting on the fluid at constriction the pressure profile is more intensified. The steep pressure gradients are found far the stenosis area but in different at stenosis center. The lowest value of pressure is found in the near of second stenosis region but higher than symmetric stenosis. The most negative value is originated for generalized Oldroyd-B case at second constriction area which leads to non-Newtonian fluid.

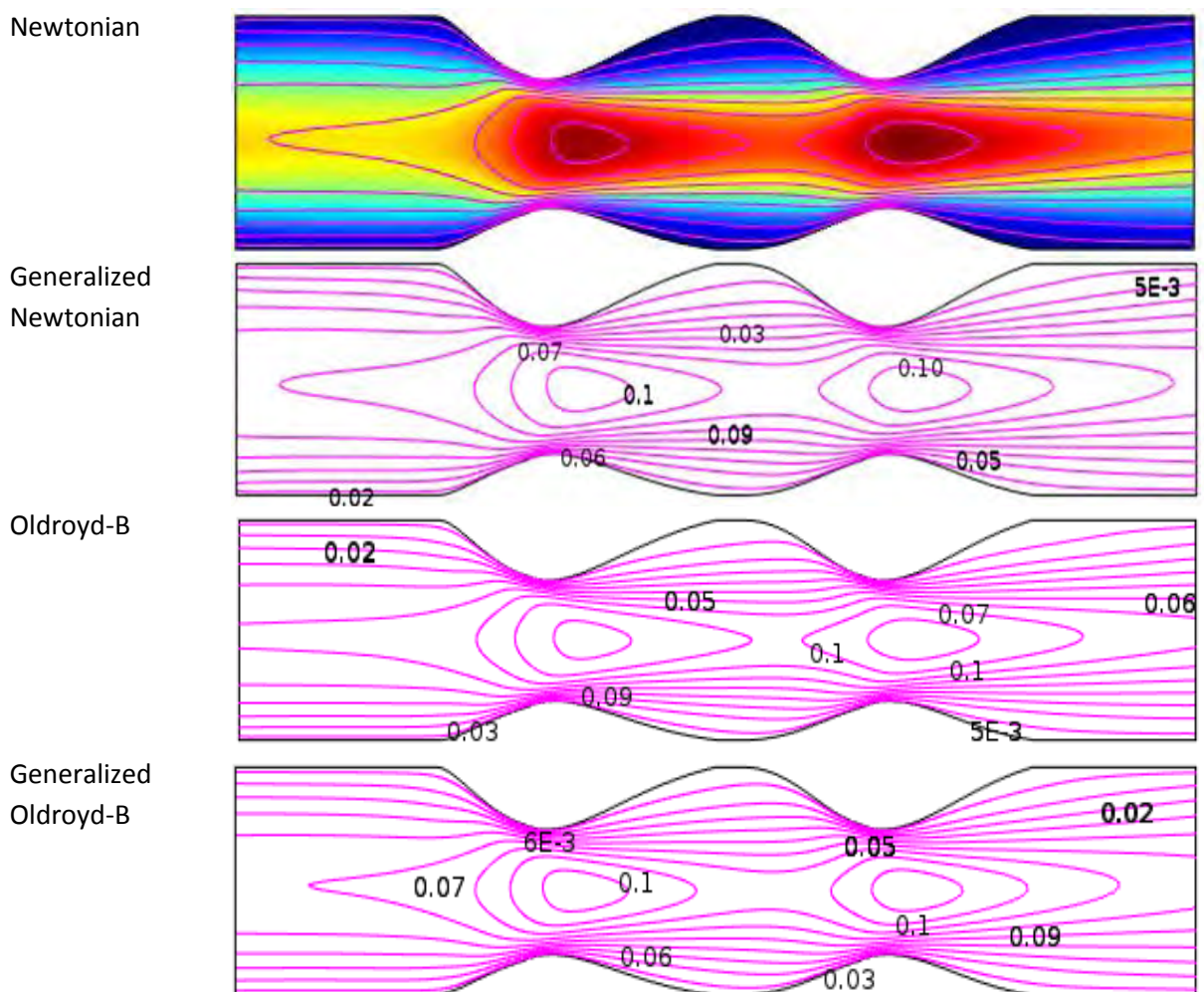


Figure 3.11: Velocity distribution on blood flow through non-symmetric Stenosis at $Re=100$ and $Wi = 0.6$ and $q = 0.1 \text{ cm}^3/\text{s}$.

CHAPTER 3 NUMERICAL STUDY OF BLOOD FLOW... ..

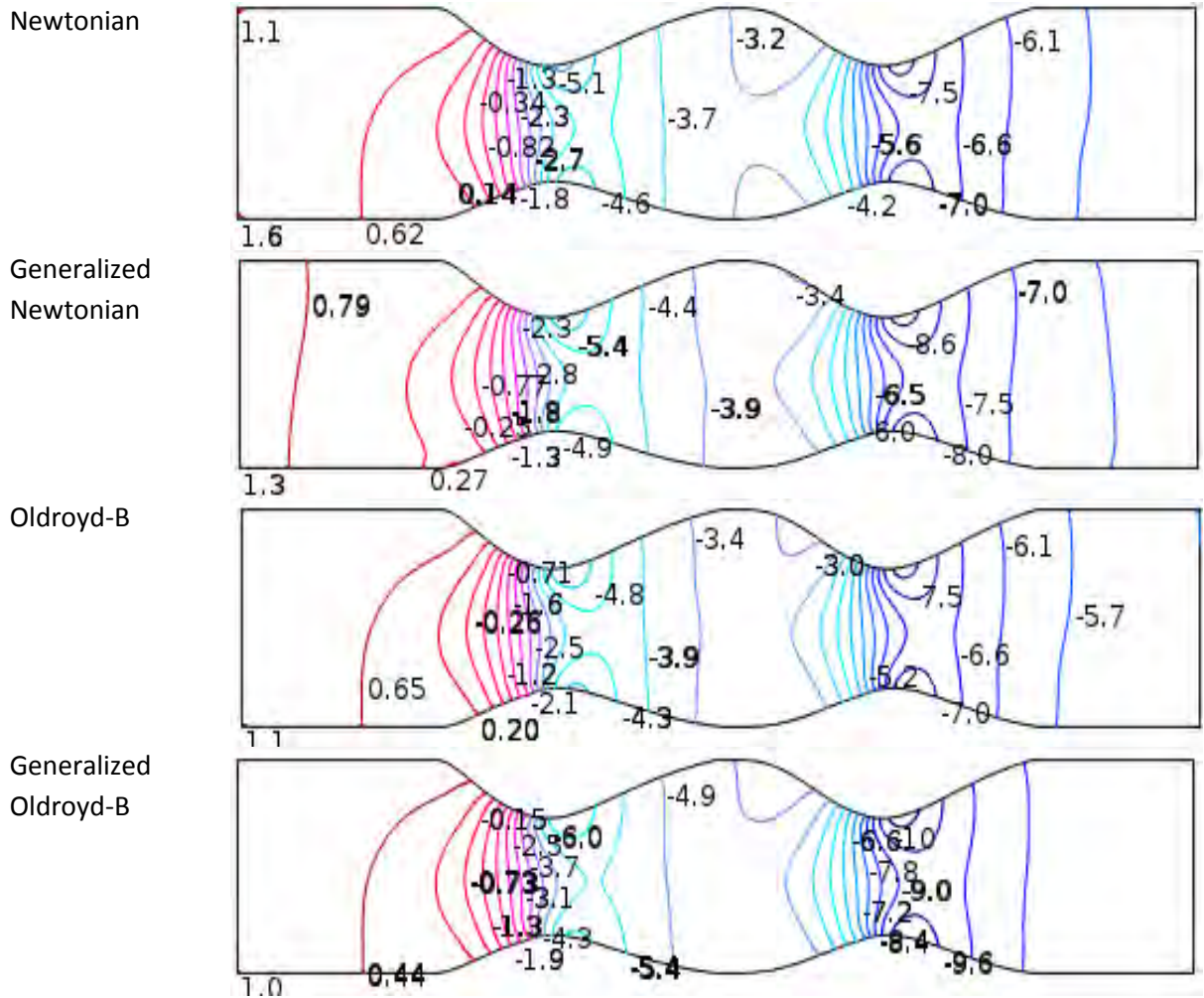


Figure 3.12: Pressure distribution on blood flow through asymmetric Stenosis at $Re=100$ and $Wi = 0.6$ and $q = 0.1 \text{ cm}^3/\text{s}$.

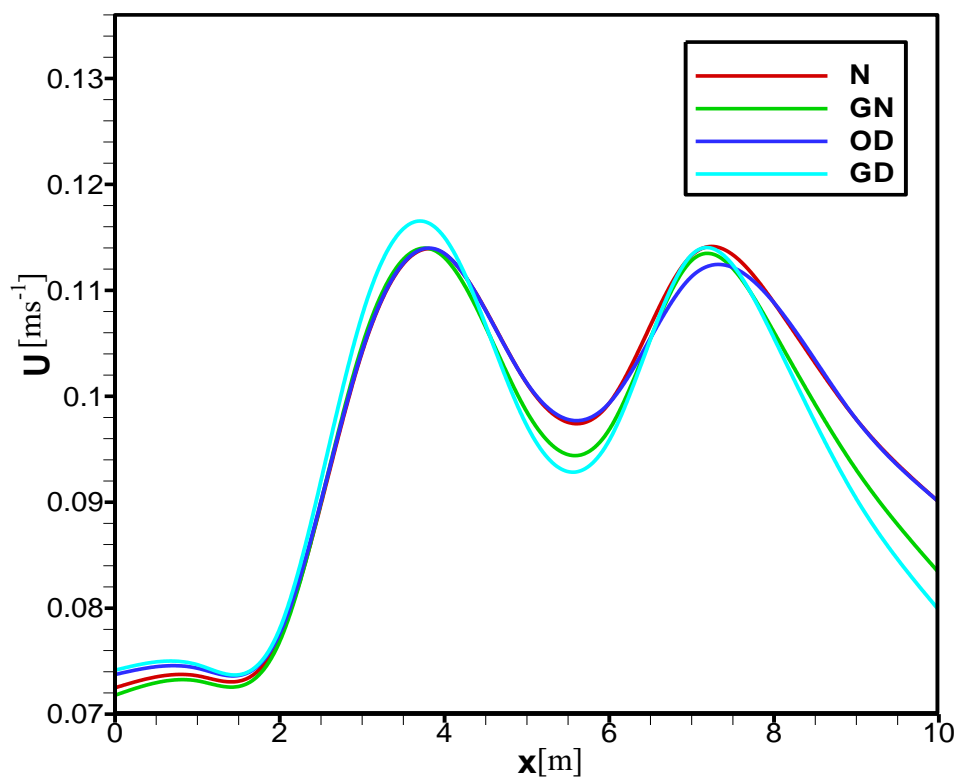


Figure 3.13a

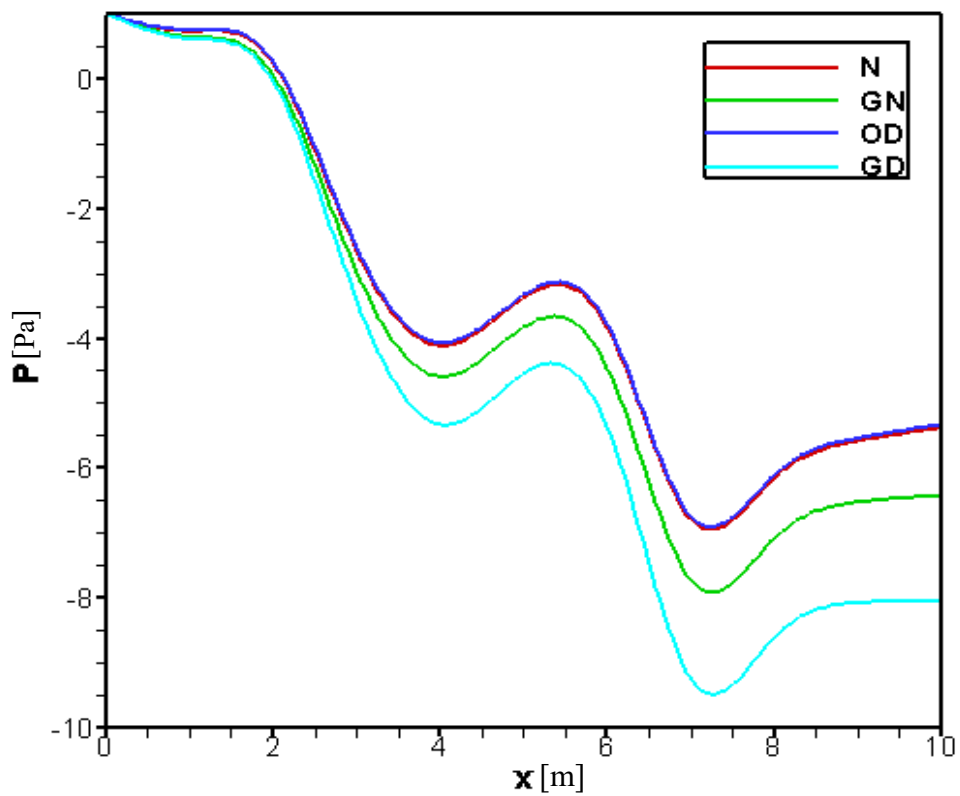


Figure 3.13b

Figure 3.13: Comparison of (Figure 3.13a) Blood Velocity and (Figure 3.13b) Blood Pressure distribution along vessel axis for asymmetric Stenosis

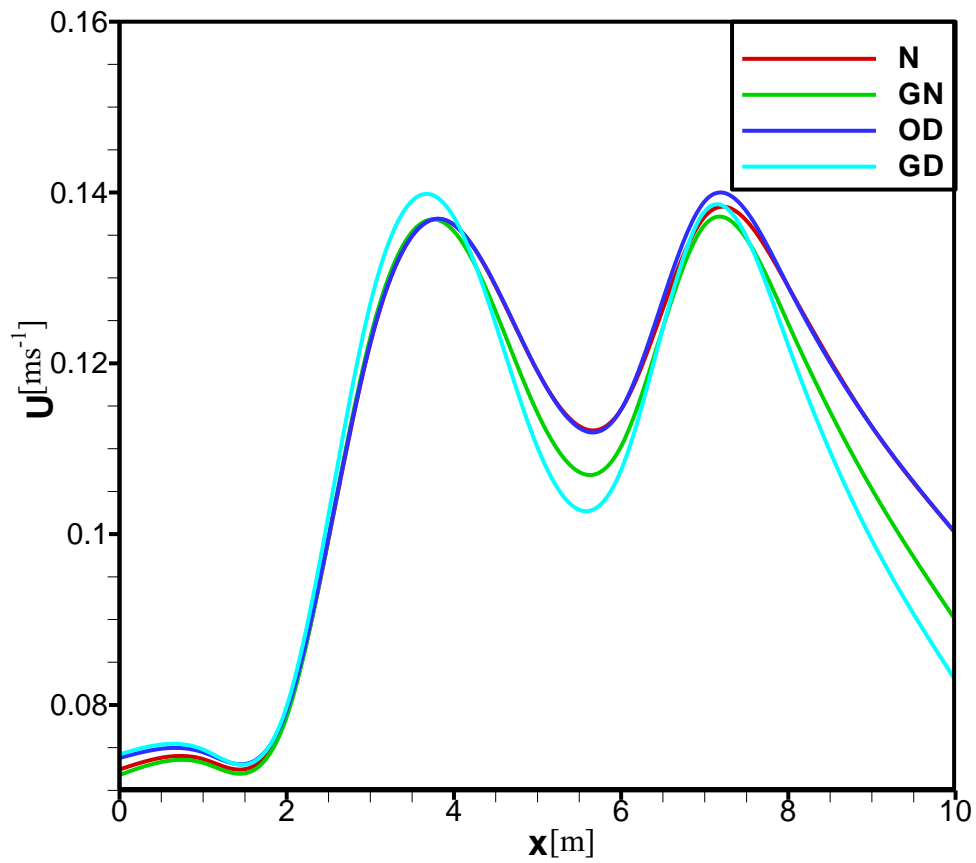


Figure 3.14a

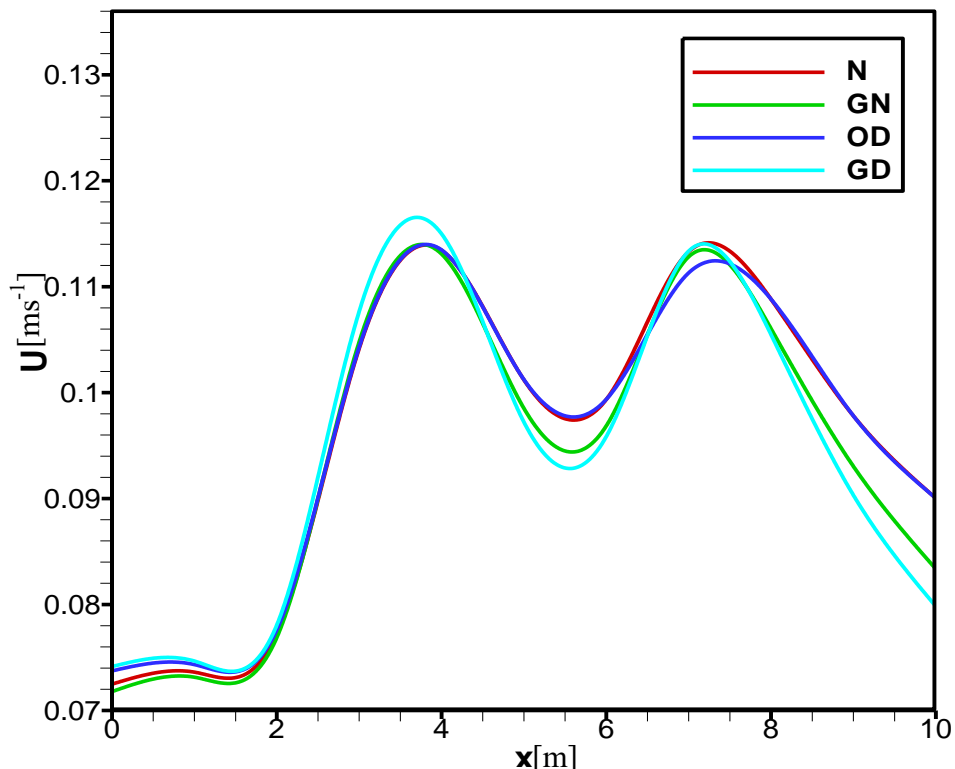


Figure 3.14b

Figure 3.14: Comparison of velocity profile for symmetric (Figure 3.14a) and asymmetric (Figure 3.14b) stenosis effects along vessel axis

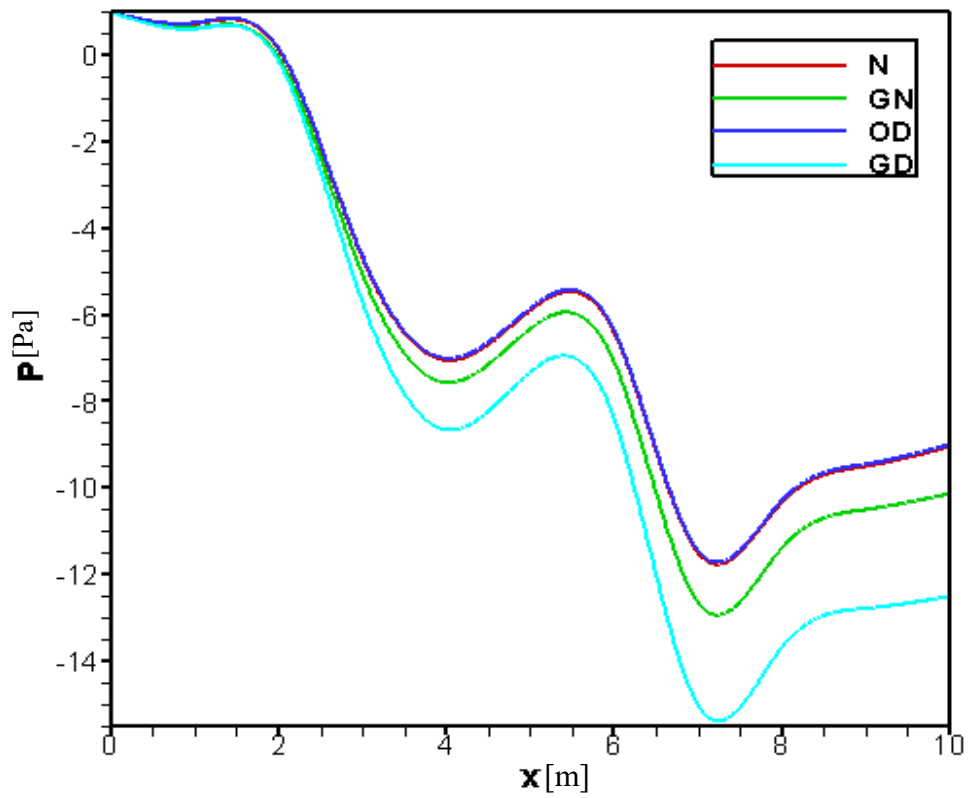


Figure 3.15a

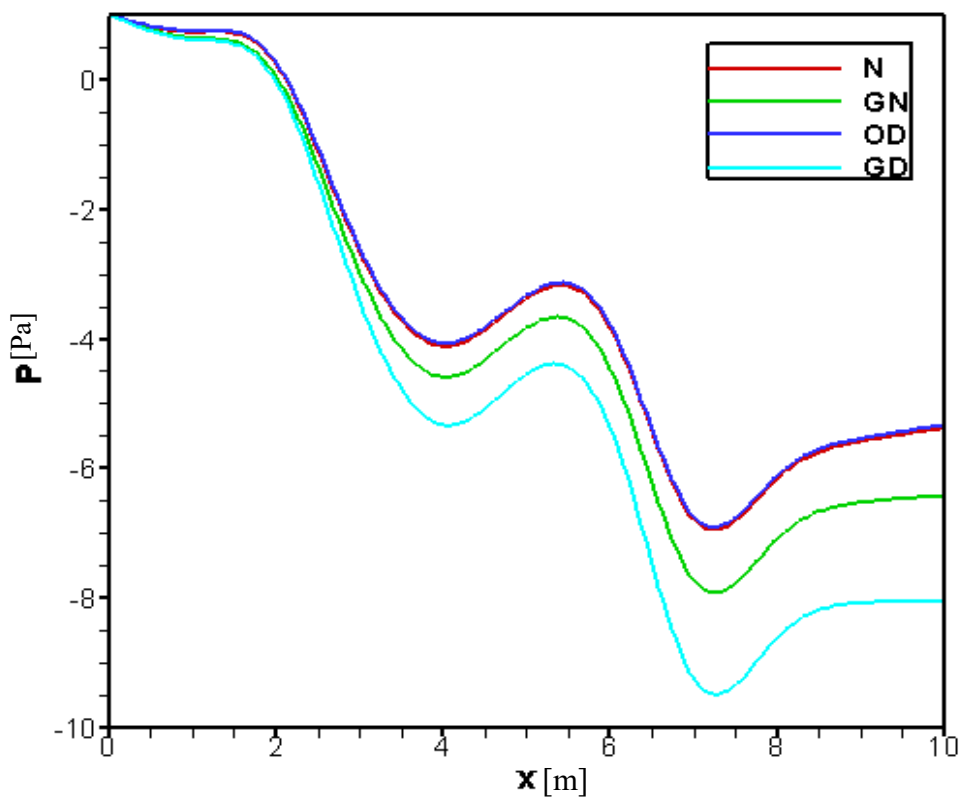


Figure 3.15b

Figure 3.15: Comparison of pressure profile for symmetric (Figure 3.15a) and asymmetric (Figure 3.15b) stenosis effects along vessel axis

3.5.4 Effects of dimensionless number

Reynold numbers (*Re*) effects

The Blood flow patterns affected by different Reynold numbers, *Re* (100, 500 and 1000) are shown in Figures 3.16-3.23 for all four models with *Wi* = 0.6 and *q* = 0.2cm³/m. It is seen that fluid developed parabolic profile at stenosis area in artery with the increases of *Re* and the pattern of blood flow for velocity and pressure distribution in terms of contour lines are shown in Figures 3.16-3.23. In Table 3.5, the average velocity obtained along vessel axis for different Reynold numbers while *Re* = 100, 500 and 1000 is presented.

Table 3.5: Velocity are obtained along vessel axis for different Reynold numbers, *Re* = 100, 500 and 1000 while *Wi* = 0.6 and *q* = 0.1 cm³/s.

Models	Velocity (<i>U</i>)					
	At first Stenosis			At second Stenosis		
	<i>Re</i> =100	<i>Re</i> =500	<i>Re</i> =1000	<i>Re</i> =100	<i>Re</i> =500	<i>Re</i> =1000
N	0.12285019	0.13841949	0.136573224	0.1544978	0.15062677	0.14515353
GN	0.12031713	0.13315758	0.13737259	0.15232078	0.15339416	0.14802205
OD	0.12283797	0.13841511	0.136613092	0.15449957	0.1506474	0.14516427
GD	0.12031713	0.13315759	0.137361681	0.15232078	0.15339419	0.14760520

For all models, the graphical representation of the average velocity and pressure variation for different Reynold numbers, *Re* = 100, 500 and 1000 with flow rate 0.2 cm³/s are shown in Figures 3.24-3.25. From these figures, we observe that average velocity speed up around stenosis area with the increases of Reynold numbers and it obtained peak value at second stenosis for all four models because of the effect of inertia. The velocity profile crosses each other between the stenosis for a little turbulence blood flow. In Figures 3.24, we also see that pressure distribution decrease along vessel axis with increases of Reynold numbers, *Re*. The lowest value of pressure is obtained at second stenosis for generalized Oldroyd-B model. In the case of generalized Oldroyd-B, pressurecontour lines becoming close each other because of blood shear-thinning behavior. In Table 3.6, the numerical value of pressureobtained along vessel axis for different Reynold numbers while *Re* = 100, 500 and 1000 is presented.

Table 3.6: Numerical value of pressure are obtained along vessel axis for different Reynold numbers, $Re = 100, 500$ and 1000 while $Wi = 0.6$ and $q = 0.1 \text{ cm}^3/\text{s}$.

Models	Pressure (P)					
	At first Stenosis			At second Stenosis		
	$Re=100$	$Re=500$	$Re=1000$	$Re=100$	$Re=500$	$Re=1000$
N	-2.18594129	-4.19061198	-6.81221242	-4.8318908	-7.8255203	-11.207662
GN	-4.07529027	-5.79128785	-8.38520390	-8.2884164	-11.142647	-14.662206
OD	-2.18706481	-4.16916653	-6.75792962	-4.8329671	-7.8034547	-11.152158
GD	-4.07623408	-5.79119330	-8.63268061	-8.2893602	-11.142555	-14.988180

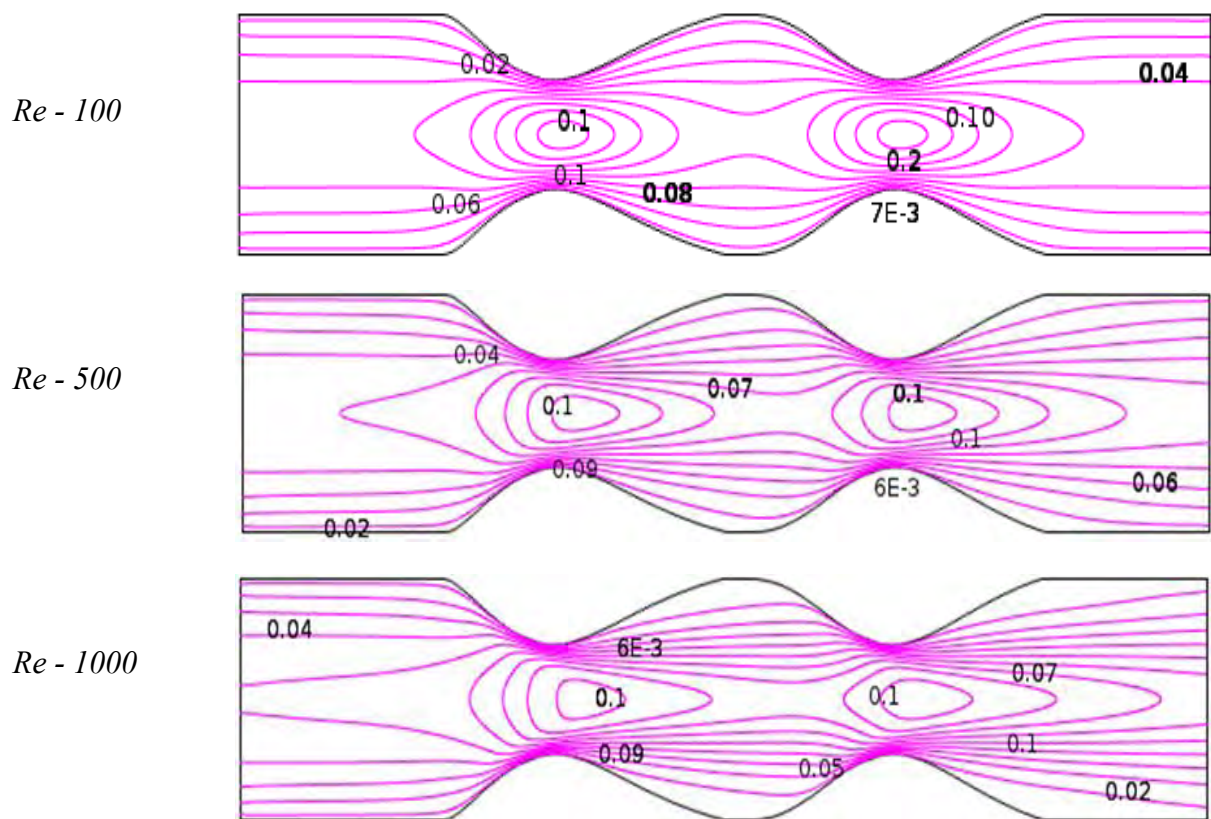


Figure 3.16: Reynlod Numbers (Re) effects on Blood flow of Newtonian Model at $Wi = 0.6$ and flow rate $0.1 \text{ cm}^3/\text{s}$.

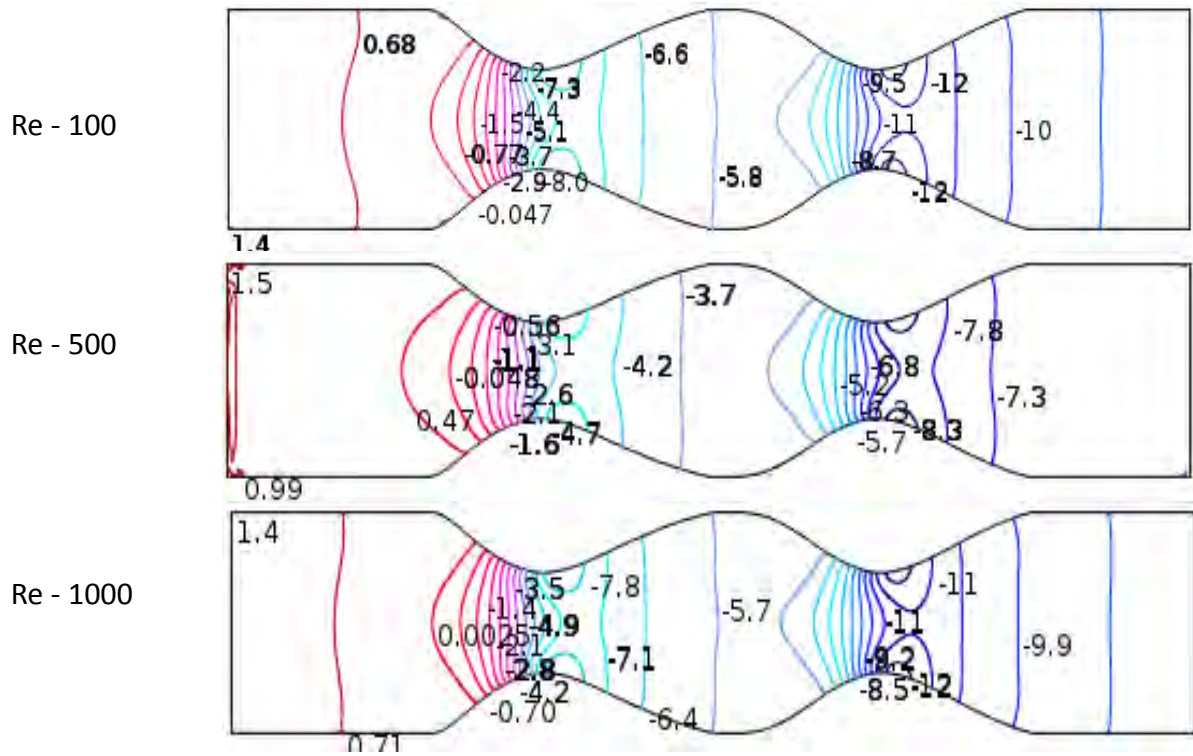


Figure 3.17: Renyld Numbers (Re) effects on pressure distribution of Blood flow for Newtonian Model at $Wi = 0.6$ and flow rate $0.1 \text{ cm}^3/\text{s}$.

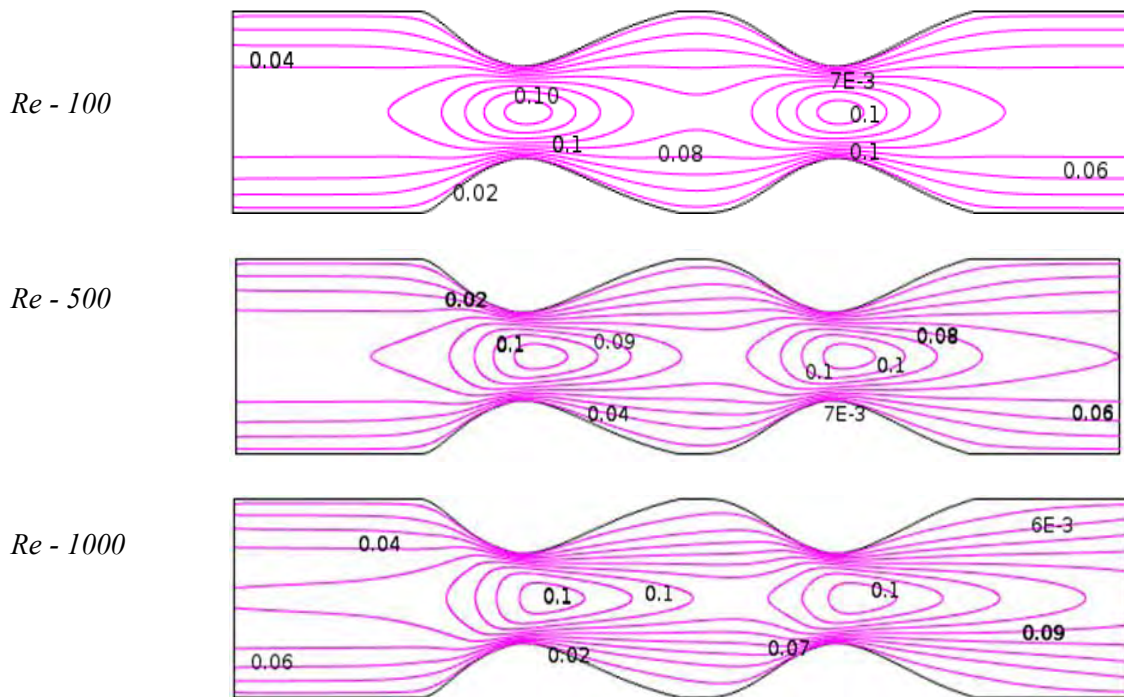


Figure 3.18: Renyld Numbers (Re) effects on Blood flow of generalized Newtonian Model at $Wi = 0.6$ and flow rate $0.1 \text{ cm}^3/\text{s}$.

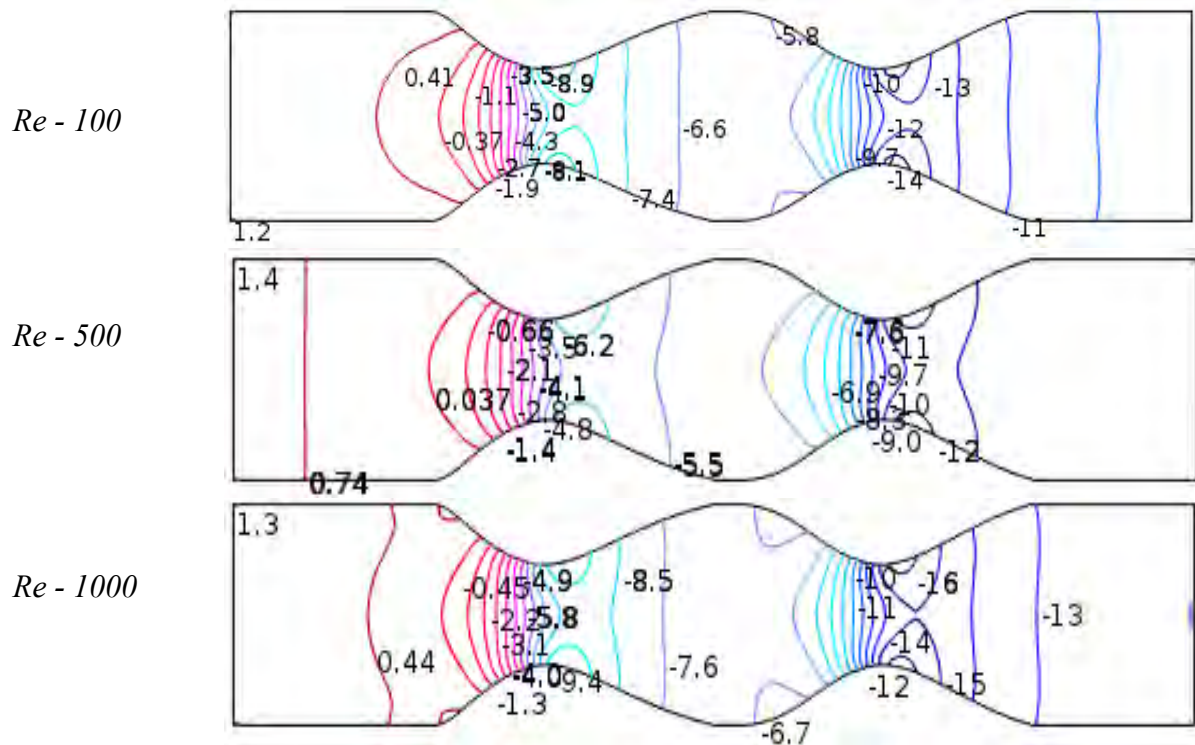


Figure 3.19: Renyloid Numbers (Re) effects on Blood flow of Generalized Newtonian Model at $Wi = 0.6$ and flow rate $0.1 \text{ cm}^3/\text{s}$.

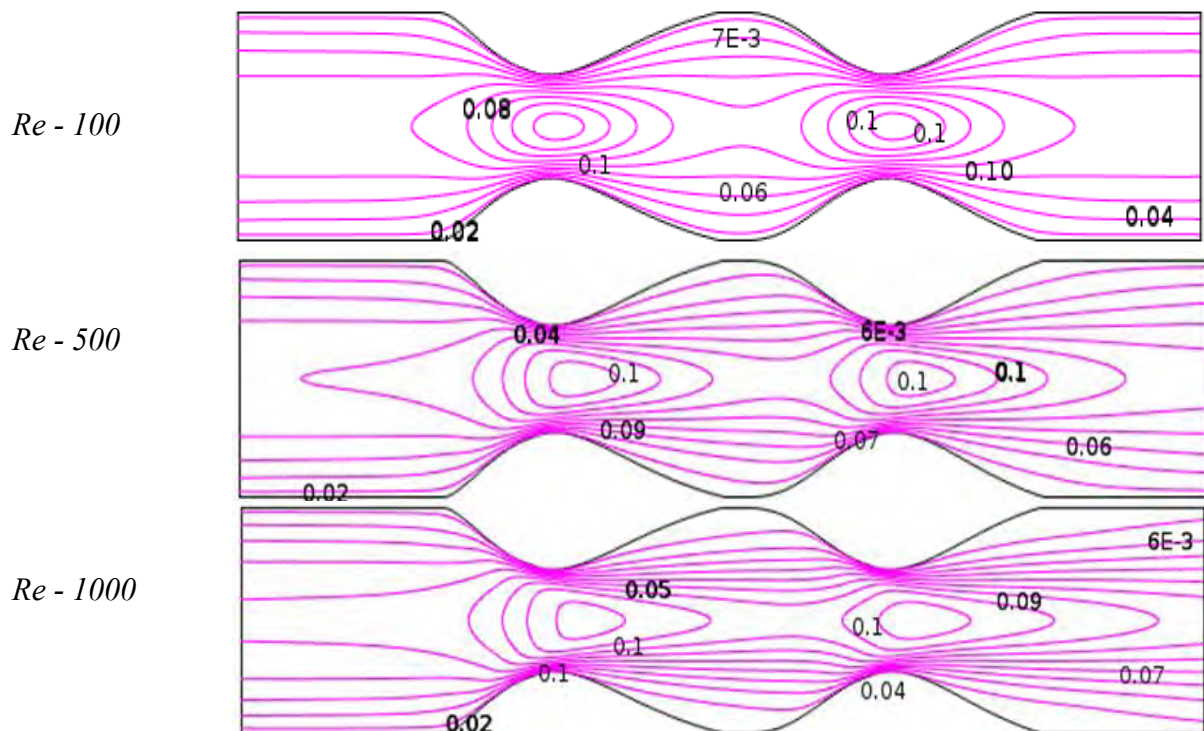


Figure 3.20: Renyloid Numbers (Re) effects on Blood flow of Oldroyd-B Model at $Wi = 0.6$ and flow rate $0.1 \text{ cm}^3/\text{s}$.

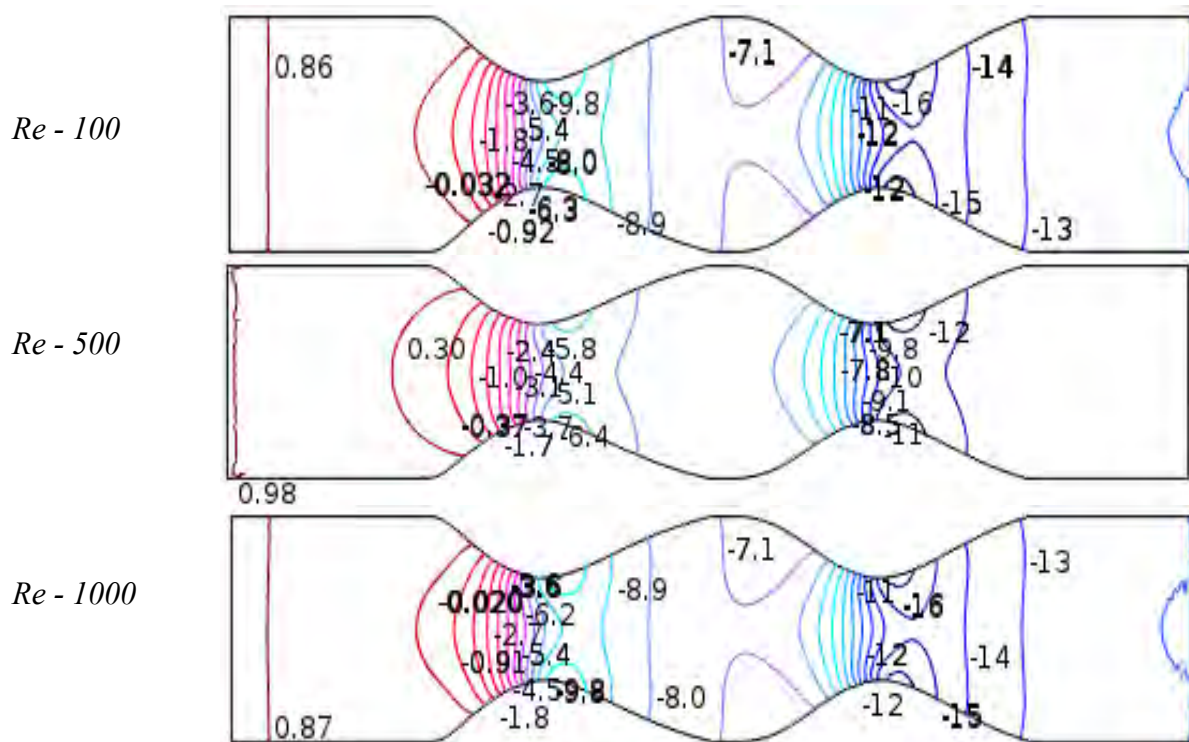


Figure 3.21: Renyod Numbers (Re) effects on pressure distribution of Blood flow for Oldroyd-B Model at $Wi = 0.6$ and flow rate $0.1 \text{ cm}^3/\text{s}$.

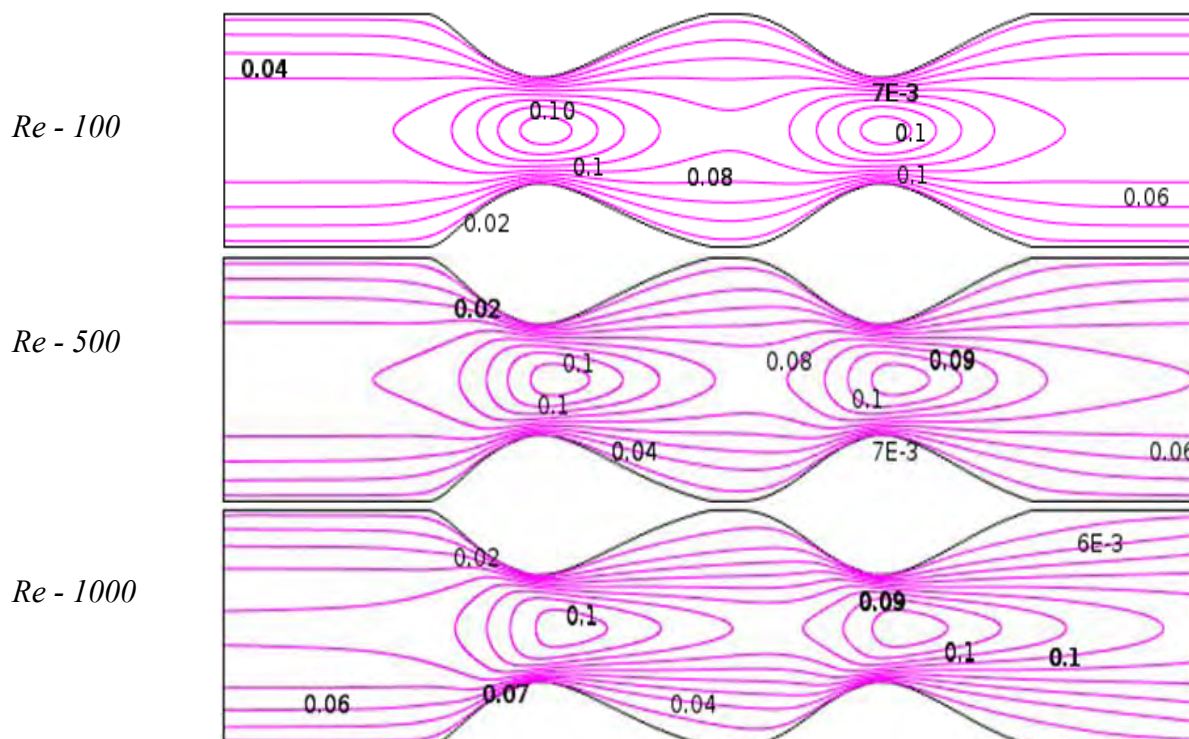


Figure 3.22: Renyod Numbers (Re) effects on Blood flow of Generalized Oldroyd-B Model at $Wi = 0.6$ and flow rate $0.1 \text{ cm}^3/\text{s}$.

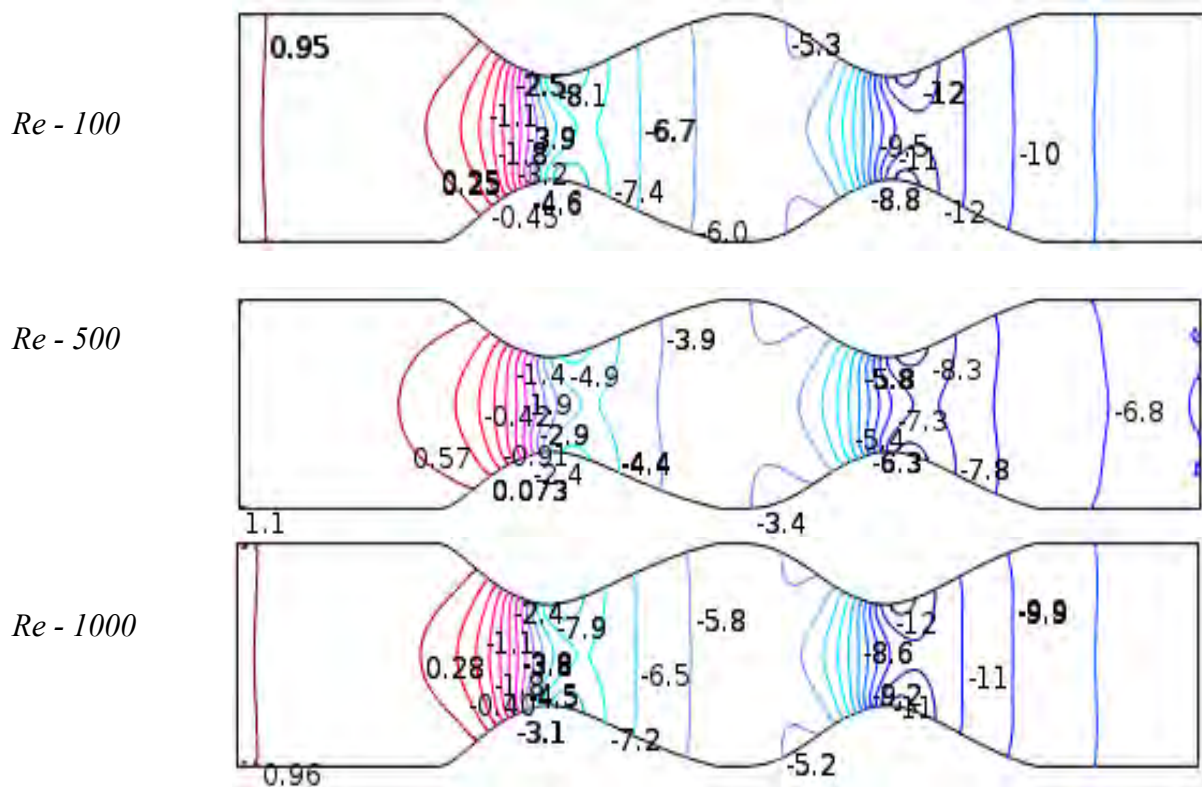


Figure 3.23: Renyloid Numbers (Re) effects on pressure distribution of Blood flow for generalized Newtonian Model at $Wi = 0.6$ and flow rate $0.1 \text{ cm}^3/\text{s}$.

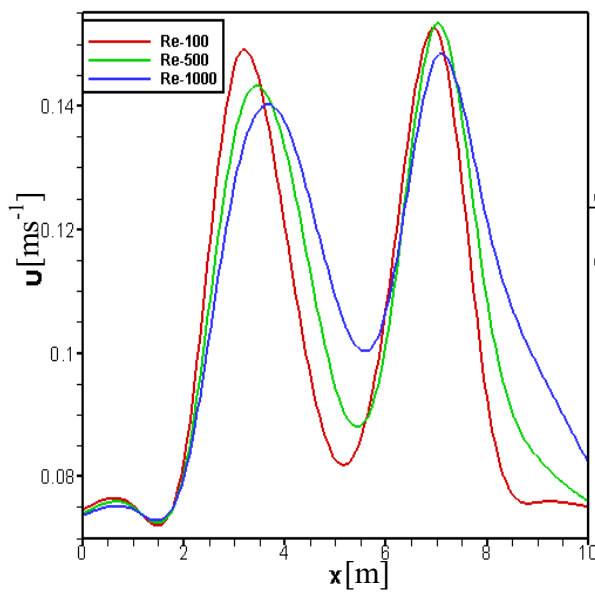


Figure 3.24a

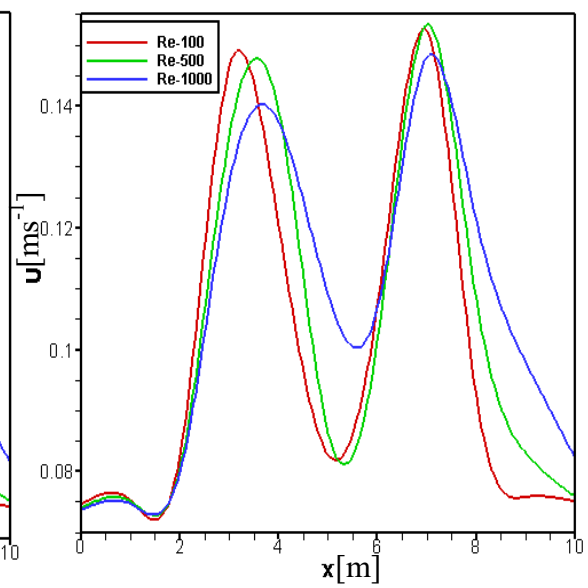


Figure 3.24b

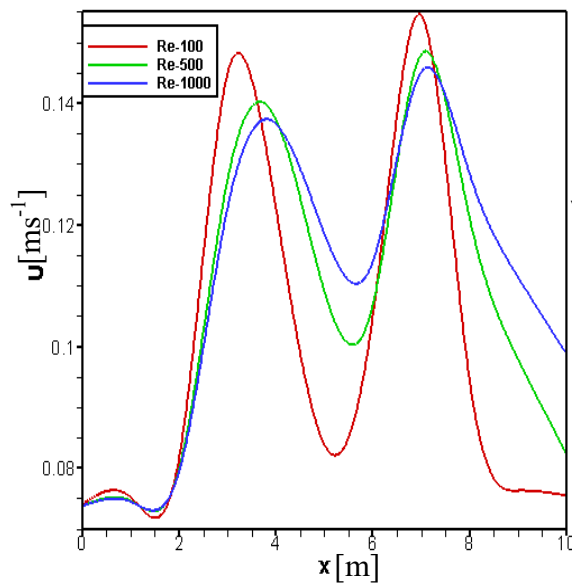


Figure 3.24c

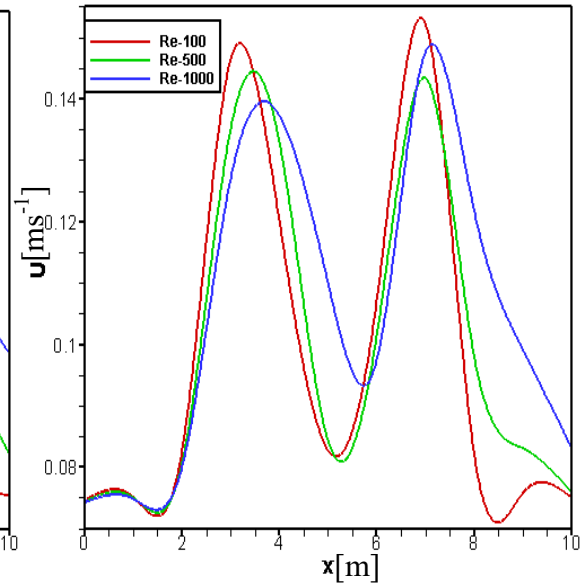


Figure 3.24d

Figure 3.24: Velocity profile of the Effects of Reynold numbers (Re) on Blood flow at $Wi = 0.6$ and flow rate $0.2 \text{ cm}^3/\text{s}$ for (Figure 3.24a) Newtonian Model, (Figure 3.24b) Generalized Newtonian Model, (Figure 3.24c) Oldroyd-B Model, and (Figure 3.24d) Generalized Oldroyd-B Model.

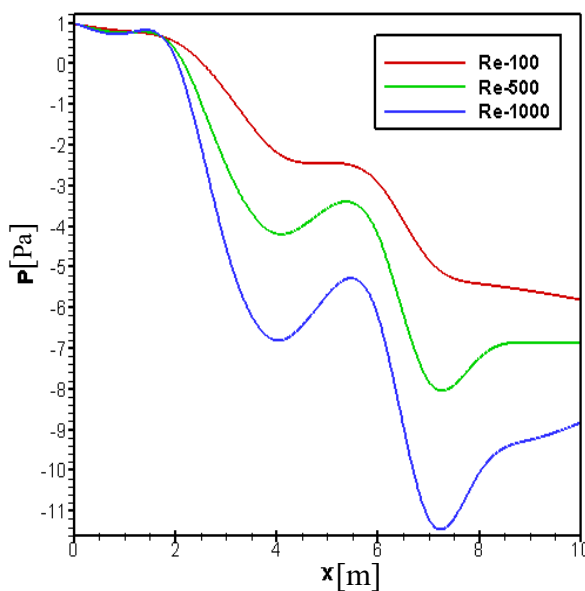


Figure 3.25a

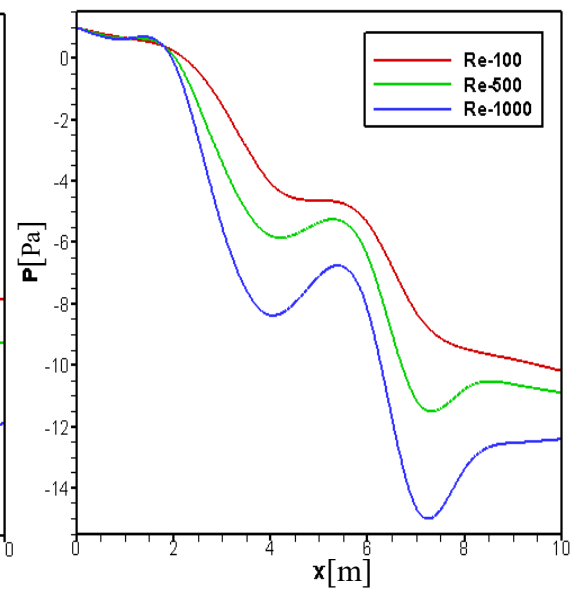


Figure 3.25b

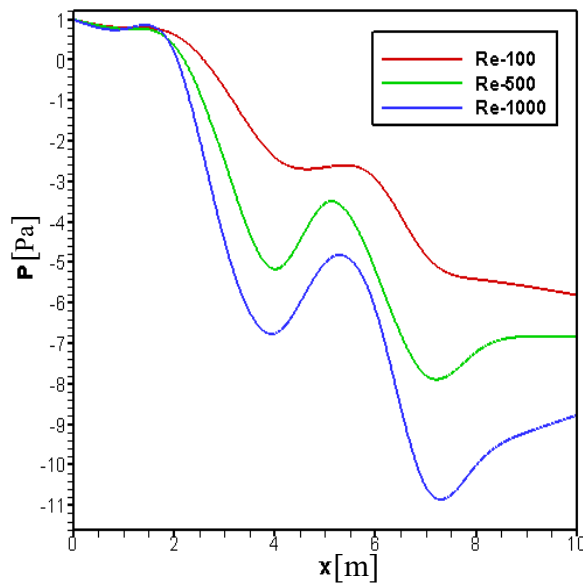


Figure 3.25c

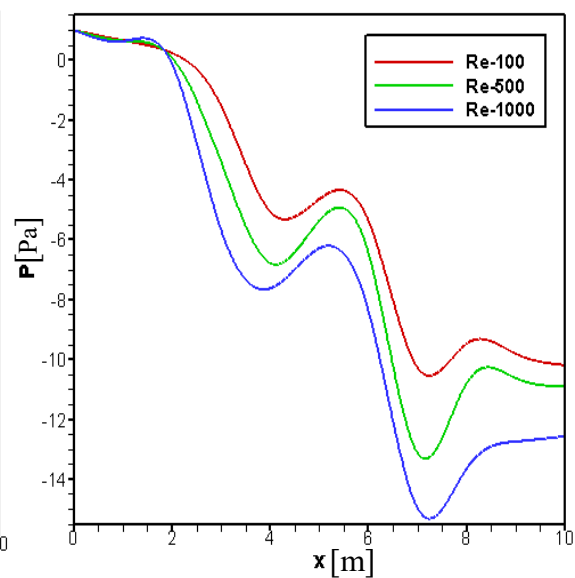


Figure 3.25d

Figure 3.25: Pressure profile of the Effects of Reynold numbers (Re) on Blood flow at $Wi = 0.6$ and flow rate $0.1 \text{ cm}^3/\text{s}$ for (Figure 3.25a) Newtonian Model, (Figure 3.25b) Generalized Newtonian Model, (Figure 3.25c) Oldroyd-B Model, and (Figure 3.25d) Generalized Oldroyd-B Model.

Weissenberg Numbers (Wi) Effects

Again, the effects of Weissenberg numbers, Wi (0.0, 0.5, 1.0) on blood flow are shown in Figures 3.26-3.33 for all four models with the flow rate at $Re = 100$. At $Wi = 0.0$ leads that the fluid is pure viscous fluid i.e. no elasticity while an infinite Weissenberg numbers limit corresponds to purely elastic response. At $Wi = 0.0$, we have found small confine area for all models. Since at low shear rate, blood aggregate are solid-like bodies, and has ability to store elastic energy. We observe that velocity contour lines have dense at the stenosis throat which indicate the blood velocity slight enlarged with the increases of Wi and create big confine zone at second constriction for $Wi = 1.0$. Due to less dominant of viscous force the velocity is higher at $Wi = 1.0$ which leads to bigger recirculation area and blood behave fluid-like bodies. At $Wi = 0.5$, a small circulation area has found at the centre of stenosis and just after stenosis velocity fall down and create a back flow adjacent to vessel wall. In Figure 3.34, we attained maximum value of velocity at center of stenosis for all four models and have little different at beginning. In Table 3.7, the numerical value of velocity obtained along vessel axis at throat of stenosis for different Weissenberg numbers while $Wi = 0.0, 0.5$ and 1.0 is presented.

Table 3.7: Blood velocity is presented for various Weissenberg numbers, $Wi = 0.0, 0.5$ and 1.0 while $Re = 100$ and $q = 0.1 \text{ cm}^3/\text{s}$.

Models	Velocity (U)					
	At first Stenosis			At second Stenosis		
	$Wi=0.0$	$Wi=0.5$	$Wi=1.0$	$Wi=0.0$	$Wi=0.5$	$Wi=1.0$
N	0.13497634	0.13619820	0.13678027	0.14506764	0.14496746	0.14475503
GN	0.13402507	0.13546135	0.13627702	0.14417983	0.14419503	0.14397909
OD	0.13490637	0.1362318	0.13683679	0.14506252	0.14497107	0.14474881
GD	0.13622025	0.13749055	0.13836750	0.14763397	0.14778152	0.14765851

The pressure is more dominated at the constriction area of the stenosis cavity for all models which are shown in odd number Figures 3.26-3.33. At stenosis regions pressure is lower than other region because of the shear-thinning characteristics of blood viscosity which leads the flow is faster than the non-Newtonian ones and its patterns remain in a disturbed state compare to others. From Figure 3.35, the minimum value of pressure is found at second stenosis area and pressure profiles are almost similar at generalized Oldroyd-B model. In Figure 3.35, the numerical values of pressure distribution are presented for all the four models Newtonian, Generalized Newtonian, Oldroyd-B, Generalized Oldroyd-B with the flow rate $q = 0.2 \text{ cm}^3/\text{s}$. In Table 3.8, the pressure obtained along vessel axis at constriction for different Weissenberg numbers while $Wi = 0.0, 0.5$ and 1.0 is presented.

Table 3.8: Numerical pressure is obtained along vessel axis at constriction for different Weissenberg numbers while, $Wi = 0.0, 0.5$ and 1.0 while $Re = 100$ and $q = 0.1 \text{ cm}^3/\text{s}$.

Models	Pressure (P)					
	At first Stenosis			At second Stenosis		
	$Wi=0.0$	$Wi=0.5$	$Wi=1.0$	$Wi=0.0$	$Wi=0.5$	$Wi=1.0$
N	-6.69929172	-7.04994131	-7.09259017	-11.2366119	-11.5143189	-11.5077824
GN	-7.37517020	-7.56501574	-7.58516418	-12.5500529	-12.6642887	-12.6323679
OD	-6.85269457	-7.00316541	-7.03559779	-11.3926709	-11.4672491	-11.4486727
GD	-8.61595339	-8.66326103	-8.65927274	-15.0563381	-15.0390610	-14.9913434

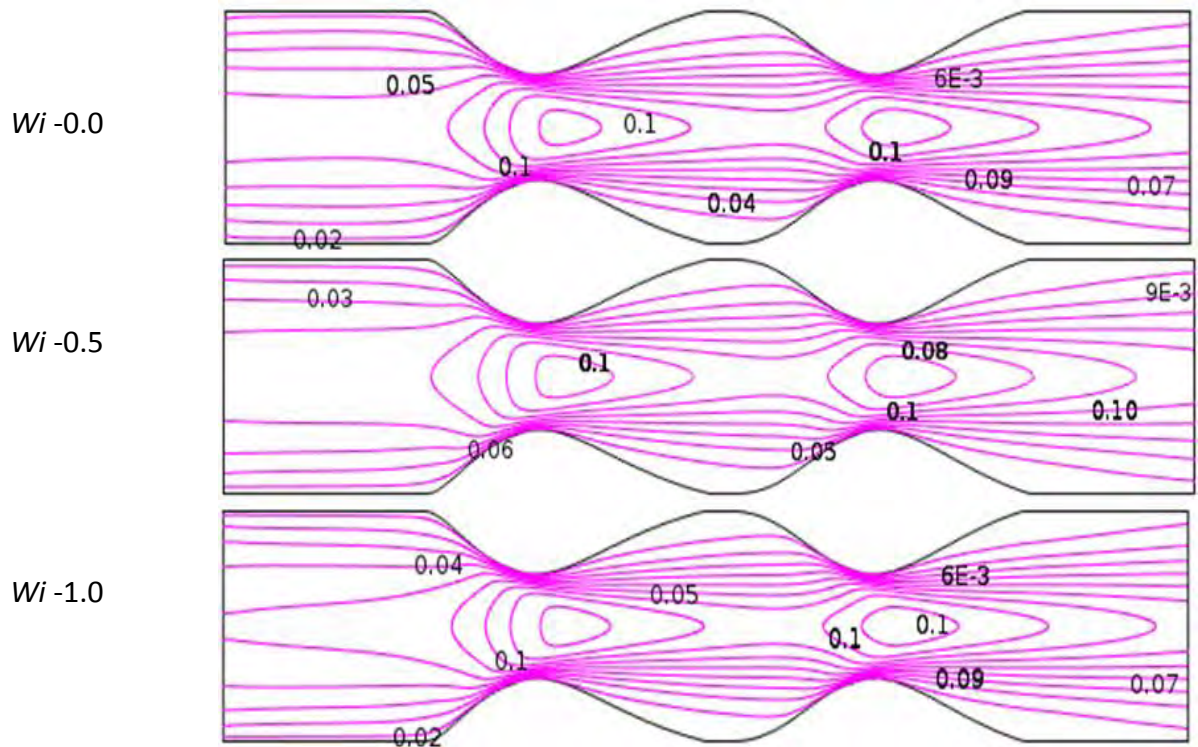


Figure 3.26: Weissenberg Numbers (Wi) effects on blood flow of Newtonian model at $Re = 100$ and flow rate $0.1 \text{ cm}^3/\text{s}$.

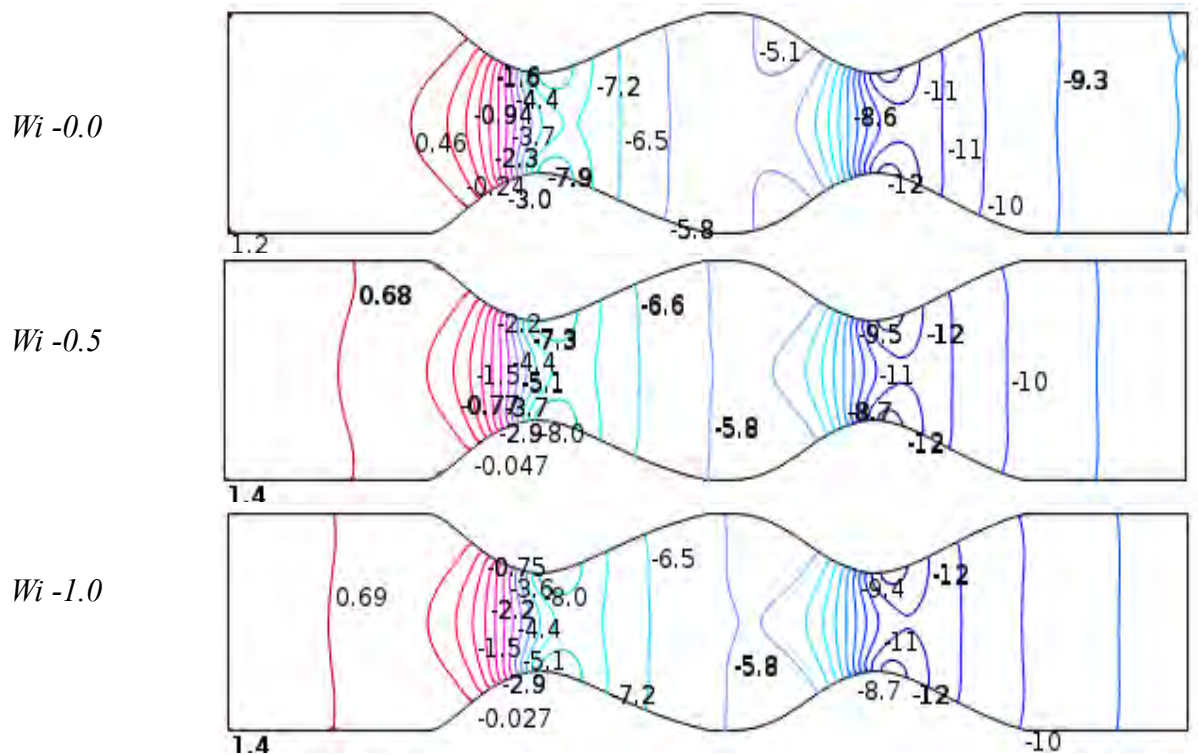


Figure 3.27: Weissenberg Numbers (Wi) effects on pressure distribution of blood flow for Newtonian model at $Re = 100$ and flow rate $0.1 \text{ cm}^3/\text{s}$.

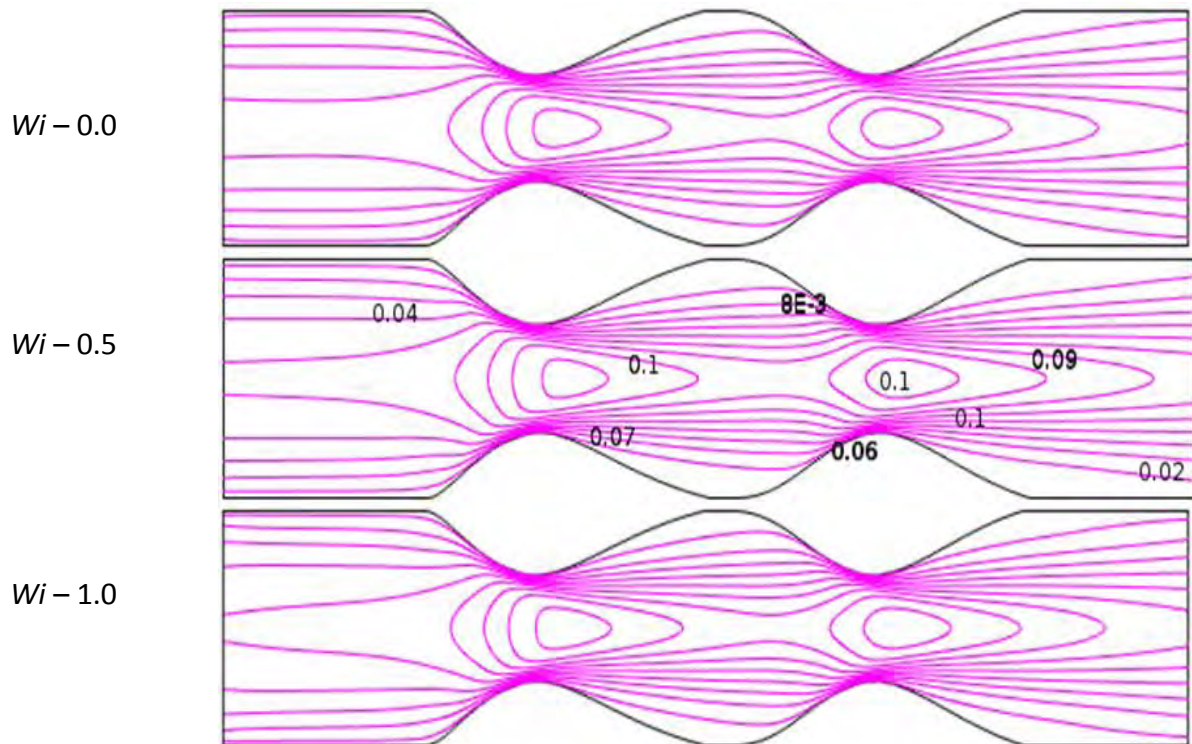


Figure 3.28: Weissenberg Numbers (Wi) effects on velocity distribution of blood flow for Generalized Newtonian model at $Re = 100$ and flow rate $0.1 \text{ cm}^3/\text{s}$.

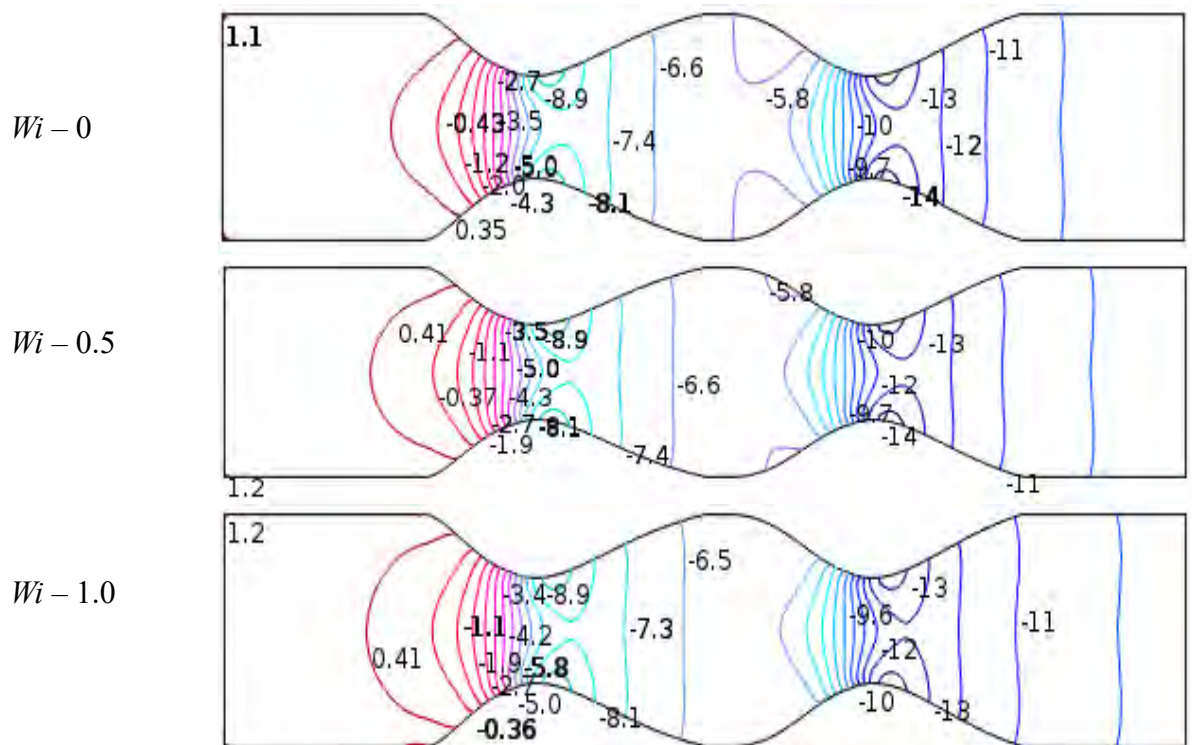


Figure 3.29: Weissenberg Numbers (Wi) effects on pressure distribution of blood flow for Generalized Newtonian model at $Re = 100$ and flow rate $0.1 \text{ cm}^3/\text{s}$.

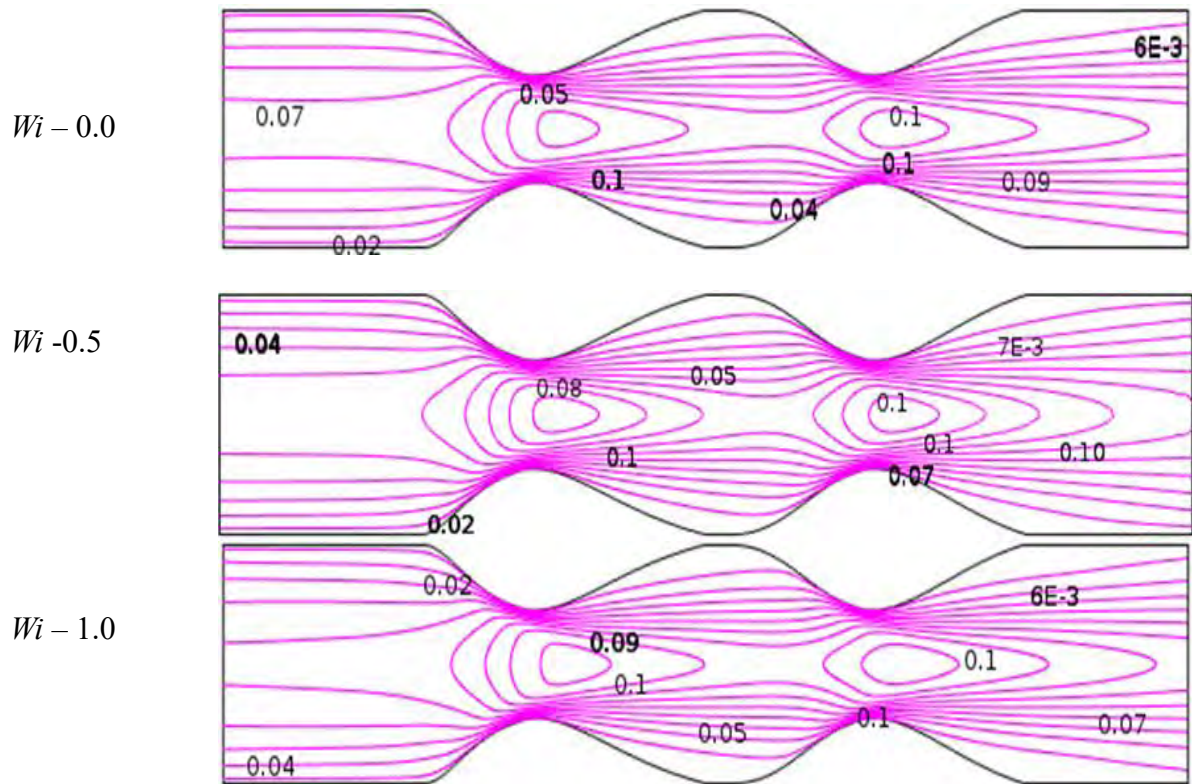


Figure 3.30: Weissenberg Numbers (Wi) effects on velocity distribution of blood flow for Oldroyd-B model at $Re = 100$ and flow rate $0.1 \text{ cm}^3/\text{s}$.

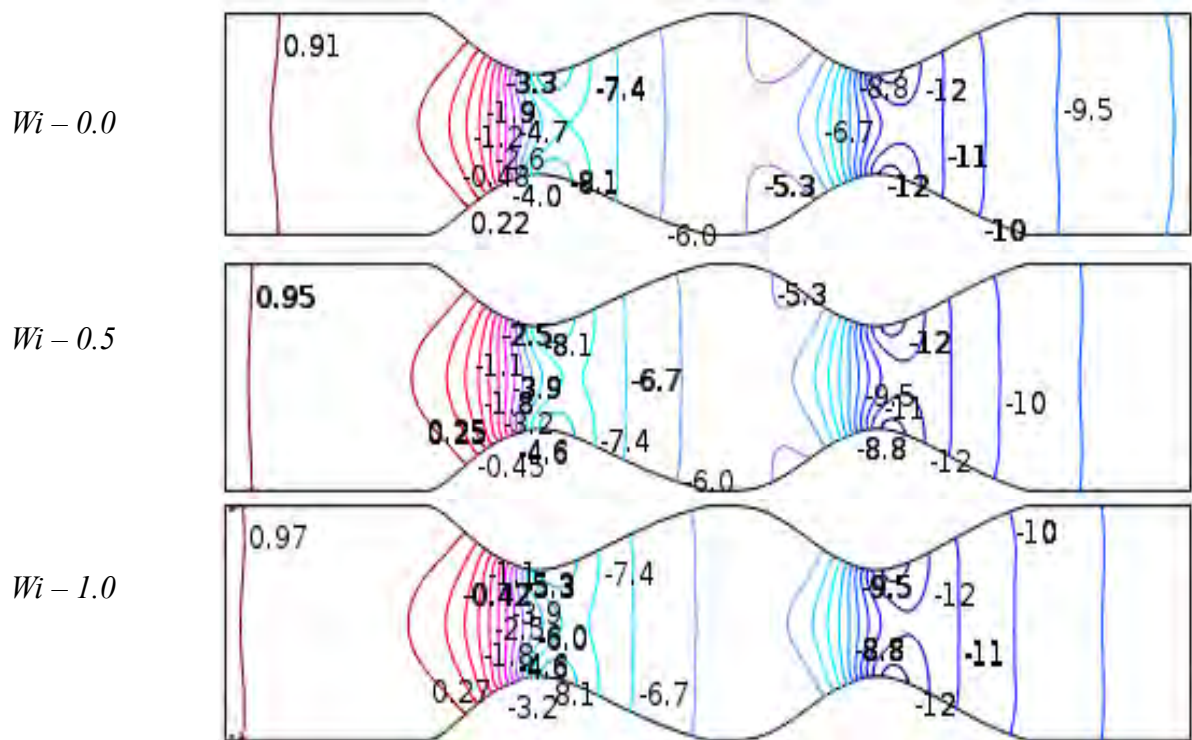


Figure 3.31: Weissenberg Numbers (Wi) effects on pressure distribution of blood flow for Oldroyd-B model at $Re = 100$ and flow rate $0.1 \text{ cm}^3/\text{s}$.

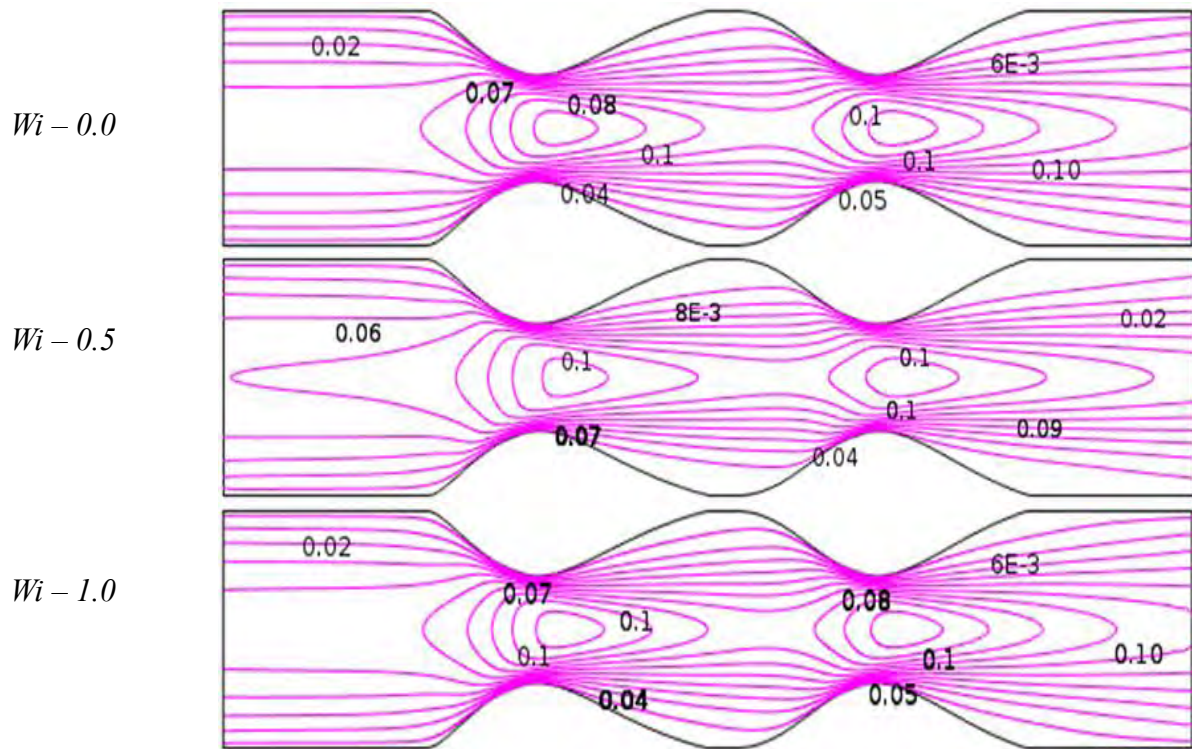


Figure 3.32: Weissenberg Numbers (Wi) effects on velocity distribution of blood flow for Generalized Oldroyd-B model at $Wi = 0.6$ and flow rate $0.1 \text{ cm}^3/\text{s}$.

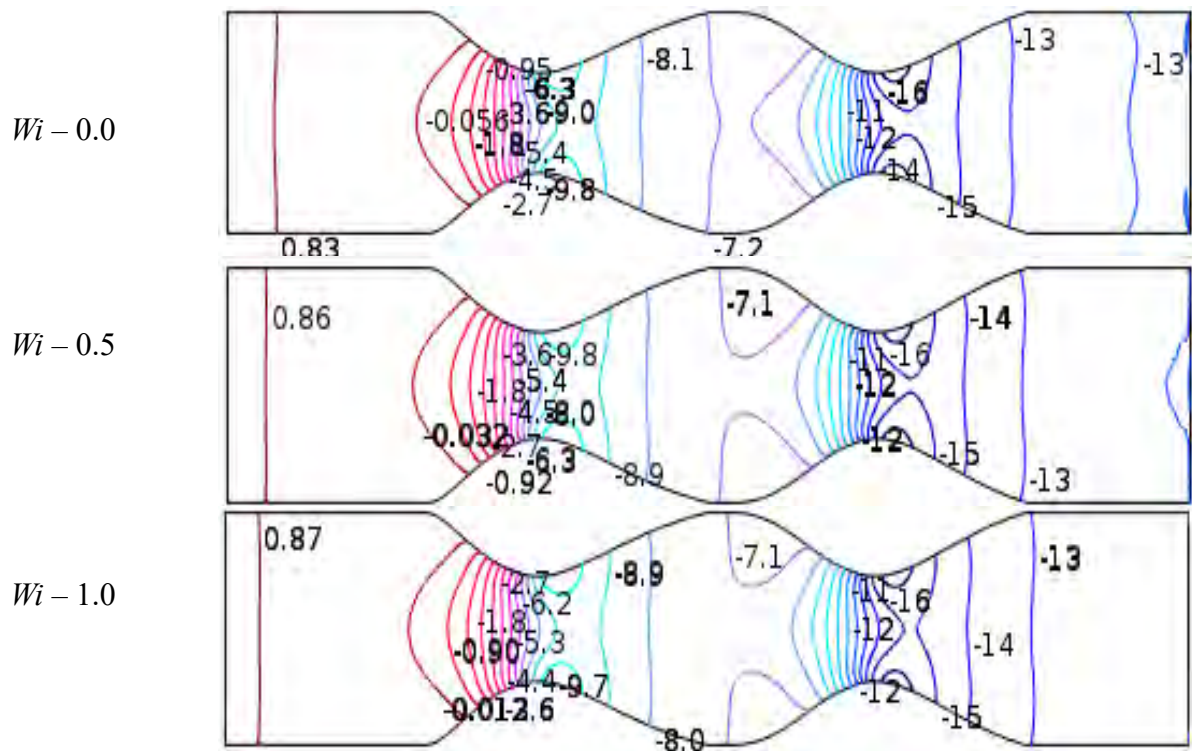


Figure 3.33: Weissenberg Numbers (Wi) effects on pressure distribution of blood flow for generalized Oldroyd-B model at $Wi = 0.6$ and flow rate $0.1 \text{ cm}^3/\text{s}$.

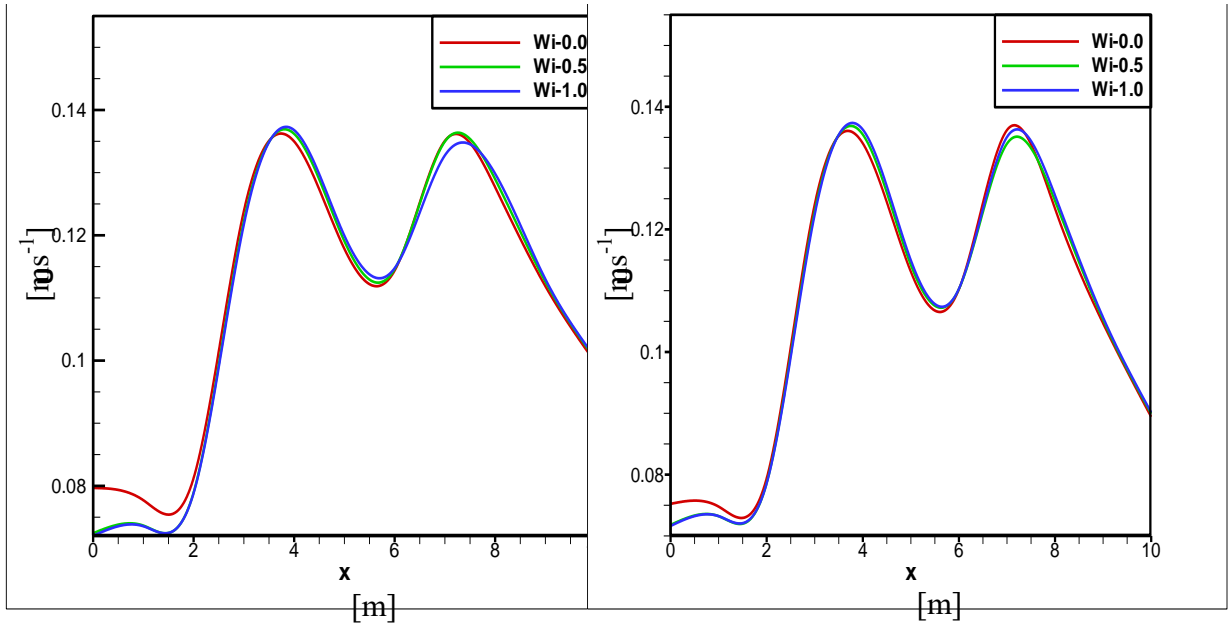


Figure 3.34a

Figure 3.34b

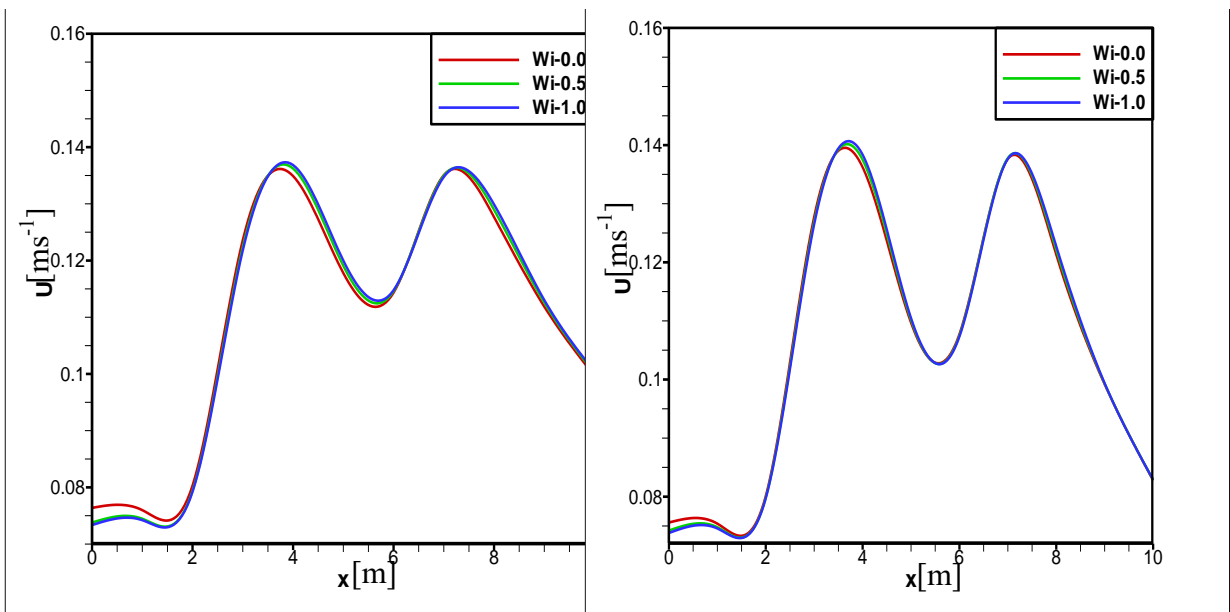


Figure 3.34c

Figure 3.34d

Figure 3.34: Velocity profile of the Effects of Reynold numbers (Re) on Blood flow at $Wi = 0.6$ and flow rate $0.1 \text{ cm}^3/\text{s}$ for (Figure 3.34a) Newtonian Model, (Figure 3.34b) Generalized Newtonian Model, (Figure 3.34c) Oldroyd-B Model, and (Figure 3.34d) Generalized Oldroyd-B Model.

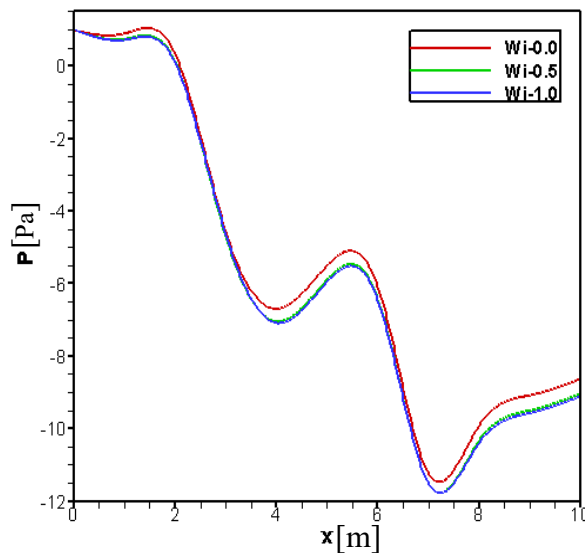


Figure 3.35a

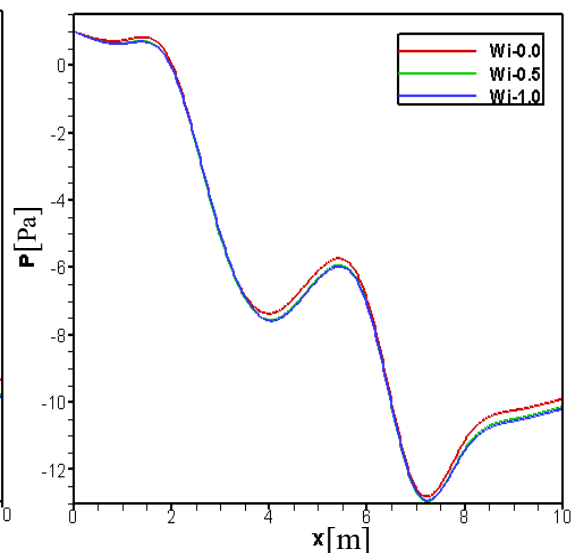


Figure 3.35b

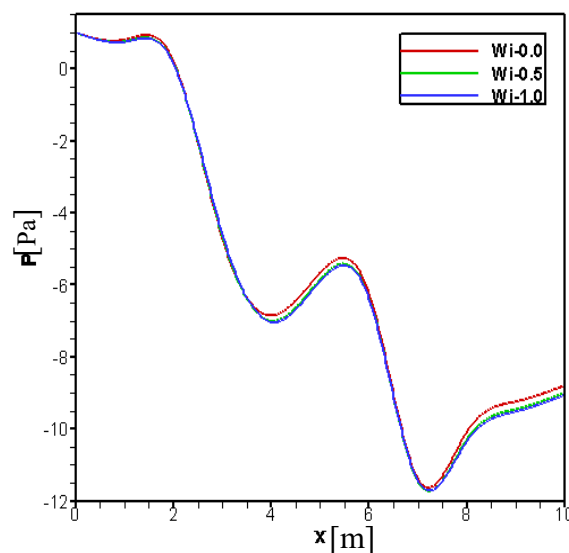


Figure 3.35c

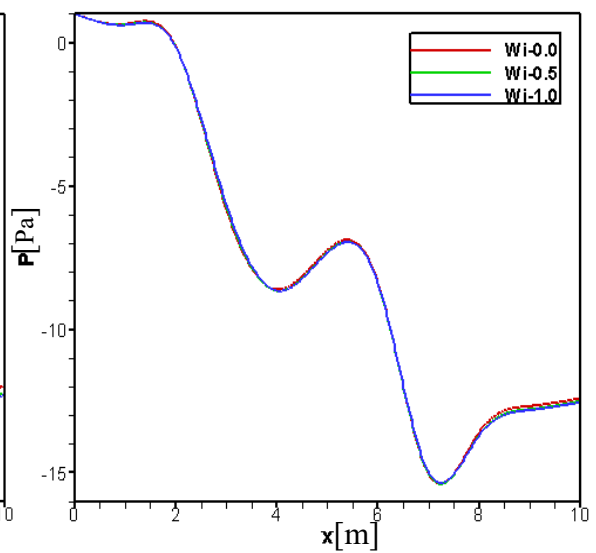


Figure 3.35d

Figure 3.35: Pressure profile of the Effects of Weissenbegr numbers (Re) on Blood flow at $Re = 100$ and flow rate $0.1 \text{ cm}^3/\text{s}$ for (Figure 3.35a) Newtonian Model, (Figure 3.35b) Generalized Newtonian Model, (Figure 3.35c) Oldroyd-B Model, and (Figure 3.35d) Generalized Oldroyd-B Model.

3.5.5 Different Flow rates on Blood flow

The axial pressure profiles are shown in Figures 3.36-3.37 at various flow rates for the four models Newtonian, Generalized Newtonian, Oldroyd-B, Generalized Oldroyd-B. By simple analysis from the figure the blood shear -thinning behavior is more intensified at stenosis area compare to non-stenosis. The velocity is little lower for generalized

CHAPTER 3 NUMERICAL STUDY OF BLOOD FLOW... ..

Oldroyd-B model compare to others. At flow rate $2 \text{ cm}^3/\text{s}$, the Newtonian and Oldroyd-B model very close and same result for generalized models. On the other hand, the pressure distributions along vessel axis are presented in Figure 3.37 with different flow rates. The pressure is decreased with respect to vessel axis for all four models. At second stenosis, we obtained lowest value of pressure. For higher flow rate, the pressure profiles almost same for all models because of less viscoelastic response of blood with increases of blood flow rate. The numerical data is shown in Table 3.9 and 3.10 as follows. In Tables 3.9 and 3.10, the blood velocity and pressure obtained along vessel axis at first and second stenosis for different flow rate (q) while $q = 0.05, 0.2$ and $2.0 \text{ cm}^3/\text{s}$ are presented.

Table 3.9: Blood velocity is obtained along vessel axis at first and second stenosis for different flow rate , $q = 0.05, 0.2$ and $2.0 \text{ cm}^3/\text{s}$ at $Re=100$ and $Wi = 0.6$.

Flow rates / Models	Velocity (U)					
	First stenosis			Second stenosis		
	$q= 0.05$	0.2	2.0	$q= 0.05$	0.2	2.0
N	0.1362328	0.136398205	0.136251668	0.145971072	0.144967463	0.144995957
GN	0.135461351	0.135461351	0.135461351	0.144195034	0.144195034	0.144195034
OD	0.1362318	0.1362318	0.1362318	0.144971072	0.144971072	0.142971072
GD	0.137490551	0.137490551	0.137490551	0.147781529	0.147781529	0.147781529

Table 3.10: Pressure are presented at first and second stenosis along vessel axis for different flow rate, $q = 0.05, 0.2$ and $2.0 \text{ cm}^3/\text{s}$ at $Re=100$ and $Wi = 0.6$.

Flow rates / Models	Pressure (P)					
	First stenosis			Second stenosis		
	$q = 0.05$	0.2	2.0	$q = 0.05$	0.2	2.0
N	-7.00016541	-7.0499413	-8.6632610	-11.4172491	-11.467249	-21.0498156
GN	-7.56501574	-7.5650157	-8.6632610	-14.7070610	-12.464288	-21.0598156
OD	-7.00426541	-7.0031654	-8.6632610	-11.4683491	-11.5143189	-21.0398156
GD	-8.66326103	-8.6632610	-8.6632610	-15.0390610	-12.6642887	-21.0798156

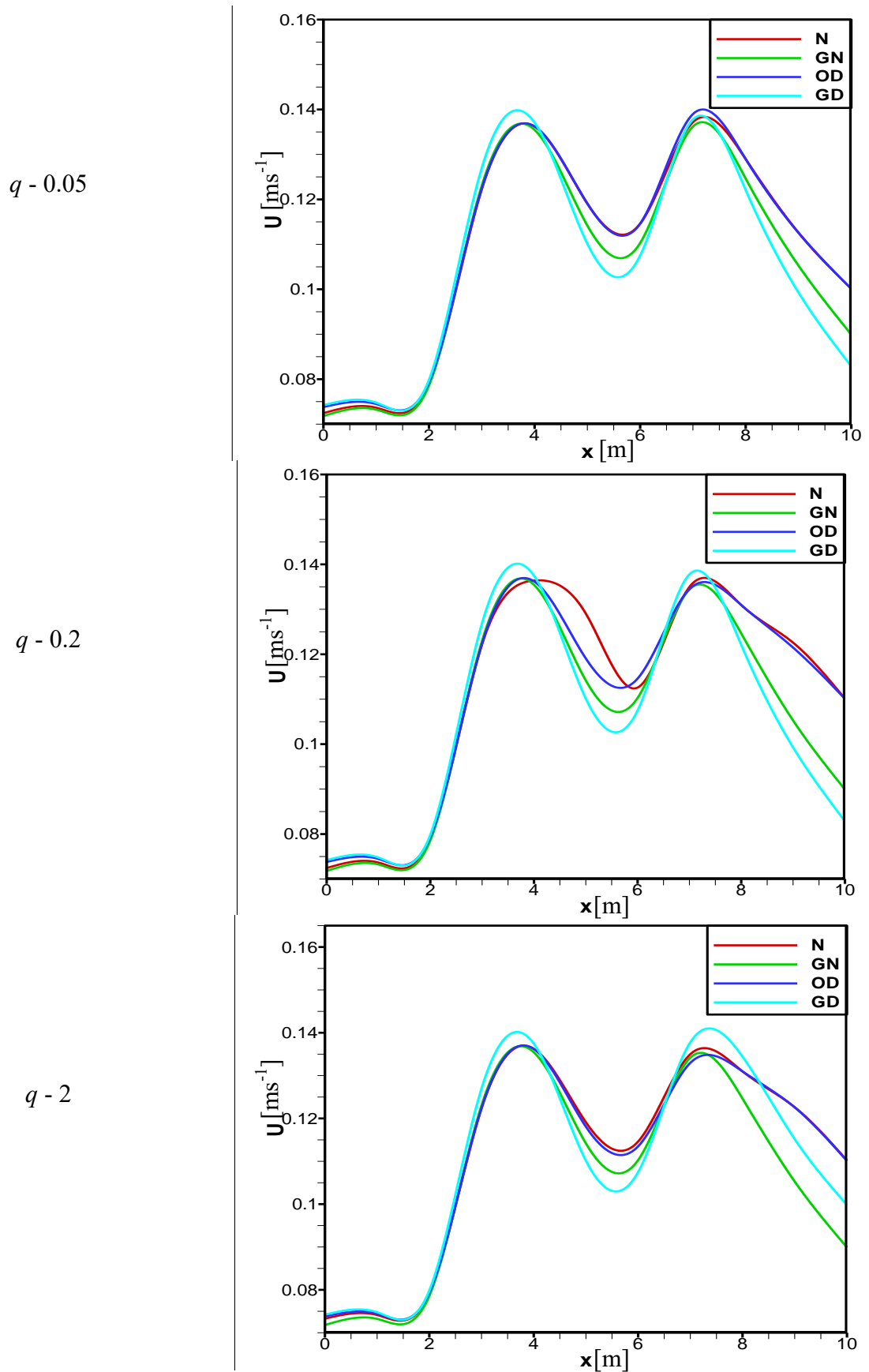


Figure 3.36: Velocity profile on Blood flow with various flow rate ($q = 0.05, 0.1, 2$ cm^3/s) at $Wi = 0.6$ and $Re = 100$

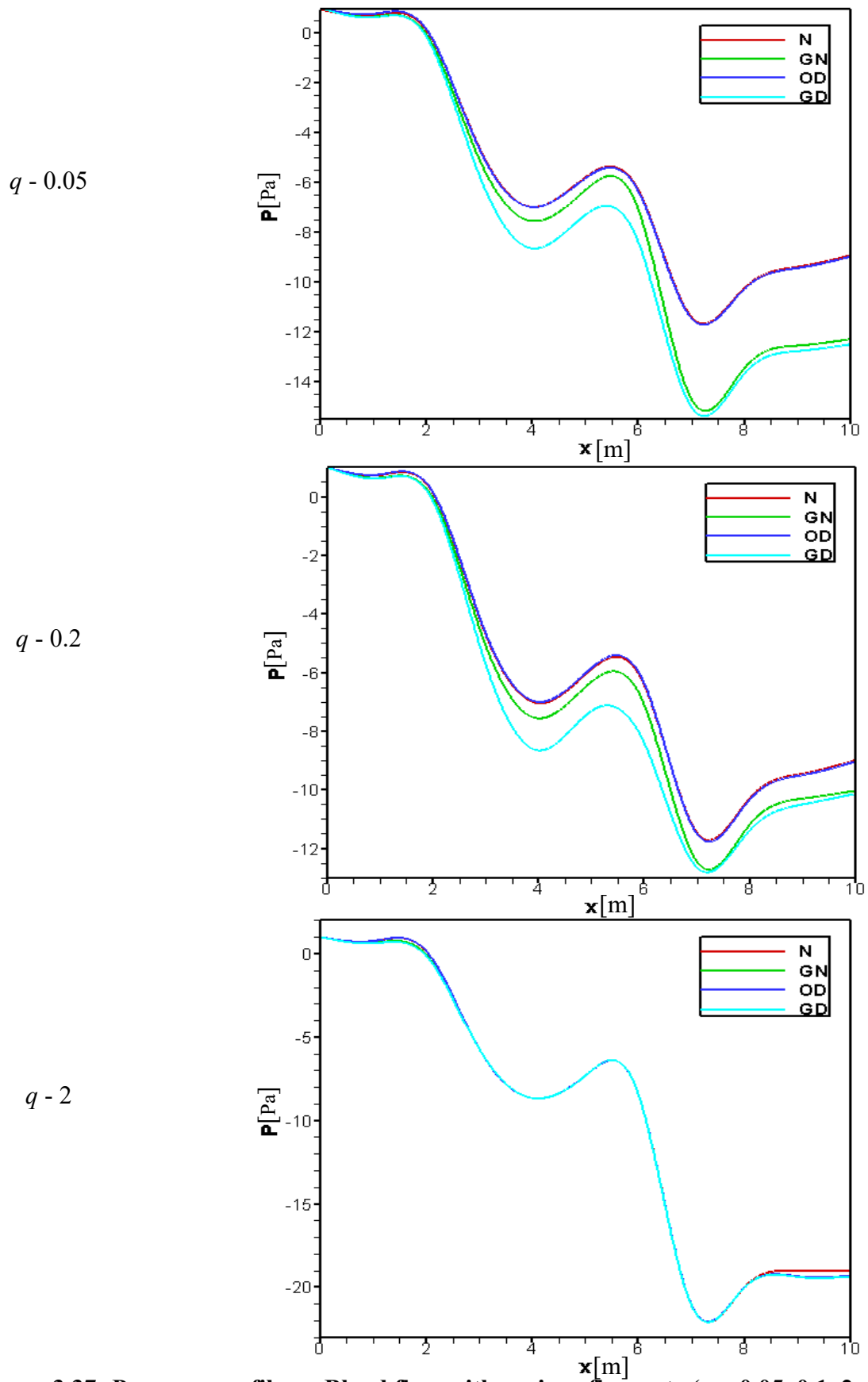


Figure 3.37: Pressure profile on Blood flow with various flow rate ($q = 0.05, 0.1, 2$ cm^3/s) at $Wi = 0.6$ and $Re = 100$

3.5.6 Wall Shear Stress effects

The effect of the blood flow behaviour on the wall shear stress is a significant factor in the onset of arterial diseases. In Figure 3.38 show the variation of the wall shear stress for the four models Newtonian, Generalized Newtonian, Oldroyd-B, Generalized Oldroyd-B with the flow rate $q = 0.1 \text{ cm}^3/\text{s}$. The wall shear stress (Wss) is another vital parameter in blood flow simulation. It represent the tangential component of the surface force at the vessel wall, acting against the fluid flow and can define as follows

$$W_{ss} = \boldsymbol{\sigma} \cdot \boldsymbol{n} \cdot \boldsymbol{t}$$

Here \boldsymbol{n} is the local wall normal vector (pointing towards the fluid) and \boldsymbol{t} is the corresponding unit tangential vector. The wall shear stress profiles for all the models at $Wi = 0.6$ and $Re = 100$ are shown in Figure 3.38. At the genesis of stenosis region, the wall shear stress have a significant change for all cases. It is found that the wall shear stress suddenly at the beginning of recirculation zones and depressed in non stenosis area. It is observed that the wall shear stress of generalized Newtonian and Oldroyd-B model is marginally lower than the others model and the wall shear stress is the lowest for generalized Oldroyd-B model. It is also found that the wall shear stress is higher for higher value of Weissenberg numbers. The negative values of wall shear stress are found in the region of reversal flow area. In Table 3.11, the numerical value of wall shear stress obtained along blood vessel axis for all four models while $Re = 100$, $Wi = 0.6$ and $q = 0.1 \text{ cm}^3/\text{s}$ are presented.

Table 3.11: Numerical values of wall shear stress are obtained at beginning of 1st and 2nd stenosis of artery for all four models while $Re = 100$, $Wi = 0.6$ and $q = 0.2 \text{ cm}^3/\text{s}$.

	Wall shear stress (Wss)	
	1 st Stenosis	2nd Stenosis
Newtonian Model	0.0064	0.0062
Generalized Newtonian Model	0.0061	0.0058
Oldroyd-B Model	0.0051	0.0057
Generalized Oldroyd-B Model	0.0458	0.0455

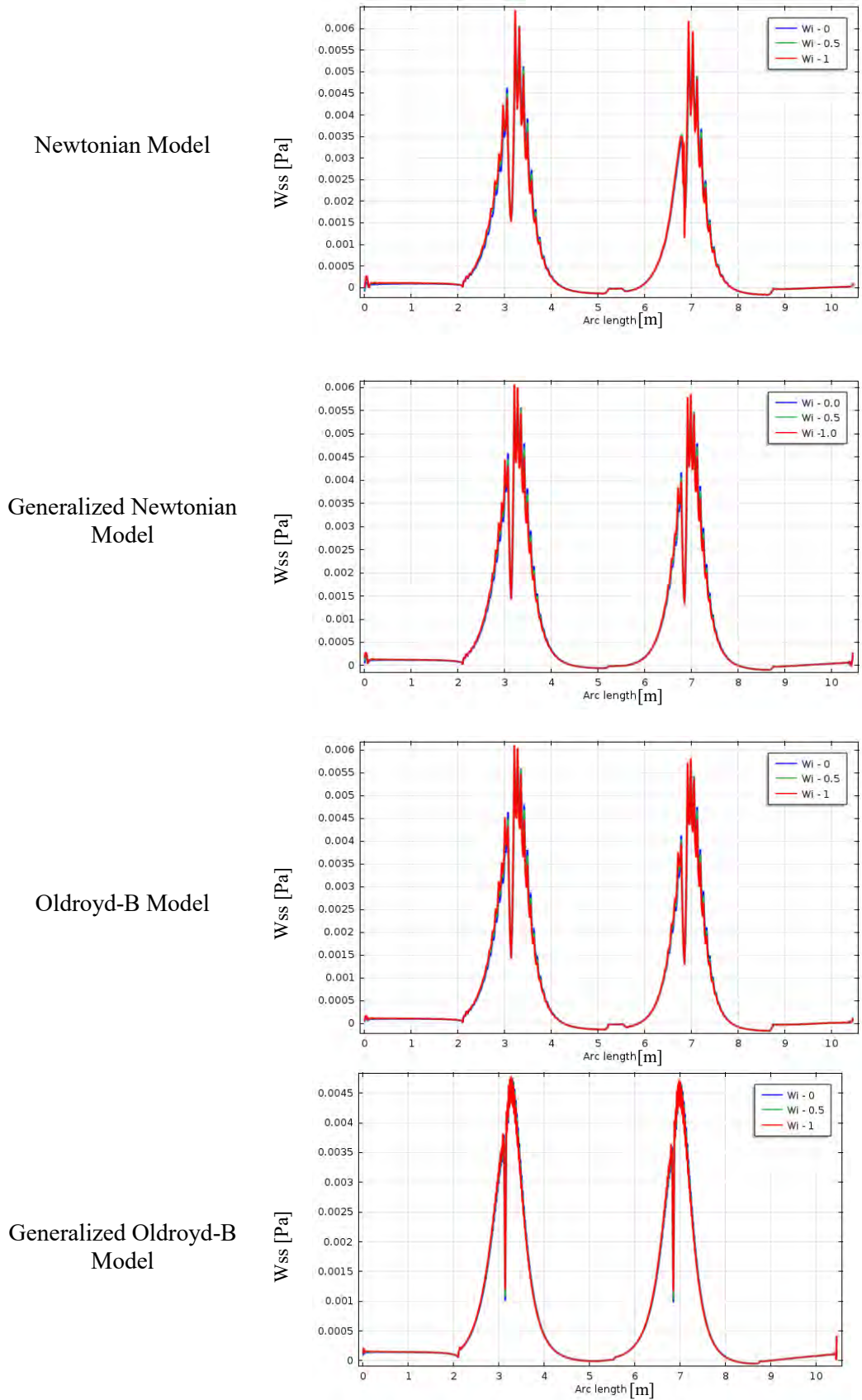


Figure 3.38: Wall shear stress distribution on blood flow along vessel axis through symmetric stenosis at $Re=100$ and $Wi = 0.6$ with various flow rate $q = 0.05$ (top) and 2 (bottom) cm^3/s .

3.6 Chapter Summary

The blood flow in wavy stenosis artery is simulated by finite element method. Four constitutive laws (Newtonian model, generalized Newtonian model, Oldroyd-B models and generalized Oldroyd-B models) have been proposed to describe the non-Newtonian shear-thinning blood viscosity. The numerical investigation of Newtonian and Oldroyd-B models, and their generalized (shear-thinning) models have been considered to the blood flow through symmetric and asymmetric stenosis in steady flow simulations. From the computational results, we conclude that the effect of flow variables and wall shear stress are related to viscoelasticity (shear-thinning) are more noticeable than the viscoelastic ones. At the throat of stenosis, the flow variables are predominant and increased with the flow rate decreased consequently. The specific choice of the characteristic viscosity μ_n for the reference Newtonian and (non-generalized) Oldroyd-B solution is main reason. The apparent viscosity is close to μ_0 in the large part of vessel at low shear rates and the difference for the Newtonian solution at high flow rate. For the given problems, the numerical method used to solve the governing equations seems to be sufficiently robust and efficient for the appropriate resolution.

The finite element equations derived from the governing flow equations that consist of the conservation of mass, momentum, and Oldroyd-B equations. The derived finite element equations are nonlinear requiring an iterative technique solver. The Newton-Raphson iteration method has been applied to solve these nonlinear equations for solutions of the nodal velocity component, tensor component, and pressure by considering Weissenberg numbers of 0.0, 0.5 and 1.00 and Reynold numbers of 10^2 to 10^3 . The results show the following aspects:

- ◆ The effect of flow variables (velocity and Pressure) have more significant changed at the throat of stenosis for all four models. The Peak value of blood velocity and lowest value of blood pressure are found at second constriction region for our considerable models.
- ◆ The effect of the blood flow behavior on the wall shear stress is an important factor in the onset of arterial diseases.

CHAPTER 3 NUMERICAL STUDY OF BLOOD FLOW... ..

- ◇ In blood flow, the effect of dimensionless numbers Re and Wi are remarkable and flow variables are more affected at stenosis area. With increase of Wi the blood flow patterns and pressure distribution are almost alike for generalized Oldroyd-B model.
- ◇ It is another remarkable effect on blood flow if the height of stenosis is different of the four dissimilar models.
- ◇ Various types of recirculation zones are originated at the throat of stenosis regions for all four models.

CHAPTER 4

BLOOD FLOW STUDY THROUGH ANEURYSMATIC ARTERY WITH PERMEABLE WALLS

The study of the blood flow has attracted many researchers over the past years. Due to its significant effect on several human cardiovascular diseases such as heart attacks, strokes, atherosclerosis, bleeding, stenosis and aneurysms, detailed knowledge of blood flow in physiological conditions is required. The frequently affected arteries are the aorta, the coronary, the carotid, and the femoral arteries. It is a vital area of research for the flow behavior of blood, as well as the shear-thinning viscosity of blood. Medical problems, genetic conditions, and trauma can damage or injure artery walls. The force of blood pushing against the weakened or injured walls can cause an aneurysm. An aneurysm can grow large and rupture (burst) or dissect. A rupture causes dangerous bleeding inside the body. A dissection is a split in one or more layers of the artery wall. The split causes bleeding into and along the layers of the artery wall. Cronenwett et al. (1985) have studied that the risk of rupture increases and size of aneurysm of artery. Theoretical and experimental studies of fluid dynamics through differently geometries of constriction or expansion have been discussed to evaluate the flow pattern are cited in Pincombe and mazumdar (1957), Muraki (1983), Pincombe et al. (1995), and Fakour et al. (2015).

In the present chapter the main objective is to examine the effects of the blood flow behaviour through aneurysmatic artery with permeable wall for Newtonian, Oldroyd-B and their generalized fluids. A set of partial differential equations of conservation of mass, momentum and Oldroyd-B equations are expressed in a normalized primitive variables formulation and then a finite element model has been developed for the present problem.

The blood flow patterns have shown in terms of velocity contour lines, pressure plots, streamlines with vectors and we have found that the blood flow variables are correlated to blood shear thinning properties for all four models. The blood variables have a significant changed along vessel axis for the presence of porosity at vessel walls. It is found that the hemodynamical factors- blood velocity, pressure, stress components and wall shear stress, permeability play important roles in the localization of healthy and unhealthy conditions of cardiovascular diseases. The effects on blood flow of aneurysmatic artery are presented graphically for all modifications.

This chapter has covered the following contents. The problem descriptions of the current investigation are presented in section 4.1. It has carried out the mathematical model with boundary conditions in section 4.2. The computational analysis have discussed in section 4.3 with grid freedom test for problem accuracy. In section 4.4, the result discussion of the current problem are presented and finally chapter summary in section 4.5.

4.1 Problem Statement

In the present study, the aneurysmatic model is considered along with the important geometric parameters as shown in Fig. 4.1. The two-dimensional partial permeable aneurysmatic vessel is assumed with diameter $D=2R= 6.2\text{mm}$ which enlarge smoothly to one half of the vessel width. At inlet, the parabolic velocity profile and extra stress tensor is prescribed and pressure is fixed to constant at outlet with Peclet number, $Pe=1000$ and Weissenberg number, $Wi = 0.6$. On the walls no-slip conditions are used for velocity and homogeneous Neumann condition for the pressure. The blood fluid is uniformly injected or removed with speed V_0 at first aneurysmatic vessel wall. A significant local acceleration of the blood flow is expected for the aneurysmatic cross-sectional area.

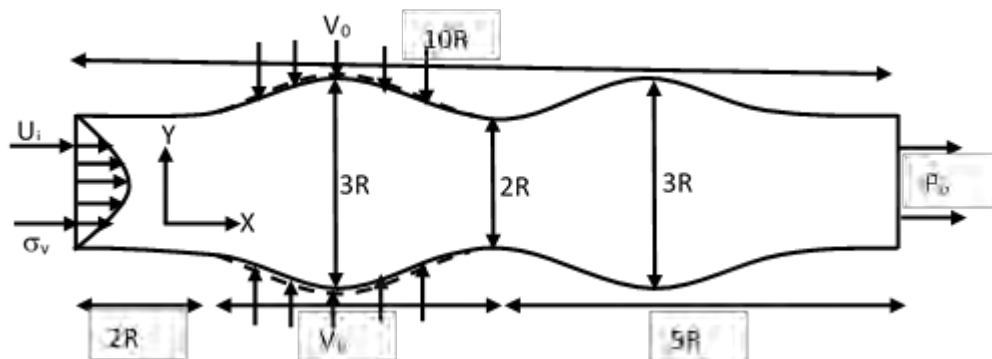


Figure 4.1: Geometry of the physical system

4.2 Mathematical Formulation

The Mathematical formulation of the above problem are shown as follows

4.2.1 Non-dimensional governing mathematical equations

The steady state laminar blood flow is generalized to consider viscoelasticity and shear-thinning properties based on incompressible Navier-Stokes equations. To capture viscoelastic properties of the blood flow, the generalized Oldroyd-B model is used. The solution of the governing system of equations is based on the finite element discretization. The governing equations for steady state blood flow can be written as:

CHAPTER 4 BLOOD FLOW STUDY THROUGH... ..

Continuity Equation

$$\nabla \cdot \mathbf{u} = 0 \quad (4.1)$$

Momentum Equations

$$\rho \frac{\partial \mathbf{u}}{\partial t} + \rho(\mathbf{u} \cdot \nabla) \mathbf{u} = -\nabla p + \mu_n \Delta \mathbf{u} + \nabla \cdot \boldsymbol{\sigma} + \rho \mathbf{f} \quad (4.2)$$

Oldroyd-B constitutive equation:

$$\boldsymbol{\sigma} + \lambda_x \left[\frac{\partial \boldsymbol{\sigma}}{\partial t} + (\mathbf{u} \cdot \nabla) \boldsymbol{\sigma} \right] = 2\mu_v \mathbf{V}(\mathbf{u}) + \lambda_x [\boldsymbol{\sigma} \mathbf{V}' - \mathbf{V}' \boldsymbol{\sigma} - \boldsymbol{\sigma} \mathbf{V} - \mathbf{V} \boldsymbol{\sigma}] \quad (4.3)$$

Here \mathbf{u} is the velocity vector, $\mathbf{u} = (u_1, u_2, u_3)^T$, ρ is the constant density, $\boldsymbol{\sigma}$ is the extra stress tensor, μ is dynamic viscosity, λ_x the relaxation and the symmetric part of the velocity gradient, $\mathbf{V} = \frac{1}{2}(\nabla \mathbf{u} + \nabla \mathbf{u}^T)$ i.e. $\boldsymbol{\sigma} = 2\mu \mathbf{V}$.

To obtain a system of dimensionless variables, we use some scaling properties of the system to introduce Peclet number (Pe), Schmidt number (Sc) and Weissenberg number (Wi) that measures the effect of viscosity and elasticity on blood flow for steady state. We introduce the following dimensionless variables for the non-dimensional governing equations are the continuity equation, momentum equation, and Oldroyd-B equation.

$$x = LX, \quad t = Lt^*/U, \quad \mathbf{u} = UU_o, \quad \mathbf{v} = VU_o, \quad p = \mu UP/L, \quad \boldsymbol{\sigma} = U\mu\boldsymbol{\sigma}^*/L, \\ f = f^* \mu U/L^2, \quad \nabla = \nabla^*/L, \quad Wi = \lambda_x U/L, \quad Pe = UL/\alpha = Re Sc, \quad Sc = \mu/\rho L,$$

Peclet number (Pe), Schmidt number (Sc) and Weissenberg number (Wi) are dimensionless numbers. The fluid is very viscous for small Pe and the fluid is more elastic at big Wi . For two dimensional aneurysmatic vessel in domain Ω , the non-dimensional governing equations are as follows:

Continuity Equation

$$\nabla \cdot \mathbf{U} = 0 \quad (4.4)$$

Momentum Equations

$$\frac{Pe}{Sc} [(\mathbf{U} \cdot \nabla) \mathbf{U}] = -\nabla P + (1 - \lambda) \Delta \mathbf{U} + \nabla \cdot \boldsymbol{\sigma} + \mathbf{f} \quad (4.5)$$

$$\frac{Pe}{Sc} [(\mathbf{V} \cdot \nabla) \mathbf{V}] = -\nabla P + (1 - \lambda) \Delta \mathbf{V} + \nabla \cdot \boldsymbol{\sigma} + \mathbf{f} \quad (4.6)$$

Oldroyd-B constitutive equation:

$$\boldsymbol{\sigma} + Wi_i [(\mathbf{U} \cdot \nabla) \boldsymbol{\sigma} - (\nabla \mathbf{U}) \boldsymbol{\sigma} - \boldsymbol{\sigma} (\nabla \mathbf{U})^t] = 2\mu_v \mathbf{V}(\mathbf{U}) \quad (4.7)$$

CHAPTER 4 BLOOD FLOW STUDY THROUGH... ..

4.2.2 Boundary conditions

The confined computational domain is divided into four mutually disjoint parts: a solid wall, an outlet, an inlet and porous wall.

(i) At inlet:

- a. Dirichlet boundary conditions for velocity vector are used on the boundary $\partial\Omega$

$$u = g \text{ on } \partial\Omega \text{ with compatibility condition } \int_{\partial\Omega} \mathbf{g} \cdot \mathbf{n} = 0, \text{ where } \mathbf{n} \text{ is the unit outward}$$

normal vector to Ω at the boundary $\partial\Omega$. For homogenous case, $g=0$.

- b. For a pressure and the stress tensor Neumann boundary condition is used on the boundary $\partial\Omega$. This boundary condition can be defined by

$$\boldsymbol{\sigma} \cdot \mathbf{n} = (-p\mathbf{I} + \nu \nabla \cdot \mathbf{u}). \mathbf{n} = \mathbf{h}$$

- c. The developed parabolic velocity profile and the corresponding extra stresses components

$$\mathbf{u} = 1.5 U_i (1 - y^2), \mathbf{v} = 0$$

$$\sigma_{11} = 2\mu_v Wi \left(\frac{\partial \mathbf{u}}{\partial y}\right)^2, \sigma_{12} = \mu_v \frac{\partial \mathbf{u}}{\partial y}, \sigma_{22} = 0$$

Where y is along the inlet boundary, and U_i is the average fluid velocity at the inlet.

(ii) At outlet:

- a. At outflow boundary pressure value is constant and for the velocity vector and the stress tensor Neumann boundary condition is used.

- b. Due to pressure force (P_o) the stress is acting at the boundary

$$\boldsymbol{\sigma} \cdot \mathbf{n} = -P_o \mathbf{n}$$

(iii) At boundary wall:

- a. On the walls no slip conditions are used for the velocity together with the condition for the normal component of the extra stress:

$$\mathbf{u} = 0 \text{ and } (\boldsymbol{\sigma} \cdot \mathbf{n}) \cdot \mathbf{n} = 0$$

Where \mathbf{n} is the boundary unit normal vector.

- b. Homogenous Neumann boundary conditions are used for the pressure.

(iv) Permeable walls:

- a. Permeable conditions is used at first aneurysmatics wall for the velocity $V=V_0$.

- b. No slip condition is used for velocity at second aneurysmatics wall.

CHAPTER 4 BLOOD FLOW STUDY THROUGH... ..

4.3 Computational Analysis

The discretized momentum and Oldroyd-B equations subjected to the boundary conditions simultaneously will be solved using the Matlab programming & Mathematical programming package COMSOLMULTIPHYSICS for the dependent variables (velocity, pressure and stress tensor). The numerical procedure to be used in this work is based on the Galerkin weighted residual method of finite element formulation.

4.3.1 Computational procedure

In present work, the non-linear parametric solution method is chosen to solve the governing differential equations which are based on the Galerkin weighted residual method of finite-element formulation. For brevity in at this time, the detailed formulation scheme is provided in Appendix A.

4.3.2 Grid independence test

Preliminary results are obtained to inspect the field variables grid independency solutions. Test for the accuracy of grid fineness has been carried out to find out the optimum grid number.

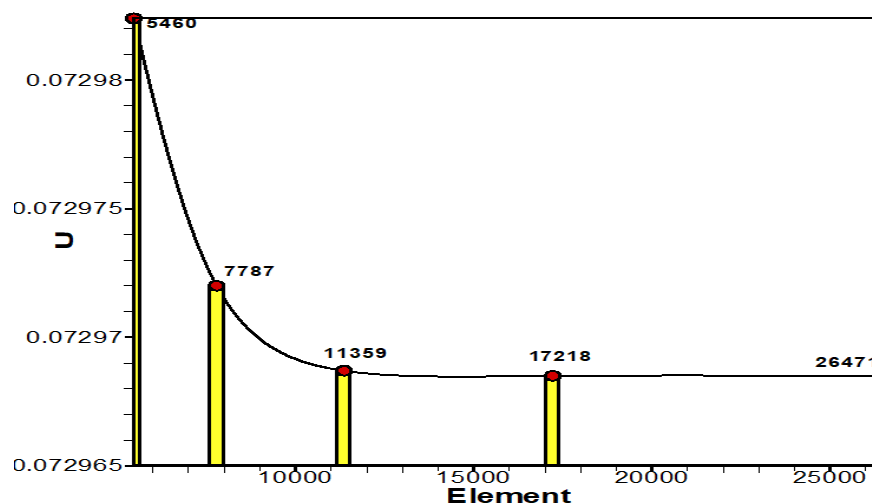


Figure 4.2: Convergence of average velocity with grid refinement for $Pe = 10^2$, $Sc = 1$ and $Wi = 0.6$ with blood flow rate $0.1 \text{ cm}^3/\text{s}$

To obtain grid independent solution, a grid refinement study is performed for aneurysm cavity with $Pe = 10^3$, $Sc = 1$ and $Wi = 0.6$ with blood flow rate $0.1 \text{ cm}^3/\text{s}$. Figure 4.2 shows the convergence of the average velocity (U) along the vessel axis with grid refinement. It is observed that grid independence is achieved with 17218 elements where there is insignificant change in velocity with further increase of mesh elements. Five different non-uniform grids with the following number of nodes and

CHAPTER 4 BLOOD FLOW STUDY THROUGH... ..

elements were considered for the grid refinement tests: 3118 nodes, 5460 elements; 4219 nodes, 7787 elements; 6199 nodes, 11359 elements; 8936 nodes, 17218 elements; 13629 nodes, 26471 elements. From these values, 8936 nodes, 17218 elements can be chosen throughout the simulation to optimize the relation between the accuracy required and the computing time.

Table 4.1: Grid Sensitivity Check at $Pe = 100$, $Sc=1$, $Wi = 0.6$ and $q= 0.1 \text{ cm}^3/\text{s}$

Nodes (elements)	3118 (5460)	4219 (7787)	6199 (11359)	8936 (17218)	13629 (26471)
$U[\text{ms}^{-1}]$	0.0729824	0.0729720	0.0729687	0.0729685	0.0729685
Time (s)	358.6	483.53	611.51	832.5	981.71

4.4 Results and Discussion

The aim of this mathematical model is to know and discuss the effects of permeable aneurysmatic artery, wall shear stress, and dimensionless numbers and stress tensor components on blood flow for all four models. We have used the Newtonian (N), generalized Newtonian (GN), Oldroyd-B (OD) and generalized Oldroyd-B (GD) models to study the influence of the shear-thinning and viscoelastic behavior of blood with blood flow. To develop models, we have only changed blood viscosity μ_n and extra stress σ_v . We have used same parameters for blood flow simulations and numerical investigation of all models which is detailed in Prokop and Kozel (2013).

The effect of permeable aneurysmatic blood vessel wall is examined for four different models with flow rates at $Pe = 1000$ and $Wi = 0.6$. A contrast blood flow simulation between velocity and pressure distribution is presented in Figures 4.3- 4.5 and 4.7- 4.9 respectively for above mentioned models with $Wi = 0.6$ and $Pe = 1000$. The blood velocity and pressure profile have a significant changed between two aneurysms. The important parameter wall shear stress is used to identify the artery diseases and its effect have shown in Figure 4.34. The effects of dimensionless numbers have been shown in Figures 4.11- 4.30 at Peclet number, Pe (1000, 2000 and 3000) and Weissenberg number, Wi (0.0, 0.5, 1.0). The axisymmetric profile has developed at inlet and outlet of blood vessel and the pattern of blood flow for velocity and pressure distribution are shown in Figures 4.1- 4.14 and 4.16-4.19 in terms of contour lines. The graphical presentation of the velocity, pressure, wall shear stress and stress tensor of blood flow are shown in Figures 4.6, 4.10, 4.15, 4.20, 4.31- 4.35 respectively.

CHAPTER 4 BLOOD FLOW STUDY THROUGH... ..

4.4.1 Aneurysm blood vessel effects on blood flow field

The velocity profiles are of particular interest, since they provided a detailed description of the blood flow field. The velocity distribution of blood flow of the four different models Newtonian, Generalized Newtonian, Oldroyd-B, Generalized Oldroyd-B are presented in Figures 4.3-4.11 with the flow rate $q = 0.1 \text{ cm}^3/\text{s}$. It is very interesting that the only confine or recirculation zones are originated in generalized Oldroyd-B model and absent at rest of the models for simple aneurysm (no permeability) blood vessel. At permeable aneurysm, there are some permanent oval or recirculation zones are found between the aneurysms. It is noted that the recirculation zones are migrating toward the proximal end of the aneurysm cavity and adjacent to vessel wall for all models. These recirculation zones are symbolic of regions over a significant portion of each model where the flow is reparated. At generalized Newtonian and Oldroyd-B model the recirculation zone has shrunk considerably. Because of a shear-thinning viscosity of blood which leads to the increase of the local viscosity in the low-shear regions.

In Figure 4.3, the flow separation regions are initiated at the beginning of both aneurysm and blood flow patterns are symmetric along vessel axis. But in the case of permeable boundary conditions, the flow separation regions are created at the bottom section of first aneurysm but different in second aneurysm and the blood flow patterns are migrating towards upper vessel wall.

The graphical presentation of velocity profiles is shown in Figure 4.12 for all four models at dimensionless number $Wi = 0.6$ and $Pe = 1000$ with absent of permeable, partial permeable and both permeable aneurysm. Form the Figure 4.12a, the minimum value of velocity is found in second enlargement regions and peak value is at outlet of both permeable aneurysm blood vessels. Due to permeability, the velocity has increased and provides highest velocity at generalized models. In the recirculation zone, the blood shear-thinning behavior is remarkable and local viscosity increases significantly. The viscoelastic effects may become more important for other cases. In Table 4.2, numerical value of velocity of partial permeable aneurysm obtained along blood vessel axis for all four models while $Pe = 1000$, $Wi = 0.6$ and $q = 0.1 \text{ cm}^3/\text{s}$ is presented.

CHAPTER 4 BLOOD FLOW STUDY THROUGH... ..

Table 4.2: Blood velocity is presented for partial permeable aneurysm along vessel axis for all cases while $Pe = 1000$, $Wi = 0.6$ and $q = 0.1 \text{ cm}^3/\text{s}$.

Along vessel axis	Velocity (U)			
	Newtonian Model	Generalized Newtonian Model	Oldroyd-B Model	Generalized Oldroyd-B Model
0	0.07219593	0.071947966	0.072666483	0.073896793
1	0.072034546	0.072317805	0.072571894	0.073940868
2	0.067408478	0.068766528	0.067882095	0.070420396
3	0.054435704	0.057225749	0.054882349	0.059043454
4	0.048987098	0.05208039	0.049244453	0.053982804
5	0.057362406	0.059983122	0.057406782	0.062135892
6	0.060962859	0.062899398	0.060963094	0.064755497
7	0.060212369	0.061026684	0.060212788	0.061905042
8	0.063881523	0.063957738	0.063878267	0.064483371
9	0.069802714	0.069574757	0.069783652	0.070465528
10	0.073008783	0.072444045	0.072996248	0.074037812

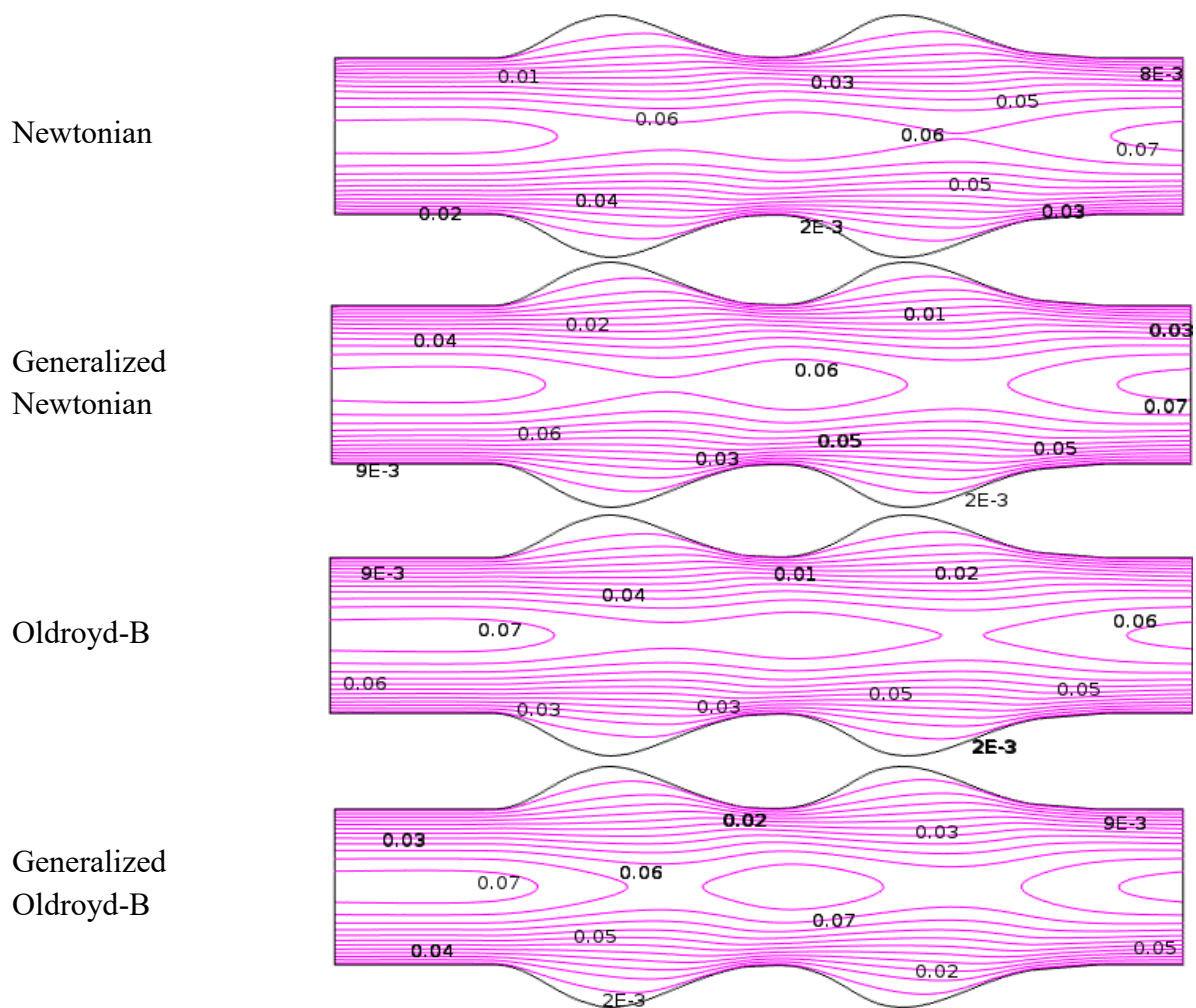


Figure 4.3: Velocity contour line on blood flow through aneurysmatic (without permeable) blood vessel at $Pe = 1000$ and $Wi = 0.6$ with $q = 0.1 \text{ cm}^3/\text{s}$.

CHAPTER 4 BLOOD FLOW STUDY THROUGH... ..

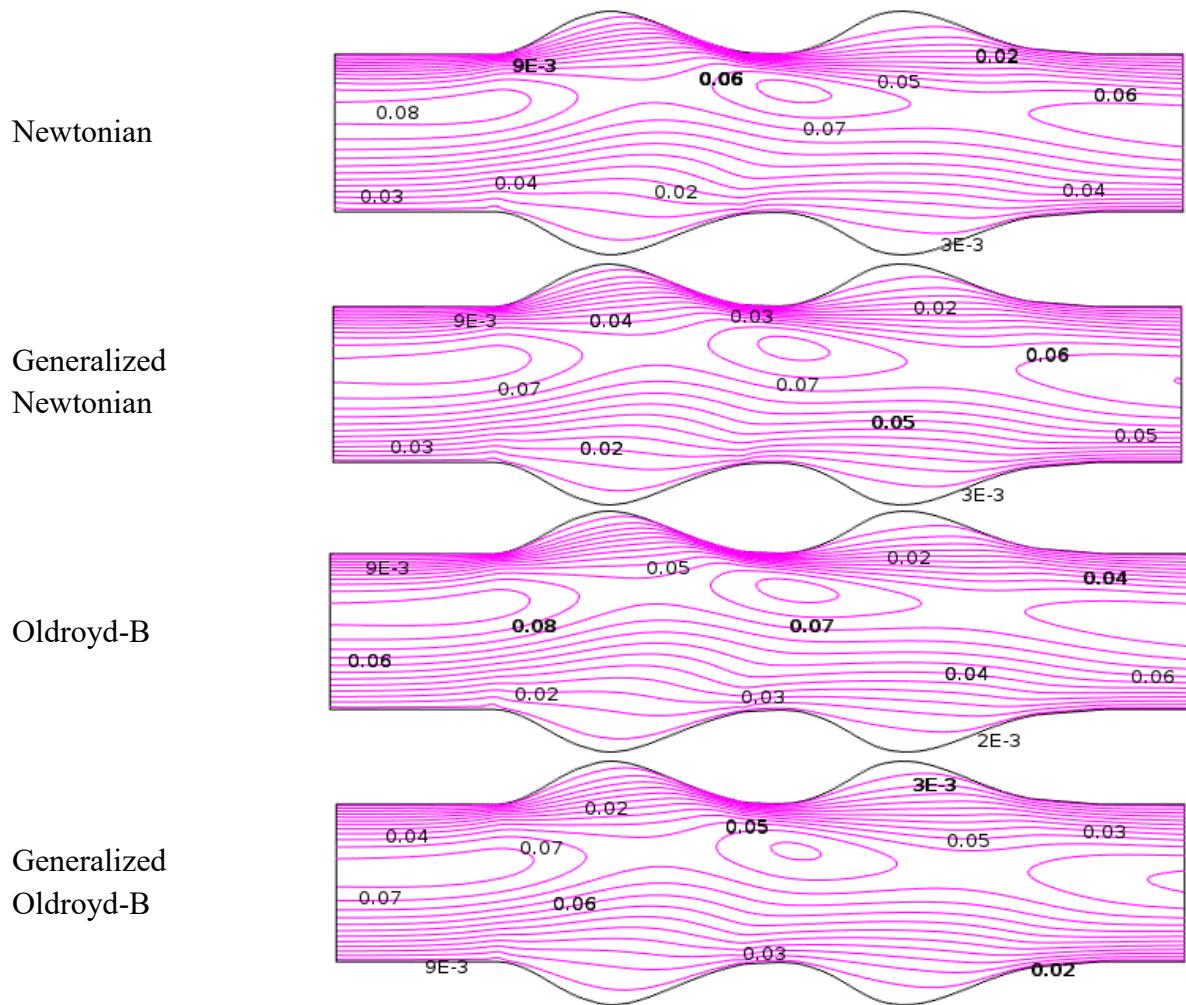
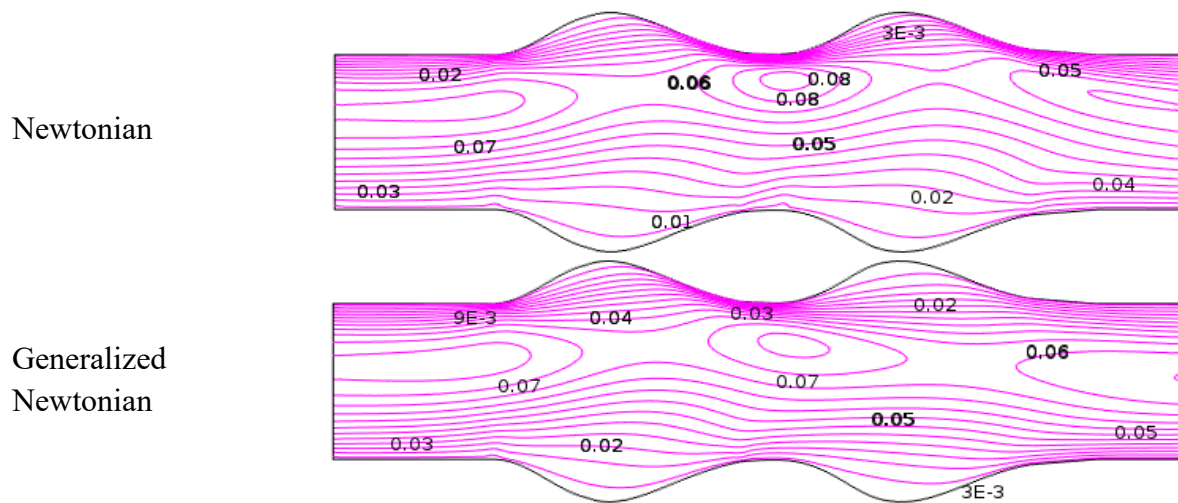


Figure 4.4: Velocity contour line on blood flow through partial permeable aneurysmatic blood vessel at $Pe=1000$ and $Wi = 0.6$ with $q = 0.1 \text{ cm}^3/\text{s}$.



CHAPTER 4 BLOOD FLOW STUDY THROUGH... ..

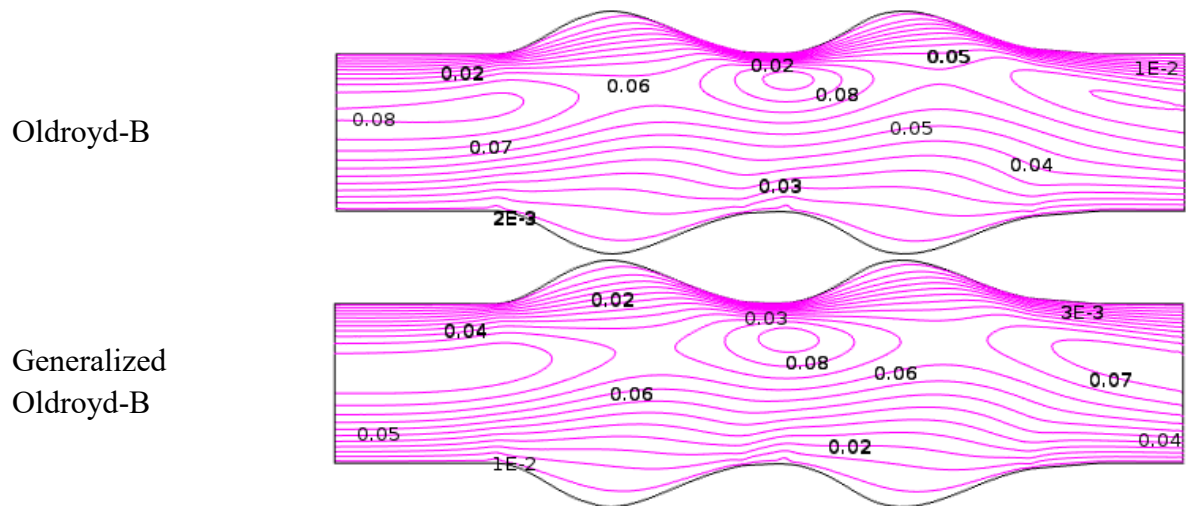


Figure 4.5: Velocity distribution on blood flow through permeable aneurysmatic blood vessel at $Pe=1000$ and $Wi = 0.6$ with $q = 0.1 \text{ cm}^3/\text{s}$.

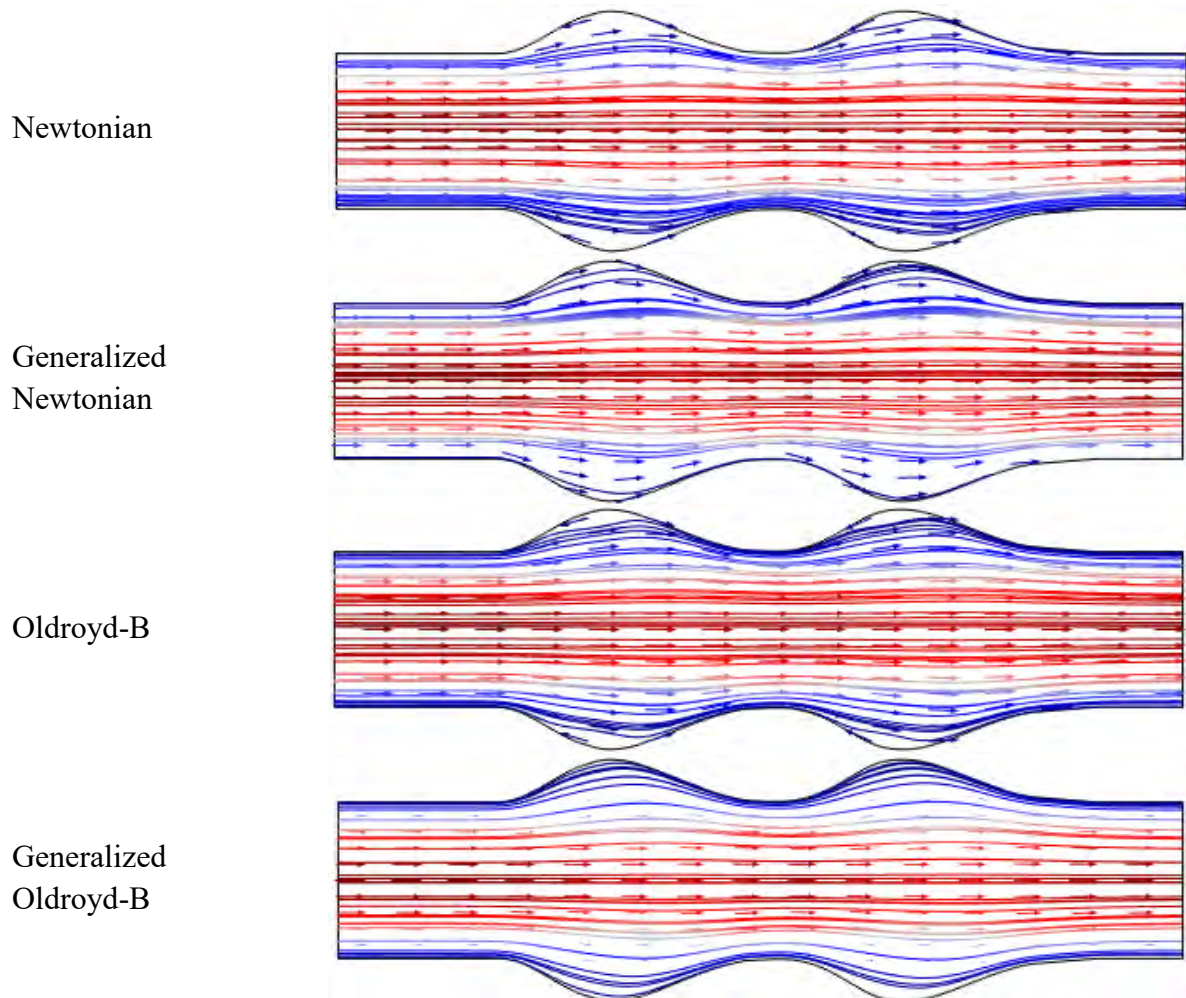


Figure 4.6: Stream lines on blood flow through aneurysmatic (without permeable) blood vessel at $Pe=1000$ and $Wi = 0.6$ with $q = 0.1 \text{ cm}^3/\text{s}$.

CHAPTER 4 BLOOD FLOW STUDY THROUGH... ..

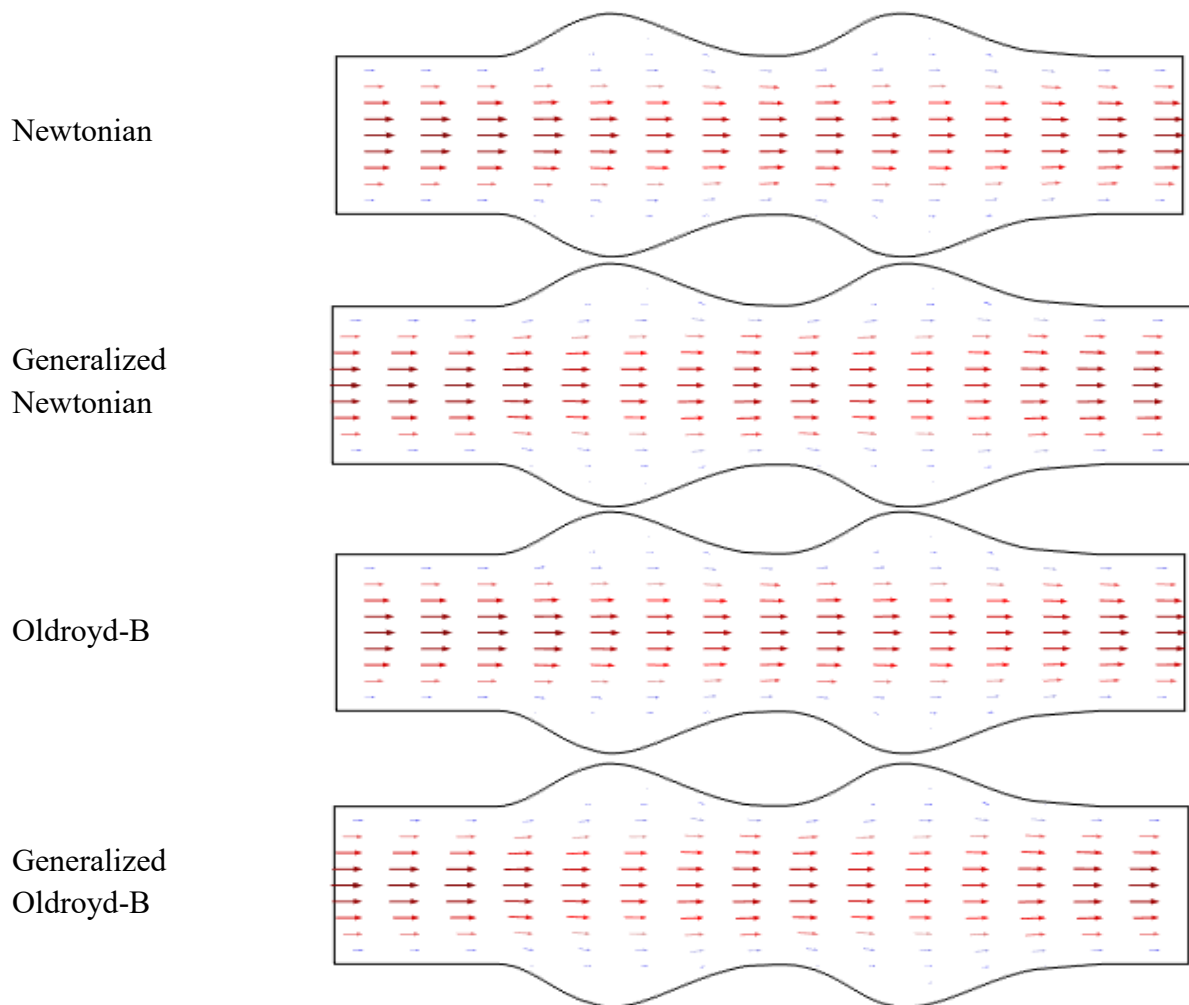
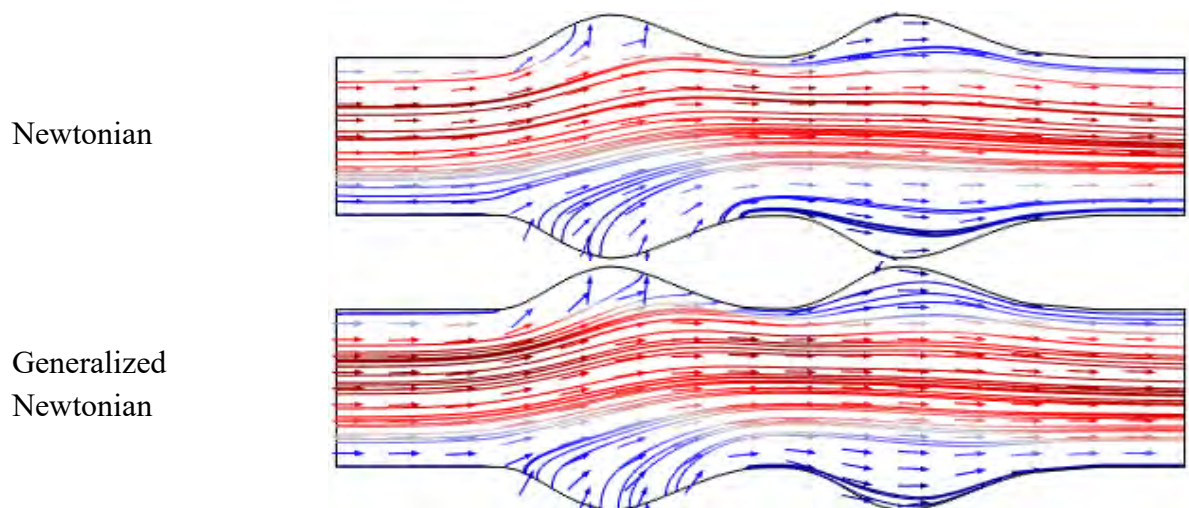


Figure 4.7: Blood flow with vectors through aneurysmatic (without permeable) blood vessel at $Pe=1000$ and $Wi = 0.6$ with $q = 0.1 \text{ cm}^3/\text{s}$.



CHAPTER 4 BLOOD FLOW STUDY THROUGH... ..

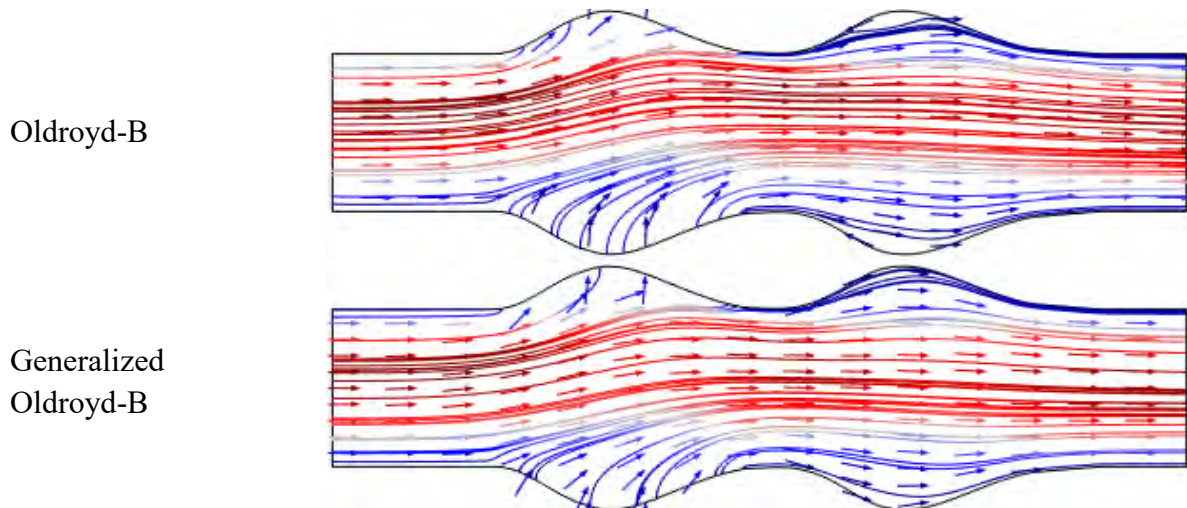


Figure 4.8: Stream lines on blood flow through permeable anuerysmatic blood vessel at $Pe=1000$ and $Wi = 0.6$ with $q = 0.1 \text{ cm}^3/\text{s}$.

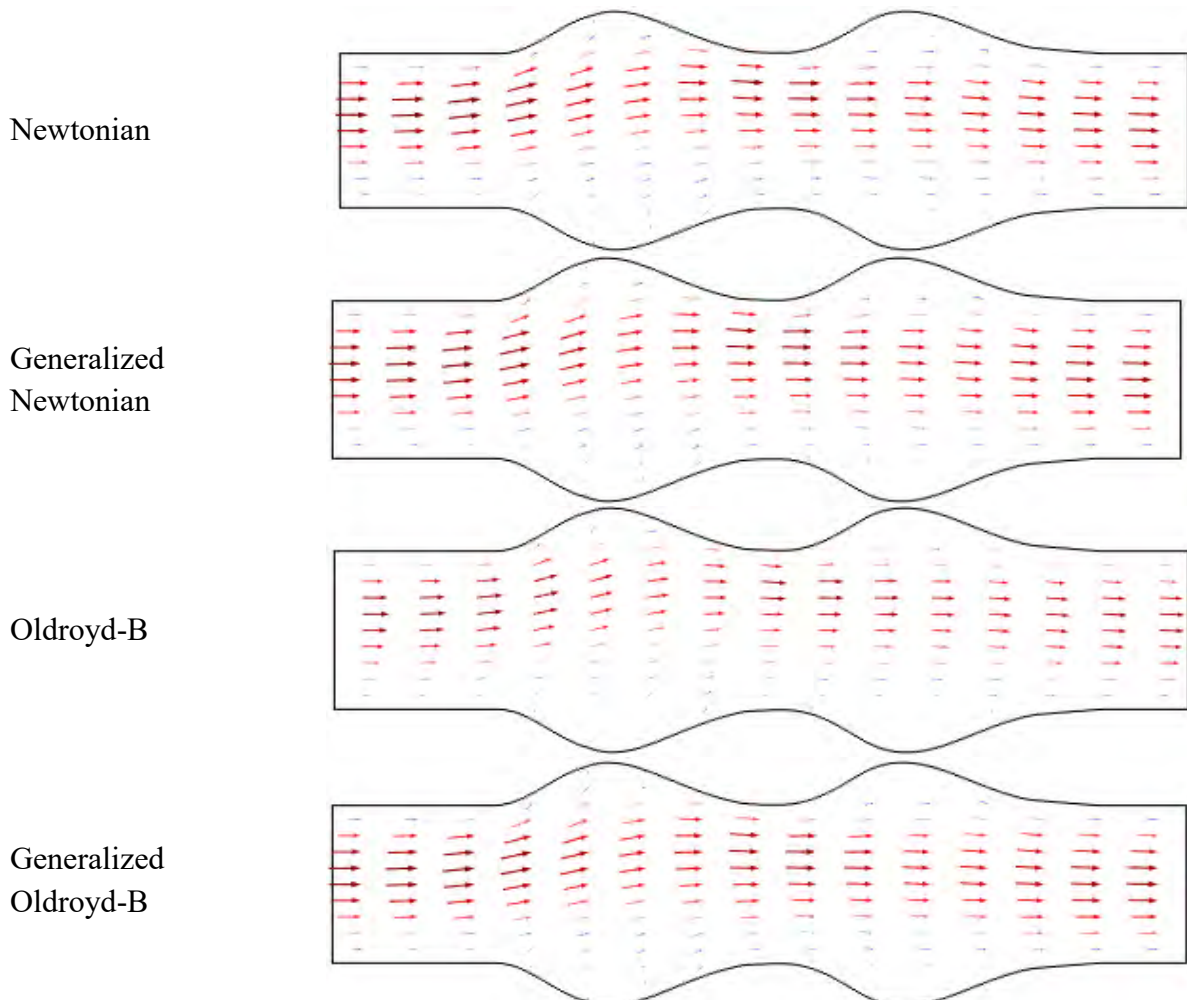


Figure 4.9: blood flow patterns with vectors through anuerysmatic (without permeable) blood vessel at $Pe=1000$ and $Wi = 0.6$ with $q = 0.1 \text{ cm}^3/\text{s}$.

CHAPTER 4 BLOOD FLOW STUDY THROUGH... ..

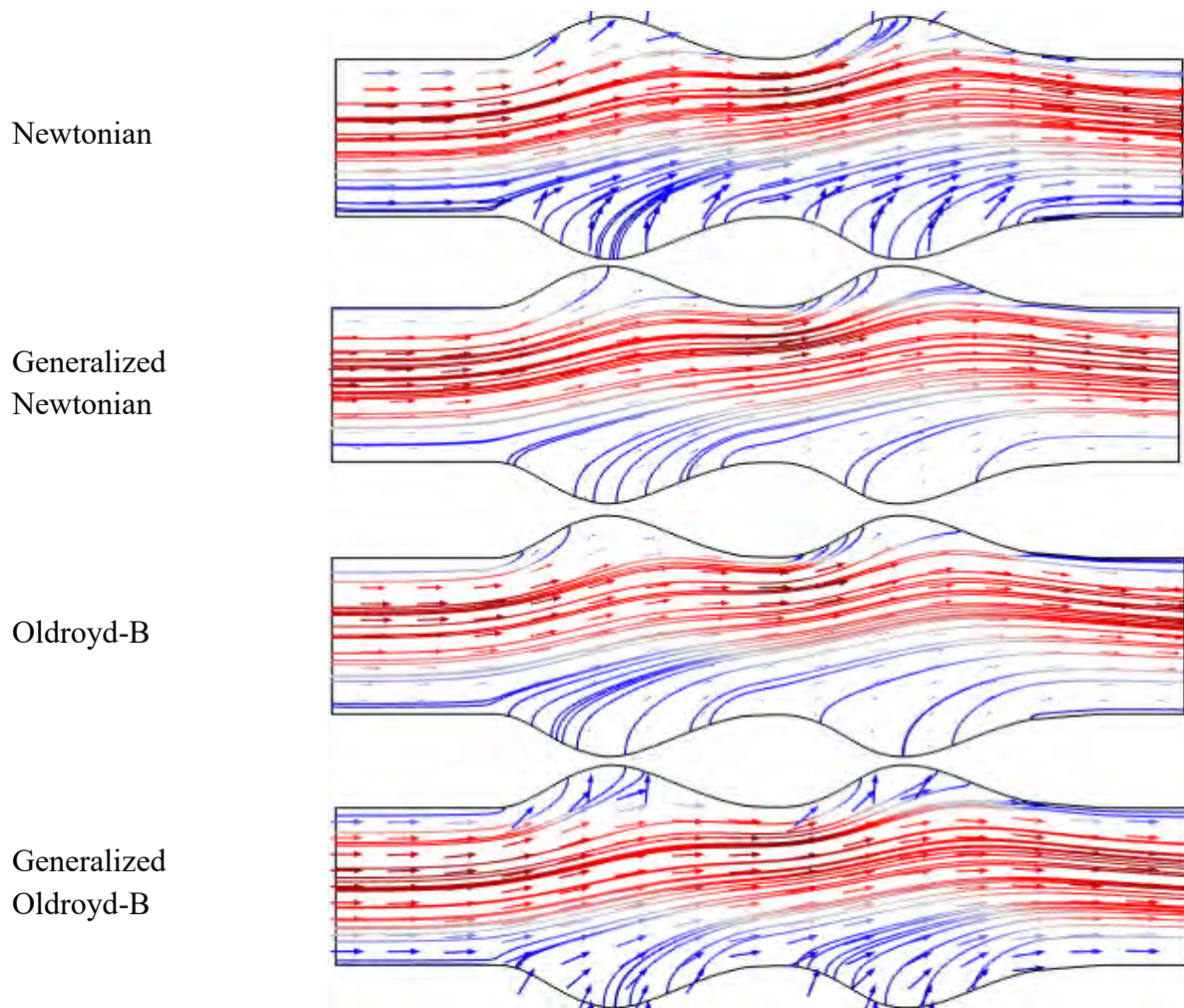
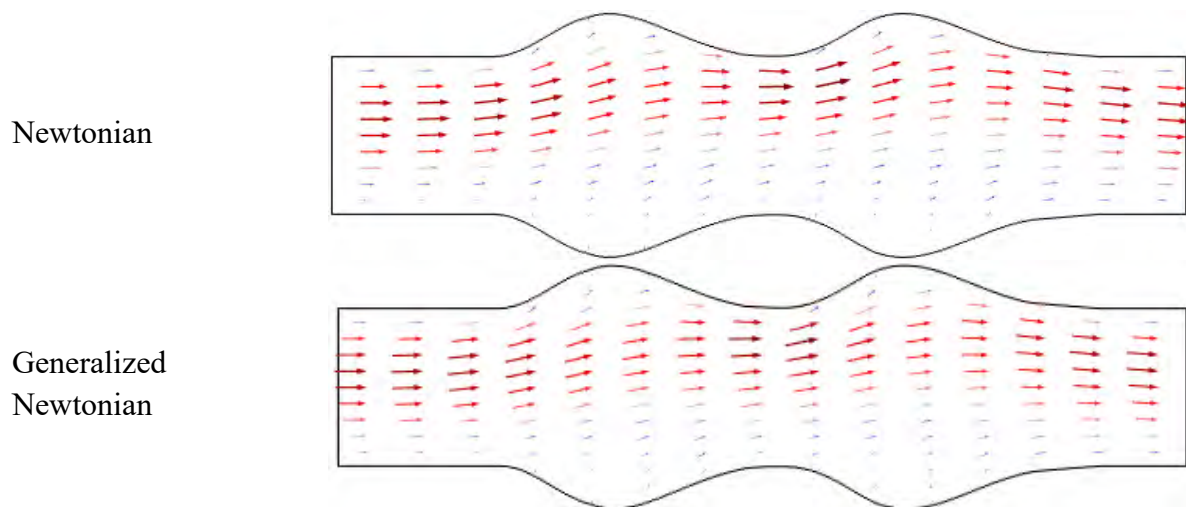


Figure 4.10: Stream lines on blood flow through partial permeable aneurysmatic blood vessel at $Pe=1000$ and $Wi = 0.6$ with $q = 0.1 \text{ cm}^3/\text{s}$.



CHAPTER 4 BLOOD FLOW STUDY THROUGH... ..

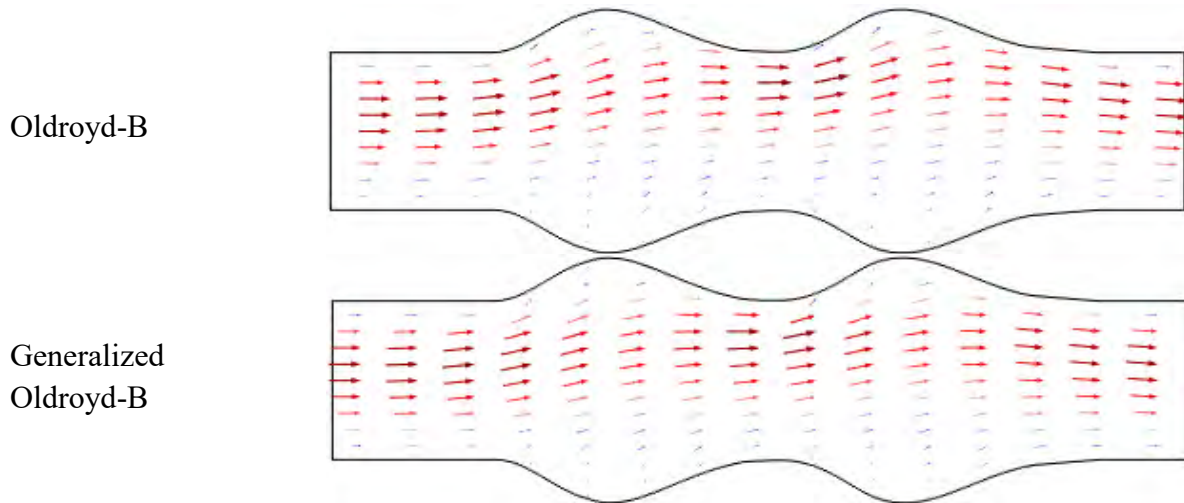
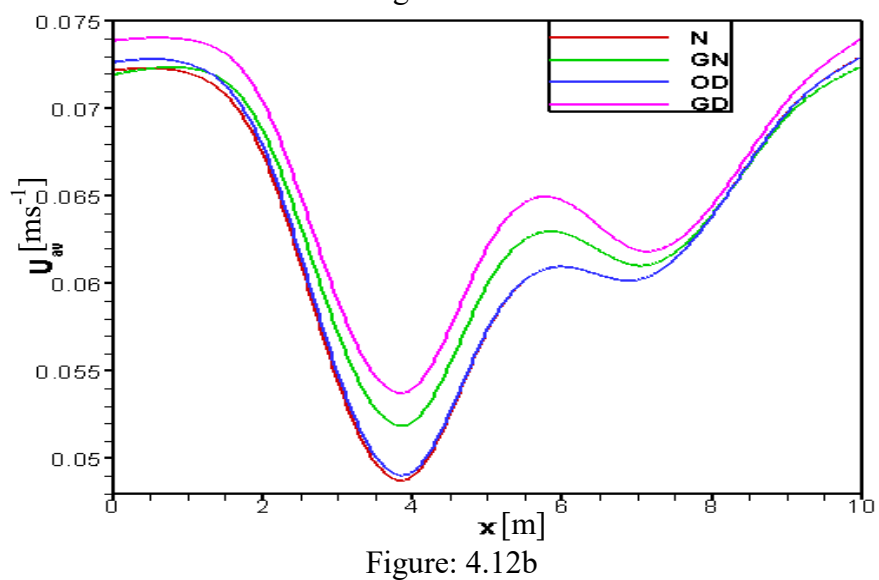
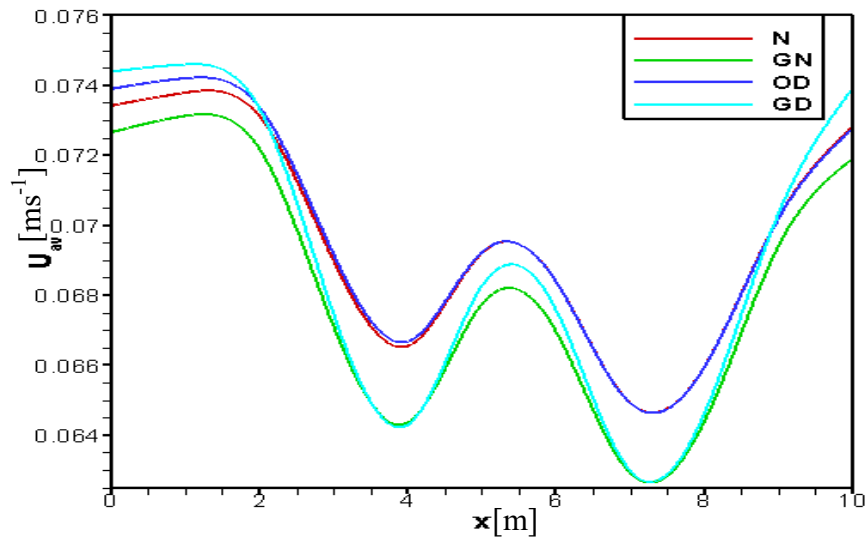


Figure 4.11: Blood flow patterns with vectors through permeable aneurysmatic blood vessel at $Pe=1000$ and $Wi = 0.6$ with $q = 0.1 \text{ cm}^3/\text{s}$.



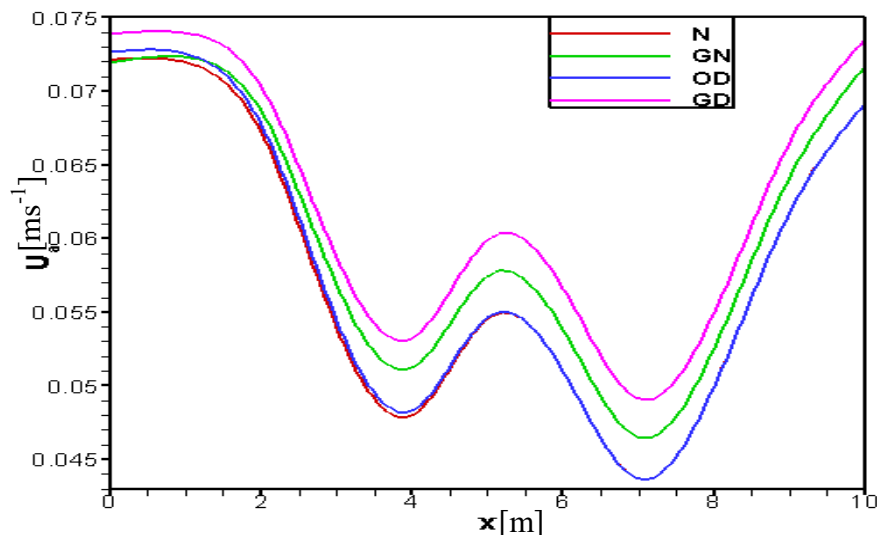


Figure: 4.12c

Figure 4.12: Velocity profile with no permeable (Figure: 4.12a), partial permeable (Figure: 4.12b) and both permeable (Figure: 4.12c) aneurysm along vessel when $Pe=1000$ and $Wi = 0.6$ with $q = 0.1 \text{ cm}^3/\text{s}$.

4.4.2 Aneurysm blood vessel effects on pressure distribution

The blood flow simulation of pressure circulation is present in terms of contour plot for all models in Figures 4.13-4.15 with absence and presence of permeability aneurysm. In Figure 4.13, the iso-pressure contours show how the pressure reached a minimum at the separation point and decreased monotonously along aneurysm. The pressure has peaked at the reattachment point, which constituted a stagnation point, and fell sharply at the beginning of first aneurysm. Due to presence of permeability, the pressure has decreased rapidly and gained minimum value at outlet in Figure 4.14. The flow separation points and stagnation point has migrated towards upper blood vessel wall. The patterns of pressure distribution have a magnificent changed along aneurysm for porosity of vessel wall and pressure contour lines converted steep to slant gradually at second aneurysm. The pressure gradient is very intensive at the end of second aneurysm and has a substantial changed throughout the blood vessel. The pressure distribution results indicate that twice aneurysm is formed, the blood flow have increased the blood pressure at dilating area. The significant changes occur in blood pressure at first dilating (aneurysm) because of penetrable vessel wall. At generalized Oldroyd-B model, the pressure is more dominated compare to others due to the shear-thinning behavior of blood viscosity.

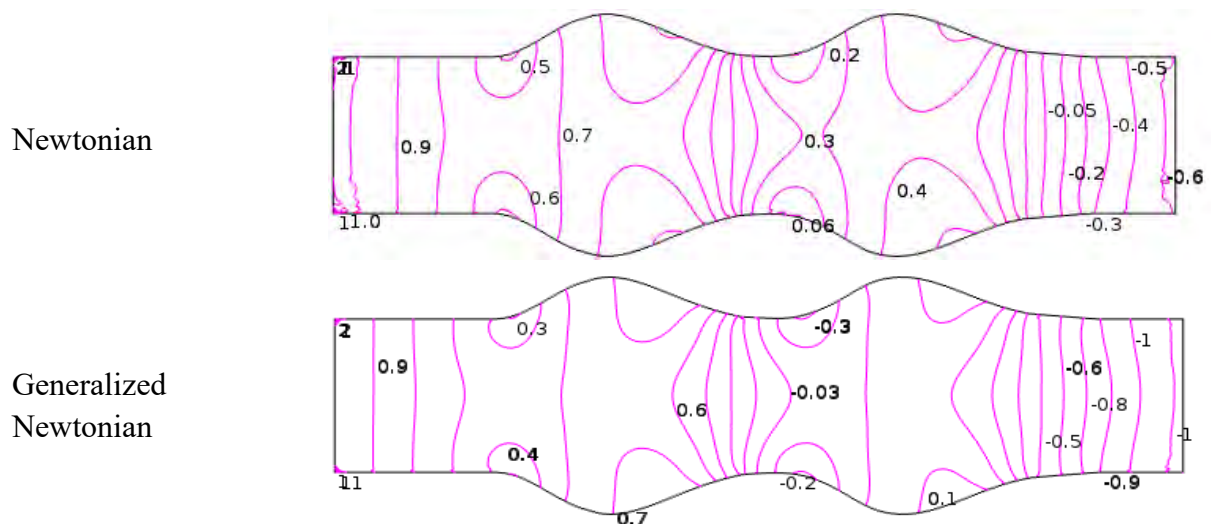
The numerical graph of pressure profiles is shown in Figure 4.16 for all four models at dimensionless number $Wi = 0.6$ and $Pe = 1000$. At Figure 4.16, the minimum pressure is

CHAPTER 4 BLOOD FLOW STUDY THROUGH... ..

originated after second dilating for all models and the lowest value is found at Oldroyd-B model due to porosity which leads to non-Newtonian fluid flow is faster than Newtonian fluid. In Table 4.3, the numerical value of pressure of partial permeable aneurysm obtained along blood vessel axis for all four models while $Pe = 1000$, $Wi = 0.6$ and $q = 0.1 \text{ cm}^3/\text{s}$ are presented.

Table 4.3: Pressure values of partial permeable aneurysm are inserted along blood vessel axis for all four models while $Pe = 1000$, $Wi = 0.6$ and $q = 0.1 \text{ cm}^3/\text{s}$.

Along vessel axis	Pressure (P)			
	Newtonian Model	Generalized Newtonian Model	Oldroyd-B Model	Generalized Oldroyd-B Model
0	0.990206222	0.992790641	0.998823145	0.998325827
1	0.831946358	0.719133323	0.799768498	0.654964065
2	0.698421401	0.523341697	0.663150523	0.404624475
3	0.705252861	0.525934623	0.672721642	0.401161015
4	0.475433218	0.277996342	0.443540628	0.144958716
5	-0.124029503	-0.371917792	-0.151624087	-0.563501083
6	-0.321290012	-0.598710361	-0.348799865	-0.822656053
7	-0.238563933	-0.526592766	-0.266772408	-0.75798542
8	-0.438662504	-0.80084777	-0.46613986	-1.090741714
9	-0.880410311	-1.335971676	-0.90656169	-1.718021646
10	-1.227242454	-10.13914344	-8.994475968	-12.51618949



CHAPTER 4 BLOOD FLOW STUDY THROUGH... ..

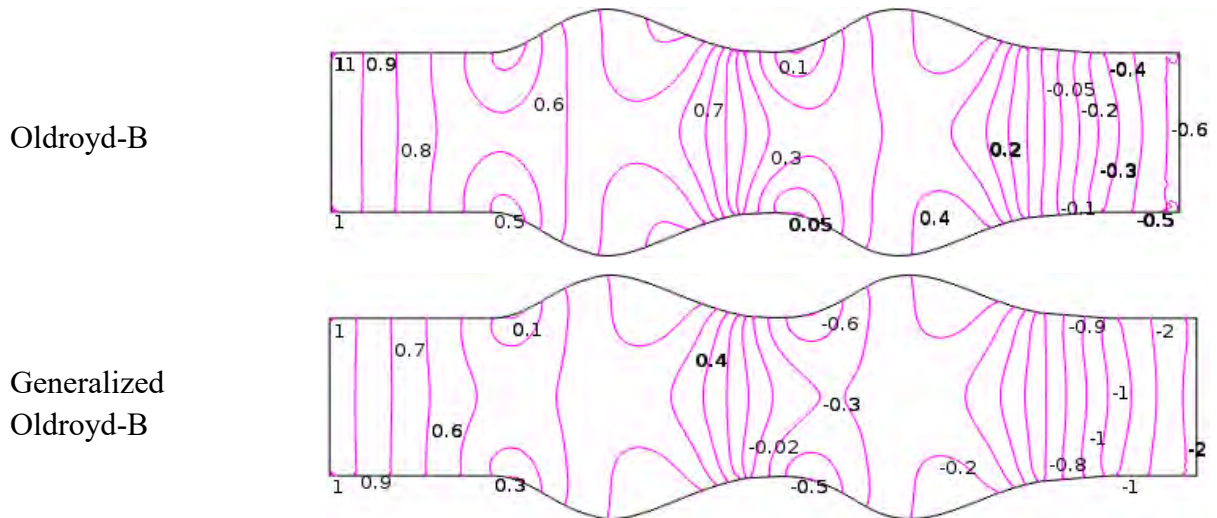


Figure 4.13: Pressure distribution on blood flow through aneurysmatic (without permeable) blood vessel at $Pe=1000$ and $Wi = 0.6$ with $q = 0.1 \text{ cm}^3/\text{s}$.

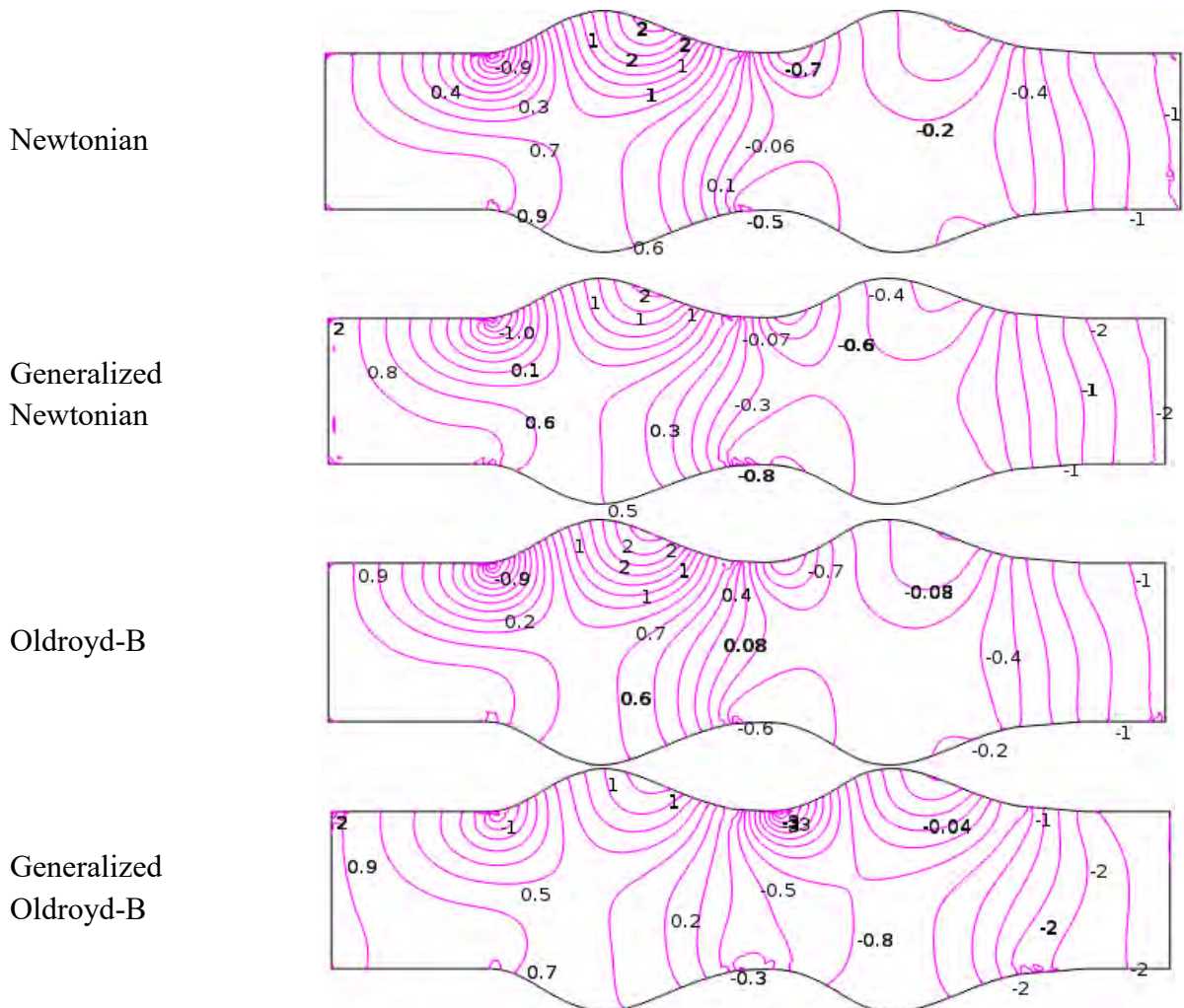


Figure 4.14: Pressure distribution on blood flow through partial permeable aneurysmatic blood vessel at $Pe=1000$ and $Wi = 0.6$ with $q = 0.1 \text{ cm}^3/\text{s}$.

CHAPTER 4 BLOOD FLOW STUDY THROUGH... ..

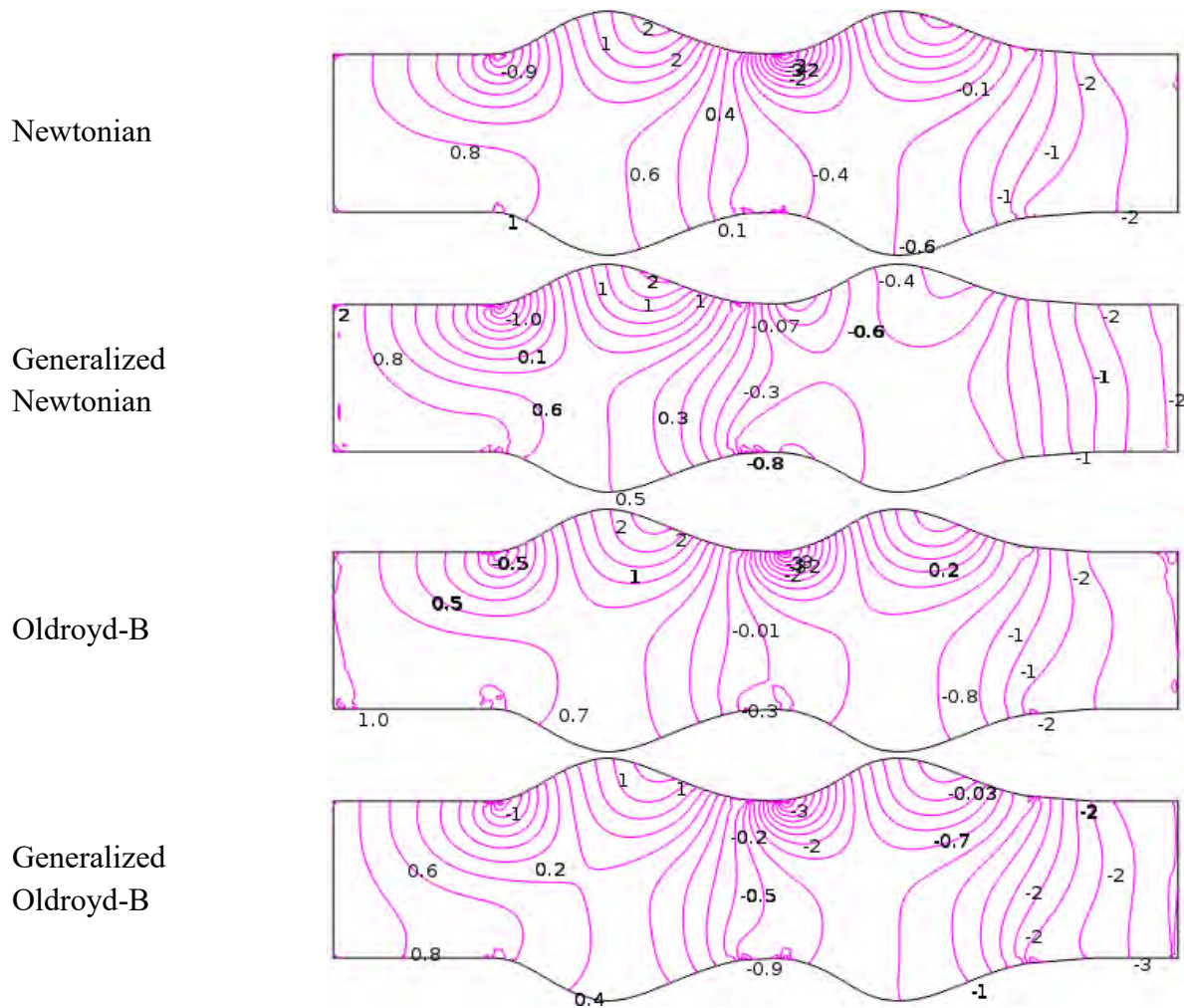
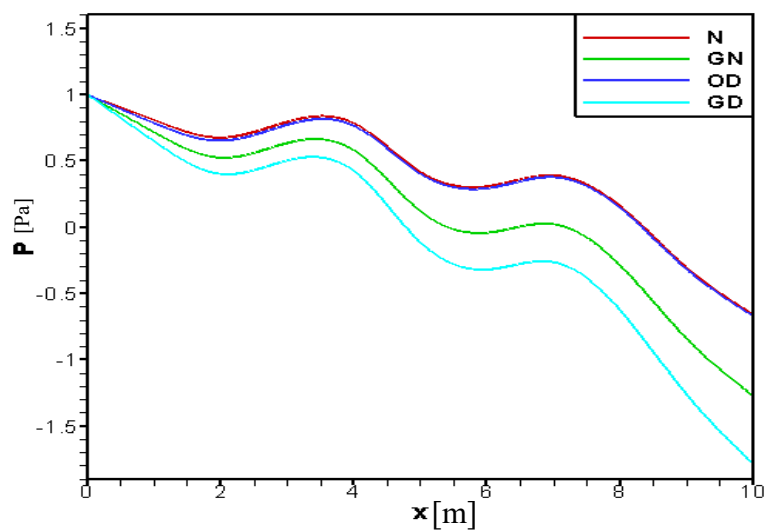


Figure 4.15: Pressure distribution on blood flow through permeable aneurysmatic blood vessel at $Pe=100$ and $Wi = 0.6$ with $q = 0.1 \text{ cm}^3/\text{s}$.



CHAPTER 4 BLOOD FLOW STUDY THROUGH... ..

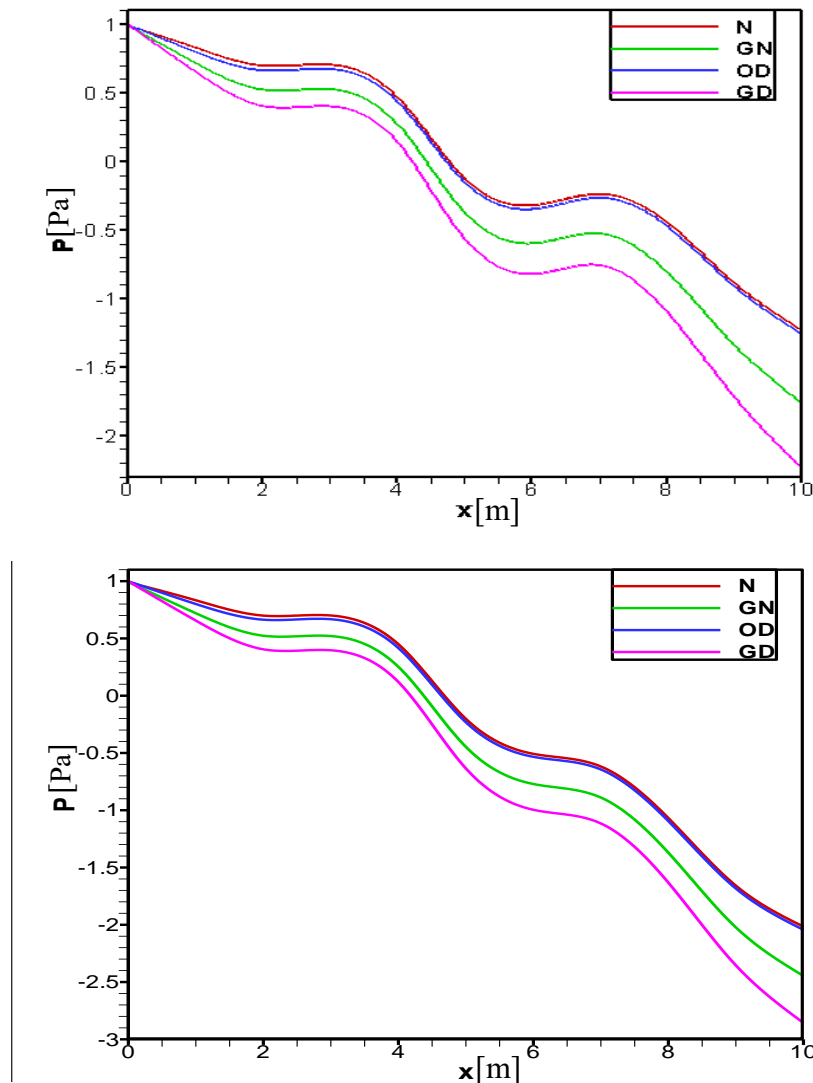


Figure 4.16: Pressure profile with no permeable (top), partial permeable (middle) and both permeable (bottom) aneurysmalong vesselwhen $Pe = 1000$ and $Wi = 0.6$.

4.4.3 Effects of dimensionless number

Peclet Numbers (Pe) Effects

The laminar blood flow patterns have obtained at Peclet numbers, $Pe = 1000$ and 2000 which is based on the diameter, length of the model and the average velocity at inlet computed from the corresponding flow rates of 0.13 L/min, and 0.25 L/min. For the flow rate 0.4 L/min., the Peclet number, $Pe = 3000$ which is indicative of turbulent blood flow.

The permanent recirculation zones are created between the dilated regions near the upper blood vessel wall for all models. For the laminar cases, the maximum core flow velocity through the aneurysm essentially remained the same as that of the entrance of the cavity in Figures 4.17 – 4.20. Therefore, the main hemodynamic mechanism for thrombus

CHAPTER 4 BLOOD FLOW STUDY THROUGH... ..

formation in the aneurysm is the slowly recirculation vortex. For the turbulent case in Figures 4.17-4.20, the maximum core flow velocity through the aneurysm (average velocity) has 6 percent slower than that of the upstream. The difference between laminar and turbulent cases stems from the fact that the recirculation zone has shrunk significantly for the turbulent case, leaving more space for the core flow to expand and slow down. It is observed that the recirculation bubbles have migrated approximately 45, 55 and 70 percent at $Pe = 1000, 2000$ and 3000 respectively from the vessel axis for all models. The reverse blood flow and blood back flow is formed at the second enlargement with the adjacent to vessel wall for higher peclet number.

It is very important findings that the turbulent velocities are reduced due to permeability aneurysm which leads to blood flow stability for all four models at Figure 4.21. The velocity has decreased 26, 46 and 62 percent for $Pe = 1000, 2000$ and 3000 at Newtonina case compare to impermeable aneurysm artery. In the case of Oldroyd-B, with the increase of Pe ($1000, 2000$ & 3000) the blood flow has reduced 26, 42 and 56 percent respectively at leaky aneurysm. From these figures, the maximum velocity deviation between upstream to downstream is 32 percents for Oldroyd-B case and minimum difference is 26.9 percent for Genelized Oldroyd-B case. In Figure 4.21, the least and most distinction of velocity between laminar and turbulent blood flow is 23 and 42.5 percent for generalized Oldroyd-B and Newtonian model respectively. In Table 4.4, the velocities deviation obtained for different Peclet numbers while $Pe = 1000, 2000$ and 3000 is presented.

Table 4.4: Velocity deviation are included for various Peclet numbers while $Pe = 1000, 2000$ and 3000 .

Models	Velocity (U)					
	Pe = 3000			Difference between Laminar and Turbulent flow		
	Up stream (inlet)	Down stream (1st Anuerysm)	Deviation (Percentage)	$Pe=1000$ (Laminar)	$Pe=3000$ (Turbulent)	Deviation (Percentage)
N	0.0721959	0.048987098	32.1470095	0.0489870	0.02810394	42.6298973
GN	0.0723178	0.05208039	27.9840015	0.0520803	0.03524744	32.3210743
OD	0.0726664	0.049244453	32.2322318	0.0492444	0.03068620	37.6859591
GD	0.0739408	0.053982804	26.9919256	0.0539828	0.04105782	23.9427791

CHAPTER 4 BLOOD FLOW STUDY THROUGH... ..

The pressure contour plots are shown in Figures 4.22 through 4.25 (odd numbers) for various Peclet numbers ($Pe=1000, 2000$ & 3000). At the entrance of the aneurysm cavity the pressure gained maximum value at the reattachment point and which constituted a stagnation point. The iso-pressure contour lines are indicative the minimum value of pressure at the end of second aneurysm and form a separation point. With the increase Peclet number the pressure contour lines are migrating to upper vessel wall and show the extreme value at reattachment point. Muraki (1983) observed that aneurysm rupture typically occurs at the bulge area and the pressure peak the highest value at the reattachment point.

In Figure 4.26, A dramatic change have occurred for blood pressure at Newtonian model Peclet number, $Pe=3000$ and pressure is intensified. The pressure has decreased along with vessel axis and highest pressure are found at turbulent blood flow ($Pe = 3000$) for Newtonian and generalized Newtonian models. But in the case of Oldroyd-B and generalized Oldroyd-B, a slight different are seen in pressure between laminar ($Pe=1000$) and turbulent ($Pe=3000$) blood flow due to permeability aneurysm. For blood shear-thinning behavior, the pressure is reverse after first aneurysm that is the lowest value are found at $Pe = 3000$ for generalized Oldroyd-B case. The pressure has dropped 35, 48 and 7 percent for different Peclet number ($Pe= 1000, 2000$ and 3000) at Newtonian case compare to impermeable aneurysm artery where maximum and minimum pressure throw down is 48% and 7% at $Pe=2000$ and 3000 respectively. On the other hand, the blood pressure has felled 40, 60 and 57 percent respectively at leaky aneurysm for $Pe = 1000, 2000$ and 3000 respectively at Oldroyd-B model. The pressure variation has mentioned in the following Table 4.5 for all models.

Table 4.5: Pressure variation at inlet and 1st aneurysm for different Pe with $Wi = 0.6$ and $q = 0.1 \text{ cm}^3/\text{s}$.

Models	Pressure (P)					
	Pe = 3000			Difference between Laminar and Turbulent flow		
	Up stream (inlet)	Down stream (1st Anuerysm)	Deviation (Percentage)	Pe=1000 (Laminar)	Pe=3000 (Turbulent)	Deviation (Percentage)
N	0.95847779	1.543063817	60.9910860	0.7052528	1.5430638	118.795825
GN	0.96214671	1.060316066	10.2031578	0.5259346	1.0603160	101.606058
OD	1.00532439	0.960631919	4.44557714	0.6727216	0.9606319	42.7978318
GD	1.00154300	0.617309048	38.3641995	0.4011610	0.6173090	53.8806175

CHAPTER 4 BLOOD FLOW STUDY THROUGH... ..

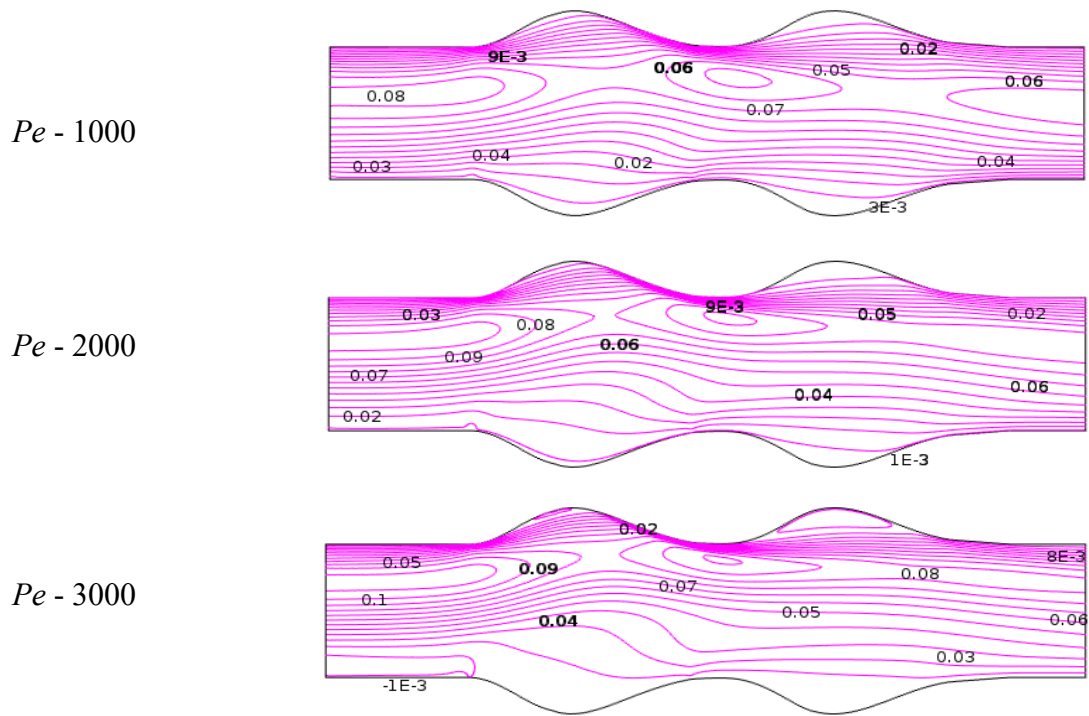


Figure 4.17: Peclet Numbers (Pe) effects on Blood flow of Newtonian Model at $Wi = 0.6$ and flow rate $0.1 \text{ cm}^3/\text{s}$.

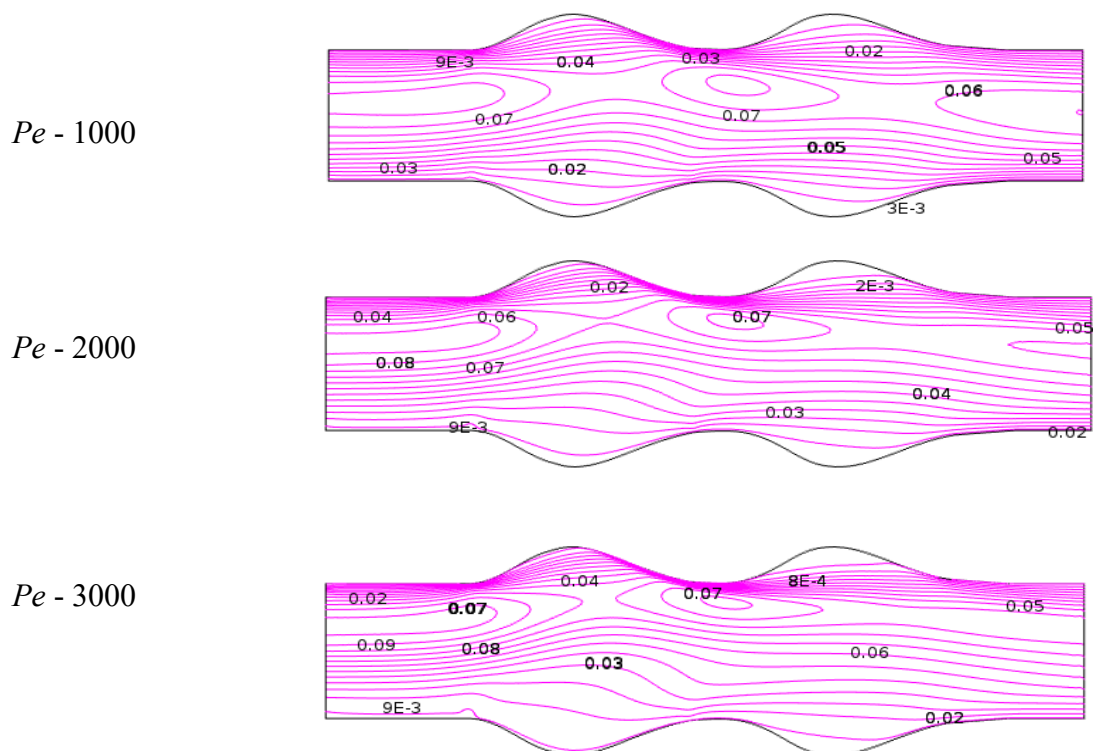


Figure 4.18: Peclet Numbers (Pe) effects on Blood flow of Generalized Newtonian Model at $Wi = 0.6$ and flow rate $0.1 \text{ cm}^3/\text{s}$.

CHAPTER 4 BLOOD FLOW STUDY THROUGH... ..

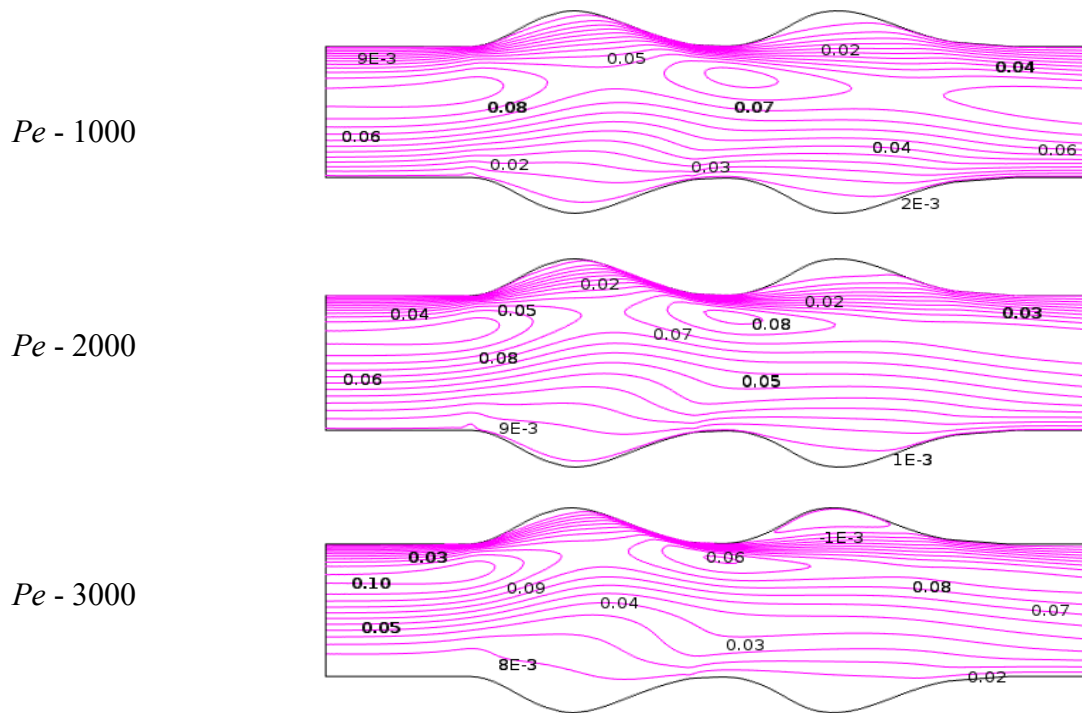


Figure 4.19: Peclet Numbers (Pe) effects on Blood flow of Oldroyd-B Model at $Wi = 0.6$ and flow rate $0.1 \text{ cm}^3/\text{s}$.

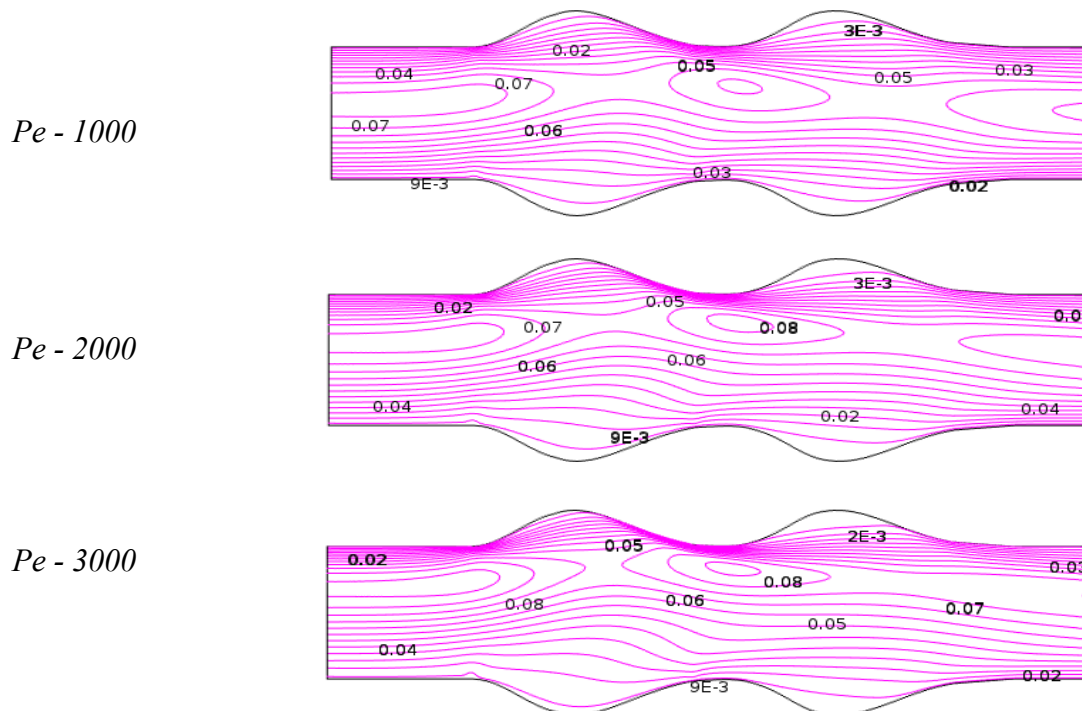


Figure 4.20: Peclet Numbers (Pe) effects on Blood flow of Generalized Oldroyd-B Model at $Wi = 0.6$ and flow rate $0.1 \text{ cm}^3/\text{s}$.

CHAPTER 4 BLOOD FLOW STUDY THROUGH... ..

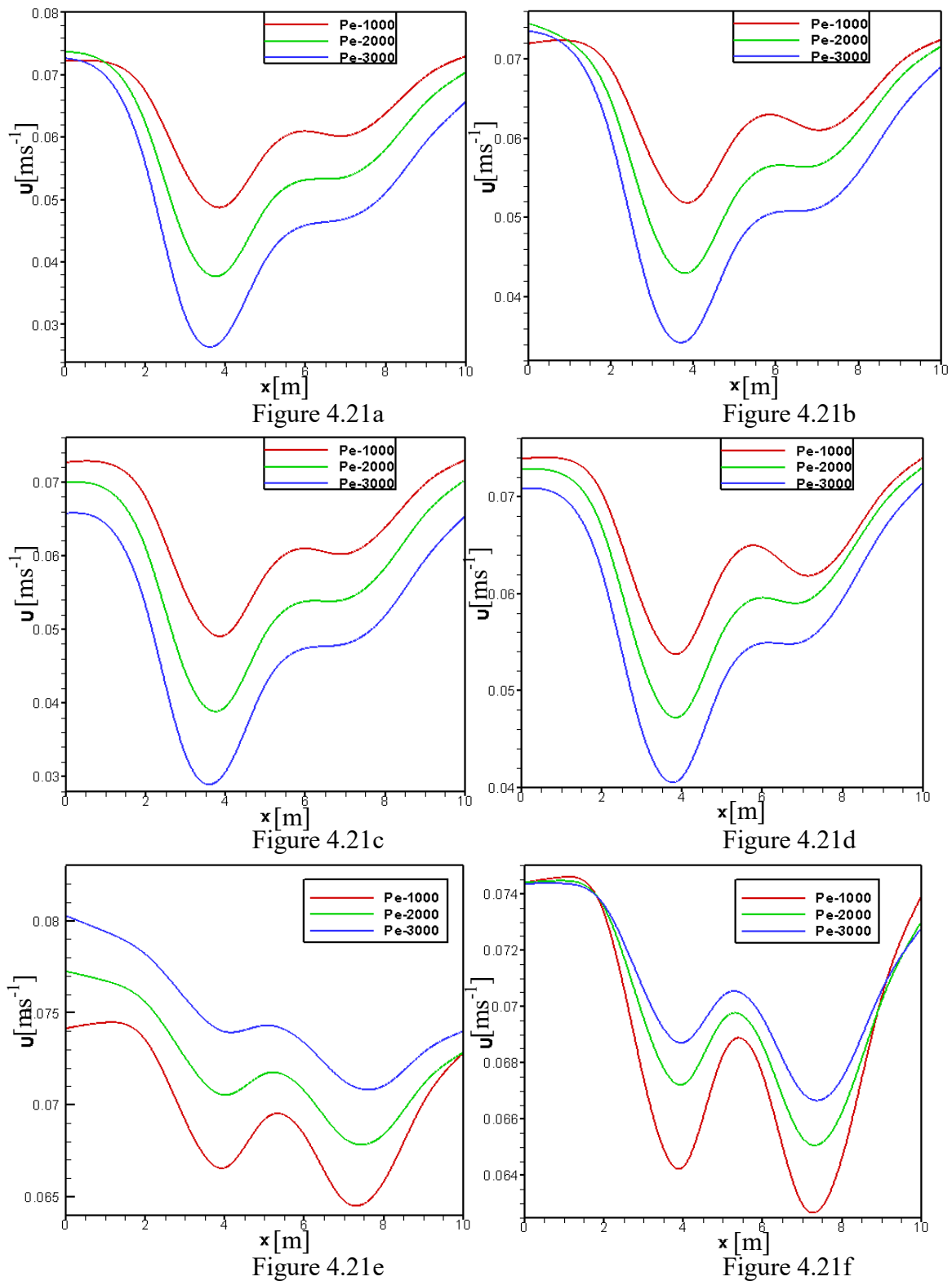


Figure 4.21: Velocity profile of Peclet numbers (Pe) on Blood flow at $Wi = 0.6$ and flow rate $0.1 \text{ cm}^3/\text{s}$ for (Figure 4.21a) Newtonian Model, (Figure 4.21b) Generalized Newtonian Model, (Figure 4.21c) Oldroyd-B Model, (Figure 4.21d) Generalized Oldroyd-B Model (Figure 4.21e) Newtonian Model without permeability, and (Figure 4.21f) Generalized Oldroyd-B Model with impermeable aneurysm wall.

CHAPTER 4 BLOOD FLOW STUDY THROUGH... ..

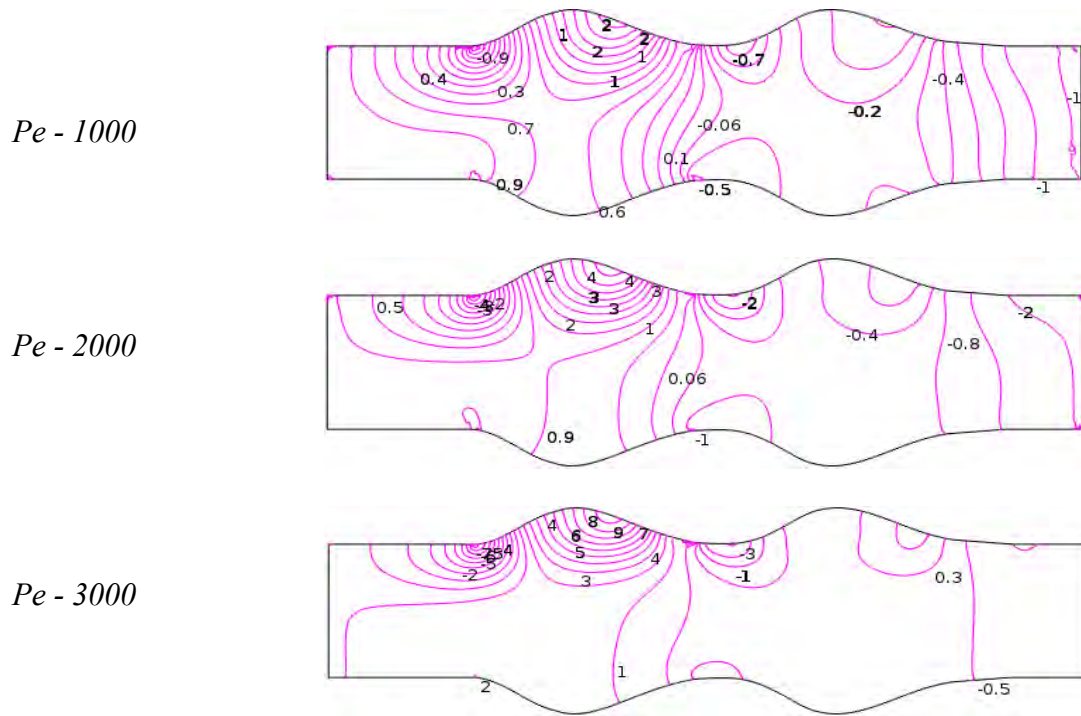


Figure 4.22: Peclet Numbers (Pe) effects on pressure distribution of Blood flow for Newtonian Model at $Wi = 0.6$ and flow rate $0.1 \text{ cm}^3/\text{s}$.

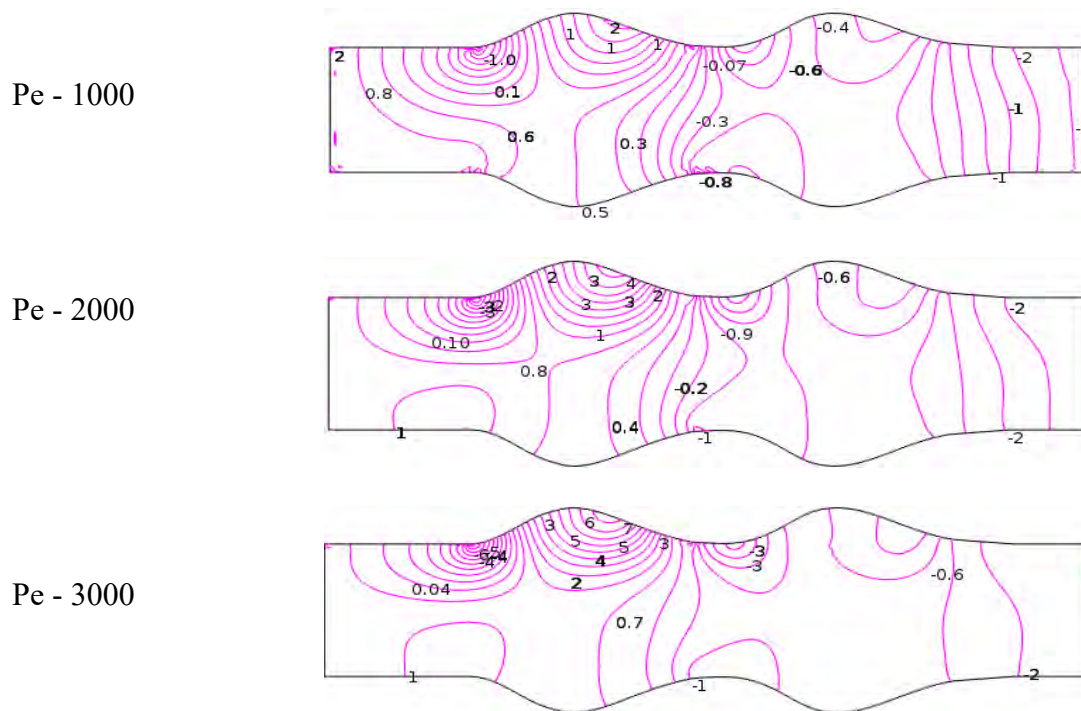


Figure 4.23: Peclet Numbers (Pe) effects on pressure distribution of Blood flow for Generalized Newtonian Model at $Wi = 0.6$ and flow rate $0.1 \text{ cm}^3/\text{s}$.

CHAPTER 4 BLOOD FLOW STUDY THROUGH... ..

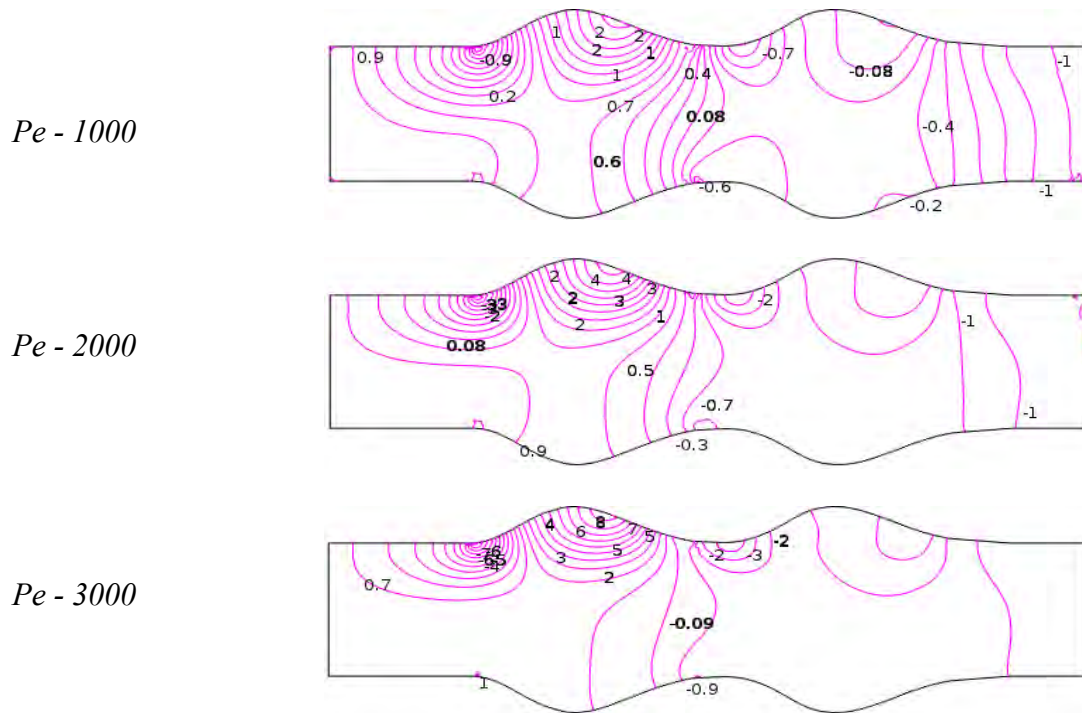


Figure 4.24: Peclet Numbers (Pe) effects on pressure distribution of Blood flow for Oldroyd-B Model at $Wi = 0.6$ and flow rate $0.1 \text{ cm}^3/\text{s}$.

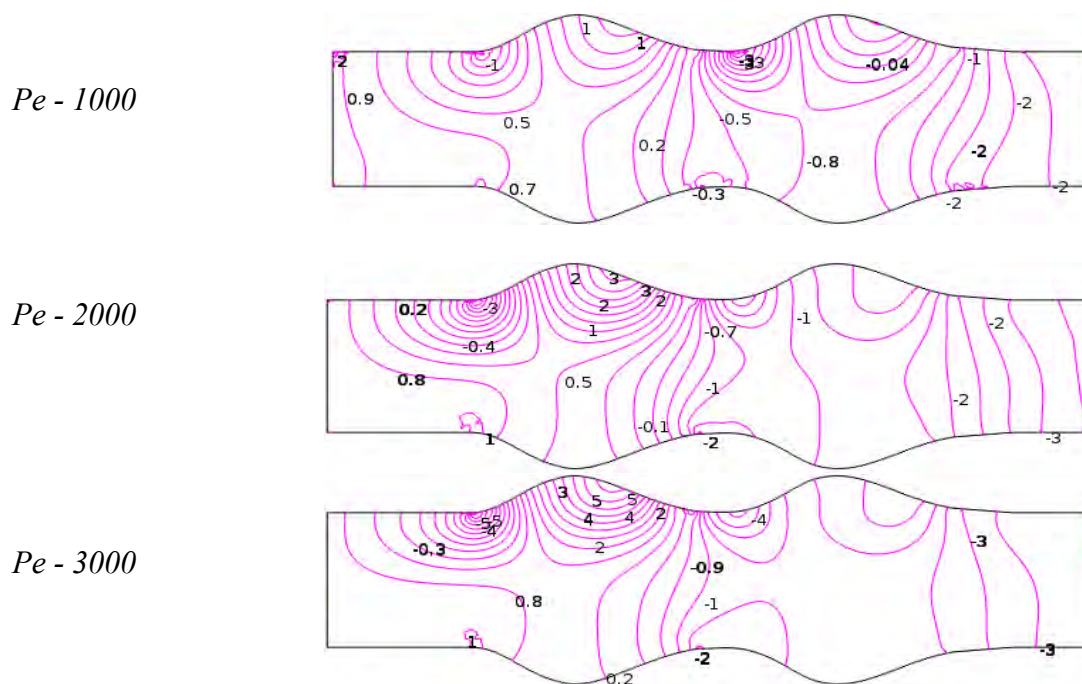


Figure 4.25: Peclet Numbers (Pe) effects on pressure distribution of Blood flow for Generalized Oldroyd-B Model at $Wi = 0.6$ and flow rate $0.1 \text{ cm}^3/\text{s}$.

CHAPTER 4 BLOOD FLOW STUDY THROUGH... ..

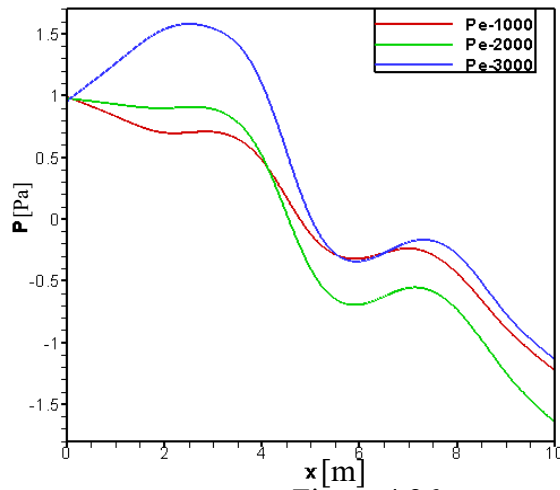


Figure 4.26a

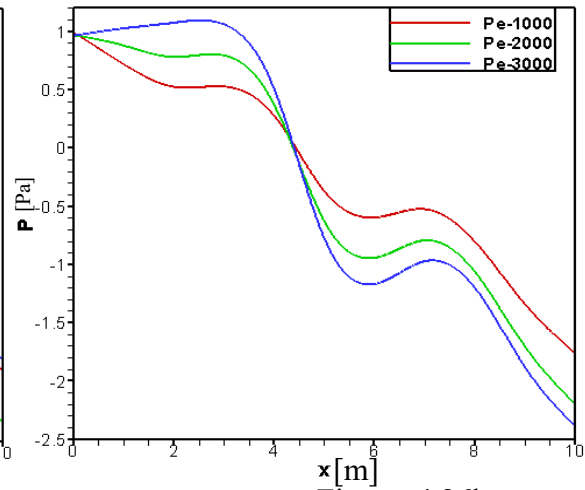


Figure 4.26b

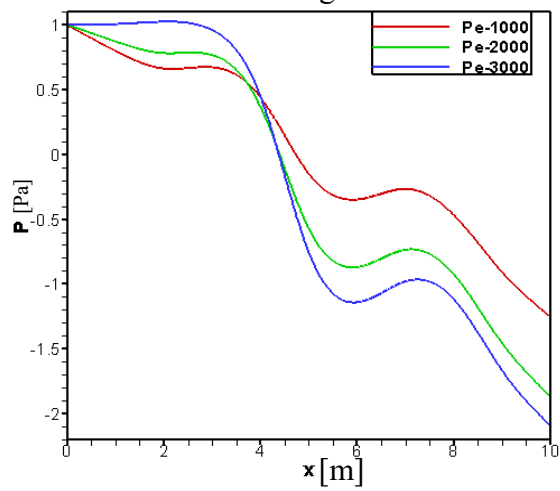


Figure 4.26c

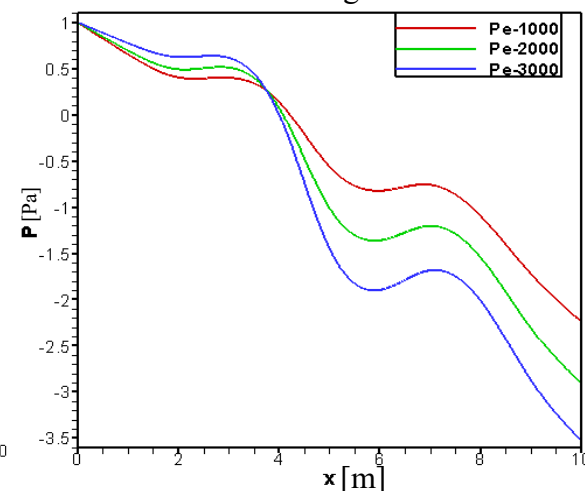


Figure 4.26d

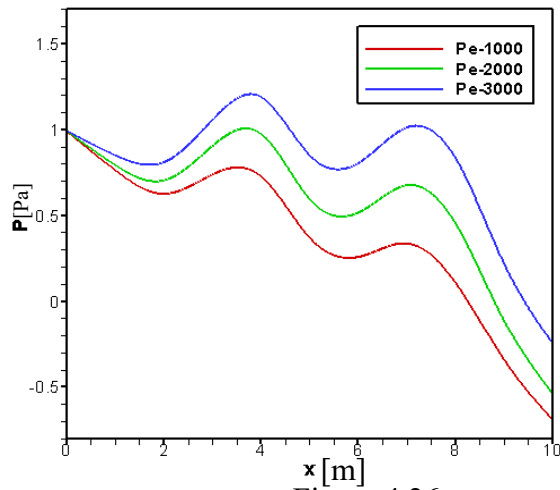


Figure 4.26e

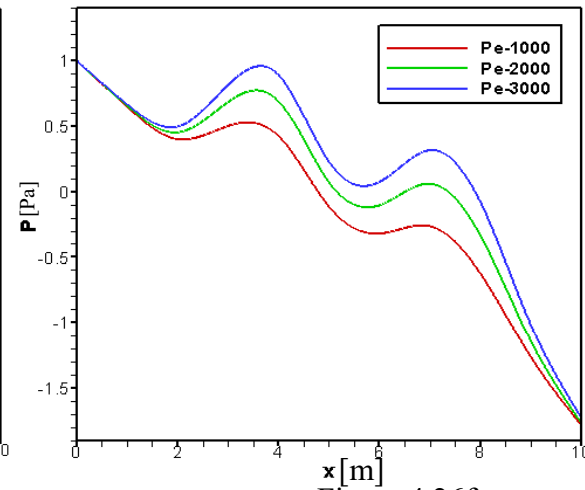


Figure 4.26f

Figure 4.26: Pressure profile of Peclet numbers (Pe) on Blood flow at $Wi = 0.6$ and flow rate $0.1 \text{ cm}^3/\text{s}$ for (Figure 4.26a) Newtonian Model, (Figure 4.26b) Generalized Newtonian Model, (Figure 4.26c) Oldroyd-B Model, and (Figure 4.26d) Generalized Oldroyd-B Model (4.26e) Newtonian Model without permeability, and (4.26f) Generalized Oldroyd-B Model with impermeable aneurysm wall.

CHAPTER 4 BLOOD FLOW STUDY THROUGH... ..

Weissenberg Numbers (Wi) Effects

Again, the simulation of blood flow is shown in Figures 4.27 through 4.30 for different Weissenberg numbers, Wi (0.0, 0.5, 1.0) in terms of velocity and pressure contour lines. The very small Wi ($Wi = 0.0$) corresponds to no elasticity and big Wi leads to pure elastic response fluid. As seen in the figures, the length of the recirculation bubble is strongly affected by the Weissenberg numbers, with small abridgment occurring as the Weissenberg numbers increases. The numbers of recirculation bubbles have increased with respect to Weissenberg numbers. The ellipse-like bubbles have originated at center of aneurysm it is shifting toward the upper vessel wall. Due to porosity, the velocity contours have developed a non-axisymmetric profile at entrance while it forms axisymmetric profile at exit of the cavity. We observe that velocity decreases at the permeable aneurysm and then increases with the increases of Wi . At $Wi = 1$, the velocity is higher except inlet velocity because of less dominant viscous force and blood behave fluid-like bodies. Just behind the porous aneurysm the separation zone has formed at the adjacent to vessel wall. In Figure 4.31d, the velocity profiles are almost same with various Wi for generalized Oldroyd-B case. We have gained minimum velocity at permeable aneurysm and maximum velocity at outlet is illustrated in Figure 4.31. It is shown from the Figures 4.31a and 4.31e that 26 to 32 percent velocity has decreased in the presence of porosity wall compare to nonporous aneurysmatic artery with the increases of Wi for Newtonian models. In the case of generalized Oldroyd-B model, the velocity variations are almost same which is approximately 16% for different Weissenberg numbers. The maximum and minimum velocity have inserted in the following table 4.6 along vessel axis for different Weissenberg numbers while $Wi = 0.0, 0.5, 1.0$.

Table 4.6: Optimal value of velocity are added for various Wi when $Pe = 1000$ and flow rate, $q = 0.1 \text{ cm}^3/\text{s}$.

Models	Velocity (U)					
	Maximum			Minimum		
	$Wi=0.0$	$Wi=0.5$	$Wi=1.0$	$Wi=0.0$	$Wi=0.5$	$Wi=1.0$
N	0.07846123	0.07300878	0.07317073	0.04576681	0.04898709	0.04917550
GN	0.07609075	0.07244404	0.07254959	0.05159760	0.05208039	0.05206627
OD	0.07468072	0.07299625	0.07316210	0.04854258	0.04924445	0.04932107
GD	0.07535079	0.07403781	0.0741205	0.0539636	0.05398280	0.05396784

CHAPTER 4 BLOOD FLOW STUDY THROUGH... ..

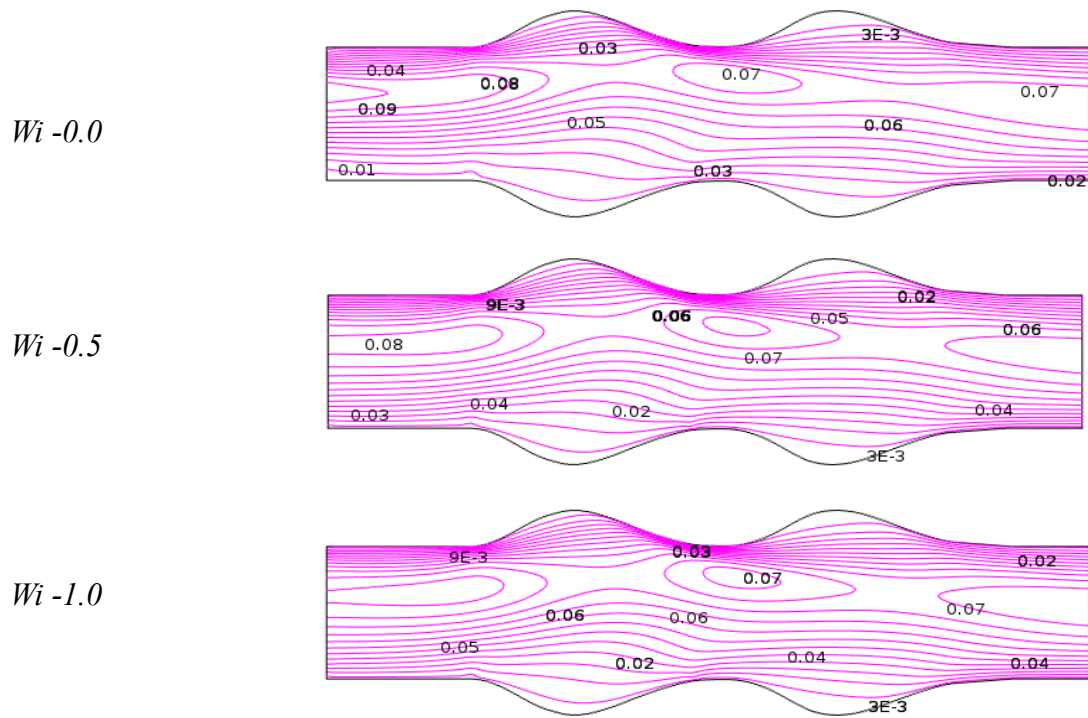


Figure 4.27: Weissenberg Numbers (Wi) effects on Blood flow of Newtonian Model at $Re = 1000$ and flow rate $0.1 \text{ cm}^3/\text{s}$.

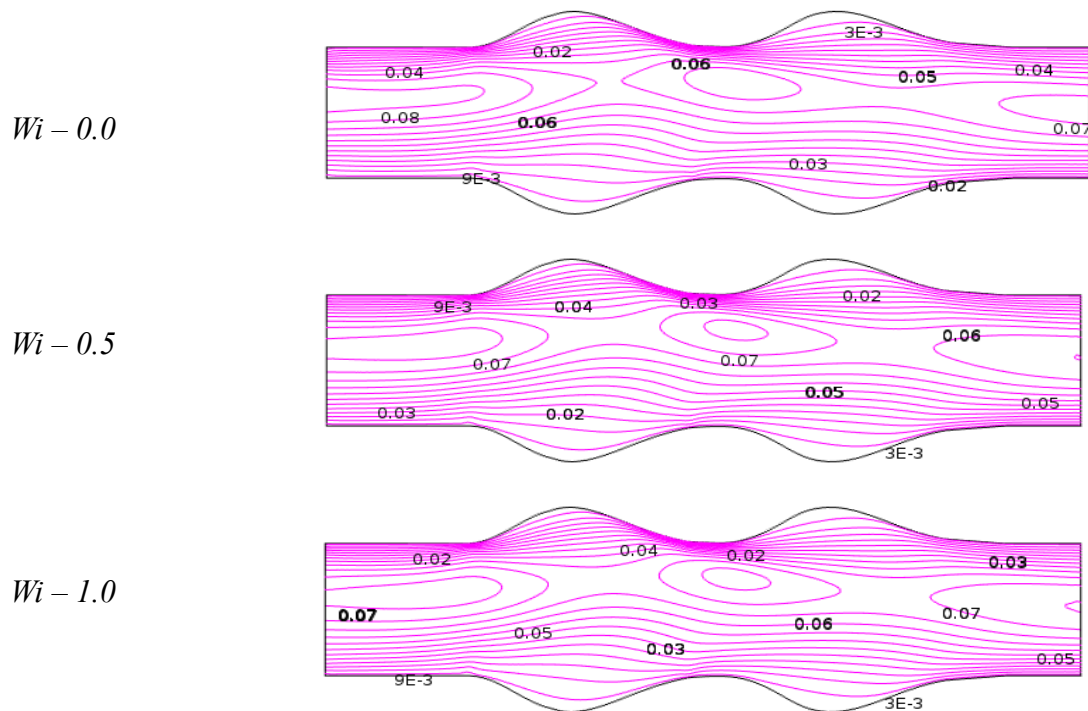


Figure 4.28: Weissenberg Numbers (Wi) effects on velocity distribution of Blood flow for Generalized Newtonian Model at $Re = 1000$ and flow rate $0.1 \text{ cm}^3/\text{s}$.

CHAPTER 4 BLOOD FLOW STUDY THROUGH... ..

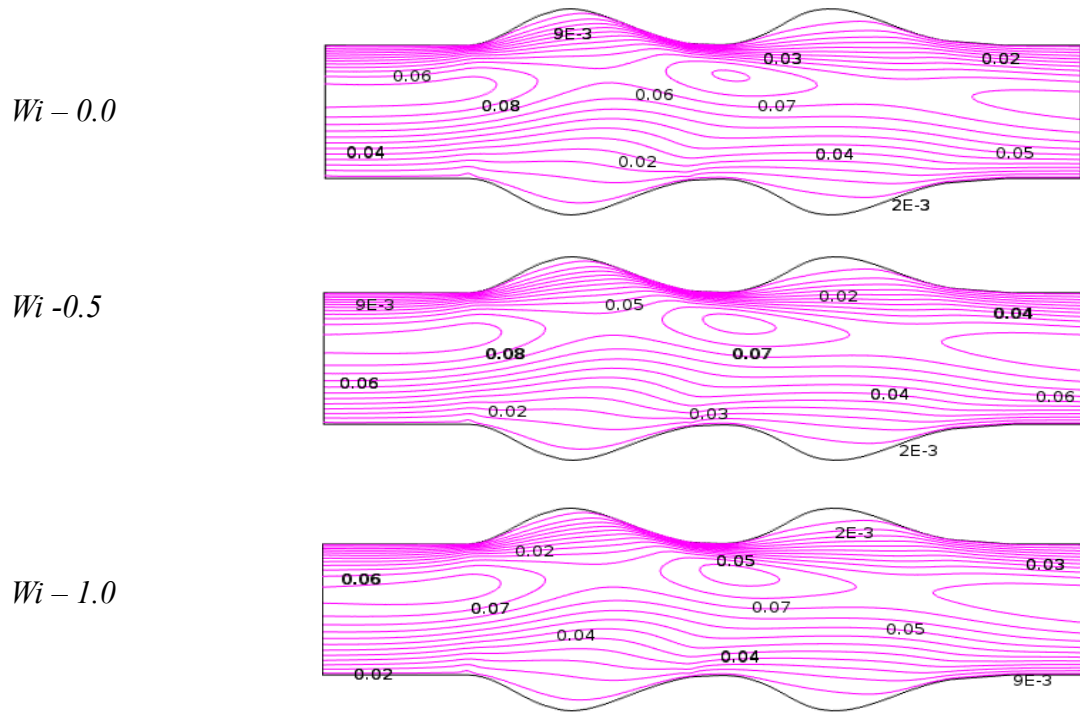


Figure 4.29: Weissenberg Numbers (Wi) effects on velocity distribution of Blood flow for Oldroyd-B Model at $Re = 1000$ and flow rate $0.1 \text{ cm}^3/\text{s}$.

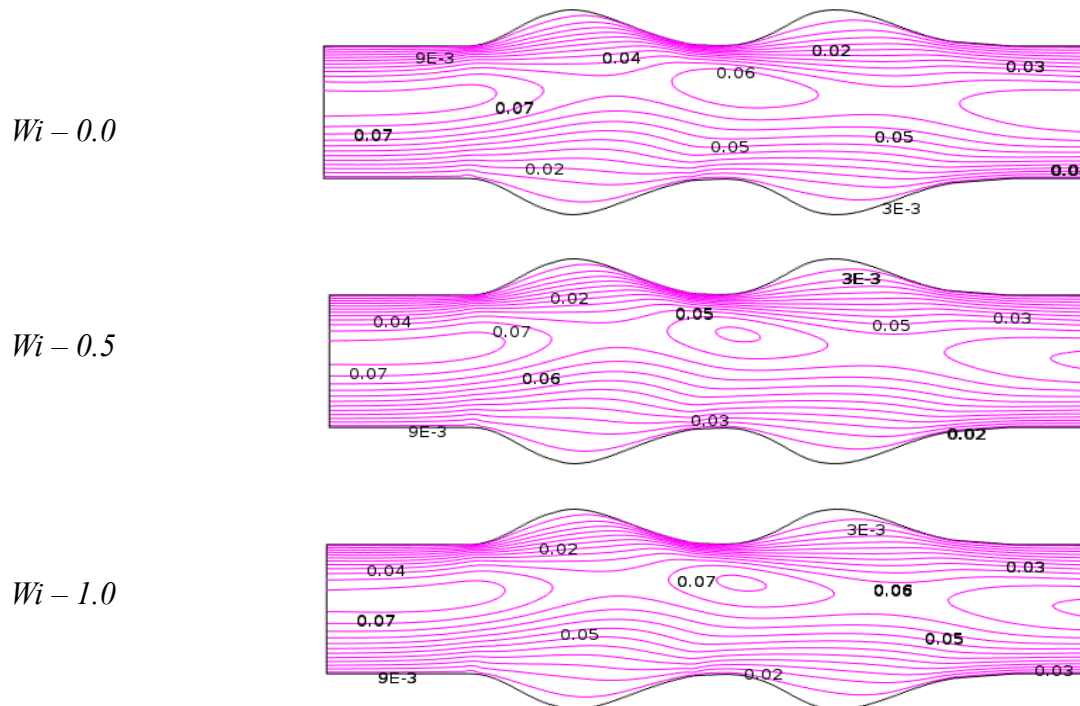


Figure 4.30: Weissenberg Numbers (Wi) effects on Velocity distribution of Blood flow for Generalized Oldroyd-B Model at $Pe = 1000$ and flow rate $0.1 \text{ cm}^3/\text{s}$.

CHAPTER 4 BLOOD FLOW STUDY THROUGH... ..

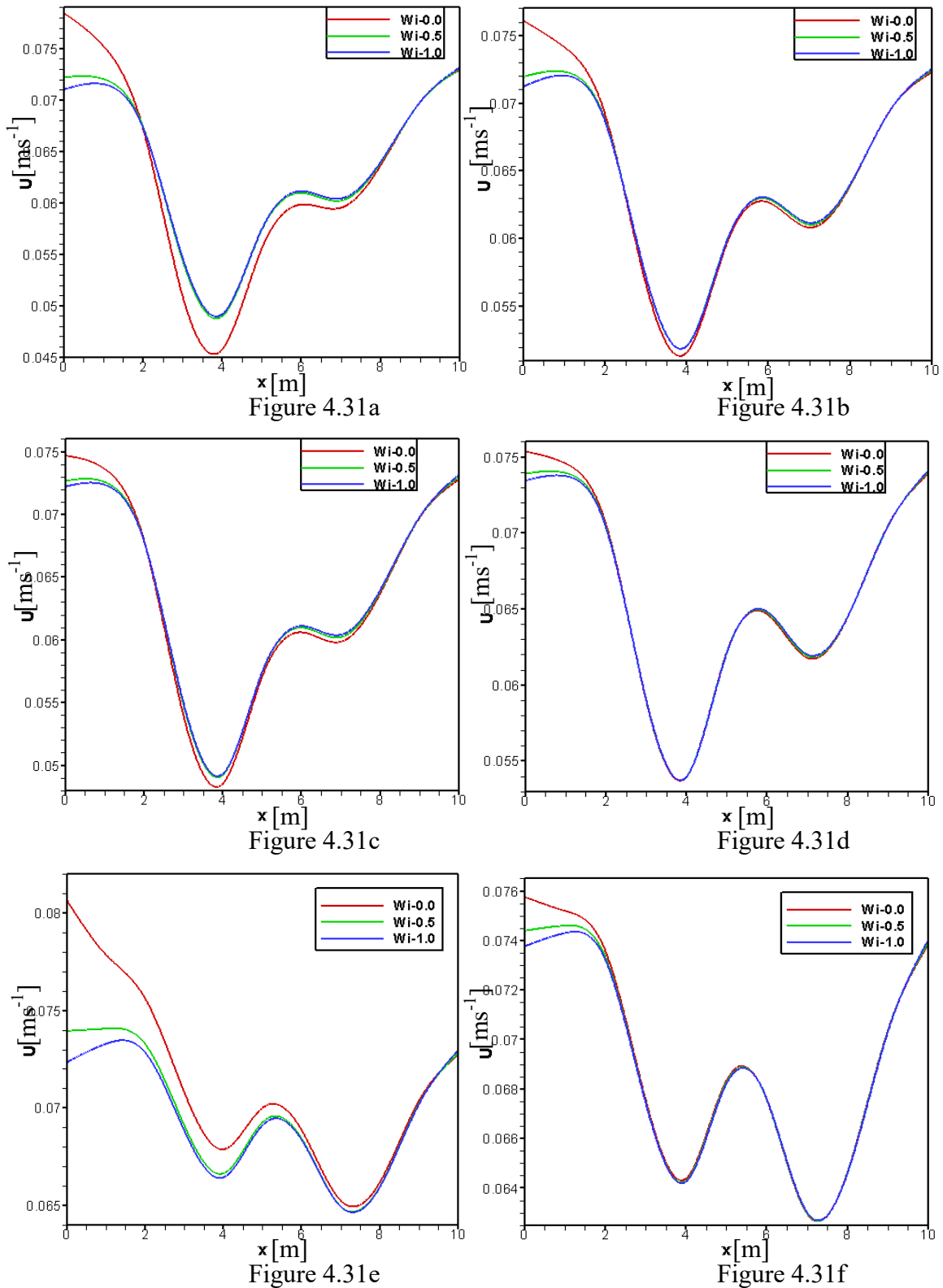


Figure 4.31: Velocity profile of the Effects of Weissenbug numbers (Wi) on Blood flow at $Pe = 1000$ and flow rate $0.1 \text{ cm}^3/\text{s}$ for (Figure 4.31a) Newtonian Model, (Figure 4.31b) Generalized Newtonian Model, (Figure 4.31c) Oldroyd-B Model, and (Figure 4.31d) Generalized Oldroyd-B Model (Figure 4.31e) Newtonian Model without permeability, and (Figure 4.31f) Generalized Oldroyd-B Model with impermeable aneurysm wall.

CHAPTER 4 BLOOD FLOW STUDY THROUGH... ..

The simulation of pressure is shown in Figures 4.32 through 4.35 for different Weissenberg numbers, Wi (0.0, 0.5, 1.0) in terms of contour lines. The pressures are more intensified at the permeable aneurysm area compare to other area in the aneurysm cavity and provide greater value at the reattachment point. At the end of second enlargement the pressure contour plots are alike and its show how the pressure reached a minimum at the separation point and decreased monotonously along the aneurysm. The pressure patterns have a little changed in non-porous aneurysm with the increases of Wi . The shear-thinning characteristic of blood viscosity which leads the flow is faster in leaky aneurysm.

The pressure decreases with the increases of Weissenberg number, $Wi = 0.0, 0.5$ & 1.0 and it is explained in Figure 4.36 graphically. From the Figure 4.36, the maximum pressure is found at $Wi = 0.0$ for Newtonian case and pressure profiles are almost similar at generalized Oldroyd-B model. In Figure 4.36, the numerical values of pressure distribution are presented for all the four models Newtonian, Generalized Newtonian, Oldroyd-B, Generalized Oldroyd-B with the flow rate, $q = 0.1 \text{ cm}^3/\text{s}$. In Table 4.7, the pressure obtained along vessel axis for different Weissenberg numbers while $Wi = 0.0, 0.5$ and 1.0 is presented.

Table 4.7: Minmax pressure are obtained along vessel axis for different Weissenberg numbers while $Wi = 0.0, 0.5$ and 1.0 .

Models	Velocity (U)					
	Maximum			Minimum		
	$Wi=0.0$	$Wi=0.5$	$Wi=1.0$	$Wi=0.0$	$Wi=0.5$	$Wi=1.0$
N	1.13254511	0.99020622	0.99314531	-0.7092817	-1.22724245	-1.29422096
GN	0.98168668	0.99279064	0.99573846	-1.5861485	-1.76730261	-1.80307929
OD	0.99465079	0.99882315	1.00083803	-1.1473296	-1.25541537	-1.28516133
GD	0.99418609	0.99832582	0.99955809	-2.1869402	-2.23774696	-2.25434182

CHAPTER 4 BLOOD FLOW STUDY THROUGH... ..

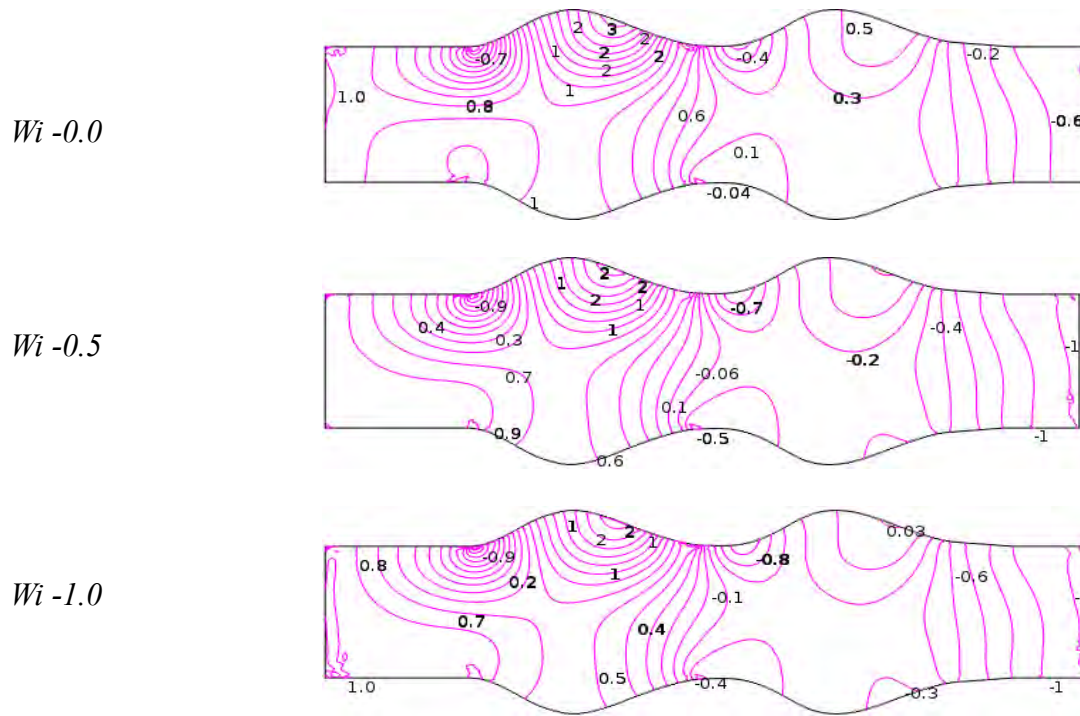


Figure 4.32: Weissenberg Numbers (Wi) effects on pressure distribution of Blood flow for Newtonian Model at $Re = 1000$ and flow rate $0.1 \text{ cm}^3/\text{s}$.

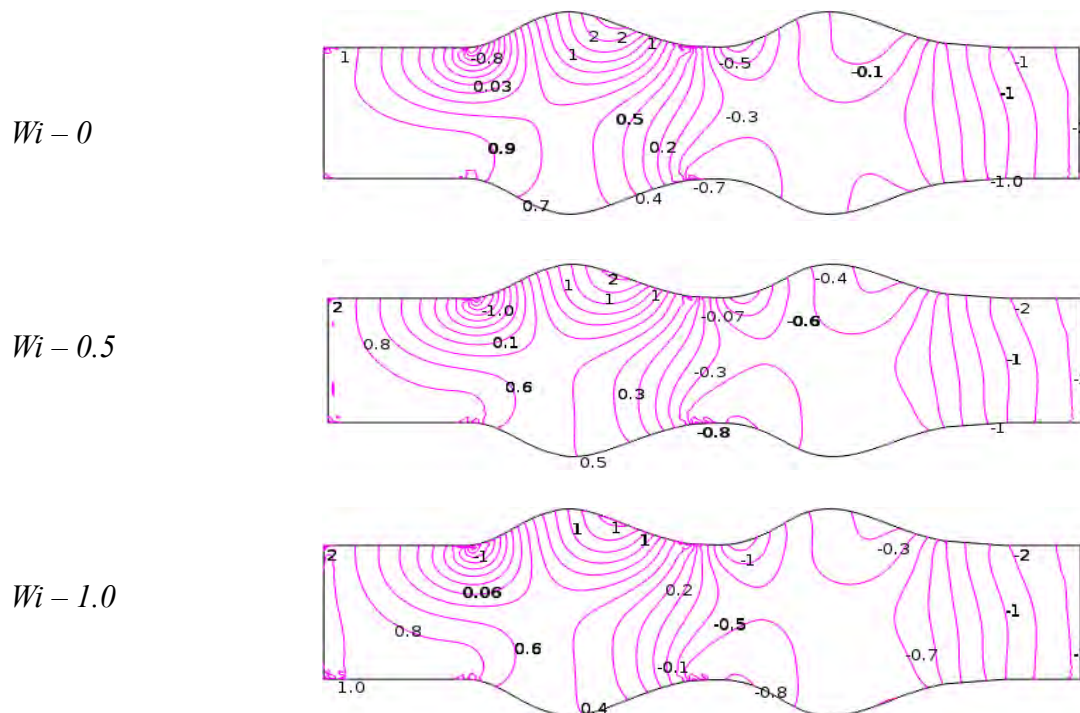


Figure 4.33: Weissenberg Numbers (Wi) effects on pressure distribution of Blood flow for Generalized Newtonian Model at $Re = 1000$ and flow rate $0.1 \text{ cm}^3/\text{s}$.

CHAPTER 4 BLOOD FLOW STUDY THROUGH... ..

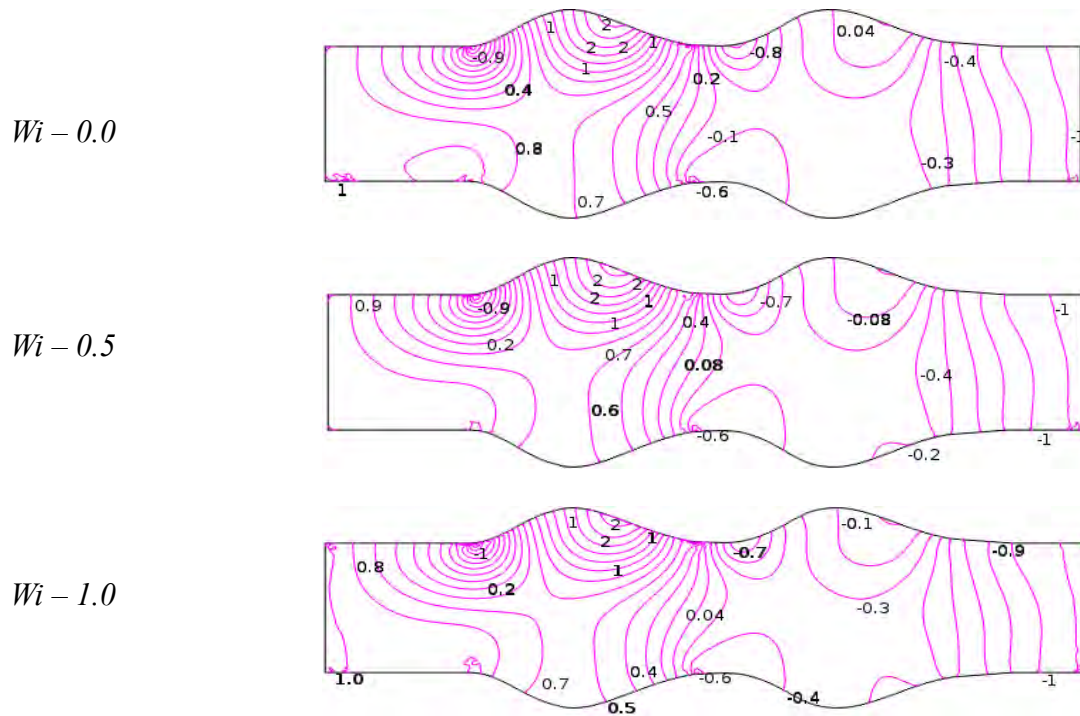


Figure 4.34: Weissenberg Numbers (Wi) effects on pressure distribution of Blood flow for Oldroyd-B Model at $Re = 1000$ and flow rate $0.1 \text{ cm}^3/\text{s}$.

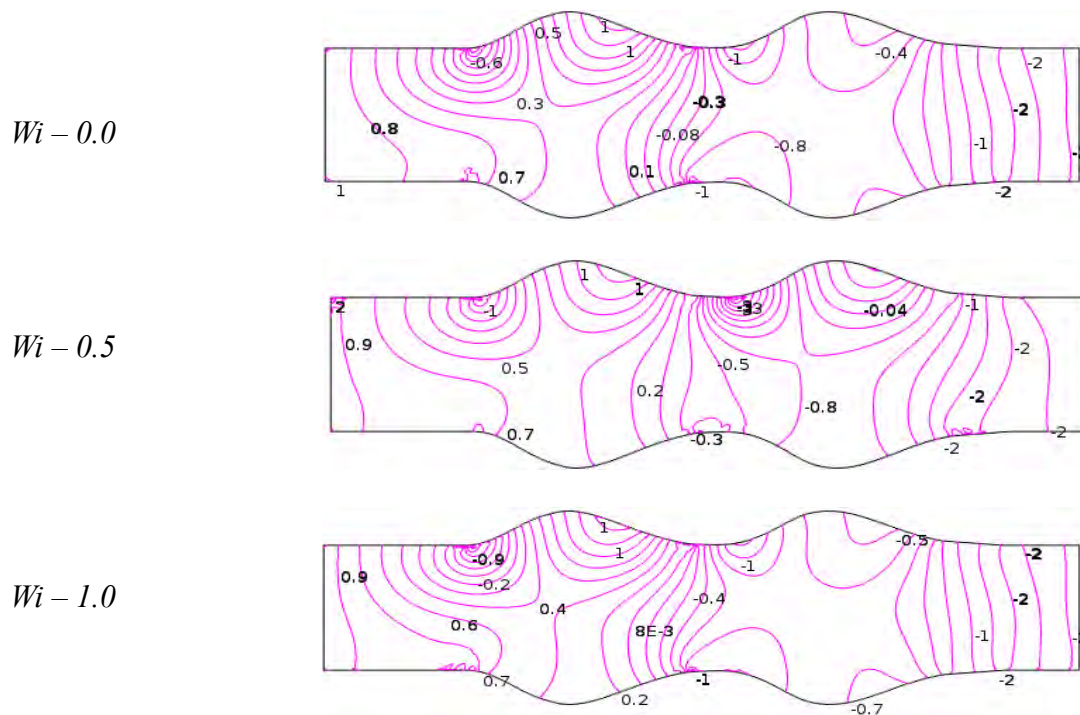


Figure 4.35: Weissenberg Numbers (Wi) effects on pressure distribution of Blood flow for Generalized Oldroyd-B Model at $Pe = 1000$ and flow rate $0.1 \text{ cm}^3/\text{s}$.

CHAPTER 4 BLOOD FLOW STUDY THROUGH... ..

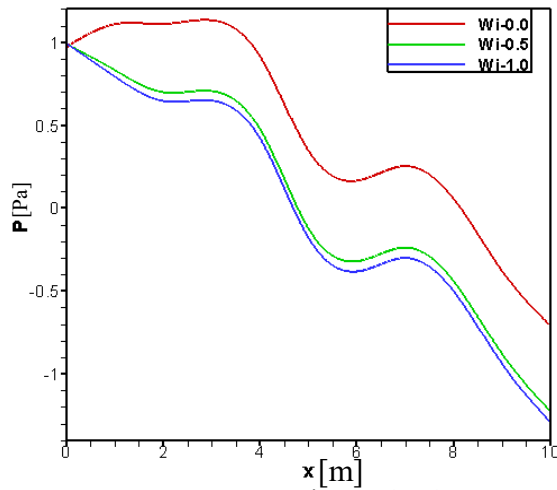


Figure 4.36a

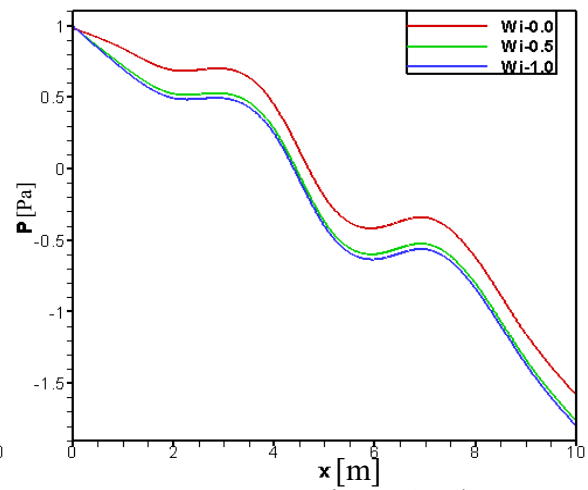


Figure 4.36b

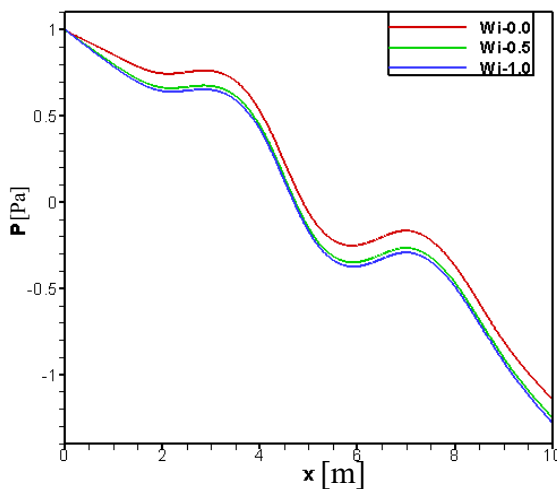


Figure 4.36c

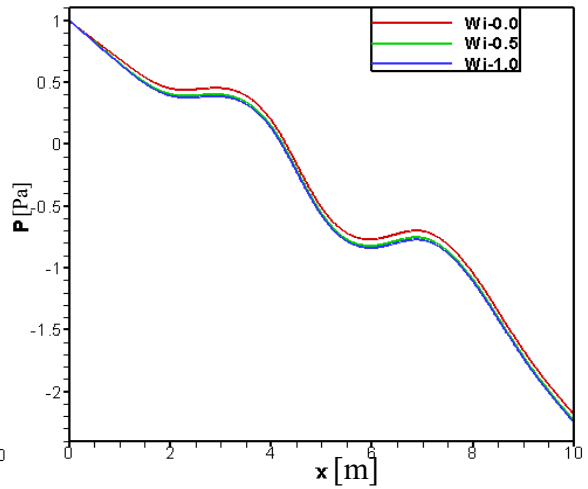


Figure 4.36d

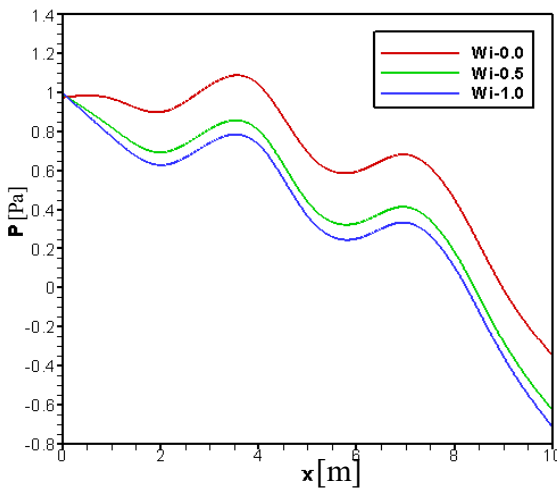


Figure 4.36e

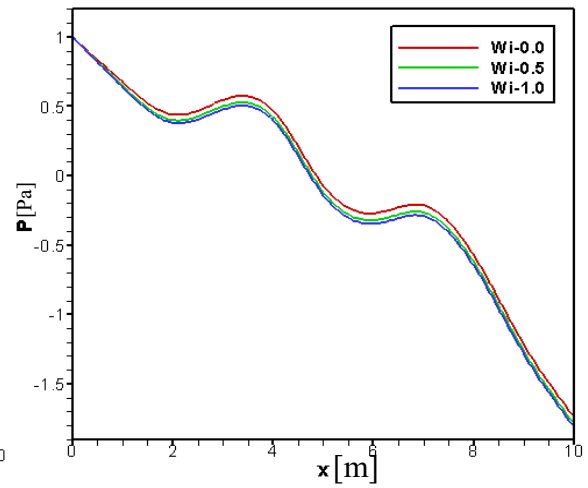


Figure 4.36f

Figure 4.36: Pressure profile of the Effects of Weissenbegr numbers (Wi) on Blood flow at $Pe = 1000$ and flow rate $0.1 \text{ cm}^3/\text{s}$ for (Figure 4.36a) Newtonian Model, (Figure 4.36b) Generalized Newtonian Model, (Figure 4.36c) Oldroyd-B Model, and (Figure 4.36d) Generalized Oldroyd-B Model (Figure 4.36e) Newtonian Model without permeability, and (Figure 4.36f) Generalized Oldroyd-B Model with impermeable aneurysm wall.

CHAPTER 4 BLOOD FLOW STUDY THROUGH... ..

4.4.4 Stress tensor effects on blood flow

Contours of extra stress components σ_{11} , σ_{12} and σ_{22} for Newtonian, Generalized Newtonian, Oldroyd-B, Generalized Oldroyd-B are shown in Figures 4.36-4.39. The stress components σ_{11} and σ_{22} on blood flow are oscillating along vessel axis for all models. The component σ_{12} provides highest stress on blood flow at the beginning of permeable aneurysm and then decreases along vessel axis for all cases. In the case of σ_{11} and σ_{22} , the stress oscillations are opposite each other and big difference is found at commencement of permeable aneurysm. We observe that the stresses are adjacent at nonpermeable aneurysm and proximate at Newtonian and Oldroyd-B model. The stress tensor component σ_{11} is fluctuating along the vessel axis and originates minimum value at the early of first aneurysm. On the other hand, the stress tensor component σ_{12} provides higher value compared to other components along blood vessel axis and peaks at the initial enlargement area for Newtonian model. From Figure 4.33, the topmost value leads the blood fluid particles exerted highest forces each other and minimum forces are applied at lowest value. For the blood viscoelasticity and shear thinning behavior, the blood particles have employed less force in generalized models compared to non-generalized models. The influence of Weissenberg numbers is shown in Figure 4.38 with $Pe = 1000$ and flow rate, $q = 0.1 \text{ cm}^3/\text{sec}$ at permeable aneurysm. With the increase of Wi , the blood fluid particles have applied more stress each other for Newtonian case but different behavior is found for σ_{22} . The lowest stress is originated at generalized Oldroyd-B case for stress components σ_{11} and σ_{12} because of intensified elastic behavior with increasing Wi . The effect of σ_{11} , σ_{12} and σ_{22} on blood flow for various Pe are depicted in Figure 4.39. The stresses have increased with respect to Pe at σ_{11} and σ_{12} but decreased at σ_{22} for all models. The peak value of stress infers that the blood fluid particles have employed more forces each other and vice versa for lowest value. In the case of generalized models, the stress value is minimum and maximum values have produced at Newtonian case. In Table 4.8, the numerical value of stress tensor components along vessel axis at permeable aneurysm and impermeable aneurysm while $q = 0.1 \text{ cm}^3/\text{s}$, $Pe = 1000$ and $Wi = 0.6$ are presented.

CHAPTER 4 BLOOD FLOW STUDY THROUGH... ..

Table 4.8: Numerical value of stress components along vessel axis at permeable aneurysm and impermeable aneurysm while $q = 0.1 \text{ cm}^3/\text{s}$, $Pe = 1000$ and $Wi = 0.6$.

Models	Stress tensor components					
	First aneurysm (permeable)			Second aneurysm (Impermeable)		
	σ_{11}	σ_{12}	σ_{22}	σ_{11}	σ_{12}	σ_{22}
N	0.010381439	0.053788133	-0.00826444	0.003558385	0.049829594	-0.00178346
GN	0.008899055	0.046426186	-0.00731837	-0.000148	0.03810832	0.0011851
OD	0.009623097	0.053839372	-0.00750608	0.003541684	0.049683179	-0.00177912
GD	0.008903874	0.042776382	-0.00755166	-0.00294549	0.032432659	0.003709123

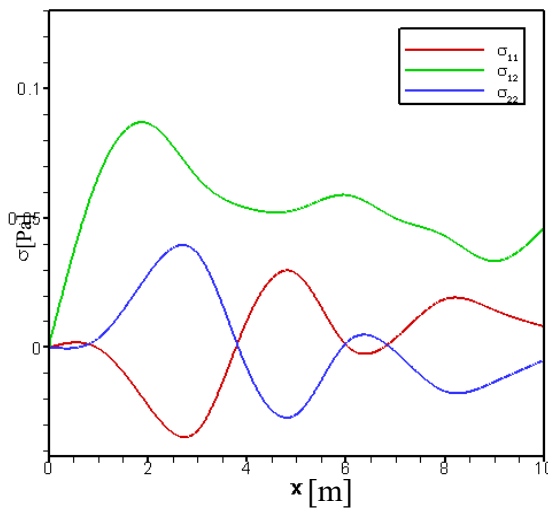


Figure 4.37a

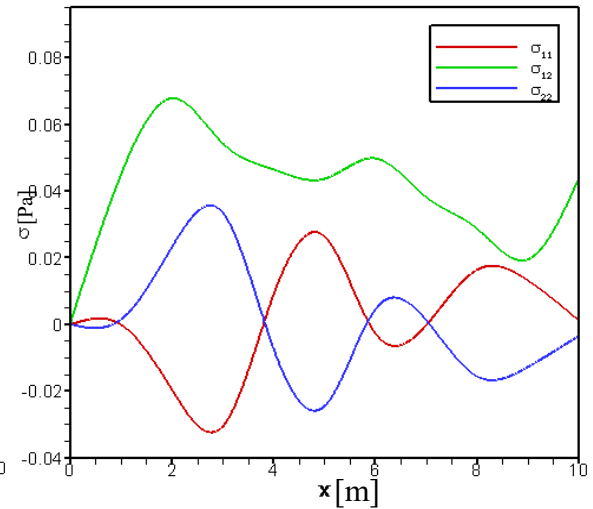


Figure 4.37b

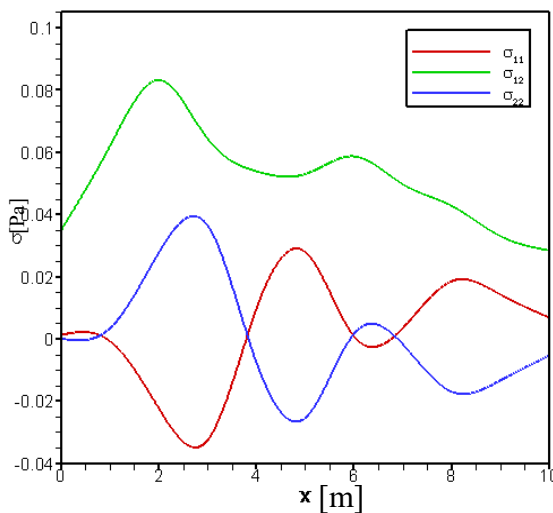


Figure 4.37c

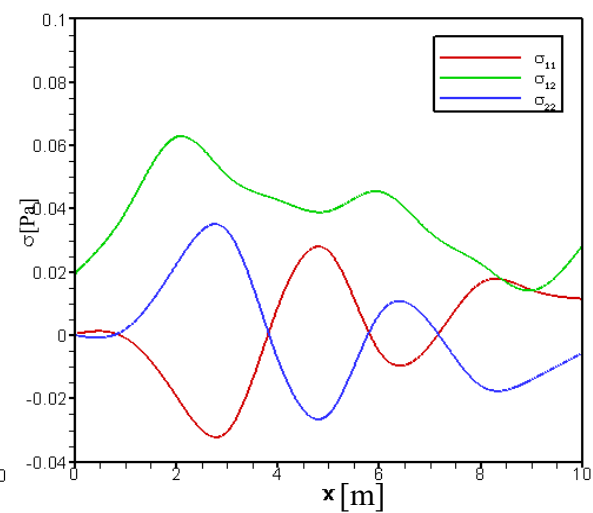


Figure 4.37d

Figure 4.37: Stress tensor profile on Blood flow at $Wi = 0.6$, $Pe = 1000$ and flow rate $0.1 \text{ cm}^3/\text{s}$ for (Figure 4.37a) Newtonian Model, (Figure 4.37b) Generalized Newtonian Model, (Figure 4.37c) Oldroyd-B Model, and (Figure 4.37d) Generalized Oldroyd-B Model.

CHAPTER 4 BLOOD FLOW STUDY THROUGH... ..

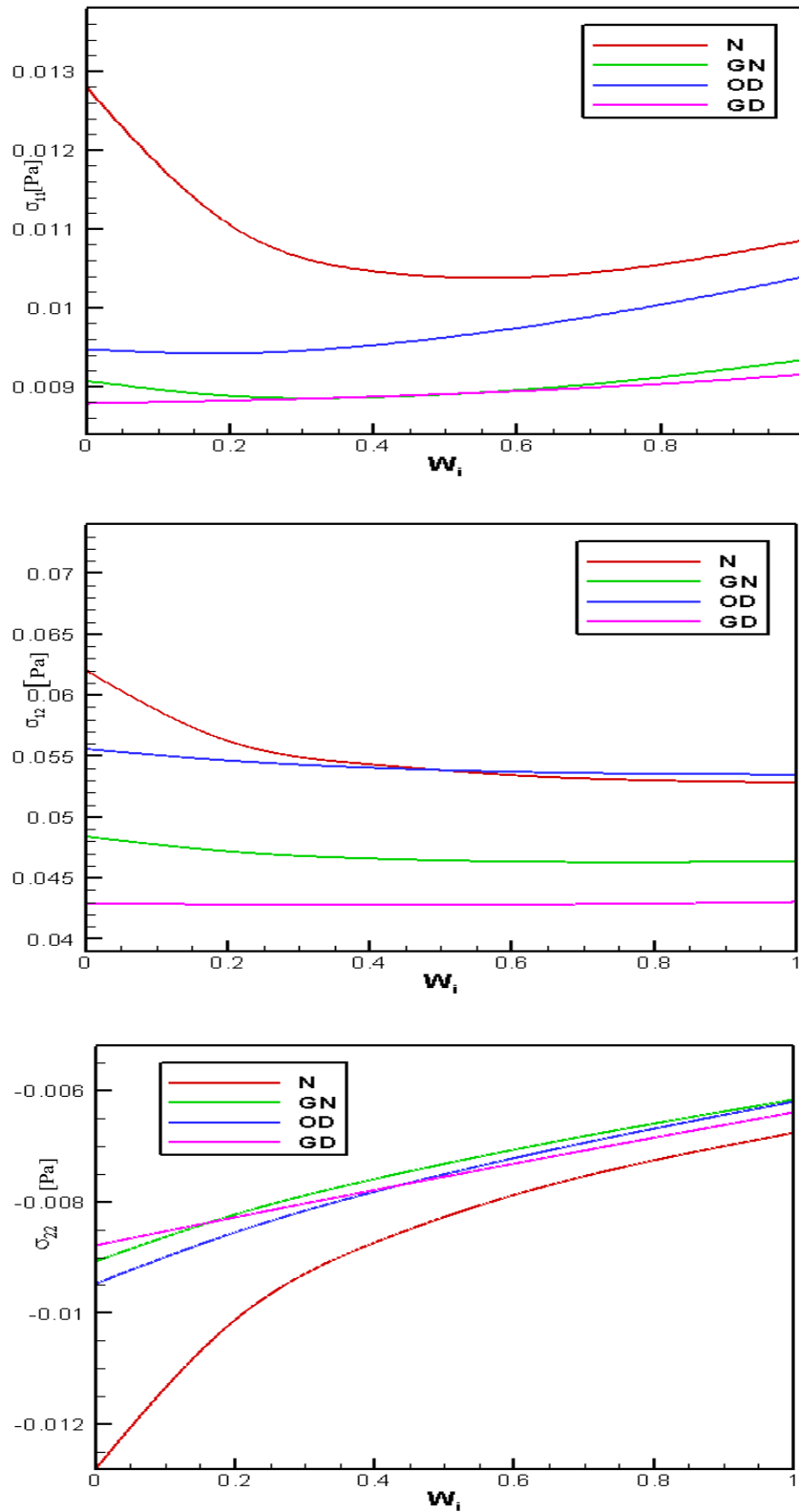


Figure 4.38: The components of σ_{11} (top), σ_{12} (middle) and σ_{22} (bottom) with $Pe=1000$ and different Wi for all models at permeable aneurysm.

CHAPTER 4 BLOOD FLOW STUDY THROUGH... ..

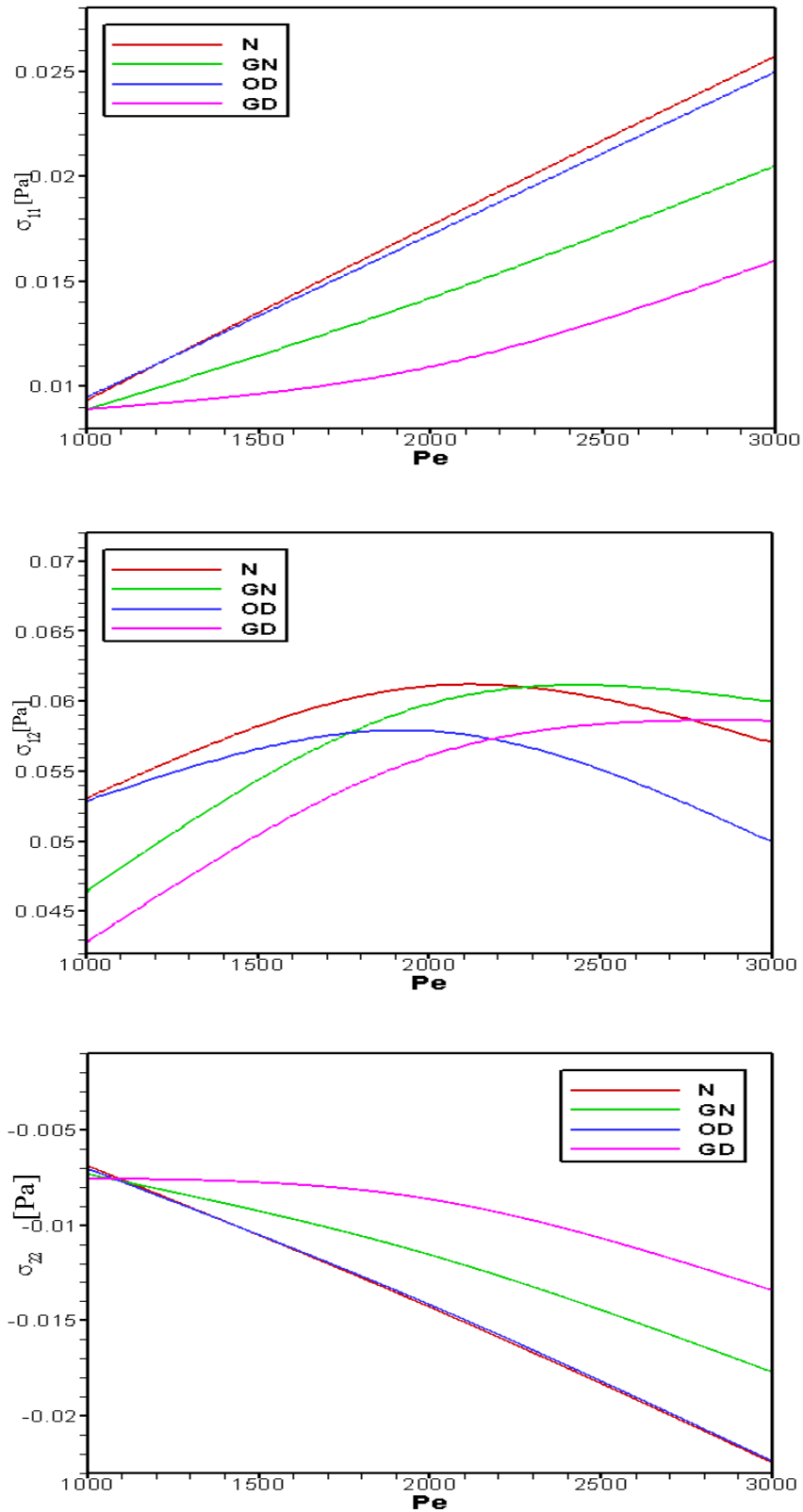


Figure 4.39: The components of σ_{11} (top), σ_{12} (middle) and σ_{22} (bottom) with $Wi=0.5$ and different Pe for all models at permeable aneurysm.

CHAPTER 4 BLOOD FLOW STUDY THROUGH... ..

4.4.5 Wall shear stress effects on blood flow

The wall shear stress effects on blood flow is an important factor to identify the fatal cardiovascular diseases in the arteries. The impact of wall shear stress on blood flow have been shown in Figures 4.40-4.41 for models Newtonian, Generalized Newtonian, Oldroyd-B, Generalized Oldroyd-B with impermeable and permeable aneurysm at the flow rate $q = 0.1 \text{ cm}^3/\text{s}$. It represents the tangential component of the surface force at the vessel wall, acting against the fluid flow and a vital parameter in blood flow simulation. In Figure 4.40, The wall shear stress profiles of bottom wall are shown at $Pe = 1000$ and $Wi = 0.6$ for impermeable model. The profiles have displayed oscillations of wall shear stress at bottom wall for all models. The maximum value are found at the beginning of impermeable aneurysm and minimum value is in dialation zones. It speeds up dramatically at the genesis of aneurysm and suddenly fall down and provides negative values in enlargement area for all models. These negative values are indicative of reversal blood flow region in the aneurysm zones. From Figure 4.41, the lowest value is found in the commencement of permeable aneurysm in the case of Oldroyd-B fluid. We observe that the wall shear stress for generalized Oldroyd-B model is marginally higher than the others model for the presence of porous dialation.

The comparable graphical study of impermeable and permeable aneurysm for the wall shear stress are shown in Figure 4.40 and 4.41 with various $Wi = 0.0, 0.5$ and 1.0 . At $Wi = 1.0$, the wall shear stress is dominated in the case of impermeable aneurysm because of viscous effect on flood flow. The influence of porosity aneurysm the wall shear stress is lower at $Wi=1.0$ in Newtonian case. From the Figure 4.41, it is clear that the wall shear stresses have a significant change due to permeability.

CHAPTER 4 BLOOD FLOW STUDY THROUGH... ..

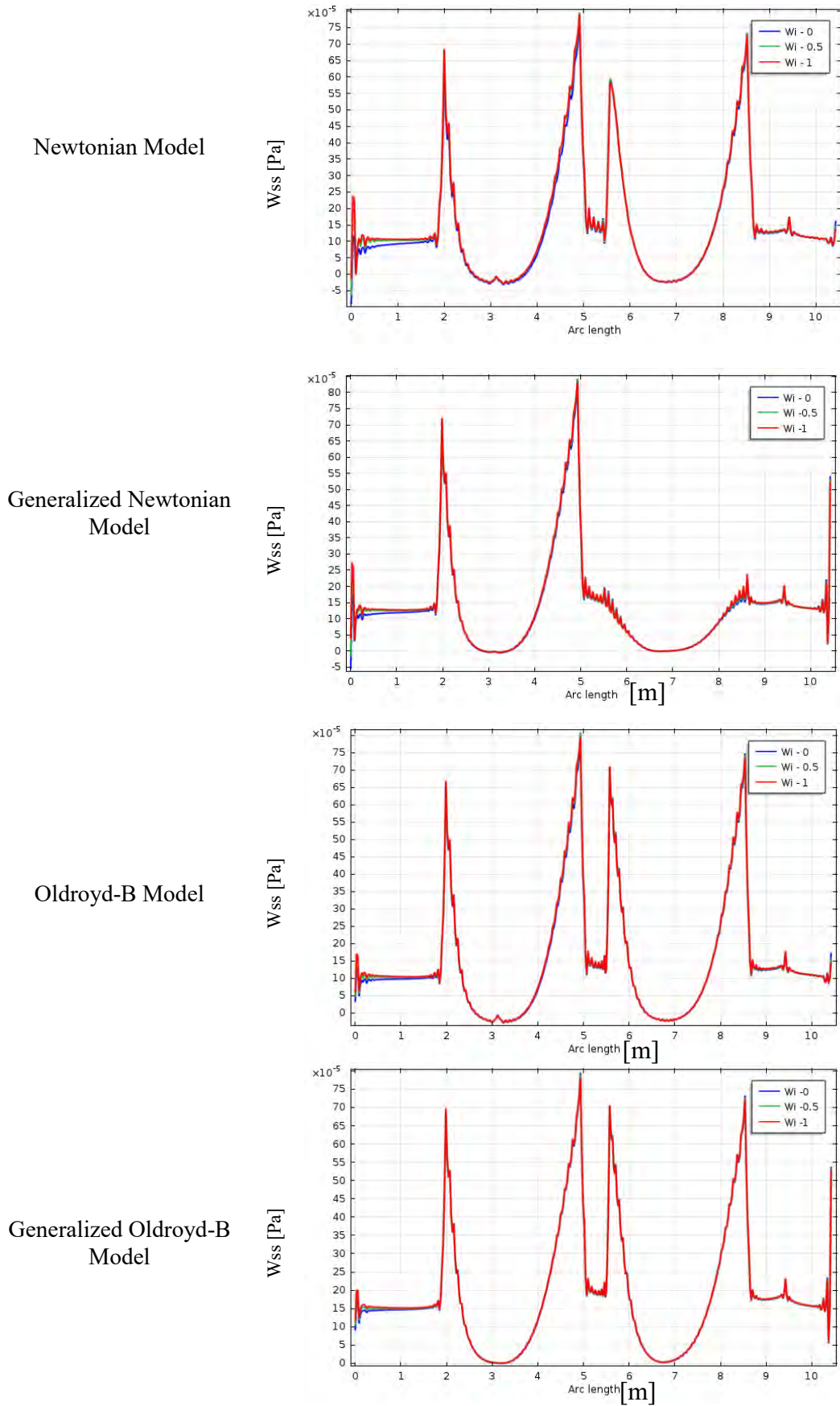


Figure 4.40: Wall shear stress effects on bottom wall of impermeable aneurysm for all cases with different Wi at $Pe=1000$ and $q = 0.1 \text{ cm}^3/\text{s}$.

CHAPTER 4 BLOOD FLOW STUDY THROUGH... ..

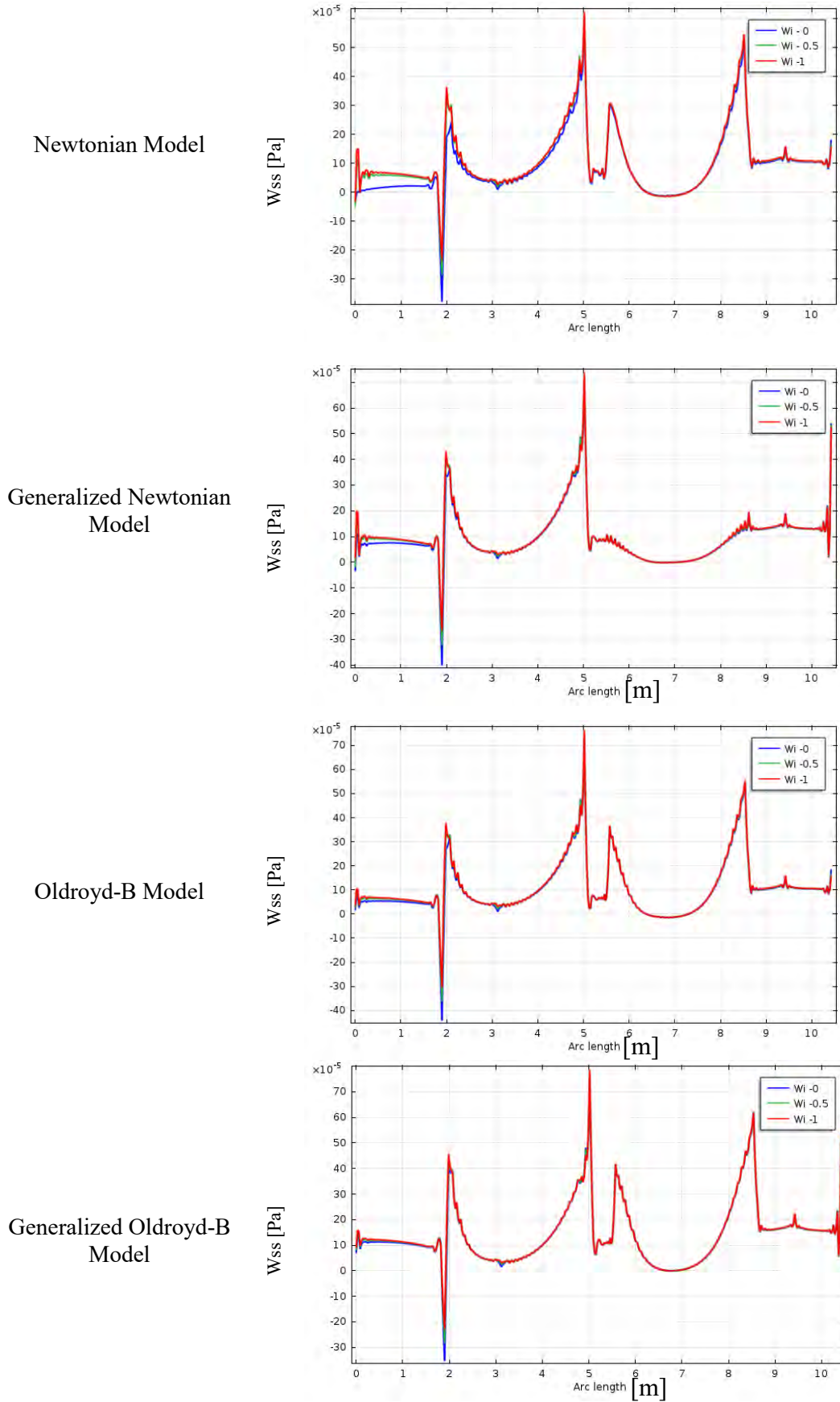


Figure 4.41: Wall shear stress effects on bottom wall of partial permeable aneurysm for all cases with different Wi at $Pe=1000$ and $q = 0.1 \text{ cm}^3/\text{s}$.

CHAPTER 4 BLOOD FLOW STUDY THROUGH... ..

4.5 Chapter Conclusion

The finite element method is used to simulate the blood flow through permeable aneurysm artery. The Newtonian model, generalized Newtonian model, Oldroyd-B models and generalized Oldroyd-B models for non-Newtonian fluid blood viscosity. The numerical study of all cases (Newtonian and Oldroyd-B models, and their generalized models) have been considered to the blood flow through permeable aneurysm in steady flow simulations. We inferred that the outcomes of blood flow characteristics, wall shear stress and stress tensor components are correlated to blood viscoelasticity and more significant. The blood flow variables are foremost and decreased for all models along vessel axis at permeable aneurysm. The porosity aneurysm and blood viscosity are main factors for the Newtonian and Non-Newtonian solution. At the present problems, the numerical method is used to solve the governing equations seems to be sufficiently strong and effective for the appropriate resolution.

The finite element equations derived from the governing blood flow equations that consist of the continuity equation (conservation of mass), momentum equation, and viscoelastic (Oldroyd-B) equation. An iterative technique solver is required to derive the finite element equations. To solve these nonlinear equations, the Newton-Raphson iteration method is used for solutions of the nodal velocity component, tensor component, and pressure by considering Weissenberg numbers of 0.0, 0.5 and 1.00 and Pectel numbers of 10^3 to 3×10^3 .

The outcomes demonstrate the following features:

- ◆ The blood flow characteristics have significant change at permeable aneurysm for all four cases.
- ◆ To determine the fatal arterial diseases, the effect of the blood flow on the wall shear stress is an important factor.
- ◆ The minimum value of blood velocity and maximum value of pressure are found at porous aneurysm. But in impermeable aneurysm, the lowest velocity are found at second aneurysm for all cases.

CHAPTER 4 BLOOD FLOW STUDY THROUGH... ..

- ◆ The dimensionless numbers (Pe and Wi) effect are more striking at porous region and blood flow variables have a dramatic change. The pressure distribution have increased with increases of Pe at permeable aneurysm but pressure patters have decreased with increases of Wi for generalized Oldroyd-B cases.
- ◆ It is very important findings that the turbulent velocity is reduced due to presence of permeability at aneurysm.
- ◆ Elliptic types of recirculation zone are originated between the aneurysm regions for all four models and non-axisymmetric profiles are found at entrance.

CHAPTER 5

NUMERICAL INVESTIGATION OF BLOOD FLOW THROUGH STENOTIC AND ANEURYSMATIC ARTERY HAVING BLOOD CLOT

The blood circulation may be poor in human body due to build up of blood clot, external force, external pressure, injury of blood artery, overgrowth of bone, tumor, hypertension, weaken of blood artery, medical surgery, inactive cells, genetic conditions, any kind of trauma are main reasons. The development of stenosis and aneurysm in artery are the main cause of cardiovascular disease arteriosclerosis which leads to serious circulatory disorders. Taylor and Yamaguchi (1994) have discussed the blood flow simulation through abdominal aortic aneurysm for unsteady flow in three dimensions. Menche (2012) and Pschyrembel (2014) have reported that the blood vessels are in network form of aorta and capillaries. Using Bingham fluid model, the effects of stenosis and dilatations of the coronary arteries with various combinations on the resistance impedance have explained by Pincombe et al. (1995).

In this chapter the major goal is to be study a numerical investigation of blood flow through stenotic and aneurysmatic artery for incompressible Newtonian and non-Newtonian fluids having blood clot. The parabolic velocity profile and stress tensor is considered at inlet and pressure is kept constant at outlet. The stenosed vessel wall is cooled and the upper surface of blood clot is heated and while no-slip velocity conditions are applicable for all walls. A set of partial differential equations for continuity, momentum, Oldroyd-B and bioheat transport have been considered and derived dimensionless equations using appropriate scale with boundary conditions. The aim of this problem is to present the influence of blood clot on blood flow in a blood vessel artery for all cases. The numerical solution is obtained using a finite element method for all models. The effects of dimensionless numbers, flow variables, drag coefficient and wall shear stress on blood flow have been examined. At low shear region, the recirculation bubbles have increased with the increase in dimensionless numbers Re and Wi . The computational results also indicate that the hemodynamical factors of blood flow depend on the various parameters.

This chapter is consists of following items. Section 5.1 provides the problem formulation of our present work. Mathematical equations with appropriate boundary condtion are in cited in section 5.2. Numerical analysis of computation have discussed in section 5.3 along with grid sensitivity test. In section 5.4, simulation and graphical result are presented. At last, section 5.5 gives a summary of this chapter.

5.1 Problem Formulation

The treated stenotic and aneurysmatic model is a two-dimensional cavity with stenosed and aneurysm vessel wall. The physical system considered in the present study is displayed in Fig. 5.1. The model is assumed with stenosed and aneurysm hight h_s and h_a respectively where $h_s=R(3.1\text{mm})$ and $h_a=3R$. The top and bottom stenosed vessel walls are cool (T_c) and heated (T_h) while the rest of the walls are adiabatic and impermeable. The velocity profile is prescribed at entrance and pressure is fixed to constant at outlet. No slip conditions are used for velocity and pressure on the vessel walls. The blood flow acceleration is expected for stenotic and aneurysmatic cross-sectional area.

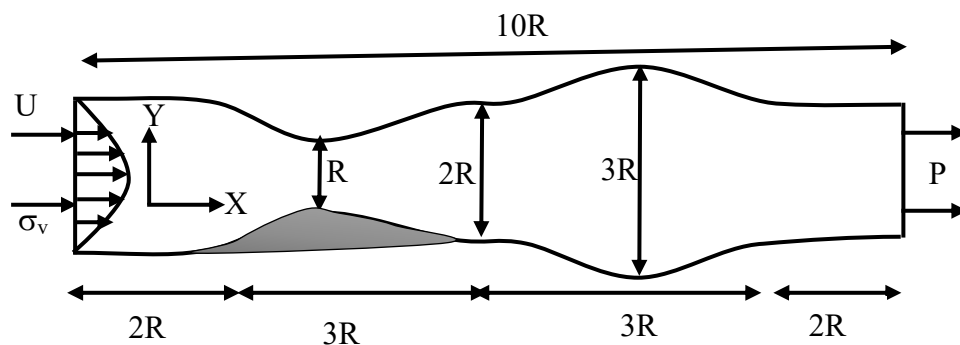


Figure 5.1: Structure of the computational domain

5.2 Mathematical Model

The Standard Mathematical equation of the above problem are exposed as follows

5.2.1 Dimensionless overning equations

The functioning fluid is assumed to be laminar blood flow and incompressible with shear-thinning and viscoelasticity properties. The generalized Oldroyd-B model is used to capture non-Newtonian properties of the blood flow. The leading differential equations are as follows:

Continuity Equation

$$\nabla \cdot \mathbf{u} = 0 \tag{5.1}$$

Momentum Equations

$$\rho \frac{\partial \mathbf{u}}{\partial t} + \rho(\mathbf{u} \cdot \nabla) \mathbf{u} = -\nabla p + \mu_n \Delta \mathbf{u} + \nabla \cdot \boldsymbol{\sigma} + \rho \mathbf{f} \quad (5.2)$$

Oldroyd-B Constitutive Equation:

$$\boldsymbol{\sigma} + \lambda_x \left[\frac{\partial \boldsymbol{\sigma}}{\partial t} + (\mathbf{u} \cdot \nabla) \boldsymbol{\sigma} \right] = 2\mu_v \mathbf{V}(\mathbf{u}) + \lambda_x [\boldsymbol{\sigma} \mathbf{V}' - \mathbf{V}' \boldsymbol{\sigma} - \boldsymbol{\sigma} \mathbf{V} - \mathbf{V} \boldsymbol{\sigma}] \quad (5.3)$$

Bio-heat Equation

$$\rho c_p \left[\frac{\partial T}{\partial t} + (\mathbf{u} \cdot \nabla) T \right] = K \nabla^2 T + q + \rho_b c_b w_b (T_b - T) \quad (5.4)$$

Here \mathbf{u} is the velocity vector, $\mathbf{u} = (u_1, u_2, u_3)^T$, ρ is the constant density, $\boldsymbol{\sigma}$ is the extra stress tensor, μ is dynamic viscosity, λ_x denote the relaxation, the symmetric part of the velocity gradient, $\mathbf{V} = \frac{1}{2}(\nabla \mathbf{u} + \nabla \mathbf{u}^T)$ i.e. $\boldsymbol{\sigma} = 2\mu \mathbf{V}$, ρ_b is the blood density, T_b is arterial blood temperature, w_b is blood perfusion rate, c_b is specific heat capacity of blood, c_p is tissue specific heat and q heat source due to metabolic activity.

To non-dimensionalized the above equations we incorporating the dimensionless variables given below:

$$\begin{aligned} x &= LX, & y &= LY, & t &= Lt^*/U, & u &= UU_o, & v &= VU_o, & p &= \mu UP/L, \\ \boldsymbol{\sigma} &= U\mu\boldsymbol{\sigma}^*/L, & f &= f^*\mu U/L^2, & \nabla &= \nabla^*/L, & Wi &= \lambda_x U/L, & Re &= \rho UL/\mu, \\ Pr &= \mu c_p/k, & \theta &= k(T-T_c)/q_0 L^2, & q &= Qq_0, & w_b &= \rho_f k / \rho c_b L^2. \end{aligned}$$

Where, the dimensionless quantities X and Y are the coordinates varying along horizontal and vertical directions respectively. U and V are the velocity components along the X and Y axes respectively, P is the pressure, L is the characteristic length, $\boldsymbol{\sigma}^*$ stress tensor, Q is heat source, ρ_f is perfusion coefficient, and Weissenberg number (Wi), Reynold number (Re), Prandtl number (Pr) are dimensionless numbers.

For two dimensional aneurysmatic vessel in domain Ω , the non-dimensional governing equations are as follows:

Continuity Equation

$$\nabla \cdot \mathbf{U} = 0 \quad (5.5)$$

Momentum Equations

$$Re [(\mathbf{U} \cdot \nabla) \mathbf{U}] = -\nabla P + (1 - \lambda) \Delta \mathbf{U} + \nabla \cdot \boldsymbol{\sigma} + \mathbf{f} \quad (5.6)$$

$$Re[(\mathbf{V} \cdot \nabla) \mathbf{V}] = -\nabla P + (1 - \lambda) \Delta \mathbf{V} + \nabla \cdot \boldsymbol{\sigma} + \mathbf{f} \quad (5.7)$$

Oldroyd-B constitutive equation:

$$W_i [(\mathbf{U} \cdot \nabla) \boldsymbol{\sigma}] + \boldsymbol{\sigma} = 2\mu_v V(\mathbf{U}) + W_i [(\nabla \mathbf{U}) \boldsymbol{\sigma} + \boldsymbol{\sigma} (\nabla \mathbf{U})^t] \quad (5.8)$$

Bio-heat Equation:

$$Re Pr(\mathbf{u} \cdot \nabla) \theta = \nabla^2 \theta + Q - \rho_f \theta \quad (5.9)$$

5.2.2 Boundary conditions

The boundary conditions for the present problem are specified as follows:

(i) At inlet:

The poiseuille (parabolic) velocity profile and the corresponding extra stresses components are

$$\begin{aligned} \mathbf{u} &= 1.5 U_i (1 - y^2), \mathbf{v} = 0 \\ \boldsymbol{\sigma}_{11} &= 2\mu_v W_i \left(\frac{\partial \mathbf{u}}{\partial y}\right)^2 \\ \boldsymbol{\sigma}_{12} &= \mu_v \frac{\partial \mathbf{u}}{\partial y}, \boldsymbol{\sigma}_{22} = 0 \end{aligned}$$

Where y is along the inlet boundary, and U_i is the average fluid velocity at the inlet.

(ii) At outlet:

At outlet homogeneous Neumann conditions for the velocity components and a constant pressure are prescribed.

(iii) At boundary wall:

a. On the vessel walls no-slip homogeneous Dirichlet conditions are prescribed for velocity field. In the case of the Oldroyd-B and generalized Oldroyd-B models, homogeneous Neumann conditions are imposed for the components of the extra stress tensor at all boundaries.

b. Homogenous Neumann boundary conditions are used for the pressure.

(iv) At stenosed vessel walls: The top and bottom walls are cooled and heated respectively. The rest of the walls of the present model are adiabatic.

5.3 Numerical Technique

The discretized momentum and Oldroyd-B equations subjected to the boundary conditions simultaneously will be solved using the MATLAB programming &

Mathematical programming package COMSOLMULTIPHYSICS for the dependent variables (velocity, pressure and stress tensor).The numerical procedure to be used in this work is based on the Galerkin weighted residual method of finite element formulation.

5.3.1 Computational procedure

By using the Galerkin weighted residual finite element method, the mass conservation, momentum, viscoelasticity and bio-heat equations have been solved that are the combinations of mixed elliptic-parabolic system of partial differential equations. More details of numerical technique are in appendix B for shortness.

5.3.2 Grid sensitivity test

A grid freedom test is reported with $Wi = 0.5$, $Re = 1000$, and flow rate $q = 0.1\text{cm}^3/\text{s}$ to decide the appropriate grid size for this study. Figure 5.2 shows the convergence of the velocity with refinement for generalized Newtonian model.

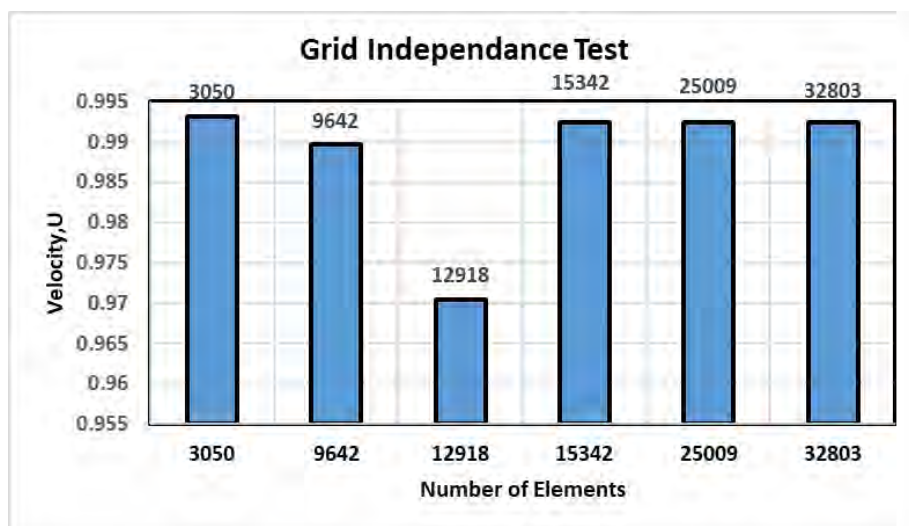


Figure 5.2: Convergence of average velocity with grid refinement for $Re = 10^3$, and $Wi = 0.6$ with blood flow rate $0.1\text{ cm}^3/\text{s}$

The following six kinds of meshes are consider for the investigation of grid sensitivity. These grid densities are 1846 nodes, 3050 elements; 5638 nodes, 9642 elements; 7276 nodes, 12918 elements; 8489 nodes, 15342 elements; 14079 nodes, 25009 elements, 17976 nodes, 32803 elements.The extreme values of the average velocity of the blood flow are used as sensitivity measures of the correctness of the solution. The current formulation is performed with 14079 nodes and 25009 elements grid system by considering both the accuracy of numerical computation.

Table 5.1: Grid Sensitivity Check at $Wi = 0.5$, $Re = 1000$ and $q = 0.1 \text{ cm}^3/\text{s}$

Nodes (elements)	1846 (3050)	5638 (9642)	7276 (12918)	8489 (15342)	14079 (25009)	17976 (32803)
U	0.13623268	0.13603243	0.13596163	0.13596162	0.13596162	0.13596162
Time (s)	46	308	558	193	354	782

5.4 Results and Discussion

The characteristics of the blood flow and pressure distribution in the stenotic and aneurysmatic artery are examined by exploring the effects Weissenberg numbers (Wi), Reynold numbers (Re), stress tensor components, drag coefficient, wall shear stress and permeable aneurysm. The blood fluid variables are analyzed by outlaying the steady state version of the velocity contour plots, pressure distribution and average temperature. In the present numerical study, the following thermal properties and tissue are considered by Shih et al. (2007): $0 \leq Wi \leq 1, 0 < Re \leq 3000, \mu_0 = 0.16 \text{ Pa.s}, \mu_n = 0.0036 \text{ Pa.s}, a = 1.23, b = 0.64, \lambda = 8.2\text{s}, \rho = 1050 \text{ kg.m}^{-3}, T_b = 37^\circ\text{C}, C_b = 3770 \text{ (J/Kg.k)}, W_b = 0.5 \text{ (Kg/sec.m}^3), K = 0.5 \text{ (J/s.m.k)}, P_f = 400, L_w = 2R, L = 0.03\text{m}, R = 3.1\text{mm}, h_s = R \text{ and } h_a = 3R$.

It is very important investigation to findout the effects of Reynold numbers, Weissenberg number, wall shear stress, stenotic and aneurysmatic artery, and drag coefficient at stenosed wall on blood flow for the various models Newtonian (N), generalized Newtonian (GN), Oldroyd-B (OD) and generalized Oldroyd-B (GD). The comparative study of blood flow simulation is shown in Figures 5.3 - 5.8 with the presence and absence of blood clot at the present model in terms of velocity, pressure contour, stream lines with vectors for all cases. The blood flow characteristics have a significant changed at the throat of stenosis. For the variations of Re and Wi , the overall features of the blood flow are depicted in Figures 5.12 -5.32. These figuers also provides the graphical illustration of the velocity, pressure, wall shear stress and drag coefficient of blood flow.

5.4.1 Stenotic and aneurysmatic effects on blood flow

The blood flow simulation is shown in Figures 5.3, 5.5 and 5.7 with the presence of blood clot at bottom stenosed wall through velocity contour plots, pressue contour lines, stream lines with vectors for all models. In Figure 5.3, the indelible recirculation zones

CHAPTER 5 NUMERICAL INVESTIGATION... ..

are originated at the constriction region of the stenotic and aneurysmatic artery for all cases. The shapes of recirculation zoens are oval-like and it has reduced at generalized Oldroyd-B model. This recirculation zones are indicative of iso-blood flow at stenotic artery. The blood shear-thinning properties are important reason to form the recirculation zone and dominate the low-shear area of stenotic and anuerysmatic artery. At aneurysm, the velocity contour lines are almost alike for Newtonian and Oldroyd-B models but little dissimilarity are found at the rest of models. In the absence of blood clot, the blood flow simulation is presented in Figure 5.4 for mentioned models where the recirculation zones are found at the throat of stenosis. These recirculation zones are symbolic of regions over a significant portion of each model where the flow is moving with same values. The recirculated area is comparable bigger at blood cloted model than non-blood cloted model for all cases. The shape of recirculation zone is another significant influence of blood clot among the models. At aneurysm, the reversal flow regions and flow separation are found with respect to vessel axis in Figures 5.5 but greater flow separation regions are created in non-blood cloted model.

Figure 5.9 provides the corresponding effects on blood velocity numerically at the being and absence of blood clot for all models where $Re=1000$ and $Wi=0.5$. It is observed that the velocity profile almost opposite for the blood clot model and non-blood clot model. The maximum blood velocity is found at the throat of stenosis for non-blood clot model and the lowest value is in blood clot model. For the existence of blood clot, the blood velocity is comparable lower to another model which leads local viscosity increases significantly. Numerical value of velocity of blood clot and non-blood clot models is presented in Table 5.2 for all four models along blood vessel axis when $Re = 1000$, $Wi=0.5$ and $q = 0.1 \text{ cm}^3/\text{s}$.

Table 5.2: Numerical value of velocity for all four models along blood vessel axis when $Re = 1000$, $Wi = 0.5$ and $q = 0.1 \text{ cm}^3/\text{s}$.

Models	Velocity (U)			
	Blood clot Model		Non-blood clot model	
	Stenosis	Aneurysm	Stenosis	Aneurysm
Newtonian Model	0.048039528	0.043678407	0.135949907	0.094392773
Generalized Newtonian Model	0.05124471	0.046487735	0.125501881	0.080989077
Oldroyd-B Model	0.048328235	0.043668155	0.135936884	0.094290511
Generalized Oldroyd-B Model	0.053240661	0.049115308	0.137238422	0.0779935

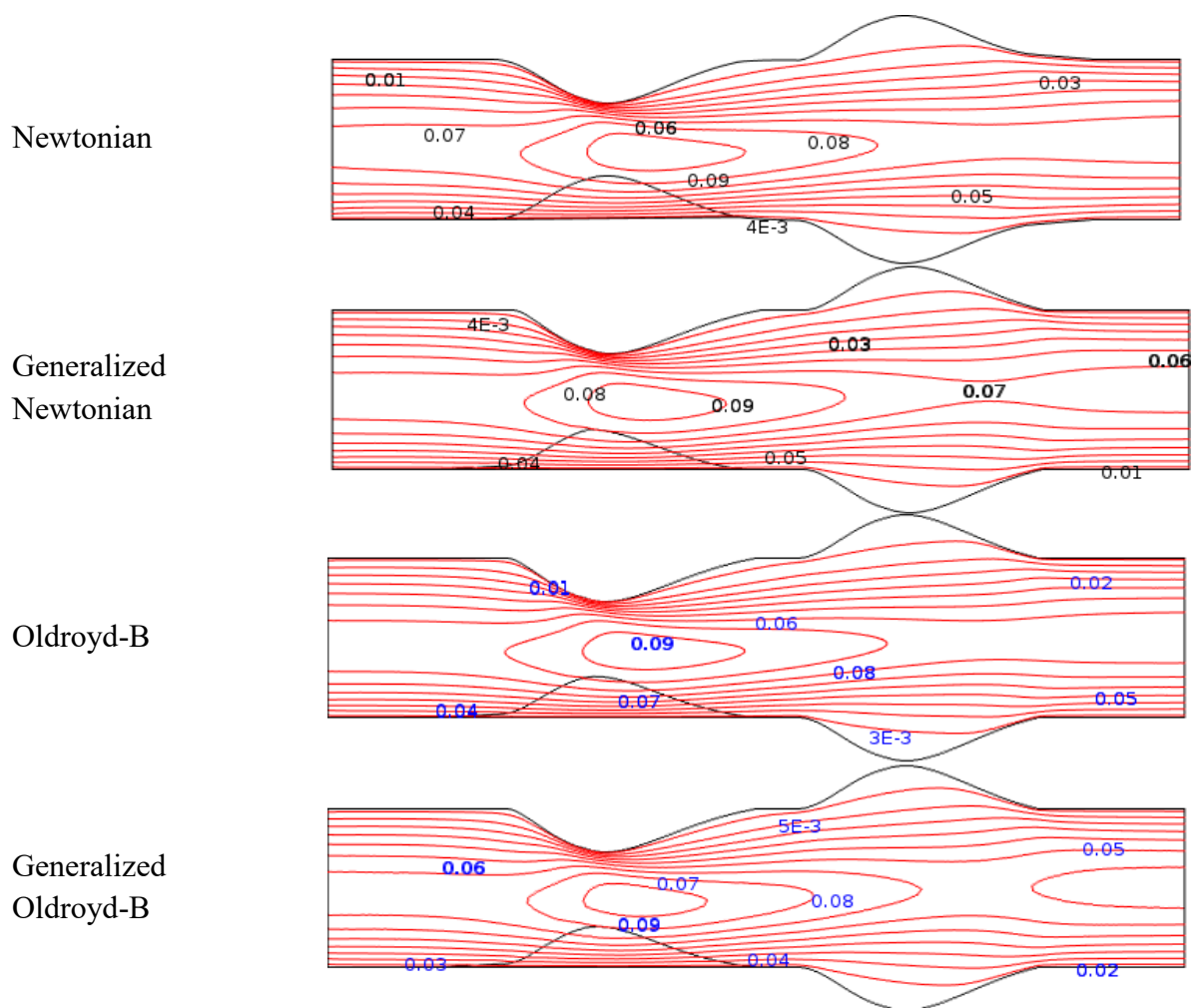
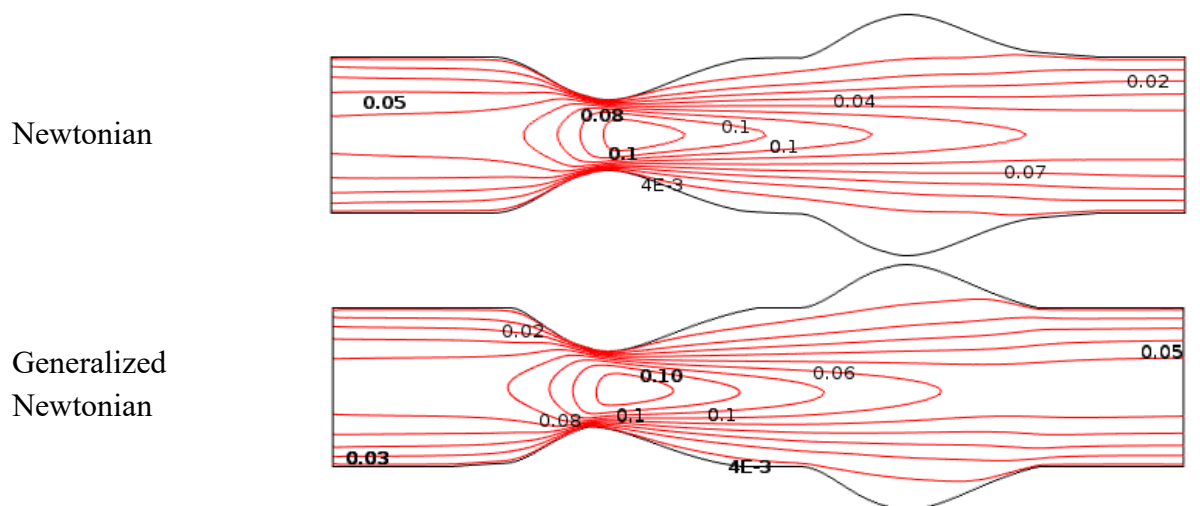


Figure 5.3: Velocity contour line on blood flow through stenosed and aneurysmatic vessel with blood clot at $Re=1000$ and $Wi = 0.6$



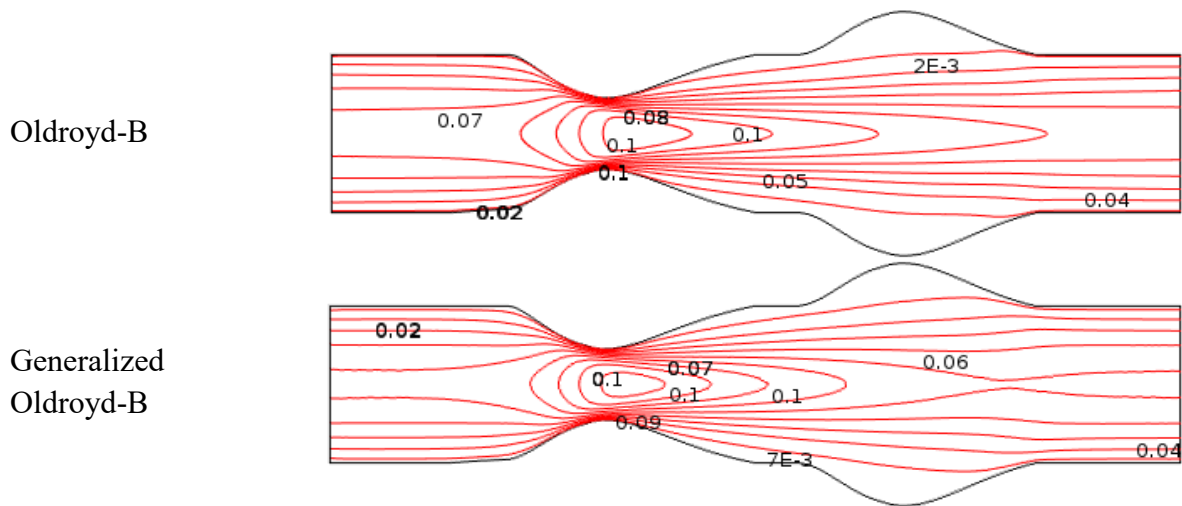


Figure 5.4: Velocity contour line on blood flow through stenosed and aneurysmatic vessel without blood clot at $Re=1000$ and $Wi = 0.6$

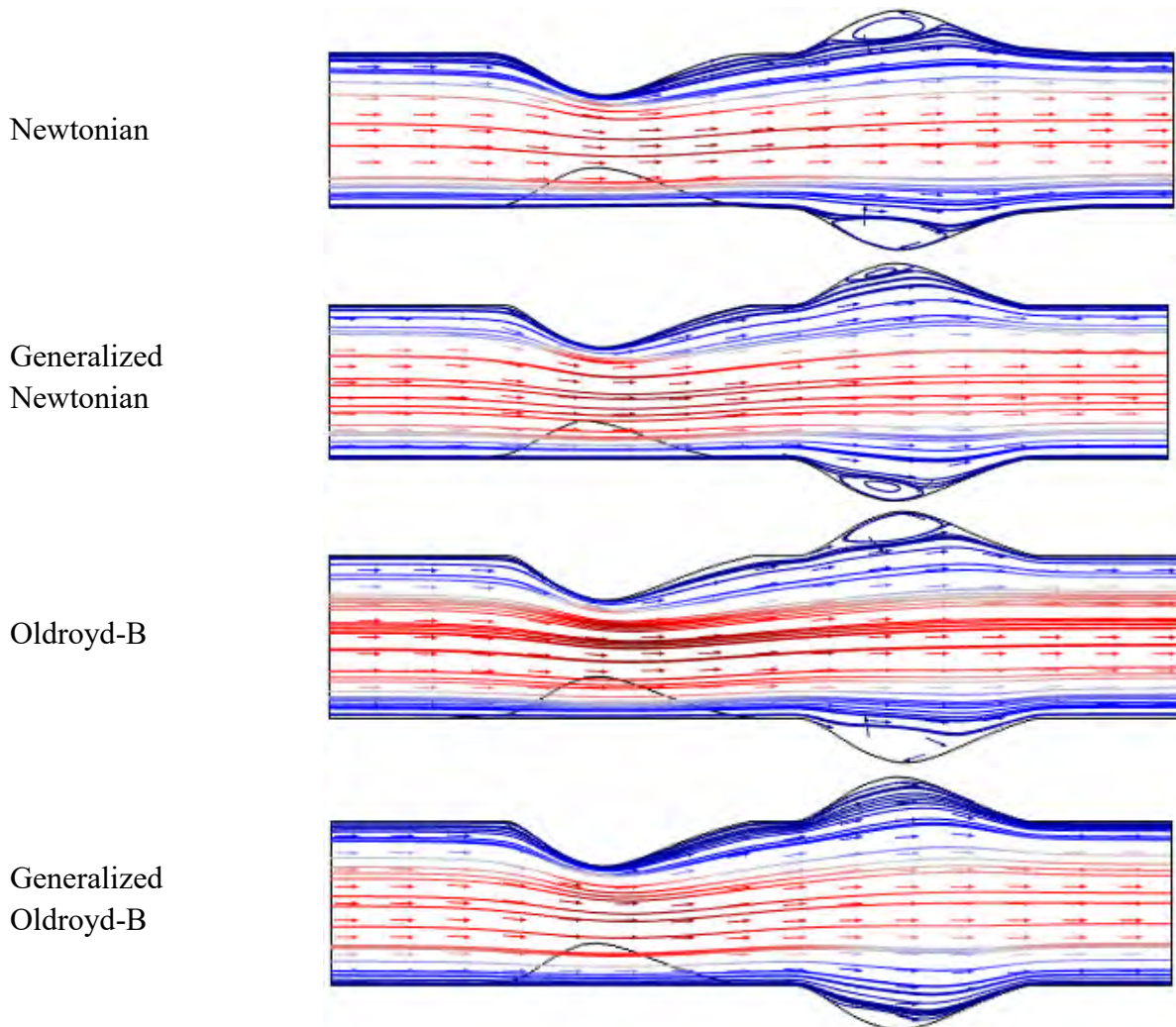


Figure 5.5: Velocity contour line on blood flow through stenosed and aneurysmatic vessel with blood clot at $Re=1000$ and $Wi = 0.6$

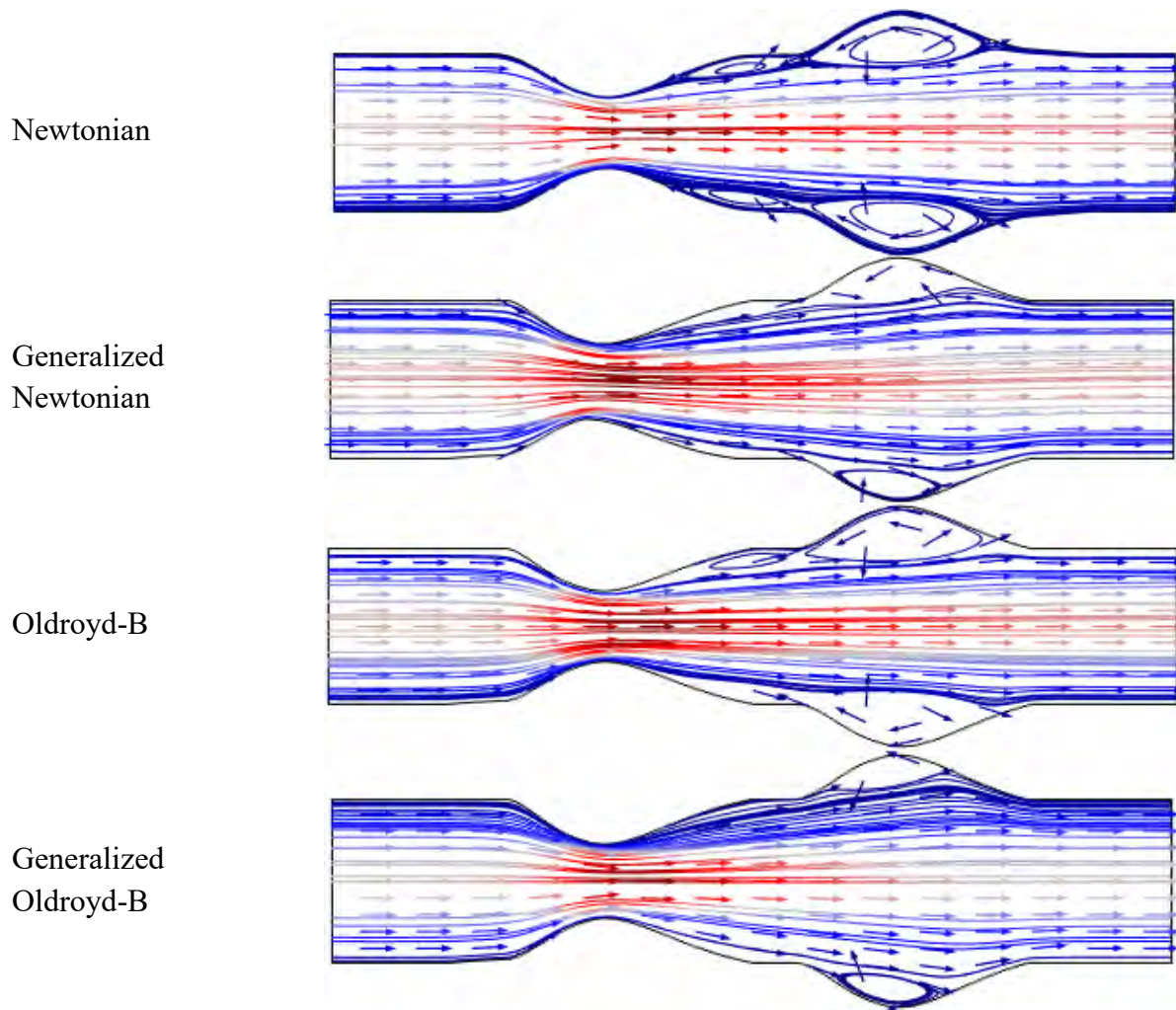
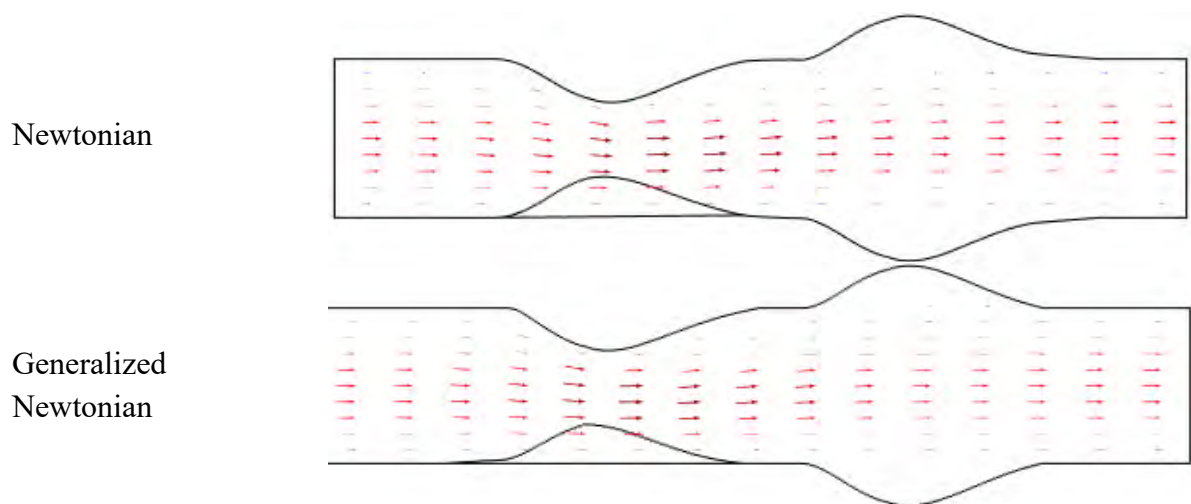


Figure 5.6: Velocity contour line on blood flow through stenosed and aneurysmatic vessel without blood clot at $Re=1000$ and $Wi = 0.6$



Oldroyd-B



Generalized Oldroyd-B

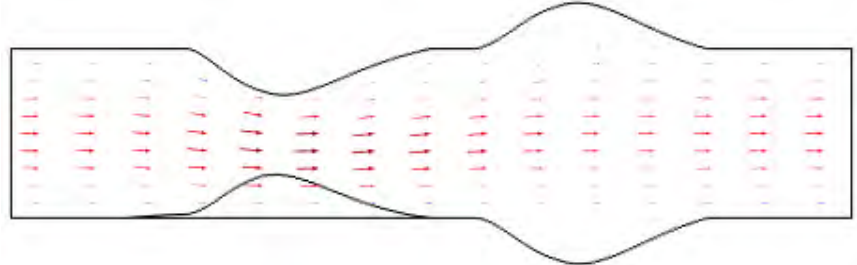
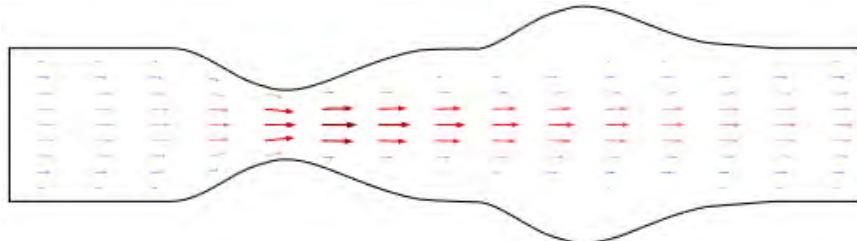
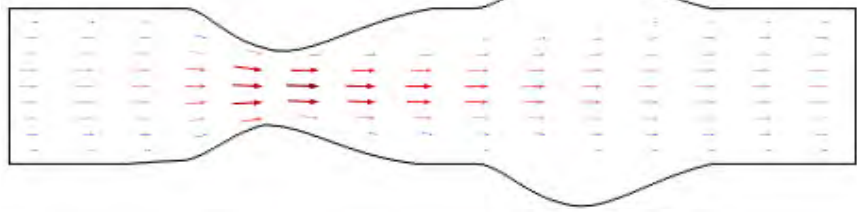


Figure 5.7: Velocity contour line on blood flow through stenosed and aneurysmatic vessel with blood clot at $Re=1000$ and $Wi = 0.6$

Newtonian



Generalized Newtonian



Oldroyd-B



Generalized Oldroyd-B

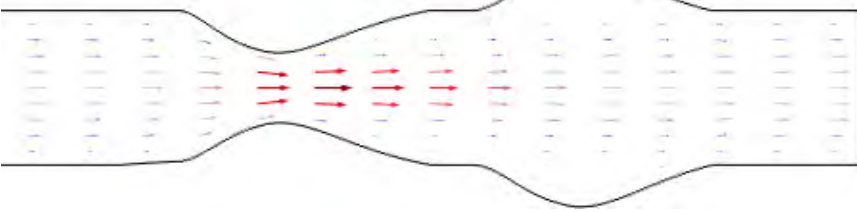


Figure 5.8: Velocity contour line on blood flow through stenosed and aneurysmatic vessel without blood clot at $Re=1000$ and $Wi = 0.6$

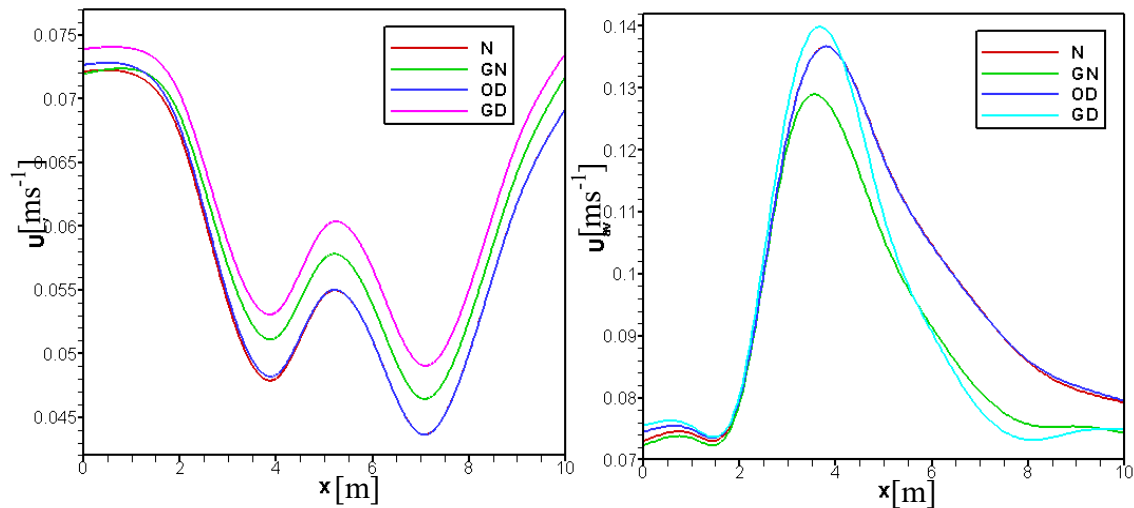


Figure 5.9: Comparison of Velocity profile with blood clot (left) and without blood clot (right)

5.4.2 Stenotic and aneurysmatic effects on pressure distribution

The pressure distribution of blood flow is exhibited for all cases in Figures 5.10 and 5.11 having blood clot and without blood clot. In Figure 5.10, the steep contour plots display the pressure gained a minimum value at the separation point and decline gradually along vessel axis. Due to clump of blood, the pressure peaked at reattachment point at stenosis region and the pressure gradient is high for all events. The pressure gradient has changed slowly and dense at clotted area. In the case of generalized Oldroyd-B model, the pressure contour lines become more compact and make distort curve withing clotted area because of shear-thinning properties of blood. The different pressure contour plots of blood flow are found in Figure 5.11 (without clotting) for all situations. The parabolic profile has developed at the throat of stenosis and separation points are originated which leads how the pressure reached a minimum point. The main difference is visible between two models at constriction area for all models. The pressure is more dominated at stenosis regions compare to blood clot model because of blood viscosity. In Figure 5.11, The pressure patterns are almost alike for all models and show the similarities at the far of stenosis, but various pressure contour plots are produce at blood clotted models. From the Figure 5.12, the blood pressure has decreased gradually in the presence of blood clot and have dramatical changed for non-blood clotting case. In the absence of blood clot, the pressure has gained the lowest value at the throat of stenosis and increased after stenosis. The Newtonian fluid is faster than non-Newtonian fluid for both cases which leads to minimum value at generalized Oldroyd-B model. The numerical value of

CHAPTER 5 NUMERICAL INVESTIGATION... ..

pressure of blood clot and non-blood clot models is inserted in Table 5.3 for all four models along blood vessel axis when $Re = 1000$, $Wi = 0.5$ and $q = 0.1 \text{ cm}^3/\text{s}$.

Table 5.3: Numerical value of pressure for blood clotted and non-blood clotted models is inserted when $Re = 1000$, $Wi = 0.5$ and $q = 0.1 \text{ cm}^3/\text{s}$.

Models	Pressure (P)			
	Blood clot Model		Non-blood clot model	
	Stenosis	Aneurysm	Stenosis	Aneurysm
Newtonian Model	0.448706443	-0.618620928	-7.05419599	-4.96725825
Generalized Newtonian Model	0.251788761	-0.889645999	-6.260098627	-4.36123117
Oldroyd-B Model	0.416478804	-0.644510712	-6.947428004	-4.84829253
Generalized Oldroyd-B Model	0.119392855	-1.115787143	-8.58277051	-6.20055391

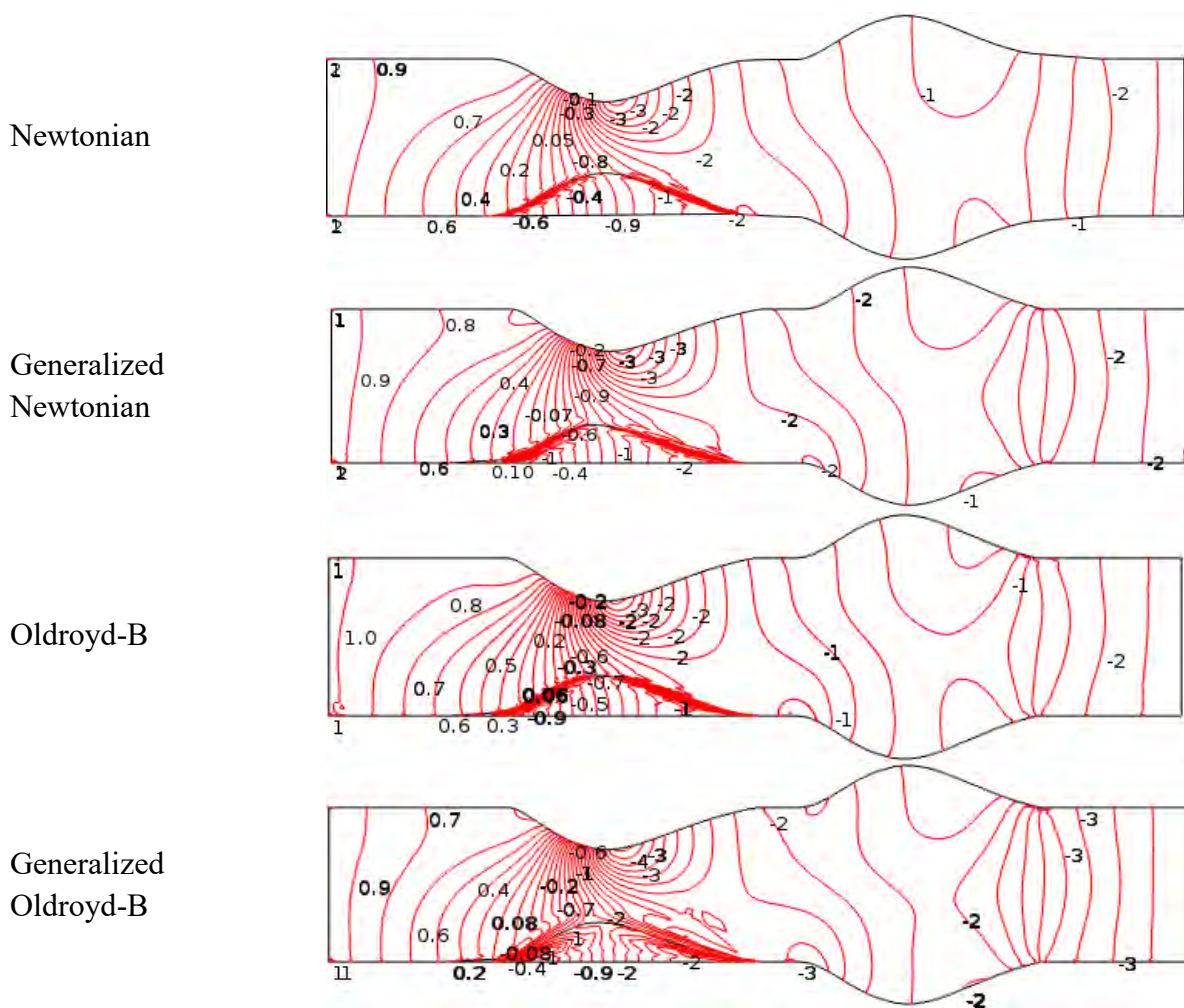


Figure 5.10: Pressure distribution on blood flow through stenosed and aneurysmatic vessel with blood clot at $Re=1000$ and $Wi = 0.6$

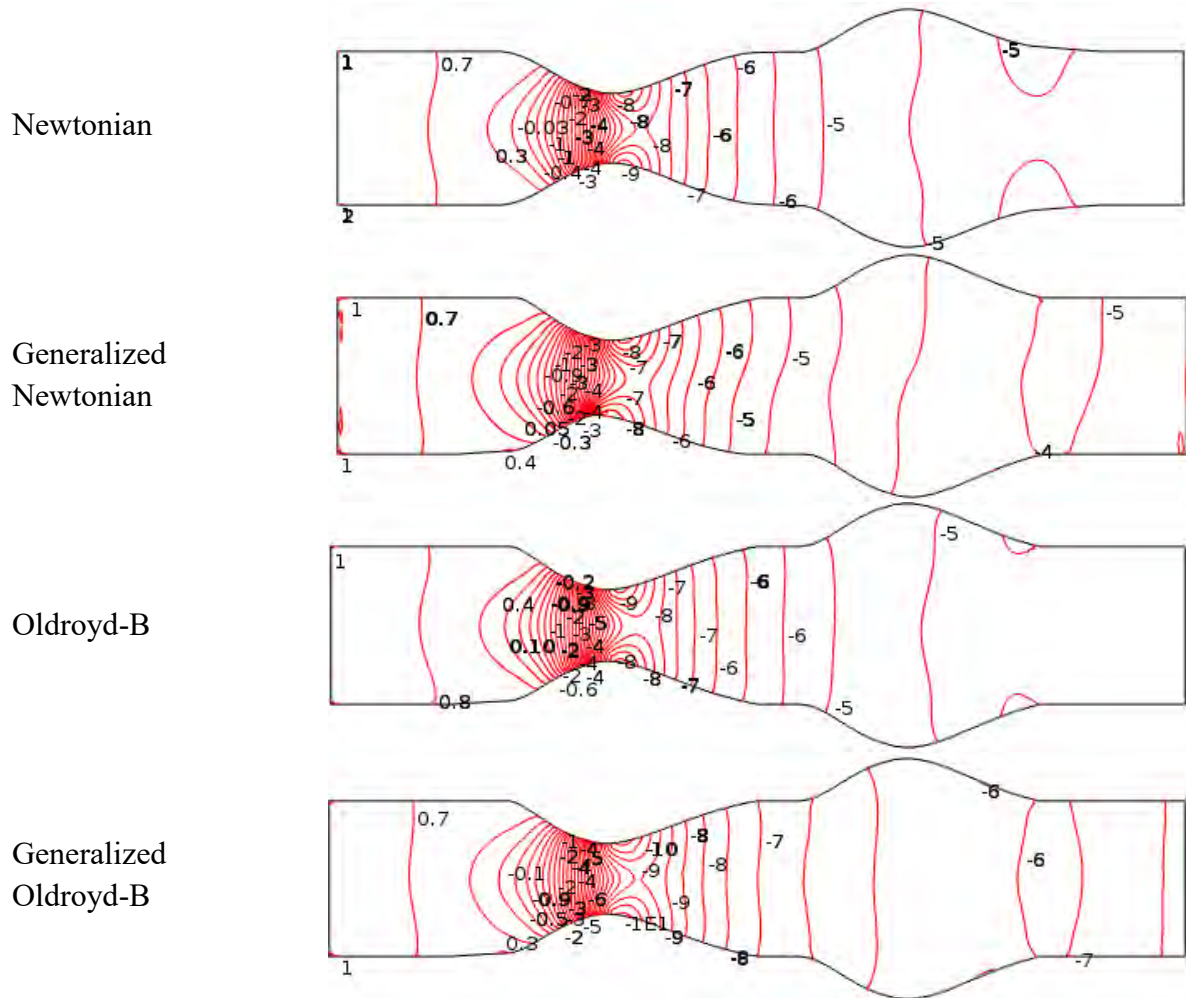


Figure 5.11: Pressure distribution on blood flow through stenosed and aneurysmatic vessel without blood clot at $Re=1000$ and $Wi = 0.6$

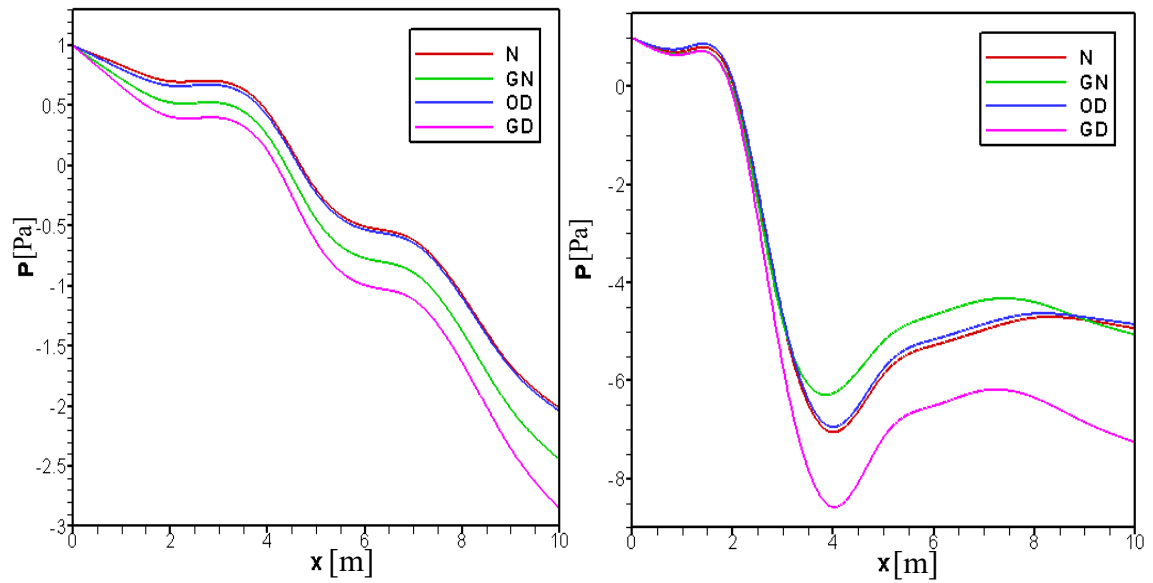


Figure 5.12: Comparison of pressure profile with blood clot (left) and without blood clot (right)

5.4.3 Effects of dimensionless number

Reynold numbers (*Re*) effects

The various Reynold numbers ($0 < Re \leq 3000$) effects on blood flow are shown in Figures 5.13 through 5.16 having blood clot for all models. The different *Re* is computed on the based on the blood density, blood viscosity, length of the model and various velocity at inlet. The recirculation zones are produced at the near of blood clot region for all events. The recirculation shape of blood flow has changed from oval to elliptic with the increases of *Re* at stenosis for all models. At *Re*=1000, the blood flow patterns have remained same at the inlet and outlet but size of recirculation zone is tiny at generalized Oldroyd-B models. At *Re*=2000, the flow separation area is comparable bigger to laminar blood flow (*Re*=1000) at aneurysm and recirculation zone have increased for all four models. At the turbulent blood flow (*Re*=3000), the blood flow velocity has changed gradually after blood lump at stenosis as a result the recirculation zones become long elliptic shape. The recirculation zones have expanded for turbulent case and occupy more space for the core blood flow and grow up swiftly at the throat of stenosis. But in the case of laminar blood flow, the blood velocity is higher compare to another *Re* numbers at the constriction area as a result the mini recirculation zones are developed and blood flow go down slow which is indicated by iso-velocity contour lines. Due to lump of blood, the turbulent flow of blood has reduced at stenosis which leads to blood flow stability for all cases. The graphical presentation of blood velocity is shown in Figure 5.17 for all models. The blood velocity has a significant changed and it gains maximum value at blood clotted regions and peak minimum value at the end of aneurysm of the vessel for Newtonian case. The lowest velocity is found at generalized Oldroyd-B model due to blood viscosity. In Table 5.4, the velocities obtained for different Reynold numbers while *Re* = 1000, 2000 and 3000 are presented.

Table 5.4: Velocities are obtained for different Reynold numbers, *Re* = 1000, 2000 and 3000 when *Wi* = 0.6 and *q*= 0.1 cm³/s.

Models	Velocity (<i>U</i>)					
	<i>Re</i> = 1000		<i>Re</i> = 2000		<i>Re</i> = 3000	
	Upstream (Stenosis)	Downstream (Aneurysm)	Upstream (Stenosis)	Downstream (Aneurysm)	Upstream (Stenosis)	Downstream (Aneurysm)
N	0.0906721	0.0749423	0.0876923	0.08053922	0.0851597	0.08198339
GN	0.0891384	0.07098498	0.0872179	0.07693232	0.0862179	0.07993232
OD	0.0895202	0.07476200	0.0862124	0.07995660	0.0832586	0.08085481
GD	0.0899349	0.06925514	0.0889029	0.07621299	0.0868359	0.07923295

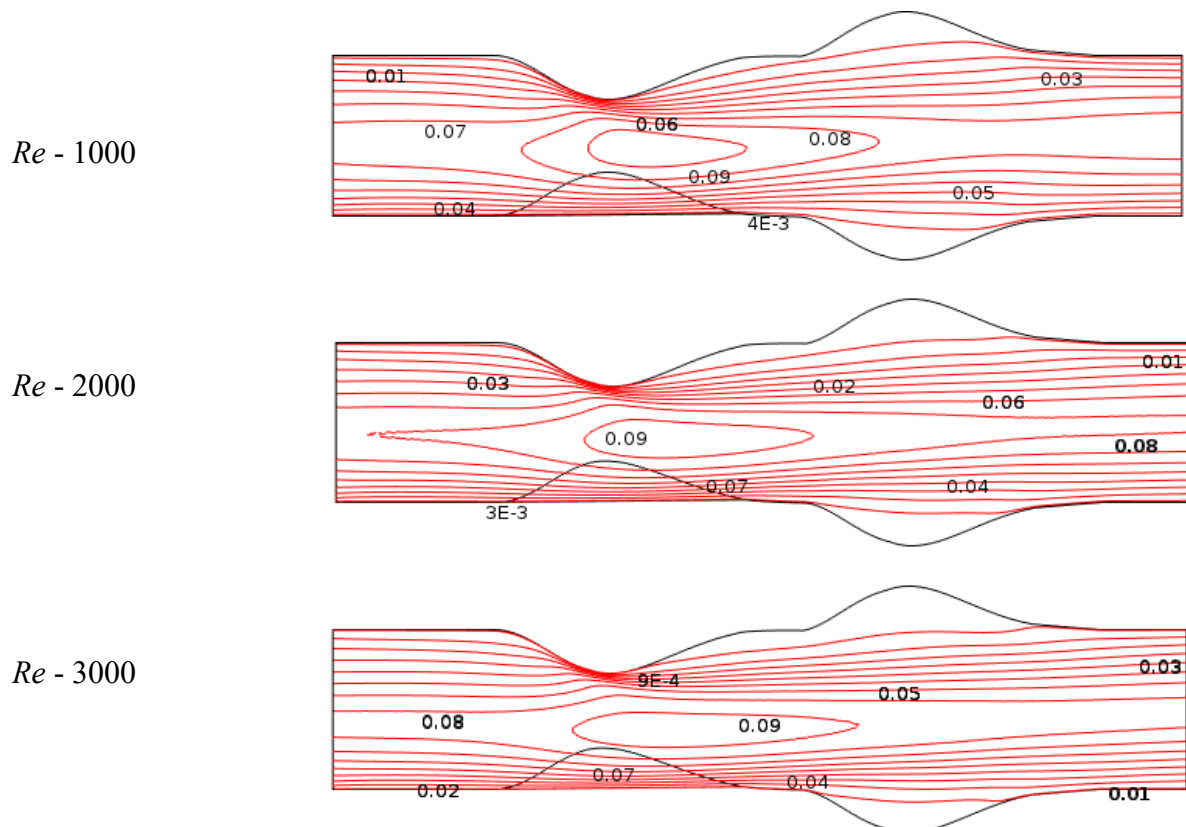


Figure 5.13: Reynold Numbers (Re) effects on Blood flow of *Newtonian Model* at $Wi = 0.6$ and flow rate $0.1 \text{ cm}^3/\text{s}$.

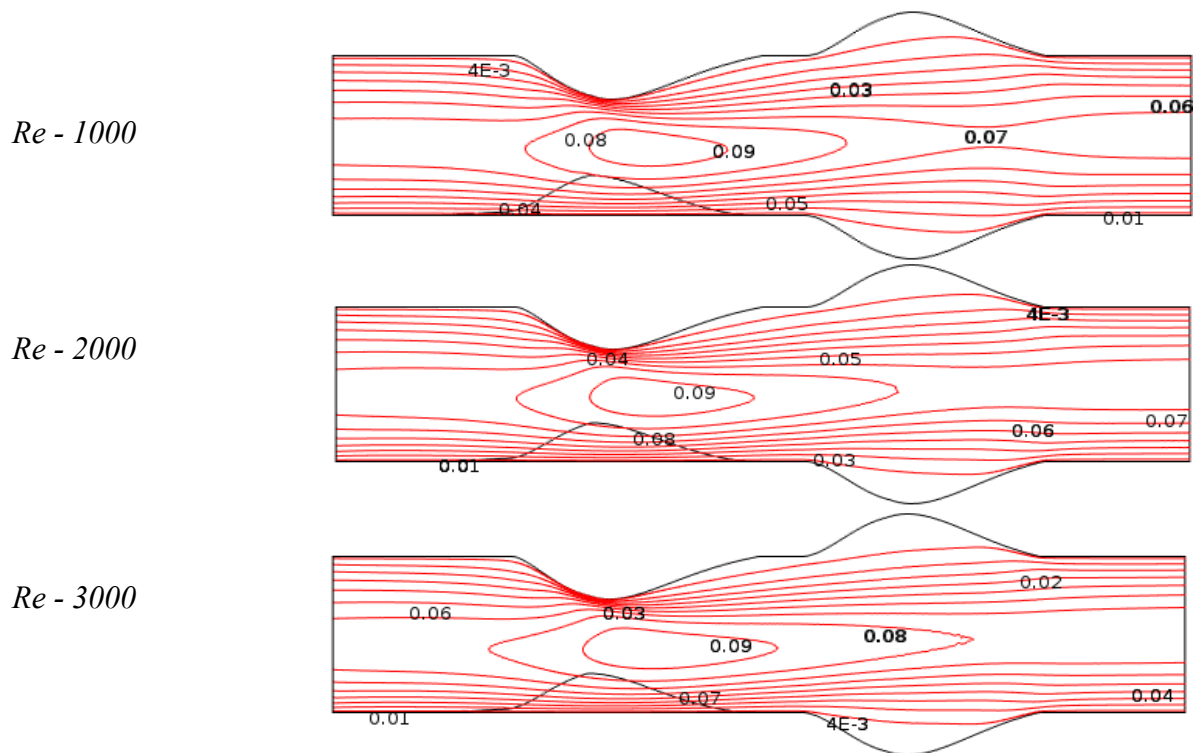


Figure 5.14: Reynold Numbers (Re) effects on Blood flow of *Generalized Newtonian Model* at $Wi = 0.6$ and flow rate $0.1 \text{ cm}^3/\text{s}$.

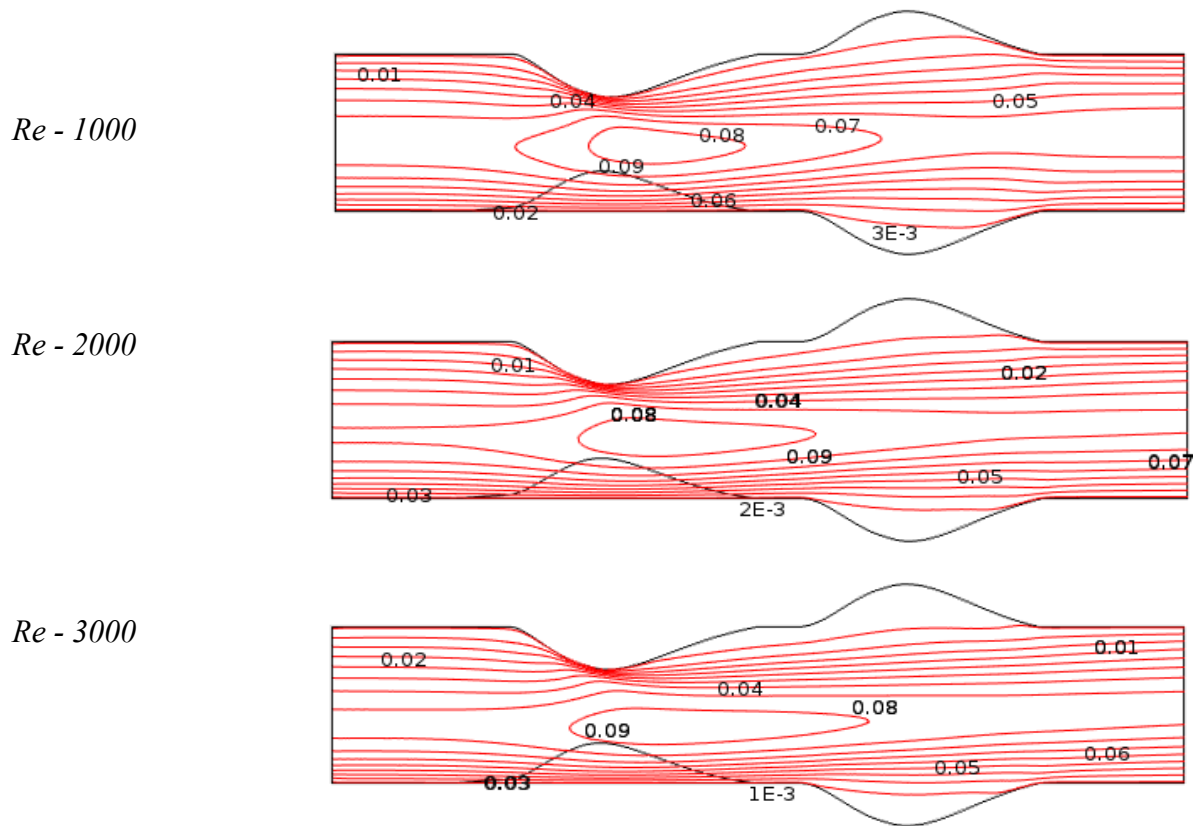


Figure 5.15: Reynold Numbers (Re) effects on Blood flow of Oldroyd-B Model at $Wi = 0.6$ and flow rate $0.1 \text{ cm}^3/\text{s}$.

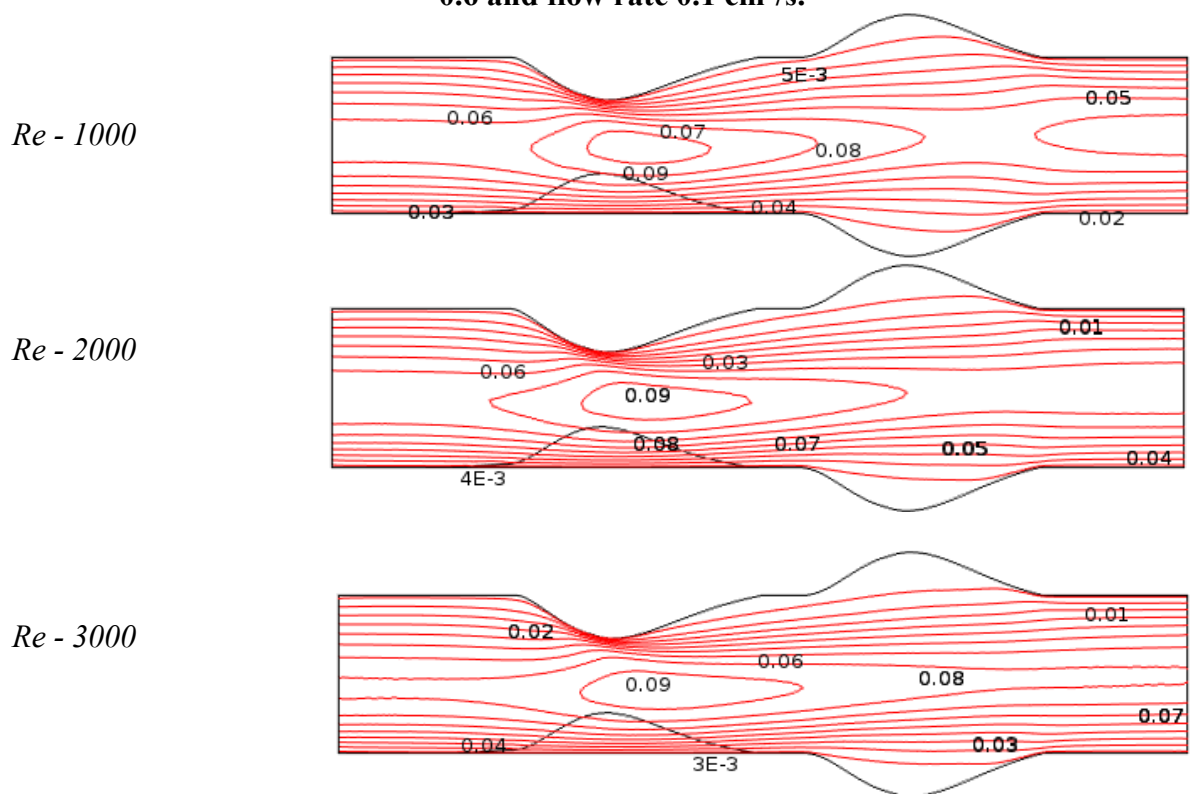


Figure 5.16: Reynold Numbers (Re) effects on Blood flow of Generalized Oldroyd-B Model at $Wi = 0.6$ and flow rate $0.1 \text{ cm}^3/\text{s}$.

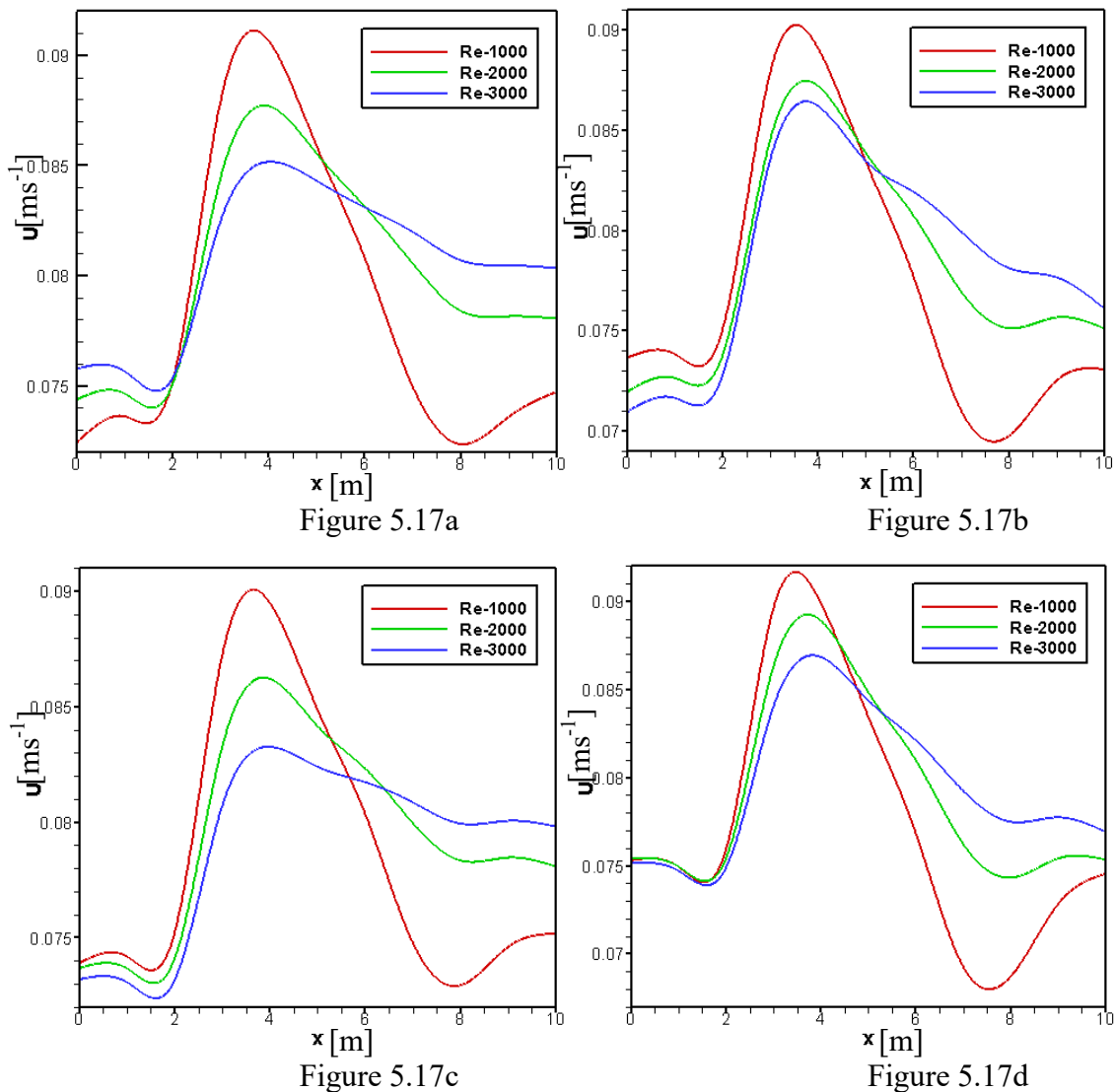


Figure 5.17: Velocity profile of the Effects of Reynold numbers (Re)on Blood flow at $Wi = 0.5$ and flow rate $0.1 \text{ cm}^3/\text{s}$ for (Figure 5.17a) Newtonian Model, (Figure 5.17b) Generalized Newtonian Model, (Figure 5.17c) Oldroyd-B Model, and (Figure 5.17d) Generalized Oldroyd-B Model.

The simulation of blood flow is exhibited in Figures 5.18 and 5.21 in terms of pressure contour plots with the range of $0 < Re \leq 3000$ for all cases. At the center of obstacle, the pressure contour lines are almost same for all Re numbers which indicate the rock-bottom value of blood pressure for all models. With the increases of Re numbers the pressure contour lines are having curls within coagulated blood which infer the minimum blood pressure level. Before aneurysm of the cavity the pressure gradient is increased and decreased at the outlet of cavity. The wavy curves are produced within coagulated blood for generalized Oldroyd-B model because of viscoelasticity and shear-thinning features of blood.

CHAPTER 5 NUMERICAL INVESTIGATION... ..

The influence of Reynold numbers on the blood flow is shown in Figure 5.22 for all four models. The pressure level is extremely lowest level at blood clot area in low shear region and it is up in the high shear area of the stenotic and aneuysmatic artery. The pressure has almost changed proportionately with respect to Reynold numbers. At $Re = 3000$, due to the presence of blood clot and viscoelastic features of blood the pressure has picked the lowest value at generalized Oldroyd-B case. The numerical value of pressure is inserted in the following Table 5.5 for different Reynold numbers while $Re = 1000, 2000$ and 3000 .

Table 5.5: Pressue value are shown at stenosis and aneurysm with different Re when $Wi=0.6$ and $q = 0.1 \text{ cm}^3/\text{s}$.

Models	Pressure (P)					
	$Re = 1000$		$Re = 2000$		$Re = 3000$	
	Upstream (Stenosis)	Downstream (Aneurysm)	Upstream (Stenosis)	Downstream (Aneurysm)	Upstream (Stenosis)	Downstream (Aneurysm)
N	-1.8844043	-1.14521587	-3.0714253	-1.88400558	-4.0050992	-2.68453688
GN	-2.1970627	-1.4898275	-3.4514261	-2.14221481	-4.4514261	-2.69221492
OD	-1.7083235	-1.00507796	-2.7907693	-1.65382281	-3.6937299	-2.41230110
GD	-2.6835676	-2.04029926	-3.7740594	-2.3944662	-4.7713939	-2.95738266

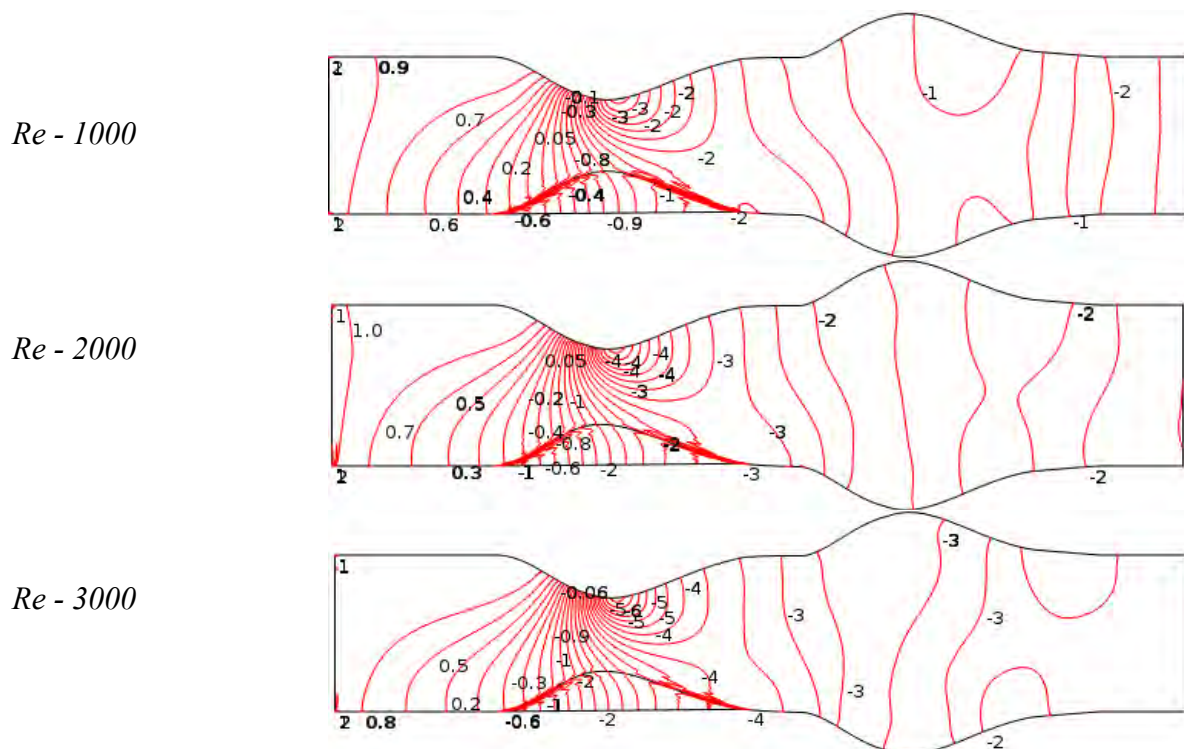


Figure 5.18: ReynoldNumbers (Re) effects on pressure distribution of Blood flow for Newtonian Model at $Wi = 0.6$ and flow rate $0.1 \text{ cm}^3/\text{s}$.

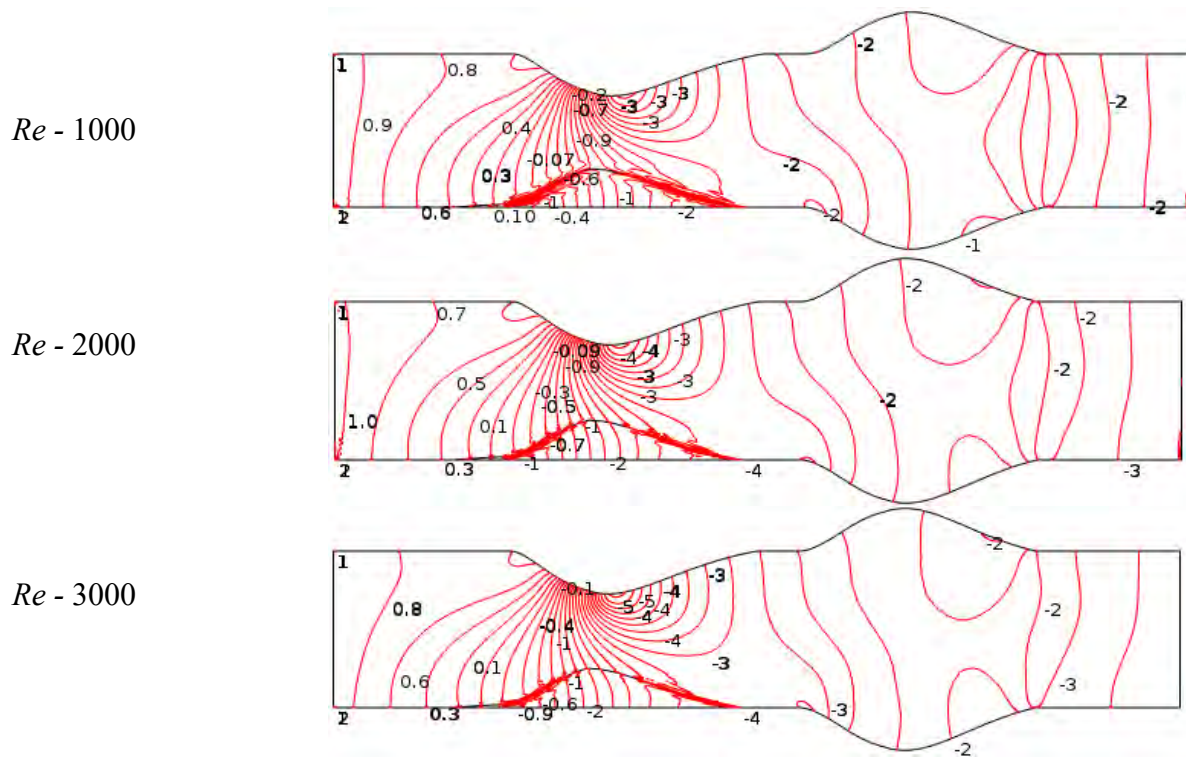


Figure 5.19: Reynold Numbers (Re) effects on pressure distribution of Blood flow for Generalized Newtonian Model at $Wi = 0.6$ and flow rate $0.1 \text{ cm}^3/\text{s}$.

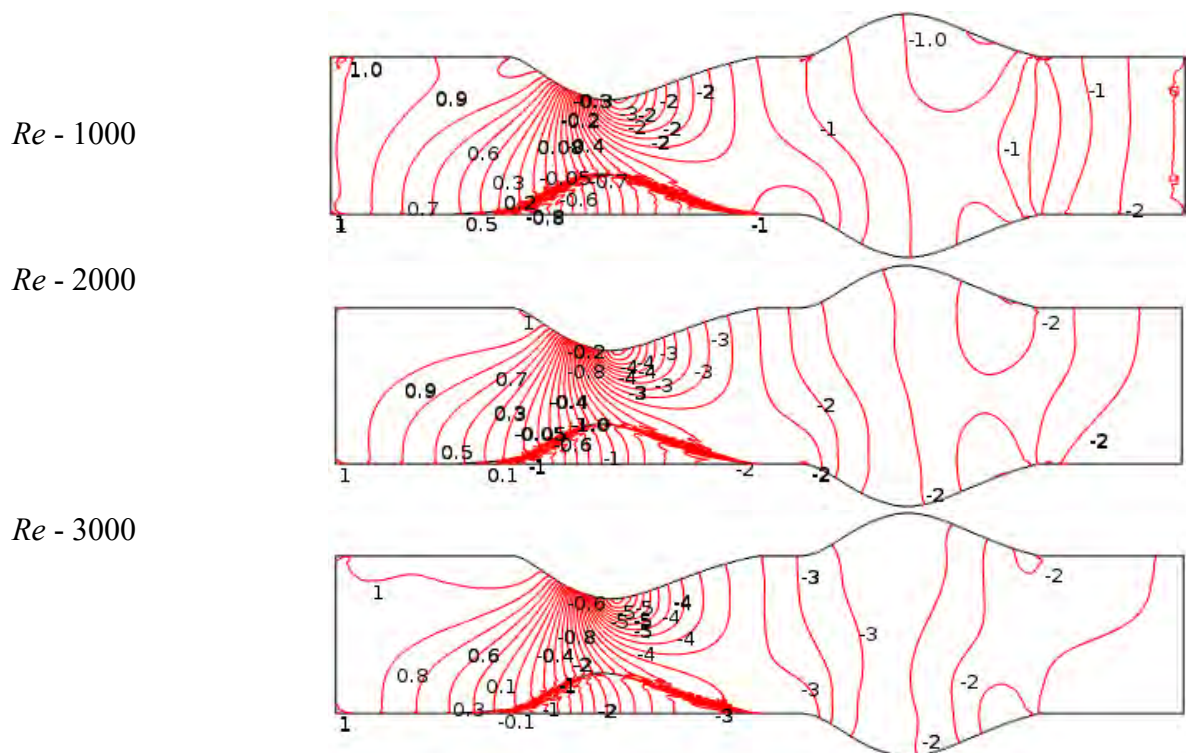


Figure 5.20: Reynold Numbers (Re) effects on pressure distribution of Blood flow for Oldroyd-B Model at $Wi = 0.6$ and flow rate $0.1 \text{ cm}^3/\text{s}$.

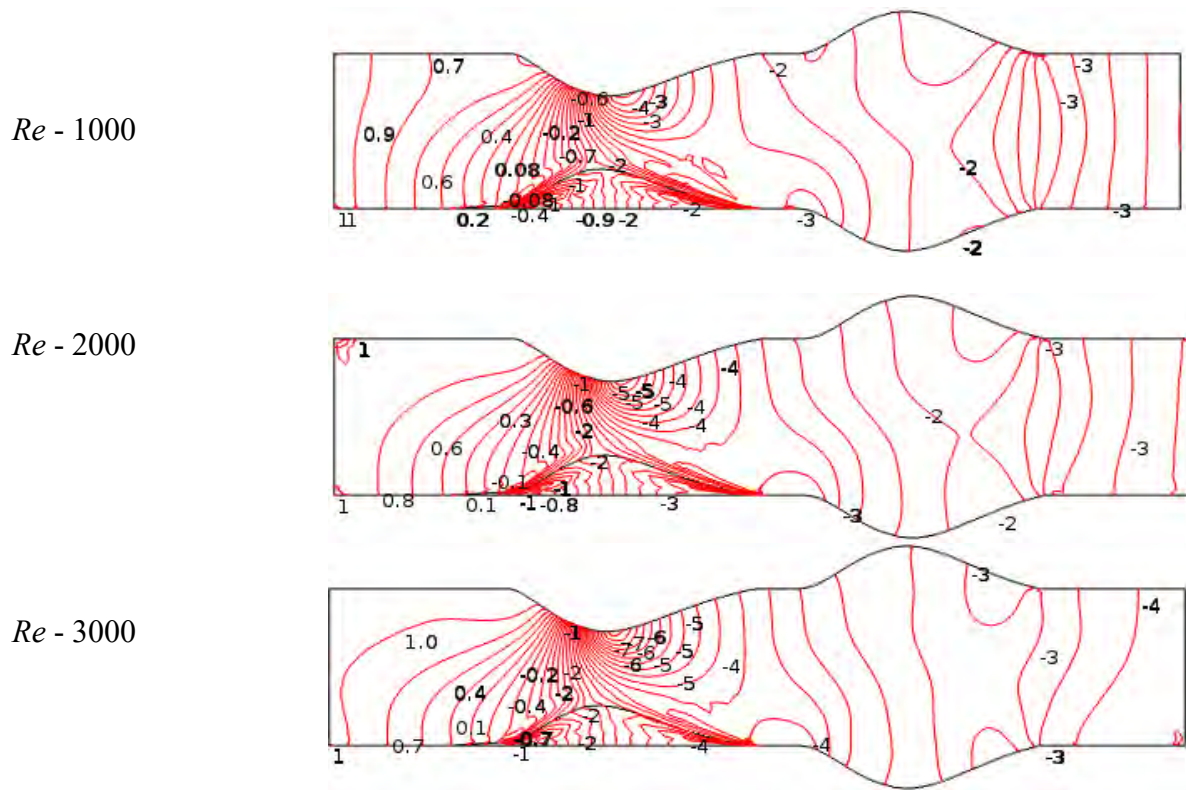


Figure 5.21: Reynold Numbers (Re) effects on pressure distribution of Blood flow for Generalized Oldroyd-B Model at $Wi = 0.6$ and flow rate $0.1 \text{ cm}^3/\text{s}$.

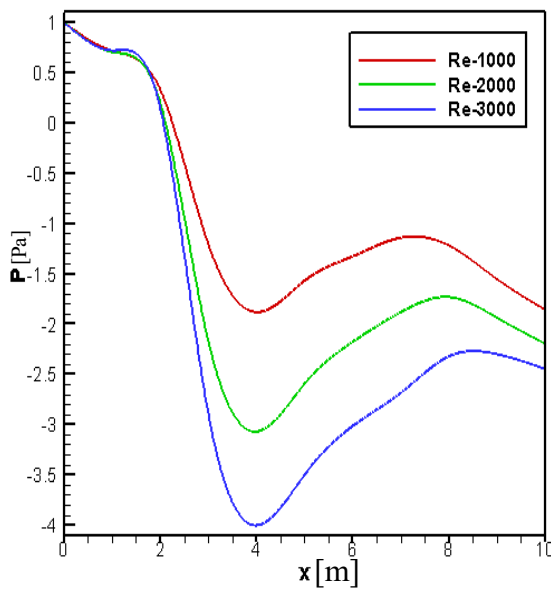


Figure 5.22a

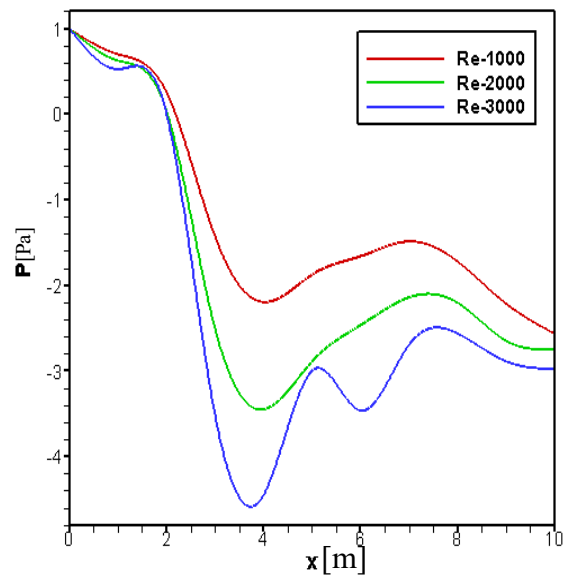


Figure 5.22b

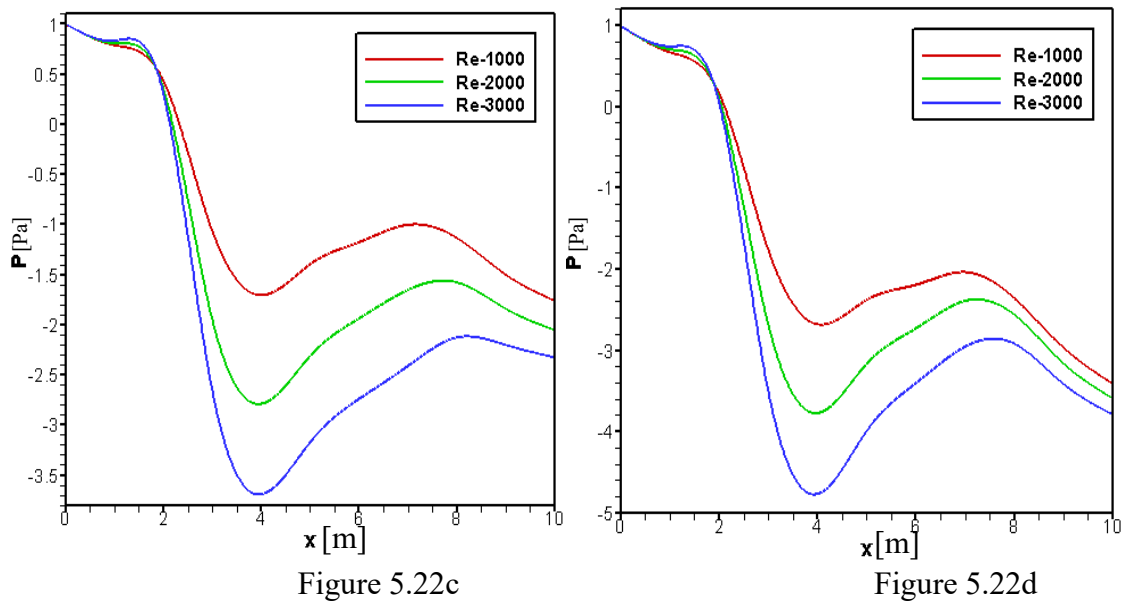


Figure 5.22: Pressure profile of the Effects of Reynold numbers (Re) on Blood flow at $Wi = 0.5$ and flow rate $0.1 \text{ cm}^3/\text{s}$ for (Figure 5.22a) Newtonian Model, (Figure 5.22b) Generalized Newtonian Model, (Figure 5.22c) Oldroyd-B Model, and (Figure 5.22d) Generalized Oldroyd-B Model.

Weissenberg Numbers (Wi) Effects

In this section, the blood flow simulation is demonstrated through the velocity and pressure contour lines in Figures 5.23 to 5.26 with the range of Weissenberg numbers ($0 \leq Wi \leq 1$) for all cases. The pure elastic response fluid and pure fluid corresponds to larger Wi ($Wi > 1$) and tiny Wi ($Wi = 0$) respectively. From the figures, the recirculation bubbles are seen at stenosis area and they have insignificantly changed by the Weissenberg numbers. With the increases of Wi , a little bit elongate of recirculation of blood flow at the constriction region has done. We observed that the bubbles are shorter in Oldroyd-B and generalized Oldroyd-B model compare to another model for blood viscosity behavior and lump of blood. The velocity contour lines are almost symmetric along the vessel axis for all models. The reverse blood flow regions are found at aneurysm to the adjacent of vessel walls and trivial change occur for different Wi .

The graphical presentations of blood velocity are described in Figure 5.27 for all events. In the low shear regions and blood clotted area, the velocity has a great important change and provided apex value of the velocity. On the contrary, the lowest velocity is found in aneurysm due to local viscosity is dominated. A little different at inlet is

CHAPTER 5 NUMERICAL INVESTIGATION... ..

noticeable and the minor variation is seen in Figure 5.27. The velocity at the throat of stenosis and aneurysm have introduced in the following table 5.6 along vessel axis for different Weissenberg numbers while $Wi = 0.0, 0.5, 1.0$.

Table 5.6: Velocity at the throat of stenosis and aneurysm with various Wi when $Re=1000$ and $q= 0.1\text{cm}^3/\text{s}$.

Models	Velocity (U)					
	$Wi = 0.0$		$Wi = 0.5$		$Wi = 1.0$	
	Up stream (Stenosis)	Down stream (Anuerysm)	Up stream (Stenosis)	Down stream (Anuerysm)	Up stream (Stenosis)	Down stream (Anuerysm)
N	0.09035163	0.07542726	0.09050904	0.07542334	0.09073528	0.07556485
GN	0.08898240	0.07091897	0.08913842	0.07098498	0.08932517	0.07106860
OD	0.08907139	0.07514768	0.08933925	0.07522795	0.08962555	0.07534929
GD	0.08983876	0.06923700	0.08993499	0.06925514	0.09003013	0.06927763

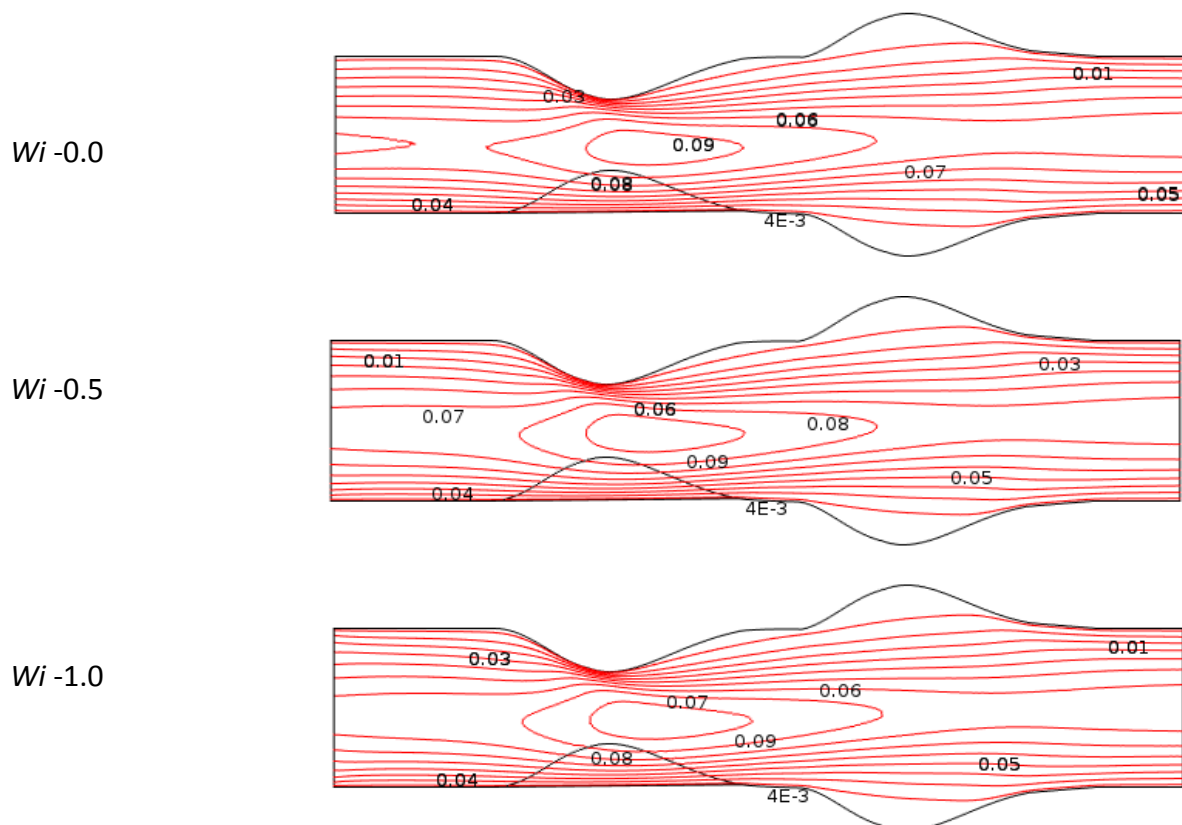


Figure 5.23: Weissenberg Numbers (Wi) effects on Blood flow of Newtonian Model with blood clot at $Re = 1000$ and flow rate $0.1 \text{ cm}^3/\text{s}$.

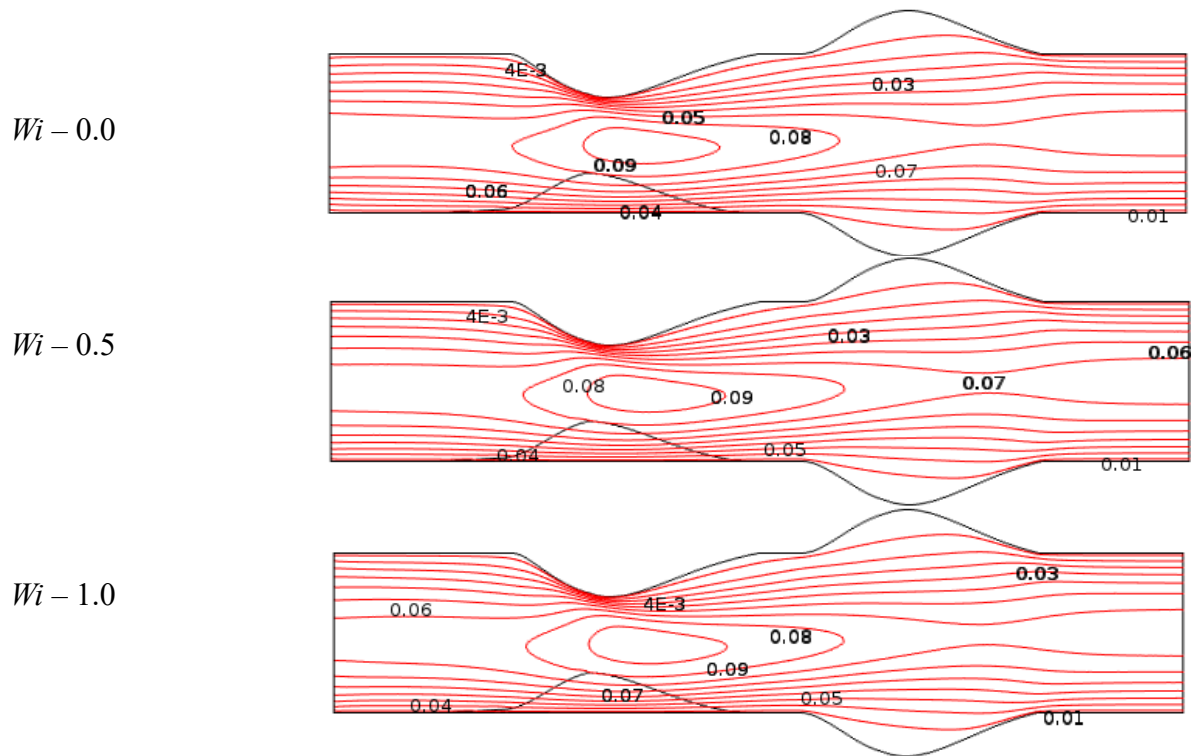


Figure 5.24: Weissenberg Numbers (Wi) effects on velocity distribution of Blood flow for Generalized Newtonian Model with blood clot at $Re = 1000$ and flow rate $0.1 \text{ cm}^3/\text{s}$.

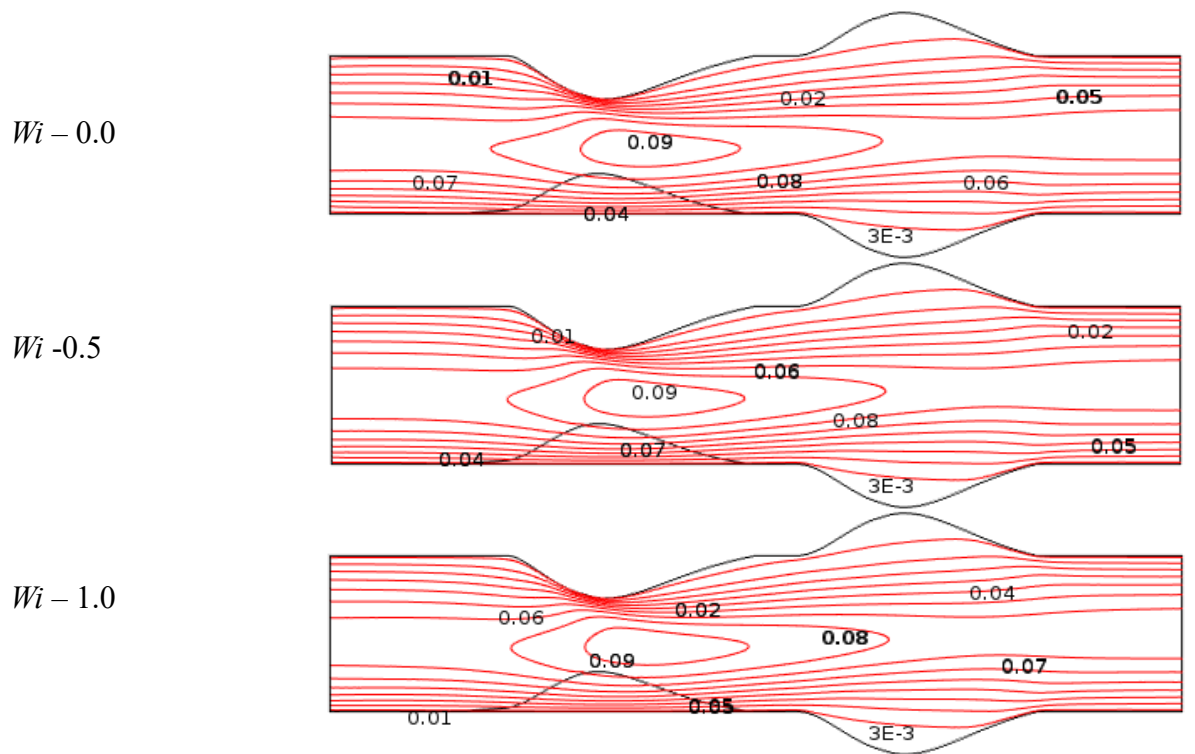


Figure 5.25: Weissenberg Numbers (Wi) effects on velocity distribution of Blood flow for Oldroyd-B Model with blood clot at $Re = 1000$ and flow rate $0.1 \text{ cm}^3/\text{s}$.

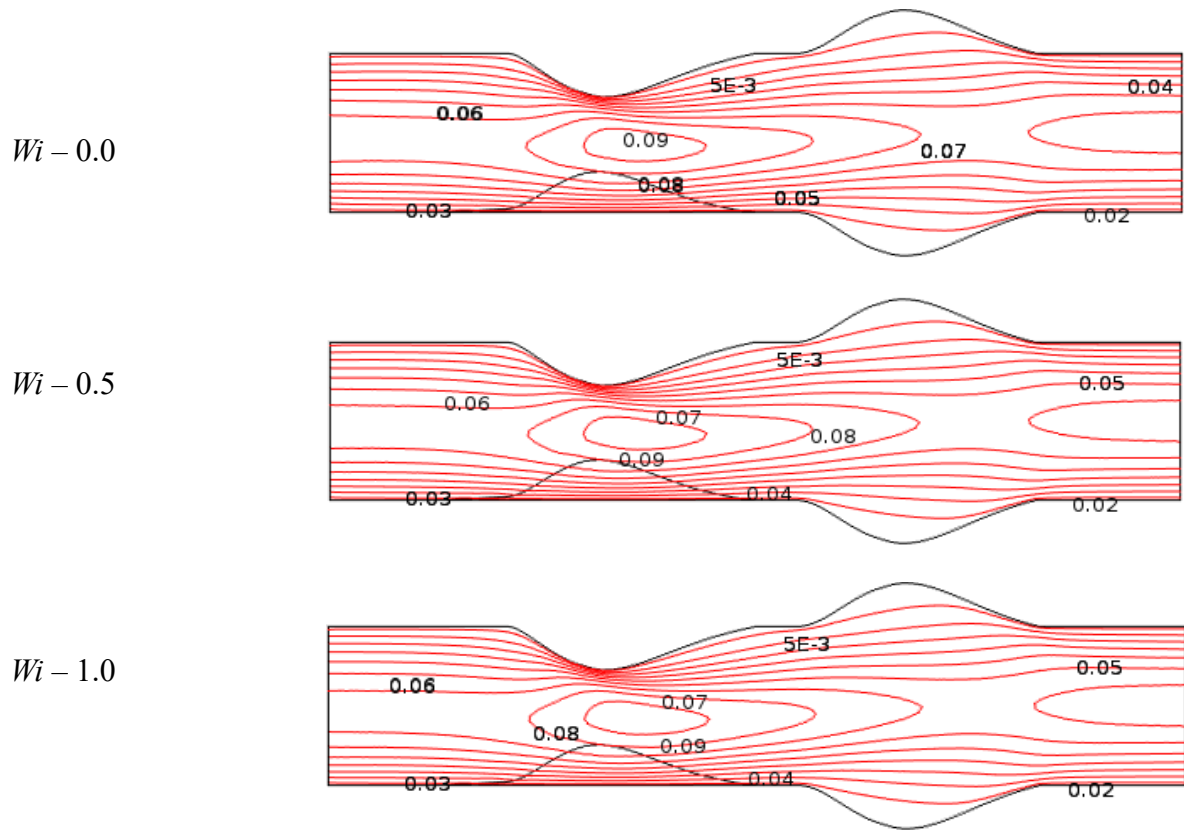


Figure 5.26: Weissenberg Numbers (Wi) effects on Velocity distribution of Blood flow for Generalized Oldroyd-B Model with blood clot at $Re = 1000$ and flow rate $0.1 \text{ cm}^3/\text{s}$.

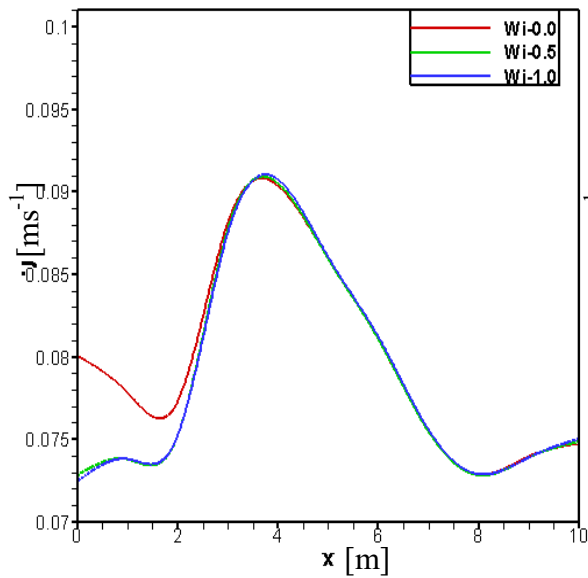


Figure 5.27a

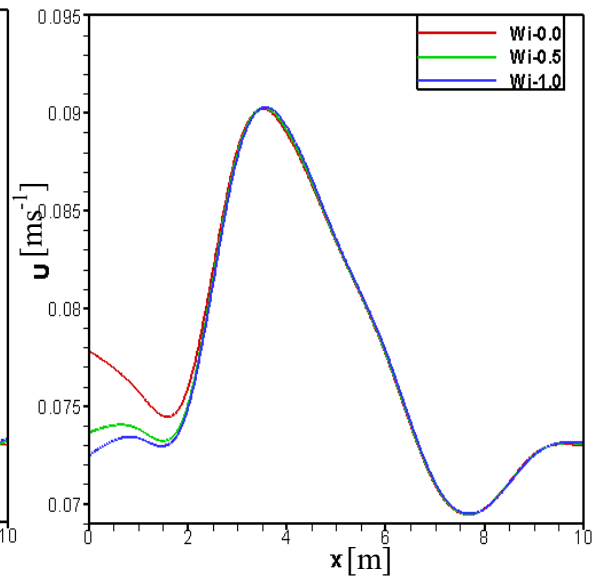


Figure 5.27b

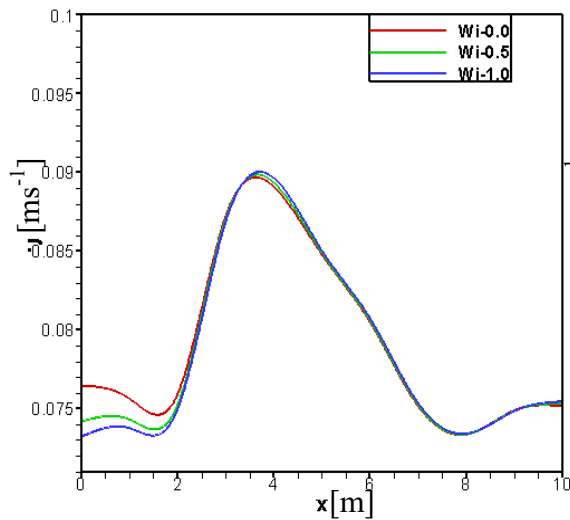


Figure 5.27c

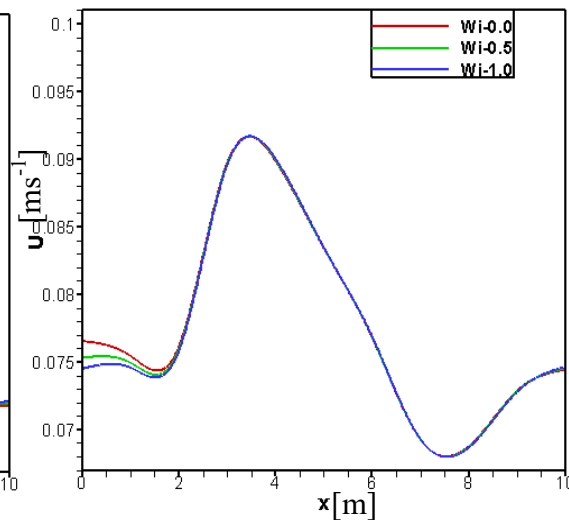


Figure 5.27d

Figure 5.27: Velocity profile of the Effects of Weissenbug numbers (Wi) on Blood flow at $Pe = 1000$ and flow rate $0.2 \text{ cm}^3/\text{s}$ for (Figure 5.27a) Newtonian Model, (Figure 5.27b) Generalized Newtonian Model, (Figure 5.27c) Oldroyd-B Model, and (Figure 5.27d) Generalized Oldroyd-B Model.

The pressure is more dominated at blood clot area and achieved the lowest value at separation point which are portray in Figures 5.28-5.31 for all four models. The iso-pressure contour lines are found at the end of bulge region and provide how the pressure changed to meet minimum value. For generalized Oldroyd-B model, the vertical fold curves are shown within coagulated blood region caused by high viscoelasticity factor of blood.

The computed pressures are visible in Figure 5.32 with respect to Weissenberg number for all cases. The pressure has swiftly decreased at blood lump area and increased in swelling region of the artery for all four models. At Newtonian model, the pressure provides higher value for $Wi = 0$ compare to others value of Wi . With the increases of Wi , the blood fluid behave like elastic response is main reason. For the blood viscoelasticity and shear thinning, the pressure are identical at generalized Oldroyd-B. In Table 5.7, the calculated pressure at blood lump and swell area of artery along vessel axis for different Weissenberg numbers while $Wi = 0.0, 0.5$ and 1.0 is presented.

Table 5.7: Pressure at blood lump and swell area of artery along vessel axis for different Weissenberg numbers, $Wi = 0.0, 0.5$ and 1.0 .

Models	Velocity (U)					
	$Wi = 0.0$		$Wi = 0.5$		$Wi = 1.0$	
	Upstream (Stenosis)	Downstream (Aneurysm)	Upstream (Stenosis)	Downstream (Aneurysm)	Upstream (Stenosis)	Downstream (Aneurysm)
N	-1.62131008	-0.83623052	-1.93433161	-1.16051297	-1.96568474	-1.19961551
GN	-2.01090580	-1.29762653	-2.19706271	-1.4898275	-2.24834425	-1.546702
OD	-1.65246867	-0.90632655	-1.75469901	-1.01716673	-1.80175259	-1.07195888
GD	-2.63812641	-1.99110761	-2.68356769	-2.04029926	-2.70928755	-2.07050651

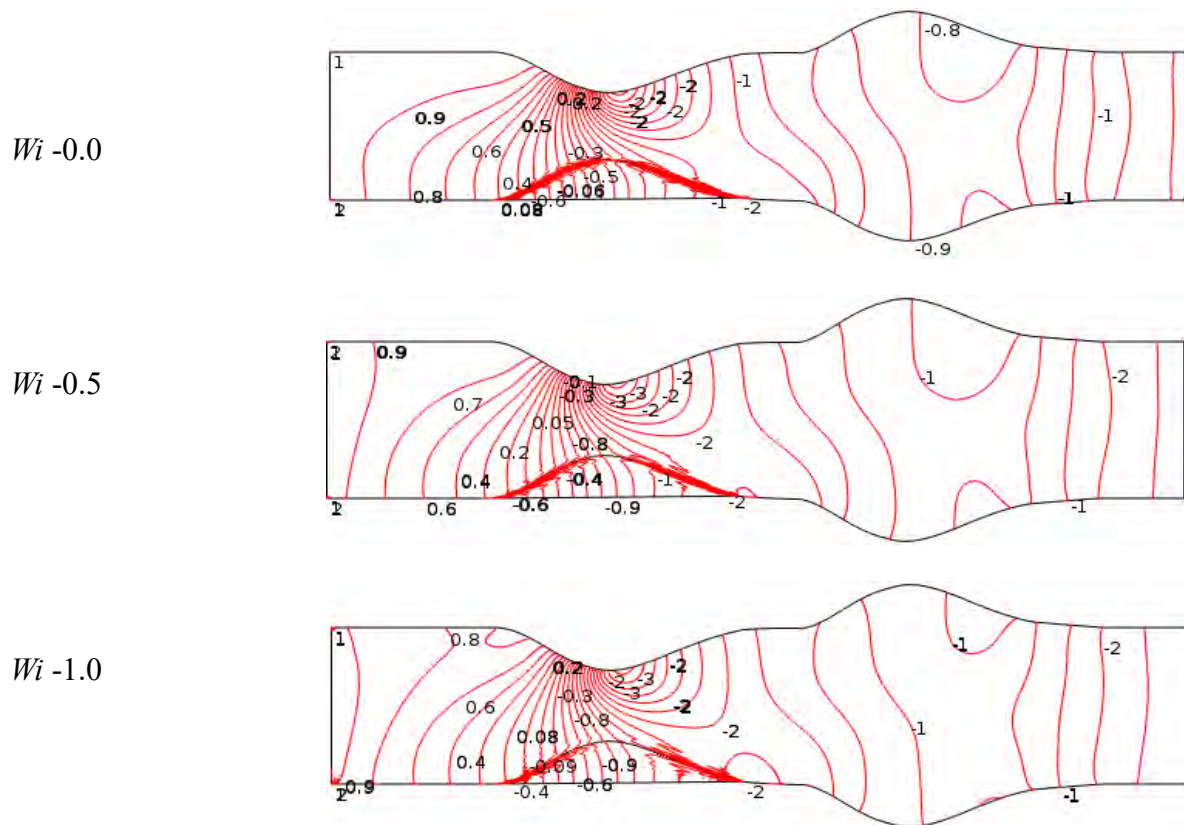


Figure 5.28: Weissenberg Numbers (Wi) effects on pressure distribution of Blood flow for Newtonian Model with blood clot at $Re = 1000$ and flow rate $0.1 \text{ cm}^3/\text{s}$.

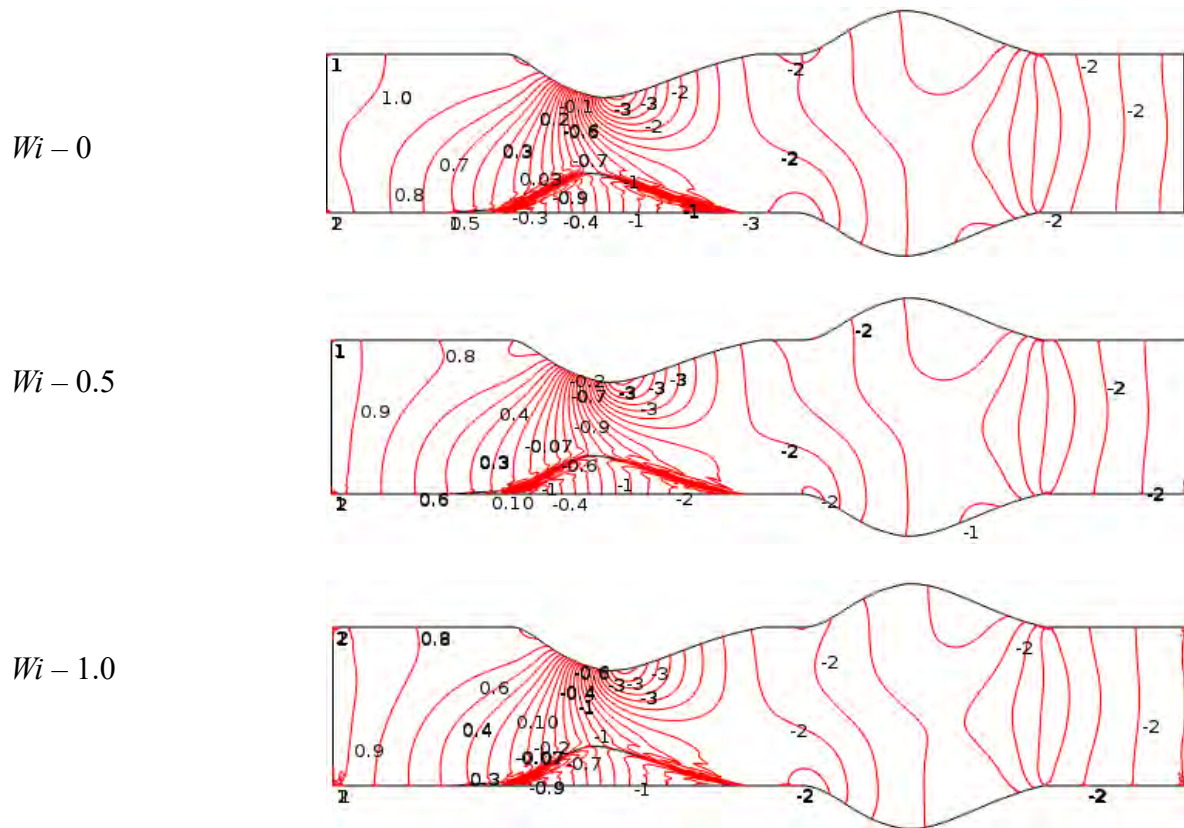


Figure 5.29: Weissenberg Numbers (Wi) effects on pressure distribution of Blood flow for Generalized Newtonian Model with blood clot at $Re = 1000$ and flow rate $0.1 \text{ cm}^3/\text{s}$.

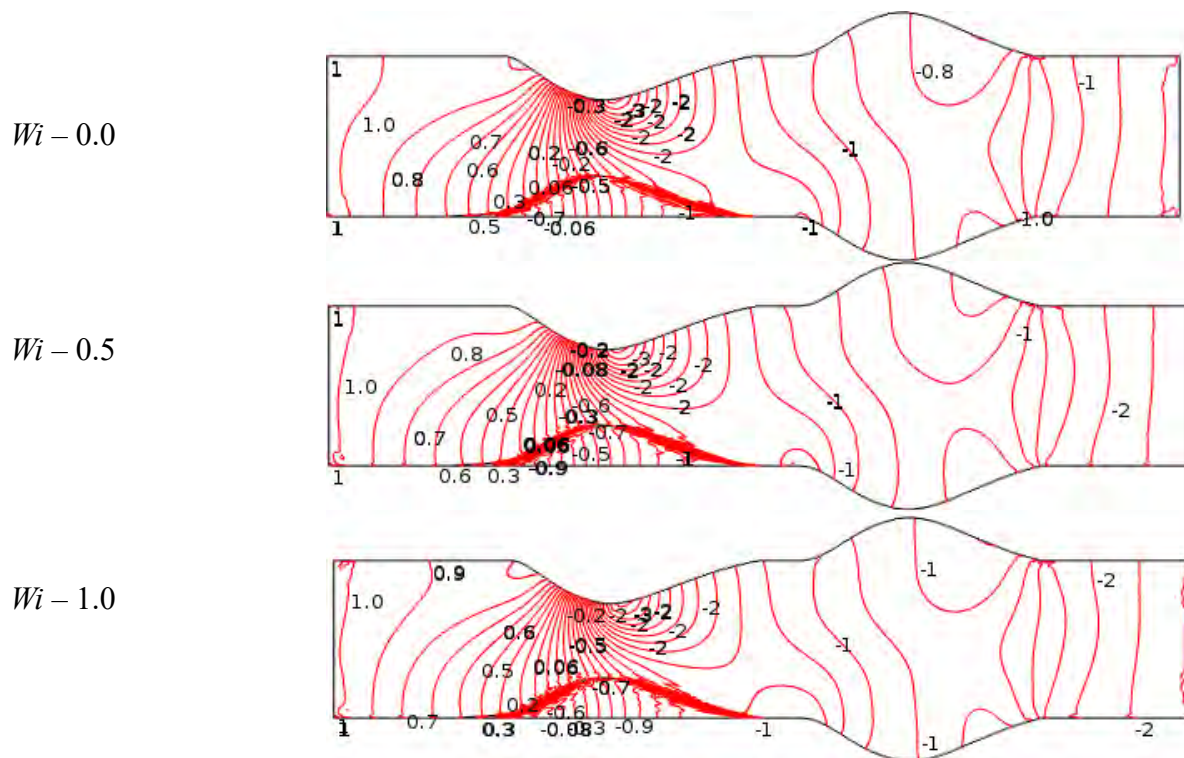


Figure 5.30: Weissenberg Numbers (Wi) effects on pressure distribution of Blood flow for Oldroyd-B Model with blood clot at $Re = 1000$ and flow rate $0.1 \text{ cm}^3/\text{s}$.

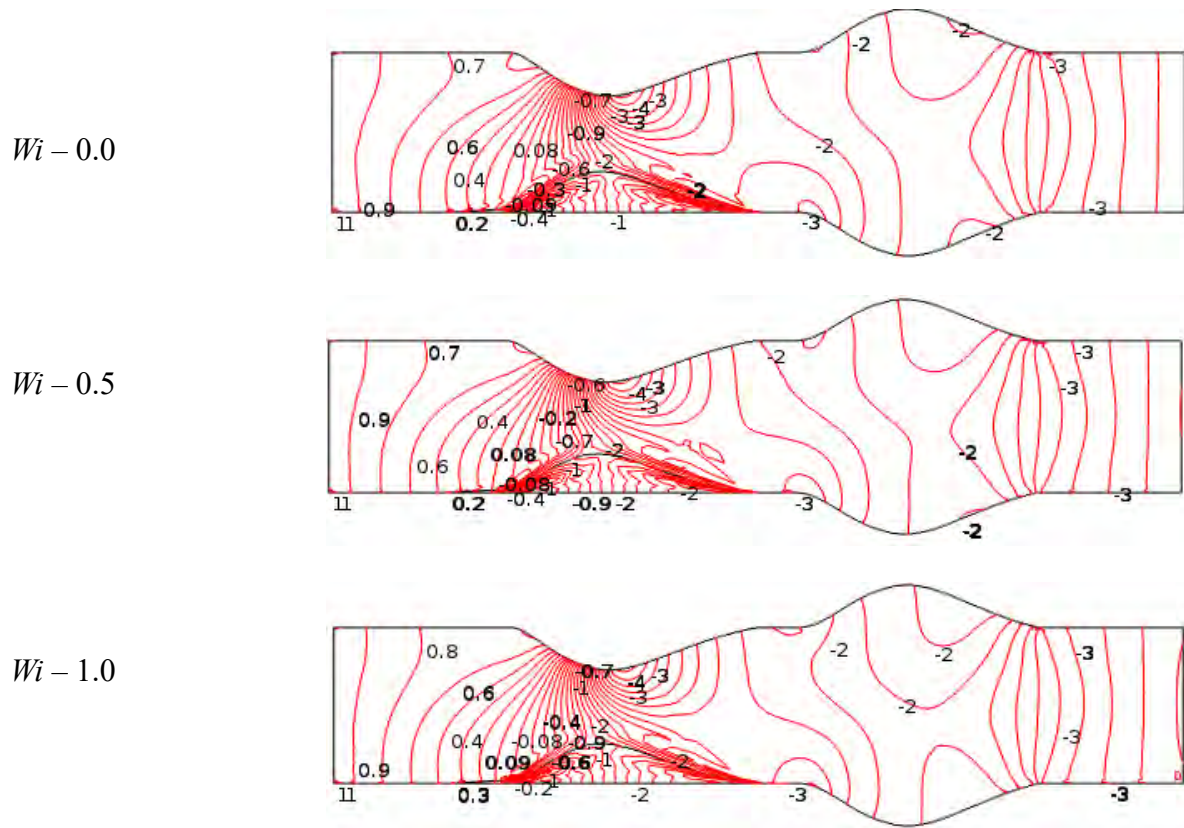


Figure 5.31: Weissenberg Numbers (Wi) effects on pressure distribution of Blood flow for Generalized Oldroyd-B Model with blood clot at $Re = 1000$ and flow rate $0.1 \text{ cm}^3/\text{s}$.

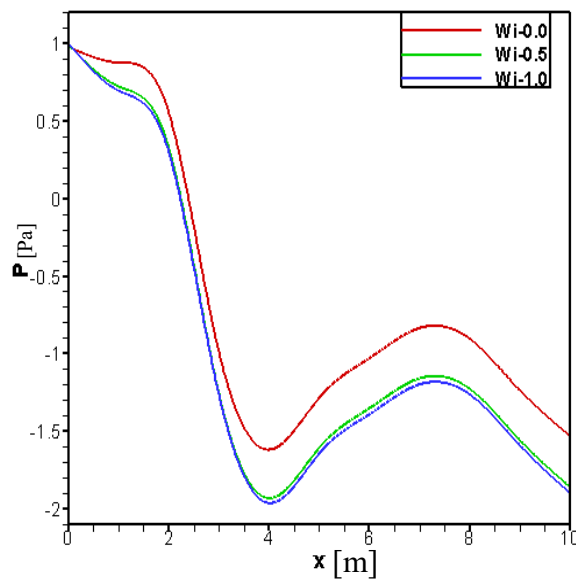


Figure 5.32a

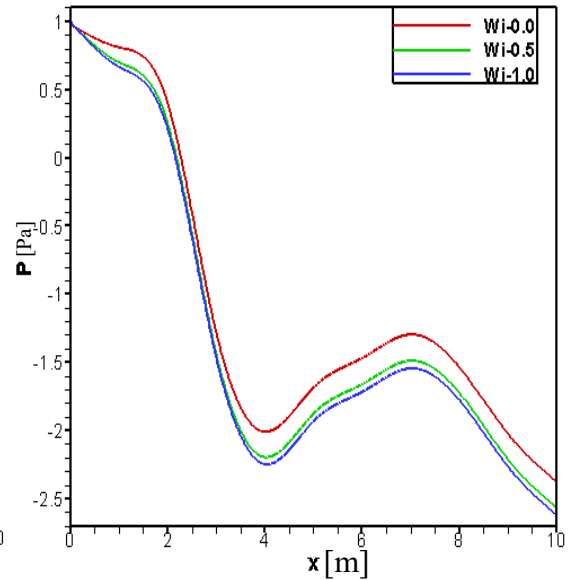


Figure 5.32b

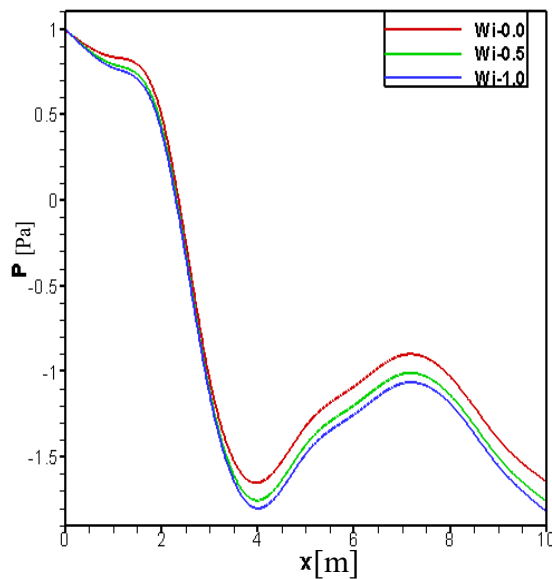


Figure 5.32c

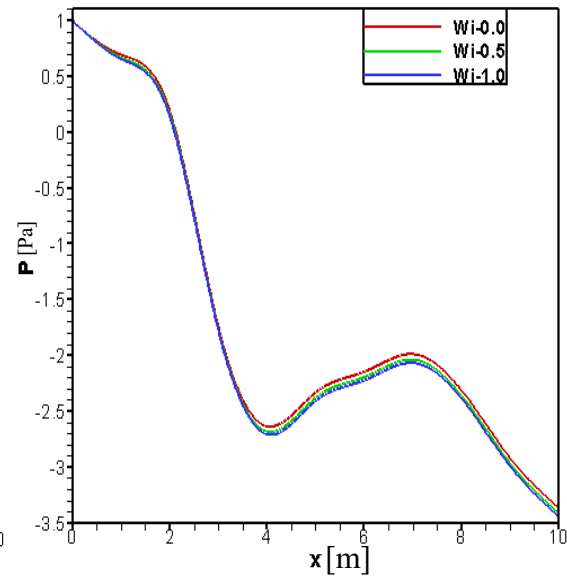


Figure 5.32d

Figure 5.32: Pressure profile of the Effects of Weissenbegr numbers (Wi) on Blood flow at $Re = 1000$ and flow rate $0.1 \text{ cm}^3/\text{s}$ for (Figure 5.32a) Newtonian Model, (Figure 5.32b) Generalized Newtonian Model, (Figure 5.31c) Oldroyd-B Model, and (Figure 5.32d) Generalized Oldroyd-B Model.

5.4.4 Wall shear stress effects on blood flow

The effects of wall shear stress at bottom wall are described in Figures 5.33 and 5.34 having blood clot and without blood clot respectively for all four models with blood flow rate $q = 0.1 \text{ cm}^3/\text{s}$. It is one of the main ingredient to findout the cardiovascular diseases in the arteries.

The friction or resistance among the fluids and between the fluid and the blood vessel wall, and is related to the fluid viscosity which leads to the pattern of the blood flow. This resistance generates a force (tangential force) exerted by the flowing fluid and is called the wall shear stress. The magnitude of wall shear stress is maximum at the beginning of blood clot area and minimum value is found at the throat of stenosis which leads how fast the blood fluid velocity changes when blood is flowing from the center of the vessel to bottom wall. The similar behavior are found for another model (without blood clot) but it attained the greatest amount of wall shear stress at the genesis of stenosis area for Newtonian case. We have found most minimum value of wall shear

stress for without blood clot model and maximum value for Newtonian models. In the case of non-blood clot, the profile of Wss has decreased slowly after stenosis region compare to blood clot model. In Figures 4.33, the rapid change of wall shear stress has occurred between blood clotted and aneurysm zone for all cases and negative values are originated at dilation area.

The contrast graphical study with the being and non existence of blood lump for the wall shear stress are shown in Figures 5.33 and 5.34 in various models. The influence of blood clot on the wall shear stress is clear from the figures and high Wss have exerted at the starting of stenotic area compare to another region. We observed that the magnitude of Wss has quickly decreased just after stenosis area for blood clot model. The negative magnitude of the wall shear stress have found in the reversalflow zones at blood clot model but the wall shear stress down significantly at non blood clot model. It is important finding that the minimum values of wall shear stress have reduced due to the presence of blood lump at stenotic arteries. In Table 5.8, the maxmini numerical value of wall shear stress along vessel axis for blood clot or non-blood clot model while $q = 0.1\text{cm}^3/\text{s}$, $Re = 1000$ and $Wi = 0.6$ are presented.

Table 5.8: The optimal value of wall shear stress along vessel axis for blood clotted and non-blood clotted model while $q = 0.1\text{cm}^3/\text{s}$, $Re = 1000$ and $Wi = 0.6$.

Models	Wall shear stress (Wss)			
	Blood clot model		Non-blood clot model	
	Maximum	Mimimum	Maximum	Mimimum
N	0.5523	-0.04214	9.8954	-1.9864
GN	0.5512	-0.04113	8.7635	-1.1563
OD	0.4595	-0.04534	8.8972	-1.8752
GD	0.4535	-0.04956	7.5486	-1.2573

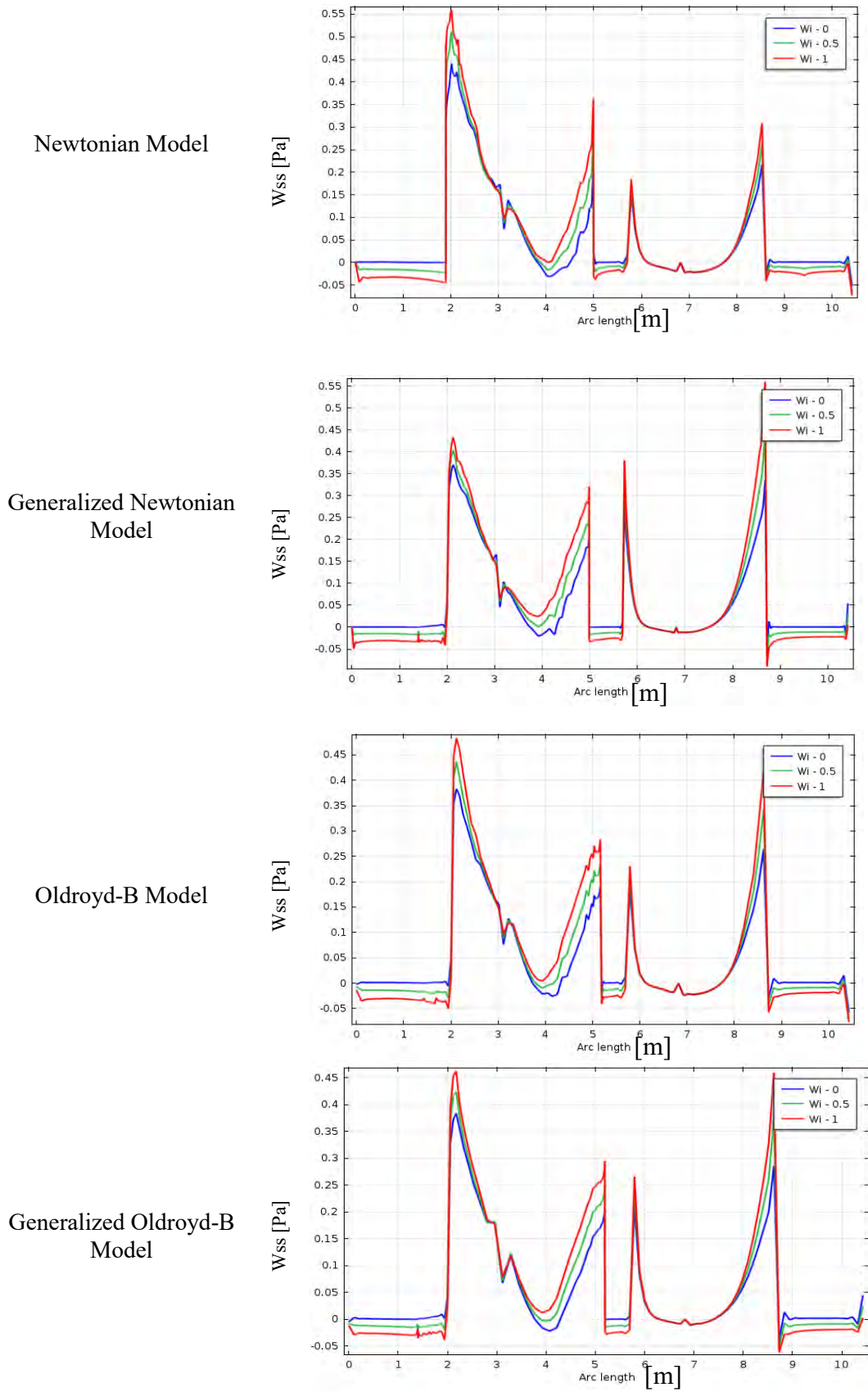


Figure 5.33: Effects of wall shear stress at upper wall without blood clot at stenotic artery for all cases with different Wi when $Re = 1000$ and $q = 0.1 \text{ cm}^3/\text{s}$.

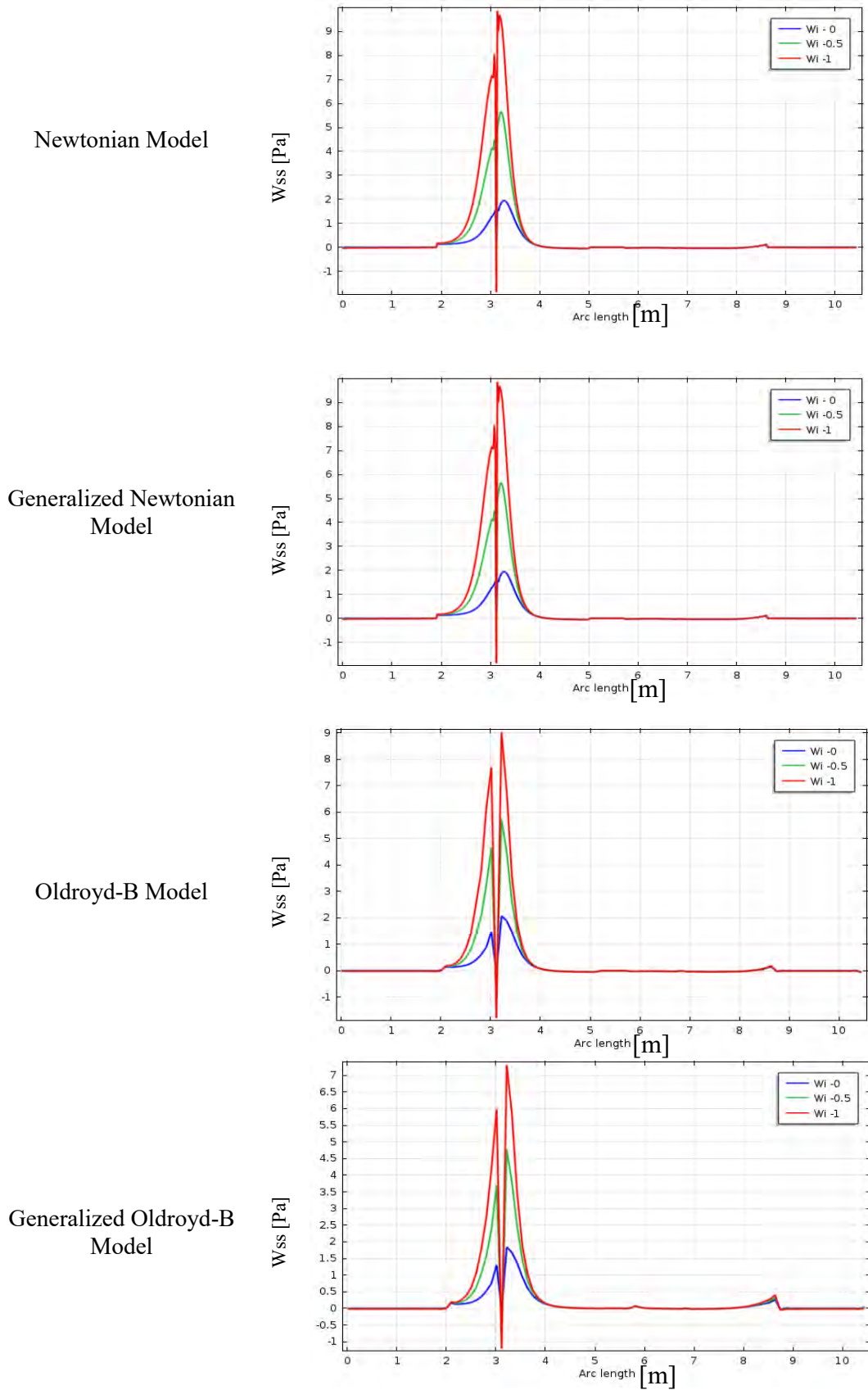


Figure 5.34: Effects of wall shear stress on blood flow through stenotic and aneurysmatic artery without blood clot for all cases at $Re=1000$ and $Wi = 0.6$.

5.4.5 Drag coefficient effects on blood flow

In Figure 5.35, the drag coefficient (resistance) of blood flow increases at blood clot model and non-blood clot model. The drag coefficient value is very high at nonblood lump case for the Newtonian, Generalized Newtonian, Oldroyd-B, Generalized Oldroyd-B models with the flow rate $q = 0.1 \text{ cm}^3/\text{s}$. In the case of non-blood clot, the resistance of blood flow is almost same for Newtonian and Oldroyd-B model but the stenotic zones (by external force) have created more obstacle to blood flow at generalized Oldroyd-B model because of viscoelastic behavior. The hindrance of blood flow over blood lump has increased for all cases but the hurdle is more at generalized model. From the Figure 5.36, the blood flow resistance increases with the increases Reynold numbers and Weissenberg numbers for all four models. The magnitude of drag coefficient is higher for generalized model and lower for Oldroyd-B model with increases of Reynold numbers. With increases of Weissenberg numbers the resistance of blood flow is more intensive at generalized Oldroyd-B model in low shear region. The magnitude of drag Coefficient (C_d) at stenosed vessel is shown in the following table 5.9 for dimensionless numbers Re and Wi .

Table 5.9: The coefficient of drag at at stenosed vessel are presented with different dimensionless numbers.

Models	Drag coefficient (C_d)					
	Re			Wi		
	1000	2000	3000	0.0	0.5	1.0
N	1.09257	1.61492	2.10357	0.40431	1.02115	1.36377
GN	0.94687	1.76125	2.10124	0.65042	0.94687	1.26045
OD	0.76539	1.27577	1.75481	0.57313	0.73852	0.99432
GD	1.16816	1.61028	2.07177	1.08912	1.16816	1.33003

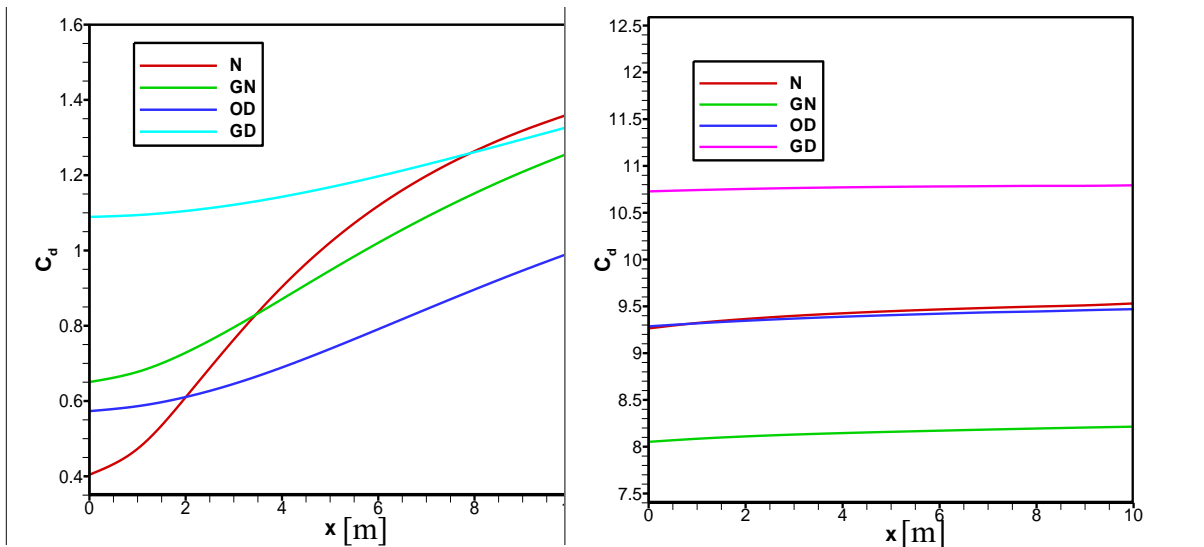


Figure 5.35: Drag effects of blood at bottom stenosed vessel wall with blood clot (left) and without blood clot (right) when $Re = 1000$ and $Wi = 0.6$.

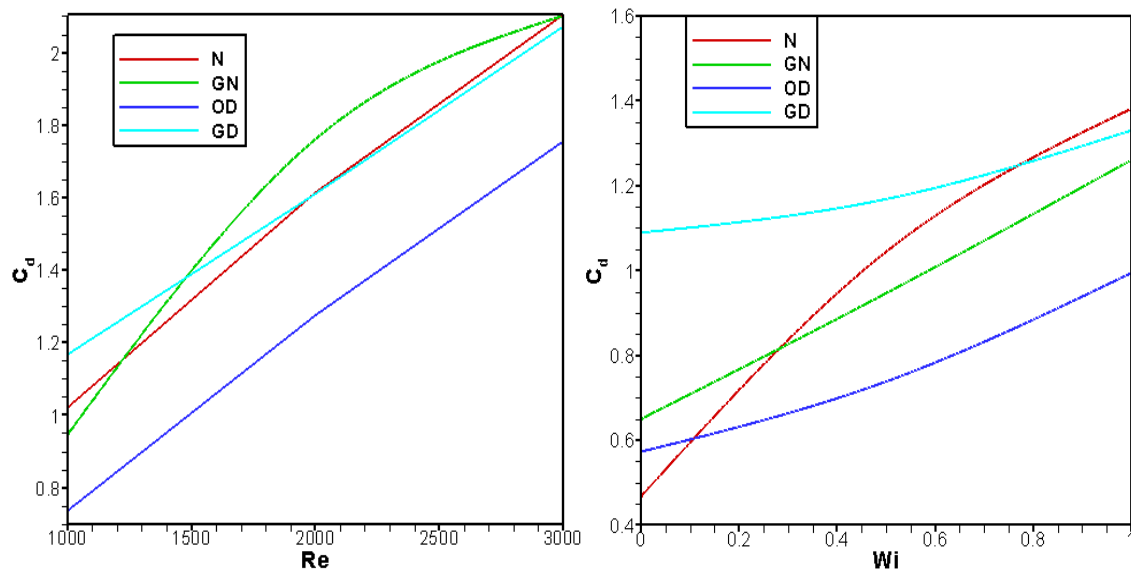


Figure 5.36: Drag effects of blood at bottom stenosed vessel wall with blood clot with respect to Re (left) and Wi (right) for all models.

5.5 Chapter Ending

This work is focused on the study of numerical investigation of blood flow through stenotic and aneurysmatic artery having or not blood clot. The simulation of the blood flow through the physical model has done by finite element method. The effect of blood flow variables, wall shear stress, dimensionless number and drag coefficients are very momentous. The above factors are correlated to blood viscoelasticity, blood shear

thinning behavior and influence the blood flow. The blood flow variables have intensive change at the throat of stenosis (no blood clot) compare to blood clot stenosis model. The blood flow patterns have more affected by high Reynold numbers (turbulence flow) at generalized Oldroyd-B case on the contrary insignificant changed occur for different Weissenberg numbers in present problem. Effects of wall shear stress and drag coefficient on blood flow at blood clot regimes are highlighted to explore their impacts on blood flow structure and its characteristics.

The governing differential equations that consist of conservation of mass, momentum equation, Oldroyd-B equations and bio-heat equation which is derived by finite element method. To solve the nonlinear differential equations the Newton-Raphson iteration is used for the dependent variables of blood velocity, pressure, drag coefficient and wall shear stress with the certain range of Reynold numbers and Weissenberg numbers.

Based on the above computational results we conclude that:

- ◆ The shear-thinning effects are related to the blood flow variables velocity and pressure are more pronounce than the viscoelastic ones.
- ◆ The blood flow parameters are predominant in the recirculation zones compare to blood clot model.
- ◆ The wall shear stress are intensified at the throat of stenosis having no blood clot for generalized models.
- ◆ The effect of drag coefficient on blood flow is more extreme in stenotic (without blood clot) artery for all models.
- ◆ The prominent changes have found on blood flow with respect to the Re through stenotic and aneurysmatic artery and the highest and lowest values are attained at stenosis and aneurysm region respectively for all cases.
- ◆ The significant change of blood flow are found with the increase of Weissenberg numbers but negligible variation among models.
- ◆ Due to presence of blood clot at the throat of stenosis the recirculation zones are more elliptic for all models.

CHAPTER 6

CONCLUSIONS

6.1 Conclusions

This thesis deals with modeling aspects of Newtonian, non-Newtonian and their generalized fluids (shear thinning) modifications, as well as with development and validation of algorithms used in simulation of such blood fluids.

The main contribution in the modeling part is the introduction and analysis of a new model for the Newtonian, generalized Newtonian, Oldroyd-B and generalized Oldroyd-B where constitutive equations are of Partial differential form. The mathematical and numerical study of the non-linear system of partial differential equations that model the motion of incompressible Newtonian and non-Newtonian fluids, in two dimensional, in case of steady flow. The numerical simulations and investigation to the problems have obtained computationally by the implementation of the finite elements method in the mathematical software COMSOL MULTIPHYSICS and MATLAB programming. The Hood-Taylor finite elements have been used to discretize the Navier-Stokes and Oldroyd-B equations and the iterative Newton-Raphson method has been applied to obtain the numerical solution of the corresponding algebraic system. In chapter-3, Numerical results have been obtained in a abrupt contraction for symmetric and non-symmetric stenosis, wall shear stress, different values of Weissenberg numbers and Reynolds numbers with various flow rates. We conclude that the effect of blood viscoelasticity are correlated to blood flow variables and wall shear stress which is more significant than non-viscoelastic ones. The blood flow variables pressure and velocity are predominant at the throat of stenosis and substantial change occurred with flow rates. With respect to the height of stenosis, the blood characteristics have a significant change at the centre of stenosis. According to the investigation, the growth of the recirculation zone at constriction regions are found, contrary to the shear-thinning blood fluid only due to the specific choice of the viscosity characteristic. The reversal blood flows have found at behind the stenosis region to the adjacent vessel wall. The finding of the blood flow behavior on the wall shear stress is an important factor in the onset of arterial diseases which may be reported in medical science.

The Second contribution of the thesis consist of development and numerical analysis of robust and reliable algorithm for blood flow simulation of Newtonian, Oldroyd-B and

CONCLUSIONS

their generalized fluids through permeable aneurysm. It is shown in this thesis at chapter-4, the objective of this mathematical model is to understand and bring out the effects of permeable aneurysmatic, wall shear stress, dimensionless numbers and stress tensor on blood flow for all four models. Moreover, to study the influence of the shear-thinning and viscoelastic behavior of blood, we have used the Newtonian (N), generalized Newtonian (GN), Oldroyd-B (OD) and generalized Oldroyd-B (GD) models. We have observed that the viscoelastic behavior of the blood fluids by comparing the results from the simulation and graphical presentation of velocity, pressure, stress tensor and wall shear stress for various values of Peclet number and Weissenberg numbers. It is shown, that the blood flow patterns have shown in terms of contour plots and developed an axisymmetric profile at entrance and exit of the model. Finally, we have inferred that the outcomes of model parameters are related to blood shear thinning properties and more significant at low shear regions. Due to permeability of aneurysm, the blood velocity and pressure have decreased at aneurysm along vessel axis for all cases. The blood flow variables have affected by wall shear stress which a vital ingredient to identify the fatal arterial diseases. The Peclet numbers and Weissenberg numbers effects are more striking at porous region and blood flow variables have a dramatic change. The turbulent blood flow have reduced for the presence of porosity at aneurysm of the model. It has also shown the elliptic recirculation bubbles have originated between the aneurysm and migrated to upper vessel wall. The numerical method is used to solve the partial differential equations seems to be sufficiently strong and effective for the appropriate resolution in this problem.

The third contribution consist of comparison and numerical study of Navier stoke's, Oldroyd-B and bio-heat equation for incompressible Newtonina and non-Newtonina fluids in two dimensional steady state flow. The numerical investigation and simulation have performed through the stenotic and aneurysmatic artery and it is shown in ch-5. The governing equations are consist of a set of partial differential equations of continuity, momentum, viscoelastic and bio-heat for all four models. The blood flow velocity and pressure distribution through the stenotic and aneurysmatic artery are examined by exploring the effects Weissenberg numbers (Wi), Reynold numbers (Re), stress tensor components, drag coefficient, wall shear stress and aneurysm. The blood flow simulation have shown in terms of velocity and pressure contour plots for this model with blood clot and without clot at the contraction stenosis. The result have shown that the blood flow

CONCLUSIONS

variables have a significant change at the abrupt contraction region having blood clot. At high Reynold numbers, the blood flow patterns is more affected for generalized Oldroyd-B and insignificant change are found for the range of Weissenberg numbers ($0 \leq Wi \leq 1$) in present problem. The effects of drag coefficient on blood flow at thrombus area are explored but more extreme in non-blood clot model compare to clotted model for all cases. It has also shown that the wall shear stresses are less intensified at the throat of stenosis at blood clot model of generalized models because of low shear regions. The recirculation bubbles are more elliptic shape due to blood clot at the constriction region for all four models. Finally, the viscoelasticity of blood is highly correlated to blood flow variables and highlighted to explore their influences on blood flow structure and its characteristics.

Summarizing, in this thesis four classes fluids described by the set of partial differential equations are considered. We have introduced new isotropic viscosity model and viscoelasticity model, describing the generalized Newtonian fluids and Oldroyd-B type fluids, which gives the ability to predict the change of the recirculation zones even if shear thinning fluid is considered. Moreover, it is shown that the constitute equations, describing viscoelastic fluids, allow to perform stable simulations for various dimensionless numbers Reynold numbers and Weissenberg numbers. Finally, systematic analysis of solution techniques for Newtonian, generalized Newtonian, Oldroyd-B and generalized oldroyd-B fluids has been performed. The above outcomes of the research may also be useful in bio-medical engineering.

6.2 Remarks on Cardiovascular Diseases

Studies have shown that atherosclerosis is a slow and progressive disease in human organ that may start in childhood. It changes faster as you age and very severe after 50 years. There are some factors such as unhealthy levels of fats and cholesterol in the blood, smoking, high blood pressure, high amounts of diabetes, obesity, physical incapability, genetic problems, abnormal growth, any kind of trauma can damage the inner layers of blood vessel. Many scientists believe plaque begins when an artery's inner layer „endothelium“ becomes damaged. Over time, deposit of plaque become hardens and contract the blood vessel which leads to barrier of blood circulation. Consequently, plaque area can blast or rupture which creates an aneurysm in arteries and

CONCLUSIONS

form blood clots through platelets in the injury cell. Blood clots reduced the blood flow in different human organ and create cardiovascular diseases (angina, stroke etc.). For treatment of these diseases, the familiar phrase of, "Prevention is better than cure" is more applicable. In the case of prevention, the following risk factors may be controlled which can help prevent or delay atherosclerosis and its related diseases.

- **Blood cholesterol levels:** Elevated levels of cholesterol and triglycerides in the blood are one of the main causes of cardiovascular diseases. Heart healthy diet is one of the best way to control these diseases taking unsaturated foods such as nuts, seeds, walnuts, olive oil, avocados, oily fish etc. to keep maintain standard level of cholesterol.
- **Cigarette smoking:** Smoking play a vital role in the growth of atherosclerosis in the coronary arteries, aorta and arteries in the legs. It also raises the blood pressure, cholesterol levels and creates barrier to move enough oxygen in our body's tissues. Smokers should quit as soon as possible and find out the ways to give up the habit to safe themselves of severe diseases.
- **High blood Pressure:** If the blood pressure is 140/90 mmHg or above leads high blood pressure and it is sources of many chronic diseases such as heart failure, stoke, diabetes, kidney disease etc. The continuous hypertension of blood on vessel wall are main reason to bulge or aneurysm in arteries. To control of high blood pressure depends on several factors, such its severity, associated risks of developing stroke or cardiovascular, disease, etc. However, change in lifestyle, exercise, keeping standard weight, regular sleep, meditation, stress reduces can help to keep in standard blood pressure.
- **Obesity:** Over weight of human being is another factor of arthrosclerosis and foundation of many diseases. WHO has shown that 39% of adults aged 18 years and 41 million children under the age of 5 were overweight in 2016. The obesity can be prevented under controlling of high fat foods, increasing in physical activities and overall consciousness of health.
- **Diabetes:** It is a disease in which blood sugar or glucose levels are too high leads to many diseases such as kidney, eye, nerves, heart diseases, stoke etc. Exercise, weight control and sticking to your meal plan can help control your diabetes. We should also monitor our blood glucose level and take medicine if prescribed.

CONCLUSIONS

- **Unhealthy diet:** It can raise our risk for cardiovascular diseases and other's diseases. High saturated foods, sodium, sugar, cholesterol and trans fats are risk factors for atherosclerosis. Adopt healthy eating habits, which include eating different fruits and vegetables (including beans and peas), whole grains, lean meats, poultry without skin, seafood, and fat-free or low-fat milk and dairy products. A heart-healthy diet is very helpful to reduce cardiovascular diseases.
- **Older age:** With the increase of age the risk for atherosclerosis will increase. Unhealthy diet, genetic or lifestyle factors cause plaque to build up in arteries during middle-aged. At studies show that the risk increases after age 45 for men and age 55 for women. Taking healthy diet, changing lifestyle and regular physical activities helps to control risk factors of such diseases at middle-aged.
- **Insulin resistance:** Insulin is a hormone that helps move blood sugar into cells where it's used as an energy source. Insulin resistance may lead to diabetes.
- **Lack of Physical activity:** It is other risk factors for atherosclerosis, such as unhealthy blood cholesterol levels, high blood pressure, diabetes, and overweight and obesity. Exercise will improve fitness levels, lower or higher blood pressure, and help reduce weight.
- **Genetic Problem:** A family history of early heart disease are risk factors for growth of atherosclerosis. Controlling other risk factors often can lessen genetic influences and prevent atherosclerosis, even in older adults.

If the above preventions aren't enough to control atherosclerosis risk factors. we may take advises from doctor about cardiovascular diseases. General treatment to cure from these diseases are adopting medicines and medical procedures which are given bellows:

- **Medicines:** Sometimes preventions or lifestyle changes alone are not enough to control your cholesterol levels. Doctors usually prescribe statin medications to control or lower cholesterol for coronary heart disease, peripheral artery disease, or stroke, diabetes and high low-density lipoprotein cholesterol levels. By controlling cholesterol level, we can change of having a heart attack or stroke. We can also take medicines to control blood pressure, sugar levels, prevent blood clots, relieving symptoms and stop swelling. We should still follow a heart healthy lifestyle, even if we take medicines to treat our cardiovascular diseases.

CONCLUSIONS

- **Medical Procedures and Surgery:** In the case of severe atherosclerosis, doctor may recommend a medical procedure or surgery to prevent cardiovascular diseases and some important surgery are discussed as follows.

- **Percutaneous coronary intervention (PCI) or coronary angioplasty:**

The Percutaneous coronary intervention (PCI) is a nonsurgical procedure that improves blood flow to our heart. It is used to open coronary arteries that are blocked or narrowed coronary (heart) arteries by the buildup of atherosclerotic plaque. PCI can improve blood flow to the heart, relieve chest pain, to relieve symptoms of coronary heart disease or to reduce heart damage during or after a heart attack. Sometimes a small mesh tube called a stent is placed in the artery to keep it open after the procedure.

- **Coronary artery bypass grafting (CABG):** The Coronary artery bypass grafting (CABG) is a type of surgery that improves blood flow to the heart. It is used for people who have severe coronary heart disease (CHD) or coronary artery disease. In CABG, arteries or veins from other areas in your body are used to bypass or go around your narrowed coronary arteries. This creates a new passage, and oxygen-rich blood is routed around the blockage to the heart muscle. Through the surgery we can improve blood flow to your heart, relieve chest pain, and possibly prevent a heart attack. Bypass grafting also can be used for leg arteries. For this surgery, a healthy blood vessel is used to bypass a narrowed or blocked artery in one of the legs. The healthy blood vessel redirects blood around the blocked artery, improving blood flow to the leg. It is also known as an open-heart surgery.

- **Carotid endarterectomy:** The Carotid endarterectomy is a surgical procedure to open or clean plaque buildup from the carotid arteries to prevent stroke. This procedure restores blood flow to the brain, which can help to avoid brain hemorrhage, clotting, bleeding etc. Taking anticlotting medicines before and after surgery can reduce this risk.

Atherosclerosis is a severe disease in our human organ which creates some obstacles to move blood smoothly throughout body. Despite a lot development in medical sector,

CONCLUSIONS

researches are still going on about cardiovascular diseases to know the sources, identification and proper treatment of these diseases.

6.3 Further Research

The consequent can be aheaded for the additional works on the base of the present research as.

- ❖ In the future, the study can be extended by dissimilar physics like bending artery, vertical artery and corss sectional arteryand arterial bifurcation effects on blood flow.
- ❖ Stenotic and Aneurysmatic artery effects on Blood flow with Magneto-hydrodynamics (MHD) for Newtonian, Oldroyd-B and their generalized models may be discussed later.
- ❖ The next work will be devoted to an extension of this numerical study to unsteady blood flow and fluid-structure interaction simulations in stenotic and anuesymatic vessels, to provide a deeper understanding of the significance of the non-Newtonian characteristics of blood and its correlation with the cardiovascular diseases like atherosclerosis.
- ❖ The study can be extended for non-uniform blood vessel with different blood flow rates.
- ❖ The present model can be explained within heat sinkor source of blood vesselfor Newtonina and non-Newtonina models.
- ❖ Two-dimensional steady blood fluid flow has been analyzed in this thesis. So, this consideration may be extended to three-dimensional analyses to explore the effects of parameters on blood flow fields in cavities.
- ❖ The analytical solution of the two or three dimensional transient bioheat equation with different boundary conditions may be done further.
- ❖ Investigation can be performed by using magnetic fluid throughstenotic or aneurysmaticartery with changing the boundary conditions of the blood vessel walls.
- ❖ We analyzed the simulation and mathematical properties of the blood flow for all four models in the case of incompressiblebut we did not verify their performance for compressible flows. Therefore, this remains for future investigation.

Appendix A

As mentioned in section 3.3.1, the finite element method can be considered to solve the governing equations. The non-linear parametric solution method is chosen to solve the governing equations. This approach will result in substantially fast convergence assurance. A non-uniform triangular mesh arrangement is implemented in the present investigation especially near the walls to capture the rapid changes in the dependent variables. For convenience, the governing Equations (3.9-3.12) to be solved are relisted below:

Continuity Equation

$$\frac{\partial U}{\partial X} + \frac{\partial V}{\partial Y} = 0 \quad (3A)$$

Momentum Equations

$$Re \left(U \frac{\partial U}{\partial X} + V \frac{\partial U}{\partial Y} \right) = -\frac{\partial P}{\partial X} + \left(\frac{\partial \sigma}{\partial X} + \frac{\partial \sigma}{\partial Y} \right) + (1-\lambda) \left(\frac{\partial^2 U}{\partial X^2} + \frac{\partial^2 U}{\partial Y^2} \right) + f \quad (3B)$$

$$Re \left(V \frac{\partial V}{\partial X} + V \frac{\partial V}{\partial Y} \right) = -\frac{\partial P}{\partial Y} + \left(\frac{\partial \sigma}{\partial X} + \frac{\partial \sigma}{\partial Y} \right) + (1-\lambda) \left(\frac{\partial^2 V}{\partial X^2} + \frac{\partial^2 V}{\partial Y^2} \right) + f \quad (3C)$$

Oldroyd-B constitutive equation:

$$W_i \left(U \frac{\partial \sigma}{\partial X} + V \frac{\partial \sigma}{\partial Y} \right) + \sigma = \left(\frac{\partial U}{\partial X} + \frac{\partial U}{\partial Y} \right) + W_i \left(\frac{\partial U}{\partial X} \sigma + \frac{\partial U}{\partial Y} \sigma + \sigma \frac{\partial U}{\partial Y} + \sigma \frac{\partial U}{\partial X} \right) \quad (3D)$$

The velocity and viscoelasticity Equations (3A-3D) result in a set of non-linear coupled equations for which an iterative scheme is adopted. To ensure convergence of the numerical algorithm the following criteria is applied to all dependent variables over the solution domain

$$\sum |\psi_{ij}^n - \psi_{ij}^{n-1}| \leq 10^{-5}$$

Where, Ψ represents a dependent variable U, V, P, σ , the indexes i, j indicates a grid point; and the index n is the current iteration at the grid level. The six-node triangular element is used in this work for the development of the finite element equations. All six nodes are associated with velocities as well as stress tensor; only the corner nodes are associated with pressure. This means that a lower order polynomial is chosen for

Appendix A

pressure and which is satisfied through continuity equation. The velocity component and the stress tensor distributions and linear interpolation for the pressure distribution according to their highest derivative orders in the differential Equations (3A-3D) as

$$U(X,Y) = N_{\alpha} U_{\alpha} \quad (\text{A.1})$$

$$V(X,Y) = N_{\alpha} V_{\alpha} \quad (\text{A.2})$$

$$\sigma(X,Y) = N_{\alpha} \sigma_{\alpha} \quad (\text{A.3})$$

$$P(X,Y) = H_{\lambda} P_{\lambda} \quad (\text{A.4})$$

Where, $\alpha = 1, 2, \dots, \dots, 6$; $\lambda = 1, 2, 3$; N_{α} are the element interpolation functions for the velocity components and the stress tensor, and H_{λ} are the element interpolation functions for the pressure.

To derive the finite element equations, the method of weighted residuals is applied to the continuity equation (3A), the momentum Equations (3B-3C) and the viscoelasticity Equation (3D), we get

$$\int_A N_{\alpha} \left(\frac{\partial U}{\partial X} + \frac{\partial V}{\partial Y} \right) dA = 0 \quad (\text{A.5})$$

$$\begin{aligned} \text{Re} \int_A N_{\alpha} \left(U \frac{\partial U}{\partial X} + V \frac{\partial U}{\partial Y} \right) dA = & - \int_A H_{\lambda} \frac{\partial P}{\partial X} dA + \int_A N_{\alpha} \left(\frac{\partial \sigma}{\partial X} + \frac{\partial \sigma}{\partial Y} \right) dA \\ & + (1 - \lambda) \int_A N_{\alpha} \left(\frac{\partial^2 U}{\partial X^2} + \frac{\partial^2 U}{\partial Y^2} \right) dA + \int_A N_{\alpha} f dA \end{aligned} \quad (\text{A.6})$$

$$\begin{aligned} \text{Re} \int_A N_{\alpha} \left(U \frac{\partial V}{\partial X} + V \frac{\partial V}{\partial Y} \right) dA = & - \int_A H_{\lambda} \frac{\partial P}{\partial Y} dA + \int_A N_{\alpha} \left(\frac{\partial \sigma}{\partial X} + \frac{\partial \sigma}{\partial Y} \right) dA \\ & + (1 - \lambda) \int_A N_{\alpha} \left(\frac{\partial^2 V}{\partial X^2} + \frac{\partial^2 V}{\partial Y^2} \right) dA + \int_A N_{\alpha} f dA \end{aligned} \quad (\text{A.7})$$

$$\begin{aligned} W_i \int_A N_{\alpha} \left(U \frac{\partial \sigma}{\partial X} + V \frac{\partial \sigma}{\partial Y} \right) dA + \int_A N_{\alpha} \sigma dA = & \int_A \mu_{\nu} N_{\alpha} \left(\frac{\partial U}{\partial X} + \frac{\partial U}{\partial Y} \right) dA + \\ & W_i \int_A N_{\alpha} \left(\frac{\partial U}{\partial X} \sigma + \frac{\partial U}{\partial Y} \sigma + \sigma \frac{\partial U}{\partial Y} + \sigma \frac{\partial U}{\partial X} \right) dA \end{aligned} \quad (\text{A.8})$$

Where, A is the element area. Gauss's theorem is then applied to Equations (A.6-A.8) to generate the boundary integral terms associated with the surface tractions and extra stress tensor. Then Equations (A.6-A.8) become,

Appendix A

$$\begin{aligned} Re \int_A N_\alpha \left(U \frac{\partial U}{\partial X} + V \frac{\partial U}{\partial Y} \right) dA + \int_A H_\lambda \frac{\partial P}{\partial X} dA - \int_A N_\alpha \left(\frac{\partial \sigma}{\partial X} + \frac{\partial \sigma}{\partial Y} \right) dA \\ - (1-\lambda) \int_A N_\alpha \left(\frac{\partial^2 U}{\partial X^2} + \frac{\partial^2 U}{\partial Y^2} \right) dA - \int_A N_\alpha f_x dA = \int_{S_0} N_\alpha S_x ds_0 \end{aligned} \quad (A.9)$$

$$\begin{aligned} Re \int_A N_\alpha \left(U \frac{\partial V}{\partial X} + V \frac{\partial V}{\partial Y} \right) dA + \int_A H_\lambda \frac{\partial P}{\partial Y} dA - \int_A N_\alpha \left(\frac{\partial \sigma}{\partial X} + \frac{\partial \sigma}{\partial Y} \right) dA \\ - (1-\lambda) \int_A N_\alpha \left(\frac{\partial^2 V}{\partial X^2} + \frac{\partial^2 V}{\partial Y^2} \right) dA - \int_A N_\alpha f_y dA = \int_{S_0} N_\alpha S_y ds_0 \end{aligned} \quad (A.10)$$

$$\begin{aligned} W_i \int_A N_\alpha \left(U \frac{\partial \sigma}{\partial X} + V \frac{\partial \sigma}{\partial Y} \right) dA + \int_A N_\alpha \sigma dA - \int_A \mu_\nu N_\alpha \left(\frac{\partial U}{\partial X} + \frac{\partial U}{\partial Y} \right) dA - \\ W_i \int_A N_\alpha \left(\frac{\partial U}{\partial X} \sigma + \frac{\partial U}{\partial Y} \sigma + \sigma \frac{\partial U}{\partial Y} + \sigma \frac{\partial U}{\partial X} \right) dA = \int_A N_\alpha \sigma_w ds_w \end{aligned} \quad (A.11)$$

Here Equations (A.6-A.7) specify surface tractions (S_x , S_y) along outflow boundary S_0 and equation (A.8) specifies velocity components and stress tensor that can be applied from domain along wall boundary S_w . Substituting the element velocity component distributions, the stress tensor distribution, and the pressure distribution from Equations (3.9 -3.12) the finite element equations can be written in the form,

$$K_{\alpha\beta^x} U_\beta + K_{\alpha\beta^y} V_\beta = 0 \quad (A.12)$$

$$\begin{aligned} Re(K_{\alpha\beta\gamma^x} U_\beta U_\gamma + K_{\alpha\beta\gamma^y} V_\beta U_\gamma) + M_{\alpha\mu^x} P_\mu + K_{\alpha\beta^x} \sigma_\beta + K_{\alpha\beta^y} \sigma_\beta \\ + (1-\lambda)(S_{\alpha\beta^{xx}} + S_{\alpha\beta^{yy}}) U_\beta - f_x K_\alpha = Q_{\alpha^u} \end{aligned} \quad (A.13)$$

$$\begin{aligned} Re(K_{\alpha\beta\gamma^x} U_\beta V_\gamma + K_{\alpha\beta\gamma^y} V_\beta V_\gamma) + M_{\alpha\mu^y} P_\mu + K_{\alpha\beta^x} \sigma_\beta \\ + K_{\alpha\beta^y} \sigma_\beta + (1-\lambda)(S_{\alpha\beta^{xx}} + S_{\alpha\beta^{yy}}) V_\beta - f_y K_\alpha = Q_{\alpha^v} \end{aligned} \quad (A.14)$$

$$\begin{aligned} W_i (K_{\alpha\beta\gamma^x} U_\beta \sigma_\gamma + K_{\alpha\beta\gamma^y} V_\beta \sigma_\gamma) + K_{\alpha\beta} \sigma_\mu - \mu_\nu (K_{\alpha\beta^x} U_\alpha + K_{\alpha\beta^y} U_\beta) \\ - W_i \left(K_{\alpha\beta\gamma^x} U_\beta \sigma_\gamma + K_{\alpha\beta\gamma^y} U_\beta \sigma_\gamma \right) = Q_{\alpha^T} \end{aligned} \quad (A.15)$$

Where, the coefficients in element matrices are in the form of the integrals over the element area and along the element edges S_0 and S_w as,

$$K_{\alpha\beta^x} = \int_A N_\alpha N_{\beta,x} dA, \quad (A.16a)$$

Appendix A

$$K_{\alpha\beta}^y = \int_A N_{\alpha} N_{\beta,y} dA, \quad (\text{A.16b})$$

$$K_{\alpha\beta\gamma}^x = \int_A N_{\alpha} N_{\beta} N_{\gamma,x} dA, \quad (\text{A.16c})$$

$$K_{\alpha\beta\gamma}^y = \int_A N_{\alpha} N_{\beta} N_{\gamma,y} dA, \quad (\text{A.16d})$$

$$K_{\alpha\beta} = \int_A N_{\alpha} N_{\beta} dA, \quad (\text{A.16e})$$

$$S_{\alpha\beta}^{xx} = \int_A N_{\alpha,x} N_{\beta,x} dA, \quad (\text{A.16f})$$

$$S_{\alpha\beta}^{yy} = \int_A N_{\alpha,y} N_{\beta,y} dA, \quad (\text{A.16g})$$

$$M_{\alpha\mu}^x = \int_A H_{\alpha} H_{\mu,x} dA, \quad (\text{A.16h})$$

$$M_{\alpha\mu}^y = \int_A H_{\alpha} H_{\mu,y} dA, \quad (\text{A.16i})$$

$$Q_{\alpha}^u = \int_{S_0} N_{\alpha} S_x dS_0, \quad (\text{A.16j})$$

$$Q_{\alpha}^v = \int_{S_0} N_{\alpha} S_y dS_0, \quad (\text{A.16k})$$

$$Q_{\alpha}^T = \int_{S_0} N_{\alpha} \sigma_w dS_w \quad (\text{A.16l})$$

These element matrices are evaluated in closed-form ready for numerical analysis. Details of the derivation for these element matrices are omitted herein for brevity.

The derived finite element equations, Equations (A.12-A.15), are nonlinear. These nonlinear algebraic equations are solved by applying the Newton-Raphson iteration technique by first writing the unbalanced values from the set of the finite element Equations (A.12-A.15) as

$$F_{\alpha}^p = K_{\alpha\beta}^x U_{\beta} + K_{\alpha\beta}^y V_{\beta} \quad (\text{A.17a})$$

$$F_{\alpha}^u = Re(K_{\alpha\beta\gamma}^x U_{\beta} U_{\gamma} + K_{\alpha\beta\gamma}^y V_{\beta} U_{\gamma}) + M_{\alpha\mu}^x P_{\mu} - K_{\alpha\beta}^x \sigma_{\beta} - K_{\alpha\beta}^y \sigma_{\beta} + (1-\lambda)(S_{\alpha\beta}^{xx} + S_{\alpha\beta}^{yy}) U_{\beta} - f_x K_{\alpha} - Q_{\alpha}^u \quad (\text{A.17b})$$

Appendix A

$$F_{\alpha^v} = Re(K_{\alpha\beta\gamma^x} U_{\beta} V_{\gamma} + K_{\alpha\beta\gamma^y} V_{\beta} V_{\gamma}) + M_{\alpha\mu^y} P_{\mu} - K_{\alpha\beta^x} \sigma_{\beta} - K_{\alpha\beta^y} \sigma_{\beta} + (1-\lambda)(S_{\alpha\beta^{xx}} + S_{\alpha\beta^{yy}}) V_{\beta} - f_y K_{\alpha} - Q_{\alpha^v} \quad (\text{A.17c})$$

$$F_{\alpha^T} = W_i(K_{\alpha\beta\gamma^x} U_{\beta} \sigma_{\gamma} + K_{\alpha\beta\gamma^y} V_{\beta} \sigma_{\gamma}) + K_{\alpha\beta} \sigma_{\beta} - \mu_v(K_{\alpha\beta^x} U_{\beta} + K_{\alpha\beta^y} V_{\beta}) - 2W_i \left(K_{\alpha\beta\gamma^x} U_{\gamma} \sigma_{\beta} + K_{\alpha\beta\gamma^y} U_{\gamma} \sigma_{\beta} \right) - Q_{\alpha^T} \quad (\text{A.17d})$$

This leads to a set of algebraic equations with the incremental unknowns of the element nodal velocity components, temperatures, and pressures in the form,

$$\begin{bmatrix} K_{uu} & K_{uv} & K_{u\sigma} & K_{up} \\ K_{vu} & K_{vv} & K_{v\sigma} & K_{vp} \\ K_{\sigma u} & K_{\sigma v} & K_{\sigma\sigma} & 0 \\ K_{pu} & K_{pv} & 0 & 0 \end{bmatrix} \begin{Bmatrix} \Delta u \\ \Delta v \\ \Delta \sigma \\ \Delta p \end{Bmatrix} = - \begin{Bmatrix} F_{\alpha^u} \\ F_{\alpha^v} \\ F_{\alpha^{\sigma}} \\ F_{\beta^p} \end{Bmatrix} \quad (\text{A.18})$$

Where,

$$K_{uu} = Re(K_{\alpha\beta\gamma^x} U_{\gamma} + K_{\alpha\gamma\beta^x} U_{\gamma} + K_{\alpha\beta\gamma^y} V_{\beta}) + (1-\lambda) \left(S_{\alpha\beta^{xx}} + S_{\alpha\beta^{yy}} \right)$$

$$K_{uv} = K_{\alpha\beta\gamma^y} U_{\gamma}, \quad K_{uT} = -K_{\alpha\beta^x} - K_{\alpha\beta^y}, \quad K_{up} = M_{\alpha\mu^x}, \quad K_{vu} = K_{\alpha\beta\gamma^x} V_{\gamma},$$

$$K_{vv} = Re(K_{\alpha\beta\gamma^x} U_{\beta} + K_{\alpha\gamma\beta^x} V_{\gamma} + K_{\alpha\gamma\beta^y} V_{\gamma}) + (1-\lambda) \left(S_{\alpha\beta^{xx}} + S_{\alpha\beta^{yy}} \right)$$

$$K_{v\sigma} = -K_{\alpha\beta^x} - K_{\alpha\beta^y}, \quad K_{vp} = M_{\alpha\mu^y}, \quad K_{\sigma u} = W_i K_{\alpha\beta\gamma^x} \sigma_c - K_{\alpha\beta^x} \mu_v,$$

$$K_{\sigma v} = W_i K_{\alpha\beta\gamma^y} \sigma_c - K_{\alpha\beta^y} \mu_v, \quad K_{TT} = K_{\alpha\beta} - 2W_i(K_{\alpha\beta\gamma^x} U_c + K_{\alpha\beta\gamma^y} U_c)$$

$$K_{Tp} = 0, \quad K_{pu} = K_{\alpha\beta^x}, \quad K_{pv} = K_{\alpha\beta^y} \quad \text{and} \quad K_{pT} = 0 = K_{pp}$$

The iteration process is terminated if the percentage of the overall change compared to the previous iteration is less than the specified value. To solve the sets of the global nonlinear algebraic equations in the form of matrix, the Newton-Raphson iteration technique has been adapted through PDE solver with COMSOL MULTIPHYSICS interface and developed MATLAB script.

Appendix B

To derive the finite element equation, which is mentioned in section 5.3.1, the method of Zienkiewicz and Taylor methods (1991) is applied to the governing equations. We recall the system of partial differential Equations (5.5 -5.9) as follows.

Continuity Equation

$$\nabla \cdot \mathbf{U} = 0 \quad (5A)$$

Momentum Equations

$$Re[(\mathbf{U} \cdot \nabla) \mathbf{U}] = -\nabla P + (1-\lambda) \Delta \mathbf{U} + \nabla \cdot \boldsymbol{\sigma} + \mathbf{f} \quad (5B)$$

$$Re[(\mathbf{V} \cdot \nabla) \mathbf{V}] = -\nabla P + (1-\lambda) \Delta \mathbf{V} + \nabla \cdot \boldsymbol{\sigma} + \mathbf{f} \quad (5C)$$

Oldroyd-B Constitutive Equation:

$$\boldsymbol{\sigma} + Wi [(\mathbf{U} \cdot \nabla) \boldsymbol{\sigma} - (\nabla \mathbf{U}) \boldsymbol{\sigma} - \boldsymbol{\sigma} (\nabla \mathbf{U})^t] = 2 \mu_v \mathbf{V}(\mathbf{U}) \quad (5D)$$

Bio-heat Equation:

$$Re Pr (\mathbf{U} \cdot \nabla) \theta = \nabla^2 \theta + Q - \rho_f \theta \quad (5E)$$

After the applying the weighted residual method then

$$\int_A N_\alpha (\nabla \cdot \mathbf{U}) dA = 0 \quad (C.1)$$

$$\begin{aligned} Re \int_A N_\alpha \mathbf{U} (\nabla \cdot \mathbf{U}) dA = & - \int_A H_\lambda \nabla P dA + \int_A N_\alpha \nabla \boldsymbol{\sigma} dA \\ & + (1-\lambda) \int_A N_\alpha \nabla^2 \mathbf{U} dA + \int_A N_\alpha \mathbf{f} dA \end{aligned} \quad (C.2)$$

$$\begin{aligned} Re \int_A N_\alpha \mathbf{U} (\nabla \cdot \mathbf{V}) dA = & - \int_A H_\lambda \nabla P dA + \int_A N_\alpha \nabla \boldsymbol{\sigma} dA \\ & + (1-\lambda) \int_A N_\alpha \nabla^2 \mathbf{V} dA + \int_A N_\alpha \mathbf{f} dA \end{aligned} \quad (C.3)$$

$$\begin{aligned} W_i \int_A N_\alpha \mathbf{U} (\nabla \cdot \boldsymbol{\sigma}) dA + \int_A N_\alpha \boldsymbol{\sigma} dA = & \int_A \mu_v N_\alpha (\nabla \cdot \mathbf{U}) dA + \\ & W_i \int_A N_\alpha (\nabla \cdot \mathbf{U}) \boldsymbol{\sigma} + \boldsymbol{\sigma} (\nabla \cdot \mathbf{U}) dA \end{aligned} \quad (C.4)$$

$$\begin{aligned} Re Pr \int_A N_\alpha (\mathbf{U} \cdot \nabla) \theta dA = & \int_A N_\alpha \nabla^2 \theta dA + \int_A N_\alpha Q dA \\ & - \int_A N_\alpha \rho_f \theta dA \end{aligned} \quad (C.5)$$

Appendix B

To generate the boundary integral terms associated with the surface tractions, extra stress tensor and temperature the Equations (C.2-C.5) become after applying Gauss's theorem.

$$\begin{aligned} Re \int_A N_\alpha U (\nabla \cdot U) dA + \int_A H_\lambda \nabla P dA - \int_A N_\alpha \nabla \cdot \sigma dA \\ - (1-\lambda) \int_A N_\alpha \nabla^2 U dA - \int_A N_\alpha f_x dA = \int_{S_0} N_\alpha S_x ds_0 \end{aligned} \quad (C.6)$$

$$\begin{aligned} Re \int_A N_\alpha U (\nabla \cdot V) dA + \int_A H_\lambda \nabla P dA - \int_A N_\alpha \nabla \cdot \sigma dA \\ - (1-\lambda) \int_A N_\alpha \nabla^2 V dA - \int_A N_\alpha f_y dA = \int_{S_0} N_\alpha S_y ds_0 \end{aligned} \quad (C.7)$$

$$\begin{aligned} W_i \int_A N_\alpha U \cdot (\nabla \sigma) dA + \int_A N_\alpha \sigma dA - \int_A \mu_v N_\alpha \nabla \cdot U dA - \\ W_i \int_A N_\alpha [(\nabla \cdot U) \sigma + \sigma (\nabla \cdot U)] dA = \int_A N_\alpha \sigma_w ds_w \end{aligned} \quad (C.8)$$

$$\begin{aligned} Re Pr \int_A N_\alpha (U \cdot \nabla) \theta dA - \int_A N_\alpha \nabla^2 \theta dA - \int_A N_\alpha Q dA \\ + \int_A N_\alpha \rho_f \theta dA = \int_{S_w} N_\alpha q_w ds_w \end{aligned} \quad (C.9)$$

Here Equations (C.2-C.3) specify surface tractions (S_x , S_y) along outflow boundary S_0 , Equations (C.4-C.5) specify velocity components, stress tensor and fluid temperature that can be applied force from domain along wall boundary S_w .

The six-node triangular element is used for the development of the finite element equations. All six nodes are associated with velocities, temperature as well as stress tensor; only the corner nodes are associated with pressure. This means that a lower order polynomial is chosen for pressure and which is satisfied through continuity equation. The basic unknowns for the above differential equations are the velocity components U , V the stress tensor, σ and the pressure, P . The velocity component and the stress tensor distributions and linear interpolation for the pressure distribution according to their highest derivative orders in the differential Equations (5A-5E) as

$$U(X,Y) = N_\alpha U_\alpha \quad (C.10)$$

$$V(X,Y) = N_\alpha V_\alpha \quad (C.11)$$

$$\sigma(X,Y) = N_\alpha \sigma_\alpha \quad (C.12)$$

$$P(X,Y) = H_\lambda P_\lambda \quad (C.13)$$

$$\theta(X, Y) = N_\alpha \theta_\alpha \quad (C.14)$$

Appendix B

Where, $\alpha = 1, 2, \dots, 6$; $\lambda = 1, 2, 3$; N_α are the element interpolation functions for the velocity components and the stress tensor, and H_λ are the element interpolation functions for the pressure. Substituting the element velocity component distributions, the stress tensor distribution, and the pressure distribution from Equations (5A-5E) the finite element equations can be written in the form,

$$K_{\alpha\beta^x} U_\beta + K_{\alpha\beta^y} V_\beta = 0 \quad (C.15)$$

$$\begin{aligned} Re(K_{\alpha\beta\gamma^x} U_\beta U_\gamma + K_{\alpha\beta\gamma^y} V_\beta U_\gamma) + M_{\alpha\mu^x} P_\mu + K_{\alpha\beta^x} \sigma_\beta + K_{\alpha\beta^y} \sigma_\beta \\ + (1-\lambda)(S_{\alpha\beta^{xx}} + S_{\alpha\beta^{yy}}) U_\beta - f_x K_\alpha = Q_{\alpha^u} \end{aligned} \quad (C.16)$$

$$\begin{aligned} Re(K_{\alpha\beta\gamma^x} U_\beta V_\gamma + K_{\alpha\beta\gamma^y} V_\beta V_\gamma) + M_{\alpha\mu^y} P_\mu + K_{\alpha\beta^x} \sigma_\beta \\ + K_{\alpha\beta^y} \sigma_\beta + (1-\lambda)(S_{\alpha\beta^{xx}} + S_{\alpha\beta^{yy}}) V_\beta - f_y K_\alpha = Q_{\alpha^v} \end{aligned} \quad (C.17)$$

$$\begin{aligned} W_i(K_{\alpha\beta\gamma^x} U_\beta \sigma_\gamma + K_{\alpha\beta\gamma^y} V_\beta \sigma_\gamma) + K_{\alpha\beta} \sigma_\mu - \mu_\nu (K_{\alpha\beta^x} U_\alpha + K_{\alpha\beta^y} U_\beta) \\ - W_i \left(K_{\alpha\beta\gamma^x} U_\beta \sigma_\gamma + K_{\alpha\beta\gamma^y} U_\beta \sigma_\gamma \right) = Q_{\alpha^T} \end{aligned} \quad (C.18)$$

$$\begin{aligned} Re Pr(K_{\alpha\beta\gamma^x} U_\beta \theta_\gamma + K_{\alpha\beta\gamma^y} V_\beta \theta_\gamma) + (S_{\alpha\beta^{xx}} + S_{\alpha\beta^{yy}}) \theta_\beta - K_\alpha Q \\ + \rho_f K_{\alpha\beta} \theta_\beta = Q_{\alpha^\theta} \end{aligned} \quad (C.19)$$

Where, the coefficients in element matrices are in the form of the integrals over the element area and along the element edges S_0 and S_w as,

$$K_\alpha = \int_A N_\alpha dA \quad (C.20a)$$

$$K_{\alpha\beta^x} = \int_A N_\alpha N_{\beta,x} dA, \quad (C.20b)$$

$$K_{\alpha\beta^y} = \int_A N_\alpha N_{\beta,y} dA, \quad (C.20c)$$

$$K_{\alpha\beta\gamma^x} = \int_A N_\alpha N_\beta N_{\gamma,x} dA, \quad (C.20d)$$

$$K_{\alpha\beta\gamma^y} = \int_A N_\alpha N_\beta N_{\gamma,y} dA, \quad (C.20e)$$

$$K_{\alpha\beta} = \int_A N_\alpha N_\beta dA, \quad (C.20f)$$

Appendix B

$$S_{\alpha\beta^{xx}} = \int_A N_{\alpha,x} N_{\beta,x} dA, \quad (C.20g)$$

$$S_{\alpha\beta^{yy}} = \int_A N_{\alpha,y} N_{\beta,y} dA, \quad (C.20h)$$

$$M_{\alpha\mu^x} = \int_A H_{\alpha} H_{\mu,x} dA, \quad (C.20i)$$

$$M_{\alpha\mu^y} = \int_A H_{\alpha} H_{\mu,y} dA, \quad (C.20j)$$

$$Q_{\alpha^u} = \int_{S_0} N_{\alpha} S_x dS_0, \quad (C.20k)$$

$$Q_{\alpha^v} = \int_{S_0} N_{\alpha} S_y dS_0, \quad (C.20l)$$

$$Q_{\alpha^{\sigma}} = \int_{S_0} N_{\alpha} \sigma_w dS_w \quad (C.20m)$$

$$Q_{\alpha} \theta = \int_{S_w} N_{\alpha} q_w dS_w \quad (C.20n)$$

Using the Newton-Raphson iteration technique the set of nonlinear algebraic Equations (C.15-C.19) are transferred into linear algebraic equations. Finally, these linear equations are solved by applying triangular factorization method and reduced integration technique of Zeinkiewicz and Taylor (1991) and the finite element Equations (C.15-C.19) as,

$$F_{\alpha^p} = K_{\alpha\beta^x} U_{\beta} + K_{\alpha\beta^y} V_{\beta} \quad (C.21a)$$

$$F_{\alpha^u} = Re(K_{\alpha\beta\gamma^x} U_{\beta} U_{\gamma} + K_{\alpha\beta\gamma^y} V_{\beta} U_{\gamma}) + M_{\alpha\mu^x} P_{\mu} - K_{\alpha\beta^x} \sigma_{\beta} - K_{\alpha\beta^y} \sigma_{\beta} \\ + (1-\lambda)(S_{\alpha\beta^{xx}} + S_{\alpha\beta^{yy}}) U_{\beta} - f_x K_{\alpha} - Q_{\alpha^u} \quad (C.21b)$$

$$F_{\alpha^v} = Re(K_{\alpha\beta\gamma^x} U_{\beta} V_{\gamma} + K_{\alpha\beta\gamma^y} V_{\beta} V_{\gamma}) + M_{\alpha\mu^y} P_{\mu} - K_{\alpha\beta^x} \sigma_{\beta} - K_{\alpha\beta^y} \sigma_{\beta} \\ + (1-\lambda)(S_{\alpha\beta^{xx}} + S_{\alpha\beta^{yy}}) V_{\beta} - f_y K_{\alpha} - Q_{\alpha^v} \quad (C.21c)$$

$$F_{\alpha^{\sigma}} = W_i (K_{\alpha\beta\gamma^x} U_{\beta} \sigma_{\gamma} + K_{\alpha\beta\gamma^y} V_{\beta} \sigma_{\gamma}) + K_{\alpha\beta} \sigma_{\beta} - \mu_v (K_{\alpha\beta^x} U_{\beta} + K_{\alpha\beta^y} V_{\beta}) \\ - 2W_i \left(K_{\alpha\beta\gamma^x} U_{\gamma} \sigma_{\beta} + K_{\alpha\beta\gamma^y} U_{\gamma} \sigma_{\beta} \right) - Q_{\alpha^{\sigma}} \quad (C.21d)$$

$$F_{\alpha} \theta = Re Pr (K_{\alpha\beta\gamma^x} U_{\beta} \theta_{\gamma} + K_{\alpha\beta\gamma^y} V_{\beta} \theta_{\gamma}) + (S_{\alpha\beta^{xx}} + S_{\alpha\beta^{yy}}) \theta_{\beta} - K_{\alpha} Q \\ + \rho_f K_{\alpha\beta} \theta_{\beta} - Q_{\alpha} \theta \quad (C.21e)$$

Appendix B

This leads to a set of algebraic equations with the incremental unknowns of the element nodal velocity components, temperatures, and pressures in the form,

$$\begin{bmatrix} K_{uu} & K_{uv} & K_{u\sigma} & K_{u\theta} & K_{up} \\ K_{vu} & K_{vv} & K_{v\sigma} & K_{v\theta} & K_{vp} \\ K_{\sigma u} & K_{\sigma v} & K_{\sigma\sigma} & 0 & 0 \\ K_{\theta u} & K_{\theta v} & 0 & K_{\theta\theta} & 0 \\ K_{pu} & K_{pv} & 0 & 0 & 0 \end{bmatrix} \begin{Bmatrix} \Delta u \\ \Delta v \\ \Delta\sigma \\ \Delta\theta \\ \Delta p \end{Bmatrix} = - \begin{Bmatrix} F \\ F \\ F \\ F \\ F \\ \alpha^u \\ \alpha^v \\ \alpha^\sigma \\ \alpha^\theta \\ \alpha^p \end{Bmatrix} \quad (C.22)$$

Where,

$$K_{uu} = Re(K_{\alpha\beta\gamma^x} U_\gamma + K_{\alpha\gamma\beta^x} U_\gamma + K_{\alpha\beta\gamma^y} V_\beta) + (1-\lambda) \left(S_{\alpha\beta^{xx}} + S_{\alpha\beta^{yy}} \right)$$

$$K_{uv} = K_{\alpha\beta\gamma^y} U_\gamma, \quad K_{uT} = -K_{\alpha\beta^x} - K_{\alpha\beta^y}, \quad K_{up} = M_{\alpha\mu^x}, \quad K_{vu} = K_{\alpha\beta\gamma^x} V_\gamma,$$

$$K_{vv} = Re(K_{\alpha\beta\gamma^x} U_\beta + K_{\alpha\gamma\beta^x} V_\gamma + K_{\alpha\gamma\beta^y} V_\gamma) + (1-\lambda) \left(S_{\alpha\beta^{xx}} + S_{\alpha\beta^{yy}} \right)$$

$$K_{v\sigma} = -K_{\alpha\beta^x} - K_{\alpha\beta^y}, \quad K_{vp} = M_{\alpha\mu^y}, \quad K_{\sigma u} = W_i K_{\alpha\beta\gamma^x} \sigma_c - K_{\alpha\beta^x} \mu_v,$$

$$K_{\sigma v} = W_i K_{\alpha\beta\gamma^y} \sigma_c - K_{\alpha\beta^y} \mu_v, \quad K_{\sigma\sigma} = K_{\alpha\beta} - 2W_i (K_{\alpha\beta\gamma^x} U_c + K_{\alpha\beta\gamma^y} U_c)$$

$$K_{\sigma p} = 0, \quad K_{pu} = K_{\alpha\beta^x}, \quad K_{pv} = K_{\alpha\beta^y} \text{ and } K_{p\sigma} = 0 = K_{pp}$$

$$K_{\theta\theta} = RePr(K_{\alpha\beta\gamma^x} U_\beta + K_{\alpha\beta\gamma^y} V_\beta) + (S_{\alpha\beta^{xx}} + S_{\alpha\beta^{yy}}) + \rho_f K_{\alpha\beta}$$

$$K_{\theta u} = K_{\alpha\beta\gamma^x} \theta_\gamma,$$

$$K_{\theta v} = K_{\alpha\beta\gamma^y} \theta_\gamma$$

$$K_{\sigma\theta} = K_{\theta\sigma} = 0$$

$$K_{\theta p} = 0, \quad K_{pu} = K_{\alpha\beta^x}, \quad K_{p\theta} = 0 = K_{pp}$$

$$K_{pv} = K_{\alpha\beta^y}$$

If the percentage of the overall change compared to the previous iteration is less than the specified value then the iteration process is terminated. The mathematical software COMSOL MULTIPHYSICS interface and inhouse MATLAB script have been used to solve the nonlinear algebraic equation in the matrix form.

References

- Akbar , N. S., Rahman, S. U., Ellahi , R., Nadeem, S., "Nano fluid ow in tapering stenosed arteries with permeable walls", *International Journal of Thermal Sciences*, vol. 85, pp 54-61, 2014.
- Anand, M., Rajagopal, K. R., "A shear-thinning viscoelastic fluid model for describing the flow of blood", *International Journal of Cardiovascular Medicine and Science*, Vol. 4 (2), pp.59–68 ,2004
- Baskurt,O.K., Meiselman, H.J., "Blood Rheology and Hemodynamics", *Seminars in Thrombosis and Hemostasis*, Vol. 29(5), pp.435-450, 2003.
- Berger, S. A., Jou, L. D., "Flows in stenotic vessels", *Ann. Rev. Fluid Mech.*, Vol.32 pp. 347–382, 2000.
- Bernsdorf, J. and Wang, D., "Non-Newtonian blood ow simulation in cerebral aneurysms", *Computers and Mathematics with Applications*, vol. 58, pp 1024-1029, 2009
- Bodnar, T., Sequeira, A., Prosi, M., "On the shear-thinning and viscoelastic effects of blood ow under various flow rates", *Applied Mathematics and Computation*, Vol. 217(11), pp. 5055-5067, 2011.
- Breithaupt-Grogler, K., Ling, M., Boudoula, H. S, Belz G.G., "Protective Effect of Chronic Garlic Intake on Elastic Properties of Aorta in the Elderly", *Circulation*, Vol. 96, pp.2649-2655, 1997.
- Budwig, R., Elgar, D., Hooper, H., Slippy, J.,' Steady Flow in Abdominal Aortic Aneurysm Models," *J. Biomed. Engr.*, Vol. 115, pp. 418-423,1993.
- Caro, C. G., Pedley, T. J., Schrote, R. C. R, Seed W. A., "The Mechanics of the Circulation", Oxford University Press, 1978.
- Chakravarty, S. and Mandal, P. K., "Two-dimensional blood flow through tapered arteries under stenotic conditions," *International Journal of Non-Linear Mechanics*, Vol. 35(5), pp. 779–793, 2000.
- Chakravarty, S., Sarifuddin, S., and Mandal, P. K., "Unsteady flow of a two-layer blood stream past a tapered flexible artery under stenotic conditions," *Computational Methods in Applied Mathematics*, vol. 4, no. 4, pp. 391–409, 2004.

References

- Charm, S.E., Kurland, G.S., “Viscometry of human blood for shear rates of 0-100,000 sec⁻¹”, *Nature*, Vol. 206, pp. 617-618, 1965.
- Chien, S., Sung, K.L.P., Skalak, R., Usami S., Tozeren, A.L., “Theoretical and experimental studies on viscoelastic properties of erythrocyte membrane”, *Biophysical Journal*, Vol.24(2), pp. 463-487, 1978.
- Chien, S., Usam, S. I, Dellenback, R.J., Gregersen, M.I., “Blood viscosity: Influence of erythrocyte aggregation”, *Science*, Vol.157(3790), pp.829-831, 1967.
- Chien, S., Usami, S., Dellenback,R.J., Gregersen, M.I., “Blood viscosity: Influence of erythrocyte deformation”, *Science*, Vol.157 (3790), pp. 827-829, 1967.
- Chien, S., Usami, S., Dellenback,R.J., Gregersen, M.I., “Shear-dependent deformation of erythrocytes in rheology of human blood”, *American Journal of Physiology*, Vol. 219, pp.136-142, 1970.
- Chien, S., Usami, S., Taylor, H.M., Lundberg, J.L., Gregersen, M.I., “Effect of hematocrit and plasma proteins on human blood rheology at low shear rates”, *Journal of Applied Physiology*, Vol. 21(1), pp. 81-87, 1966.
- Chiu, J. J., Wang, D. L., Chien, S., Skalak, R., and Usami, S., “Effects of disturbed flow on endothelial cells,” *Journal of Biomechanical Engineering*, Vol. 120(1), pp. 2–8, 1998.
- Chorin, A. J. and Marsden, J. E., “A Mathematical Introduction to Fluid Mechanics”, 3rd. edition, Springer, 2000.
- Chung, T.J., “Computational Fluid Dynamics”, Second Ed., Cambridge, 2002.
- Coleman, B. D., Markovitz, H., and Noll, W., “Viscometric flows of non-Newtonian fluids”, *Theory and experiment*, Springer-Verlag, Berlin, 1966.
- COMSOL Multiphysics, 4.3a users guide, 2013
- Cronenwett, JL; Murphy, TF; Zelenock, GB; Whitehouse WM, Jr; Lindenauer, SM; Graham, LM; Quint, LE; Silver, TM; Stanley, JC., "Actuarial analysis of variables associated with rupture of small abdominal aortic aneurysms". *Surgery*. 98 (3): 472–83, 1985.

References

- D' Elia, M., Perego, M., Veneziani A., "A variational Data Assimilation procedure for the incompressible Navier-Stokes equations in hemodynamics", *J. Sci. Comput.*, Vol. 52(2), pp. 340-359, 2011.
- Dechaumphai, P. "Adaptive finite element technique for heat transfer problems, *Energy*", *Heat & Mass transfer*, Vol. 17, pp. 87-94, 1995.
- Dechaumphai, P., "Finite Element Method in Engineering", second Ed., Chulalongkorn University Press, Bangkok, 1999.
- Dintenfass, L., "Thixotropy of Blood and Proneness to Thrombus Formation", *Circulation Research*, Vol. 11, pp. 233-239, 1962.
- Dwivedi, A. P., Pal, T. S., and Rakesh, L., "Micropolar fluid model for blood flow through small tapered tube," *Indian Journal of Technology*, Vol. 20(8), pp. 295–299, 1982.
- Ernst, C. B., "Abdominal Aortic Aneurysm," *New England J. Med.*, Vol. 328(16), pp. 1167-72, 1993.
- Evans, E.A. and Hochmuth, R.M., "Membrane viscoelasticity", *Biophysical Journal*, Vol. 16(1), pp. 1-11, 1976.
- Fakour, M., Vahabzadeh, A., Ganji, D. D. and Hatami, M., "Analytical study of micropolar fluid flow and heat transfer in a channel with permeable walls", *J. of Molecular Liquids*, Vol. 204 pp 198-204, 2015.
- Ferziger, J. H. and Perić, M., "Computational methods for fluid dynamics", Second Ed., Springer Verlag, Berlin Heidelberg, 1997.
- Fuat, Y., Ihsan, K.A., and Yasar, G.M., "Analysis of drag effects on pulsatile blood flow in a right coronary artery by using Eulerian multiphase model" *Korea-Australia Rheology Journal*, Vol. 23(2), pp. 89-103, 2011, DOI: 10.1007/s13367-011-0012-8
- Fukushima, T., Matsuzawa, T., and Homma, T., "Visualization and Finite Element Analysis of Pulsatile Flow in Models of Abdominal Aortic Aneurysm," *Biorehology*, Vol. 26, pp. 109-13, 1986.
- How, T. V. and Black, R. A., "Pressure losses in non-Newtonian flow through rigid wall tapered tubes," *Biorheology*, Vol. 24(3), pp. 337–351, 1987.

References

- Hron J., "Numerical Simulation of Visco-Elastic Fluids", In: WDS' 97, Freiburg, 1997.
- Ingoldby, C. J. H., Wujanto, R., Mitchell, J. E., "Impact of Vascular Surgery on Community Mortality From Ruptured Aortic Aneurysms," *Br. J. Surg.*, Vol. 73, pp. 551-563, 1986.
- Johansen, K. H., "Aneurysms," *Scientific American*, Vol. 247, pp. 110-125, 1982.
- Kumar, B. R., Kumar, G.A., Kumar, S.M., "MATLAB^R and its Application in Engineering", Panjab University, India, 2010.
- Landau, L. D. Lifshitz, E. M. , "Fluid Mechanics. Translated by Sykes", J. B. Reid, W. H. (2nd ed.). Butterworth Heinemann. ISBN 0-7506-2767-0, 1997
- Lee, B-K., Xue S., Nam, J., Lim, H., Shin, S., "Determination of the blood viscosity and yield stress with a pressure-scanning capillary hemorheometer using constitutive models", *Korea-Australia Rheology Journal*, Vol. 23(1), pp.1-6, 2011.
- Leuprecht, A., Perktold, K., "Computer simulation of non-Newtonian effects of blood flow in large arteries", *Computer Methods in Biomechanics and Biomechanical Engineering*, Vol. 4, pp. 149–163, 2001.
- Lubliner, J., "Plasticity Theory", Macmillan Publishing Company, 1990.
- Mandal, P. K., "An unsteady analysis of non-Newtonian blood flow through tapered arteries with a stenosis," *International Journal of Non-Linear Mechanics*, Vol. 40(1), pp. 151–164, 2005.
- Mantha, A. R., Benndorf, G., Hernandez, A., Metcalfe, R. W., "Stability of pulsatile blood flow at the ostium of cerebral aneurysms", *Journal of Biomechanics*, vol. 42, pp 1081-1087, 2009.
- Marshall, I., Zhao, S., Sopoulou P. P., Hoskins, P., and Xu, X. Y., "MRI and CFD studies of pulsatile flow in healthy and stenosed carotid bifurcation models," *Journal of Biomechanics*, Vol. 37(5), pp. 679–687, 2004.
- Mekheimer, Kh. S. and Kot, M. A. E., "The micropolar fluid model for blood flow through a tapered artery with a stenosis," *Acta Mechanica Sinica*, Vol. 24(6), pp. 637–644, 2008.
- Menche N. (ed.) *Biologie Anatomie Physiologie*. Munich: Urban & Fischer/ Elsevier; 2012.
- Mukhopadhyay, S. and Layek, G. C., "Analysis of blood flow through a modelled artery with an aneurysm", *Applied Mathematics and Computation*, vol. 217, pp 6792-6801, 2011.

References

- Muraki, N., "Ultrasonic Studies of the Abdominal Aorta with Special Reference to Hemodynamic Considerations on Thrombus Formation in the Abdominal Aortic Aneurysm," *J. Japanese College Angiology*, Vol. 23, pp. 401-413, 1983.
- Nadeem, S. and Ijaz, S., "Theoretical analysis of metallic nanoparticles on blood flow through tapered elastic artery with overlapping stenosis", *Transaction on Nanobiosciences*, doi: 10.1109/TNB.2015.2389253, 2015.
- Nasir M U and Alim M A, "Numerical Study of Blood Flow through Symmetry and Non-Symmetric Stenosis Artery under Various Flow Rates", *IOSR Journal of Dental and Medical Sciences*, Vol. 16, No. 6, pp. 106-115, 2017.
- Nasir M U and Alim M A, "Numerical Investigation of Blood Flow through stenotic Artery", *World Journal of Engineering Research and Technology (WJERT)*, Vol. 3, No. 6, pp. 93-116, 2017.
- Oka, S. and Murata, T., "Theory of the steady slow motion of non-Newtonian fluids through a tapered tube," *Japanese Journal of Applied Physics*, Vol. 8, pp. 5–8, 1969.
- Oka, S., "Pressure development in a non-Newtonian flow through a tapered tube," *Biorheology*, Vol. 10(2), pp. 207–212, 1973.
- Patankar, S. V., "Numerical Heat Transfer and Fluid Flow", New York, 1980.
- Pincombe, B., Mazumdar, I. J., Craig, I. H., "Effects of multiple stenosis and poststenotic dilatation on non-Newtonian blood flow in small arteries", *Med. Biol. Eng. Comput.*, vol. 37, pp 595-598, 1995.
- Pincombe, B. And mazumdar, J., "The effects of Post-stenotic dilatations on the flow of a blood analogue through stenosed coronary arteries", *Mathl. Comput. Modelling*, vol. 25, pp 57-70, 1997.
- Prasad, K. M., Vijaya, R. B. and Umadevi, C., "Effects of stenosis and poststenotic dilatation on Jeffrey fluid flow in arteries", *International Journal of Research in Engineering and Technology*, vol. 4, pp 195-201, 2014.
- Priyadharshini, S. and Ponalagusamy, R., "Biorheological model on flow of Herschel-Bulkley fluid through a tapered arterial stenosis and dilatation", *Applied bionics and biomechanics*, doi:org/10.1155/2015/406195, 2015.

References

- Pschyrembel W. *Klinisches Wörterbuch*. Berlin: De Gruyter; 2014.
- Prokop, V. and Kozel, K., “Numerical simulation of Generalized Newtonian and Oldroyd-B Fluids”, *Numerical Mathematics and Advanced Application 2011*, pp 579-586, 2013
- Quarteroni, A. and Formaggia, L., “Mathematical Modelling and Numerical Simulation of the Cardiovascular System”, Elsevier, Amsterdam, 2002.
- Quemada, D., “Rheology of concentrated disperse systems III. General features of the proposed non-Newtonian model”, *Comparison with experimental data. Rheol. Acta*, Vol.17, pp. 643-653, 1978.
- Radka, K., Kozel, K., “The numerical simulation of generalized Newtonian and Oldroyd-B fluid flow”, *Programs and Algorithms of Numerical Mathematics*, Vol.16, 112-117, 2013.
- Rajagopal, K., Srinivasa, A., “A thermodynamic frame work for rate type fluid models”, *Journal of Non-Newtonian Fluid Mechanics*, Vol. 80, pp. 207–227, 2000.
- Rajagopal, K.R., Srinivasa, A.R., “A Gibbs-potential-based formulation for obtaining the response functions for a class of viscoelastic materials”, *Proc. R. Soc. A*, Vol. 467, 39-58, 2011.
- Rashidi, S., Dehghan , M., Ellahi, R., Riaz , M., and Jamal-Abad M. T., "Study of stream wise transverse magnetic fluid ow with heat transfer around a porous obstacle", *Journal of Magnetism and Magnetic Materials*, vol. 378, pp 128-137, 2015.
- Reddy J.N. and Gartling, “Fundamentals of the Finite Element Method in Heat Transfer”, Second Ed., CRC Press, 2001.
- Robertson, A. M., Sequeira, A., Kameneva, M. V., Hemorheology, in: Galdi, G., Rannacher, R., Robertson, A. M., Turek, S. (Eds.), “Hemodynamical Flows: Modeling, Analysis and Simulation”, Vol. 37, pp. 63–120, 2008.
- Robertson, A. M., Sequeira, A., Owens, G. R., “Rheological models for blood, in: *Cardiovascular Mathematics*”, Modeling and Simulation of the circulatory system, Springer, Milan, 211-241, 2009.
- Robertson, A. M., Sequeira, A., Owens, R. G., “Rheological models for blood”, in: Formaggia, L., Quarteroni, A., Veneziani, A. (Eds.), “*Cardiovascular Mathematics*,

References

- Modeling and simulation of the circulatory system” MS&A, Modeling, Simulations & Applications, Vol. 1, pp. 211–241, 2009.
- Serrin, J., “Mathematical Principles of Classical Fluid Mechanics”, in Flugge, S. and Truesdell, S., Vol. VIII, Springer-Verlag, Berlin, 1969.
- Shaughnessy, E. J., Katz, I. M. and Schaer, J. P., “Introduction to Fluid Mechanics”, Oxford University Press, 2005.
- Shih, T.C., Yuan P., Lin, W., Kou, H. S., Analytical analysis of the Pennes bioheat transfer equation with sinusoidal heat flux condition on skin surface, *Medical Engineering & Physics* 29, 946– 953, 2007.
- Siddiqui, S. U., Verma, N. K., Mishra, S., and Gupta, R. S., “Mathematical modelling of pulsatile flow of Casson’s fluid in arterial stenosis,” *Applied Mathematics and Computation*, Vol. 210(1), pp. 1–10, 2009.
- Taylor, T. W., and Yamaguchi, T., "Three-Dimensional Simulation of Blood Flow in an Abdominal Aortic Aneurysm-Steady and Unsteady Flow Cases," *J. Biomech. Engr.*, Vol. 116, pp. 89-97, 1994.
- Telma, G., Jorge, T., Adelia, S., “Optimal control in blood flow simulations”, *Int. Journal of Non-Linear Mechanics*, Vol. 64, 57-69, 2014.
- Thurston, G. B., “Non-Newtonian viscosity of human blood: Flow induced changes in microstructure”, *Biorheology*, Vol. 31(2), 179–192, 1994.
- Thurston, G.B., “Frequency and shear rate dependence of viscoelasticity of blood”, *Biorheology*, Vol.10(3), 375-381, 1973.
- Thurston, G.B., “Viscoelasticity of human blood”, *Biophysical Journal*, Vol. 12, 1205-1217, 1972.
- Truesdell, C., “Rational continuum mechanics, Academic Press”, Boston, New York, London, 1991.
- Tu, C. and Deville, M., “Pulsatile flow of non-Newtonian fluids through arterial stenoses,” *Journal of Biomechanics*, Vol. 29(7), pp. 899–908, 1996.
- Verdier, C., “Rheological properties of living materials. from cells to tissues”, *Journal of Theoretical Medicine*, Vol. 5 (2), 67–91, 2003.

References

Videman, J. H., “Mathematical analysis of viscoelastic non-Newtonian fluids”, Mestre, Universidade tecnica de Lisboa, 1997.

Yeleswarapu, K. K., Kameneva, M. V., Rajagopa, K. R. I, Antaki J. F., “The flow of blood in tubes: Theory and experiment”, Mech. Res. Comm.Vol. 25, 257–262, 1998

Zeeshan , A., Ellahi, R., Hassan , M., "Magnetohydrodynamic Flow of Water/Ethylene Glycol Based Nanofluids with Natural Convection Through Porous Medium", The European Physical Journal Plus, vol. 129, pp 261, 2014.

Zienkiewicz, O. C. and Taylor, R. L. “The finite element method”, Fourth Ed., McGraw-Hill. 1991.